The Thesis Committee for Qiqi Wang
Certifies that this is the approved version of the following thesis:

Characterization of Bedding-Parallel Fractures in Shale

-Morphology, size distribution and spatial organization

APPROVED BY
SUPERVISING COMMITTEE:

Supervisor:

Stephen E. Laubach

Co-supervisor:

Julia F.W. Gale

Brian Horton

Charles Kerans

Characterization of Bedding-Parallel Fractures in Shale

- Morphology, size distribution and spatial organization

by

Qiqi Wang, B.S.

Thesis

Presented to the Faculty of the Graduate School of

The University of Texas at Austin

in Partial Fulfillment

of the Requirements

for the Degree of

Master of Science in Geological Sciences

The University of Texas at Austin

December 2016

Dedication

Dedicated to my mom and dad, Ms. Chunhua Fu and Mr. Youxiang Wang, for encouraging me to step out into a bigger world, and to find who I am and what I want to do for life.

Acknowledgements

Thank you to my supervisor, Dr. Julia Gale, for supervising my project. I appreciate all the guidance, support, and patience. You patiently taught me what scientific research is about, and significantly improved my technical writing skills. It truly has been a pleasure to be your student, and I am so happy that we shared the past two years of memories. If it turns out that I teach in university one day, I hope to be both a mentor and a companion to my students, just as you have been to me; to Dr. Stephen Laubach, my co-supervisor, for giving useful mini-lectures along the way, and for all of the suggestions, guidance, and editing. Thank you to Dr. Esti Ukar for many useful suggestions in the field; to Ms. Sara Elliott for helping me with sample preparation and SEM related work (and answering incessant questions thereafter). Thanks to my committee members Dr. Charles Kerans and Dr. Brian Horton for your suggestions and geological insight. Thanks to Dr. Richard Schultz for giving feedback on my work and being exceptionally inspiring. Thanks to Dr. Kitty Milliken for the information and suggestions on mudstone petrography and dealing with fragile samples.

Thank you to the Fracture Research and Application Consortium group for being a great teaching forum and support system. I extend thanks to the Jackson School of Geosciences, the Bureau of Economic Geology, for providing me the opportunity to learn from some of the best geologists in the world, and for continuing to fuel my passion for geology. I would like to acknowledge the financial support of FRAC and its industry partners, and the Jackson School Foundation, and YPF for funding my project. Thanks to

the Argentine geologists I worked with in the field. Rene, Ramiro, Rosina, Sebastian, Victoria, Juan Pablo, Matias, Martin, and Carolina, without you I would not have been able to get such good datasets from the field so efficiently. Thank you to the staff Nathan and Brandon at the Core Research Center for showing me how to cut rocks and to Wagner Petrographic for thin section preparation. Thanks to Philip Guerrero for always answering my questions patiently, and for being a friend who will always tell me to be careful and plan ahead!

Thank you to my friends from UT for showing me how to have a blast but still be a rocking good geologist; thanks especially Hanyue “Sophia” Zheng, who offered me a place to stay when I first arrived at Austin. Thanks for being my company through the pleasant days, exploring Texas and visiting my dreamland Yellowstone national park, and during the “Dark Ages” of thesis writing so I could have social stimulation that I so desperately needed. Thank you to my friends Meng Huo, Natchanan “Mint” Doungkaew for always being by my side. Thank you to my special friend Mr. David Nollsch for being so caring, inspiring and encouraging along the way.

Last but not least, thank you to my mother for showing me how a woman can be intelligent and strong, and showing me her work ethic and how to balance that with a joyful life. Thank you to my father for inspiring me to be a more understanding, humble and caring person and for always being there for me, without whom I wouldn't have been exposed to the wonderful world of oil and gas geology.

Abstract

Characterization of Bedding-Parallel Fractures in Shale

- Morphology, size distribution and spatial organization

Qiqi Wang, M.S. Geo Sci.

The University of Texas at Austin, 2016

Supervisor: Stephen E. Laubach, Julia F.W. Gale

Natural fracture systems are important for production in shale gas reservoirs as they may contribute to permeability of the reservoir, or they may reactivate during hydraulic fracture treatment. However, little is known about their size scaling and spatial distribution. Bed-parallel, calcite-filled fractures are common in shale. Knowing the aperture-size scaling and spatial organization of bed-parallel fractures may contribute to improved modeling of the combined fracture network (hydraulic and natural). Ten fracture data sets were collected from the Vaca Muerta (7), Marcellus (2) and Wolfcamp (1) shale formations. Bed-parallel fracture attributes such as strike, dip, aperture size, spacing, length and texture were collected from outcrops of the Vaca Muerta Formation in the Neuquén Basin, Argentina. Further fracture aperture-size and spacing data for the Vaca Muerta, and for the Marcellus and Wolfcamp, were collected through measurement direct from cores, and from photographic panels of slabbed core. A total of 1093 fractures were measured along 10 scanlines of total combined length of 629m. The aperture size of

bed-parallel fractures ranges over 4 orders of magnitude, from 15 μm to 87 mm. Nine out of ten datasets follow a negative exponential distribution. Fracture attributes such as intensity and size range are different in the 3 studied shales. Even within the same shale formation, fracture intensity and size range can be variable. Aperture size ranges of bed-parallel and vertical fractures in these shales are comparable as are fracture intensities for the Marcellus examples. Bed-parallel fractures, however, have higher intensities than vertical fractures in the Vaca Muerta examples. Spatial organization of bed-parallel fractures is investigated using a normalized two-point correlation technique that allows distinction between clustering, regular spacing and a random distribution. The relationship between fracture spatial organization and stratigraphy and mechanical interfaces within the host rock is also investigated, with preliminary results suggesting that bed-parallel fractures are more intense in organic-rich layers in some cases, but not in others.

Table of Contents

List of Tables

List of Figures

Chapter 1. Introduction

1.1 Background

1.1.1 Motivation for bedding-parallel fracture studies

Bed-parallel fractures or veins filled with fibrous mineral cements are common in in fine-grained rocks around the world, especially in organic matter-rich shales (Mackenzie, 1972; Marshall, 1982; Tobin et al., 1996; AlAasm et al., 1993, 1996; Rodrigues et al., 2009; Cobbold et al., 2013; Gale et al., 2014). Most such veins are filled with fibrous calcite that has been called *beef* on account of the resemblance of the crystal texture to the fibers of animal muscle (Buckland and De La Beche, 1835; Richardson, 1923; Lang et al., 1923; Tarr, 1933). Calcite beef are common in Cambrian-Ordovician, Devonian-Carboniferous, early Jurassic, and Cretaceous to Paleogene marine shales (Cobbold et al., 2013). In this work, the term *bed-parallel fracture* is used to refer to a bed-parallel vein filled with fibrous or non-fibrous minerals bed-parallel or open fractures Fin the same configuration relative to bedding. This is a more general terminology, and concept, than that encompassed by the historical term beef for bed-parallel veins having fibrous mineral texture.

Beef or bedding-parallel fractures that are filled with mineral cement are common, although Gale et al. (2014) noted that they are not present everywhere. Because shales are increasingly important oil and gas reservoir rocks, all of the structures within shale, including beef, are being intensely studied (Gale et al., 2014). Reasons to consider beef to be potentially important to fluid flow and the success of engineering operations in shale include the following. They are widespread but have variable, and currently unknown arrangements. They can be large features, as described more fully herein. And

they have mechanical properties that differ markedly from surrounding shale. As cement-filled veins, their compositions and textures may contain evidence useful for understanding the structural and thermal history of the shale (Bons et al., 2012).

Length, height and aperture define fracture size. Beef has a wide range of sizes. Fracture lateral extent and thickness (length and aperture size) can be highly variable. Measured in outcrop, bedding-parallel fractures can be a few millimeters to at least tens of meters long, with their thickness ranging from 10s of microns to several centimeters (Rodrigues et al., 2009; Smith et al., 2014; Maher et al., 2016) (Figure 1-1). Because these features are so large—comparable to the dimensions of beds—their presence may impact fluid flow in hydrocarbon reservoirs (Curtis, 2002; Chen et al., 2009; Ding et al., 2011; Duhalan et al., 2013; Zanella et al., 2015). Beef may also influence the propagation of hydraulic fractures, which are needed to stimulate production in shale (Zhang et al., 2007; Chuprakov et al., 2011, 2013, 2014, 2015). Natural, sealed bed-parallel fractures may facilitate horizontal growth of hydraulic fractures by acting as planes of weakness or modulus contrast that enhance the already marked strength anisotropy due to bedding-parallel laminae and planar fabric. Impacts on hydraulic fracture growth might include height growth inhibition and horizontal propagation. Several lines of evidence including mine-back experiments, microseismic data and tiltmeter data suggest that hydraulic fractures used to stimulate wells in hydrocarbon reservoirs sometimes have a horizontal (bedding-parallel) component, at various depths (Green et al., 2012; Kaiser et al., 2013; Chuprakov et al., 2015, Gale et al., 2015).

If fluid flow and hydraulic fracture propagation can be affected by bedding-parallel fractures, there are some basic fracture attributes we need to know before we can better understand the potential impact of this type of fracture.

Lateral extent and thickness of the bed-parallel fractures together defines the size of the fracture. The lateral extent of fracture is described by fracture length and width, the thickness by kinematic aperture (Figure 1-2). Kinematic aperture is the perpendicular distance between the adjacent rock walls (fracture surfaces) of a fracture, the opening displacement. The fracture may be open (containing fluid in the subsurface) or sealed (infilled by mineral cements). Beef are lens-shaped; aperture decreases along the length of a fracture toward the fracture tip. The distance between neighboring fractures is termed spacing; in the case of bed-parallel fractures it is the bed-normal distance between fractures. Other fracture attributes used to characterize bed-parallel fracture include fracture orientation, cement composition, cement texture and cement fiber orientation.

Fracture-size scaling analysis examines the relationship between fracture length/aperture sizes and their cumulative frequency. Fracture frequency is defined as the number of fractures per meter length. It is thus the inverse of average fracture spacing (Dershowitz et al., 1992; Ortega et al., 2006). Fracture size scaling describes the population distribution of different sizes of fractures. Size-scaling is an attribute that can be used as a tool to predict fracture sizes beyond the scale of observation.

For vertical fractures, average fracture spacing gained from the inverse of frequency typically is not being representative of actual fracture spacing, and this problem has not been systematically studied for bedding parallel fractures so more advanced analysis is necessary. Fracture spatial organization considers the pattern or

arrangement of fractures. As used here, this term refers to the pattern of distances between fractures (the spacing pattern). Spacing pattern indicates where the fractures are relative to each other and their location within the shale hostrock. For vertical fractures we typically look at the degree of clustering, but for bed-parallel fractures we examine the location of fractures (how they are spaced) in the stratigraphy. The type of spacing pattern is an attribute that can now be quantified (Marrett et al., in review). Evidence of typical spatial organization patterns can help predict the presence or absence of fracture clusters in shales generally. We expect that knowing the aperture-size scaling and spatial organization of bed-parallel fractures will contribute to modeling of both natural and hydraulic fracture networks.

Better characterization of shape, cement texture and cement composition of this type of fracture may improve understanding of the mechanism and environment under which bedding-parallel fractures form, and this will allow for better fracture modelling. My study focuses on bed-parallel fracture characterization, trying to gain a better understanding of their textural attributes, their relationship to host rock, their size population statistics, and their spatial distribution.

In my study, I examine beef attributes in many of the important, currently active shale oil and gas provinces including the Vaca Muerta, Marcellus, Wolfcamp and others (Table 1.)

Figure 1-1 Bedding-parallel fractures filled with fibrous calcite cement at the Arroyo Mulichinco outcrop, Neuquén, Argentina. The white fractures show positive relief relative to the softer dark shale hostrock in the river-cut cliff due to higher resistance to weathering. At this exceptionally fracture-rich outcrop, bed-parallel fractures account for as much as 10% by volume of the rock.

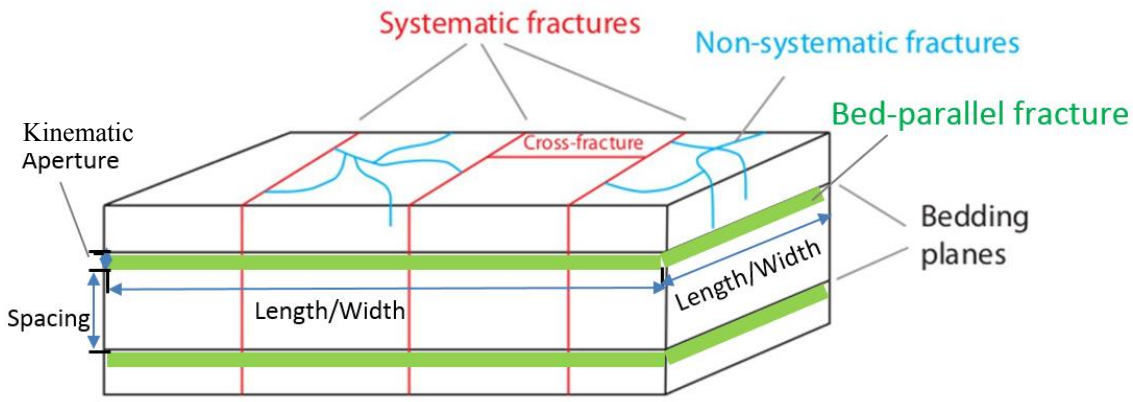

Figure 1-2 Illustration of fracture patterns developed within the hostrock, and the basic attributes used to describe bed-parallel fractures.

1.1.2 Bedding-parallel fractures around the world and previous studies

Bedding-parallel fractures occur in sedimentary basins around the world, especially within low permeability strata. In this section I review previous studies on bedding-parallel fractures, regarding where they are worldwide, and their attributes. In the past, the use of different terms in published works regarding bed-parallel fractures has probably led to some confusion. In this work, the term "bed-parallel fracture" is used to refer to a bed-parallel vein filled with fibrous or non-fibrous minerals. The term "beef" in many papers refers to bedding-parallel veins containing fibrous minerals, where the fibers have formed approximately perpendicular to the fracture margins (Cobbold et al., 2013).

Many early studies of bedding-parallel fractures are of outcrops in the United Kingdom, such as the well exposed Mesozoic strata on the coast of SW England (Brodie, 1854; Judd, 1871; Andrews, 1881; Woodward, 1893; Andrews and Jukes-Brown, 1894;

Geikie; 1902 and Reid, 1903); the Inner Hebrides Islands of NW Scotland (Judd, 1878; Harker, 1908; Lee, 1920), Ayrshire, SW Scotland (Young, 1885), the Midlands of England (Woodward, 1893; Thompson, 1902), Somerset (Short, 1904; Reynolds and Vaughan, 1904; Richardson, 1911) and South Wales (Richardson, 1905). Webster (1826) and De la Beche (1835) used the term "beef". The name "beef" comes from the resemblance of fibrous fracture cement to the fibers of animal muscle. Webster stated, "the fibers of this limestone, like those of satin spar, are at right angles to the planes of the beds which they compose, and which vary from two to six inches in thickness." Their observation is consistent with my observations nearly two hundred years later.

In the 1930s and 1940s, this type of fracture was described from localities in France, Belgium and Africa. Since then, there have been many reports of bed-parallel veins worldwide. Figure 1-3 built by Cobbold (2013) points out the worldwide localities and stratigraphic ages of hostrock for bed-parallel fractures filled with fibrous calcite and other minerals including quartz and gypsum. Based on these previous studies and my observations from this study, fibrous and non-fibrous calcite are both found in bed-parallel fractures at the same locality. According to Cobbold (2012), calcite beef (110 localities) is common in organic-rich shale of marine-carbonate origin, especially of (1) Cambrian-Ordovician, (2) Devonian-Carboniferous, (3) early Jurassic, or (4) Cretaceous to Paleogene ages. Gypsum beef (30 localities) is common in evaporitic or lacustrine strata of continental origin, especially of Triassic or Neogene ages. Quartz beef (17 localities) is common within meta-turbidite sequences, especially of Ordovician or Proterozoic ages. Bed-parallel fractures filled with multiple phases or cements are also common. Cobbold (2013) states that periods of abundant carbonate production on Earth,

as a result of a warm climate or abundant carbon dioxide in the atmosphere, correlates with high abundance of bed-parallel fractures.

Lang et al. (1923) and Rodrigues et al. (2009) reported the best evidence for fibers of beef appearing to have grown vertically, or nearly so, during progressive opening of the veins. According to them, the best evidence probably comes from split fossils. The shells lie along the median plane of a vein, and their impressions are visible at the upper and lower surfaces. Taber (1918), Durney and Ramsay (1973) and Ramsay (1980) proposed that opening and infilling occurred episodically and fibers have grown incrementally, partly or completely tracking the history of relative displacement of the walls. Ramsay (1980) termed episodic opening and sealing the crack-seal mechanism. In other examples, growth appears to have been more continuous (Taber, 1918; Durney and Ramsay, 1973; Means and Li, 2001). Bons and Jessell (1997) state that fibrous mineral growth may not have occurred during the opening of a vein, but in response to concentration gradients. There has been an inconsistent interpretation of the depth of formation, ranging from a few 10s of meters to several kilometers. (Rodrigues et al., 2009).

Another question that has been frequently discussed is whether the opening of a beef vein is due to an internal agent, such as pore fluid pressure and force of crystallization, or to an external agent, such as tectonic stress. Theoretical and experimental evidence published by Taber (1916), Means and Li (2001), Keulen et al. (2001), and Gratier et al. (2012) supports the idea that force of crystallization can make a great contribution. According to Keulen et al. (2001), pressure of crystallization can be as much as 11 MPa, equivalent to the vertical stress resulting from an overburden of 450-

600 m. Cosgrove (1995, 2001) and Lash and Engelder (2005) favor the idea that the hostrock heterogeneity, where beds are weaker parallel to bedding, and horizontal stress play the most important role. Cobbold and Rodrigues (2007) state that the vertical gradient of overpressure can trigger the fracturing. Swarbrick et al. (2002) proposed a mechanism that combines both mechanical compaction and hydrocarbon generation. A study by Aydin et al. (2014) on Marcellus black shale supports this combined mechanism. During foreland deformation, a correlation among slip surfaces that are common in the Marcellus, and organic carbon content suggests that pore pressure during maturation is important in initiating opening or slipping within the shale. Aydin et al. (2014) conclude that thermal maturation provides a mechanism for continually renewing pore pressure despite leakage during faulting, and is the source of the low effective stress, during foreland deformation. A recent study by Maher et al. (2016) proposes a mechanism on how beef mineralization is associated with growth faulting and shale diagenesis. The local fault-related stresses substantially changed during shallow diagenesis and lithification. This evolution contributed to changing pore pressures, seepage forces and material moduli. Maher et al. (2016) contend that the calcite mineralization tracks the very significant changes in mechanical properties and stress states that occur during synlithification deformation at very shallow crustal levels. This question will be explored more fully in the discussion chapter of this thesis.

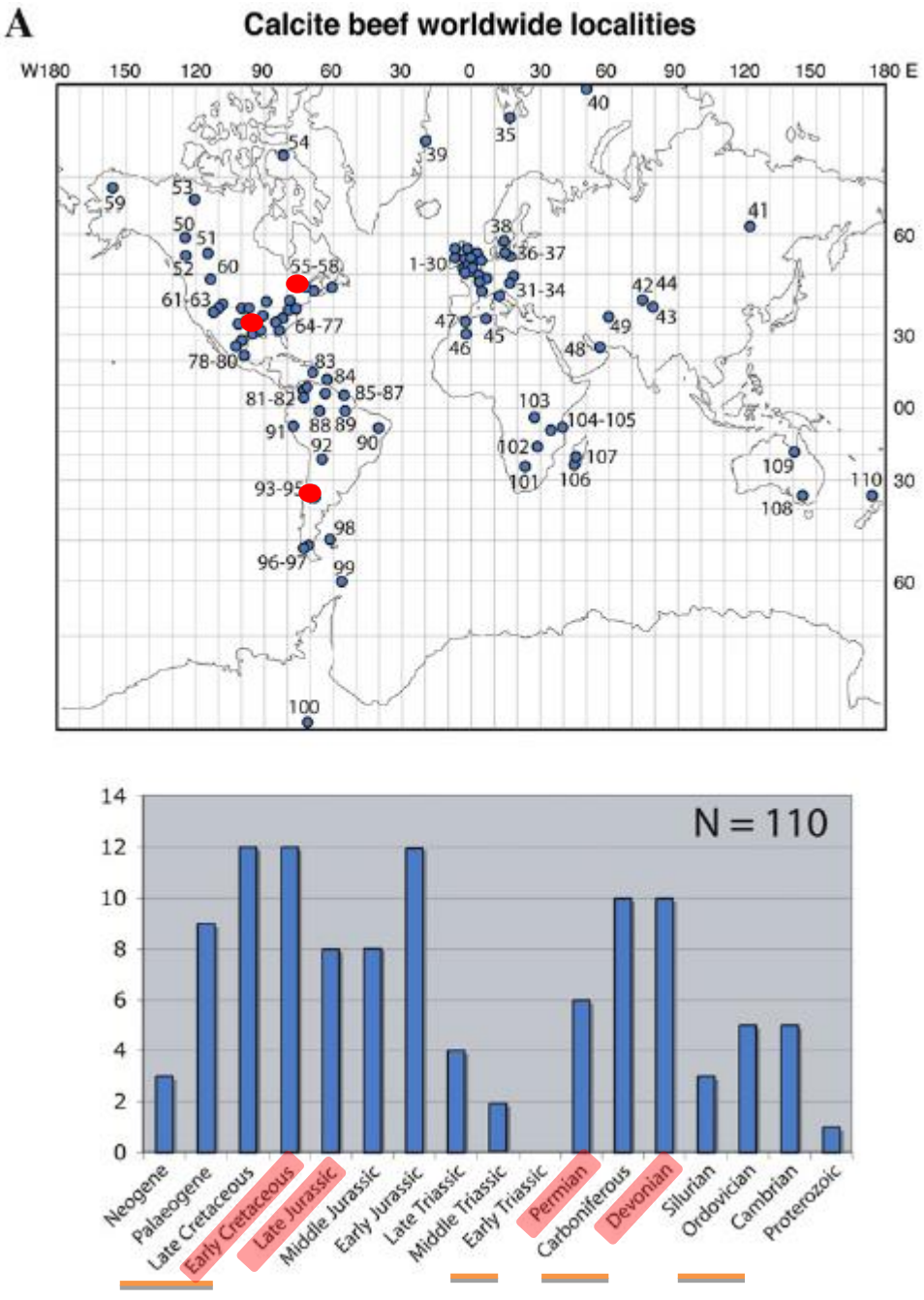
A
Calcite beef worldwide localities
W180
150
120
90
60
30
0
30
60
90
120
150
180 E
60
30
00
30
60
N = 110
14
12
10
8
6
4
2
0
Neogene
Palaeogene
Late Cretaceous
Early Cretaceous
Late Jurassic
Middle Jurassic
Early Jurassic
Late Triassic
Middle Triassic
Early Triassic
Permian
Carboniferous
Devonian
Silurian
Ordovician
Cambrian
Proterozoic

Figure 1-3 A)

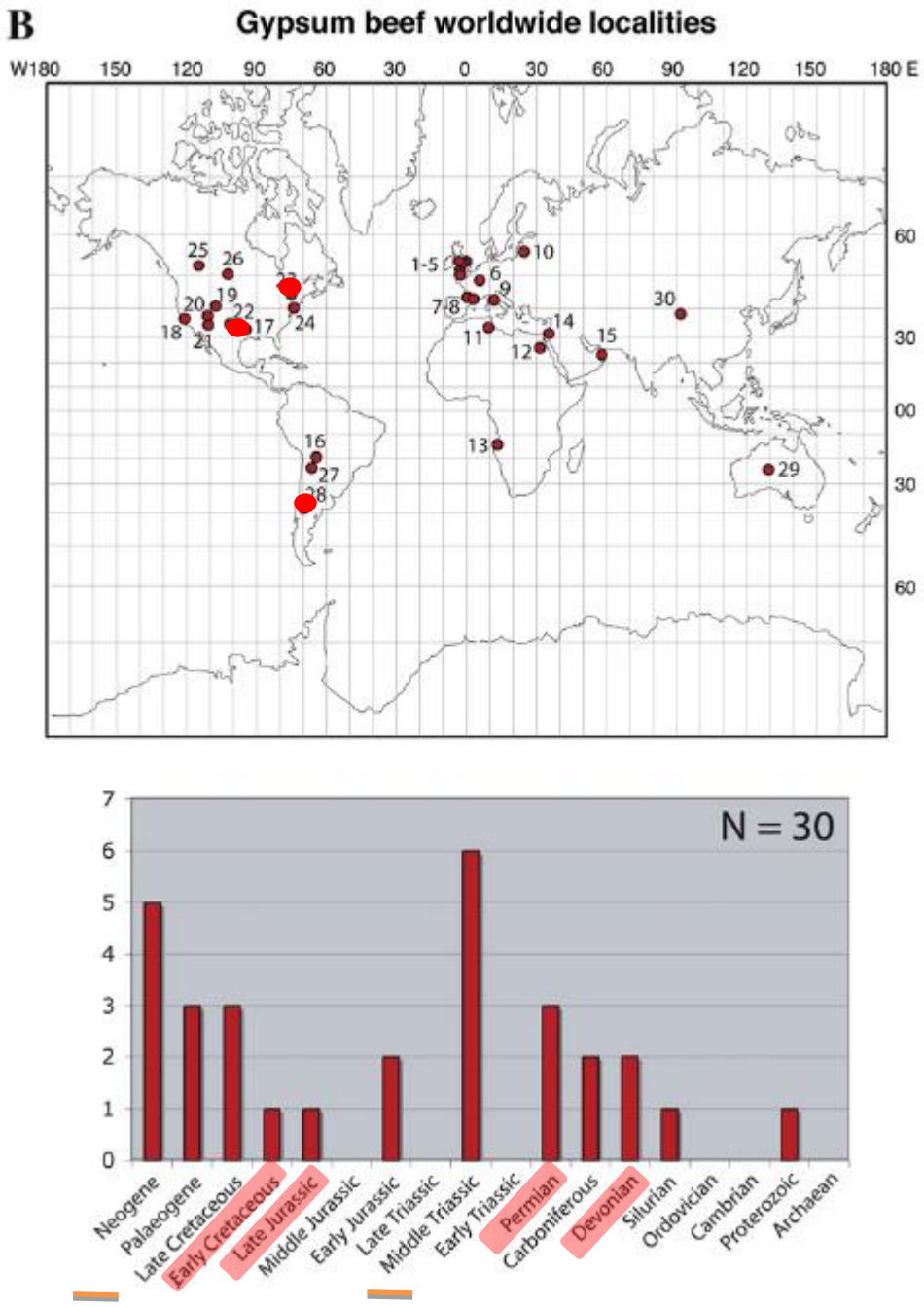
B
Gypsum beef worldwide localities
W180 150 120 90 60 30 0 30 60 90 120 150 180 E
60
30
00
30
60
1-5
6
7-8
9
10
11
12
13
14
15
16
17
18
19
20
21
22
24
25
26
27
28
29
30
N = 30
7
6
5
4
3
2
1
0
Neogene
Palaeogene
Late Cretaceous
Early Cretaceous
Late Jurassic
Middle Jurassic
Early Jurassic
Late Triassic
Middle Triassic
Early Triassic
Permian
Carboniferous
Devonian
Silurian
Ordovician
Cambrian
Proterozoic
Archaean

Figure 1-3 B)

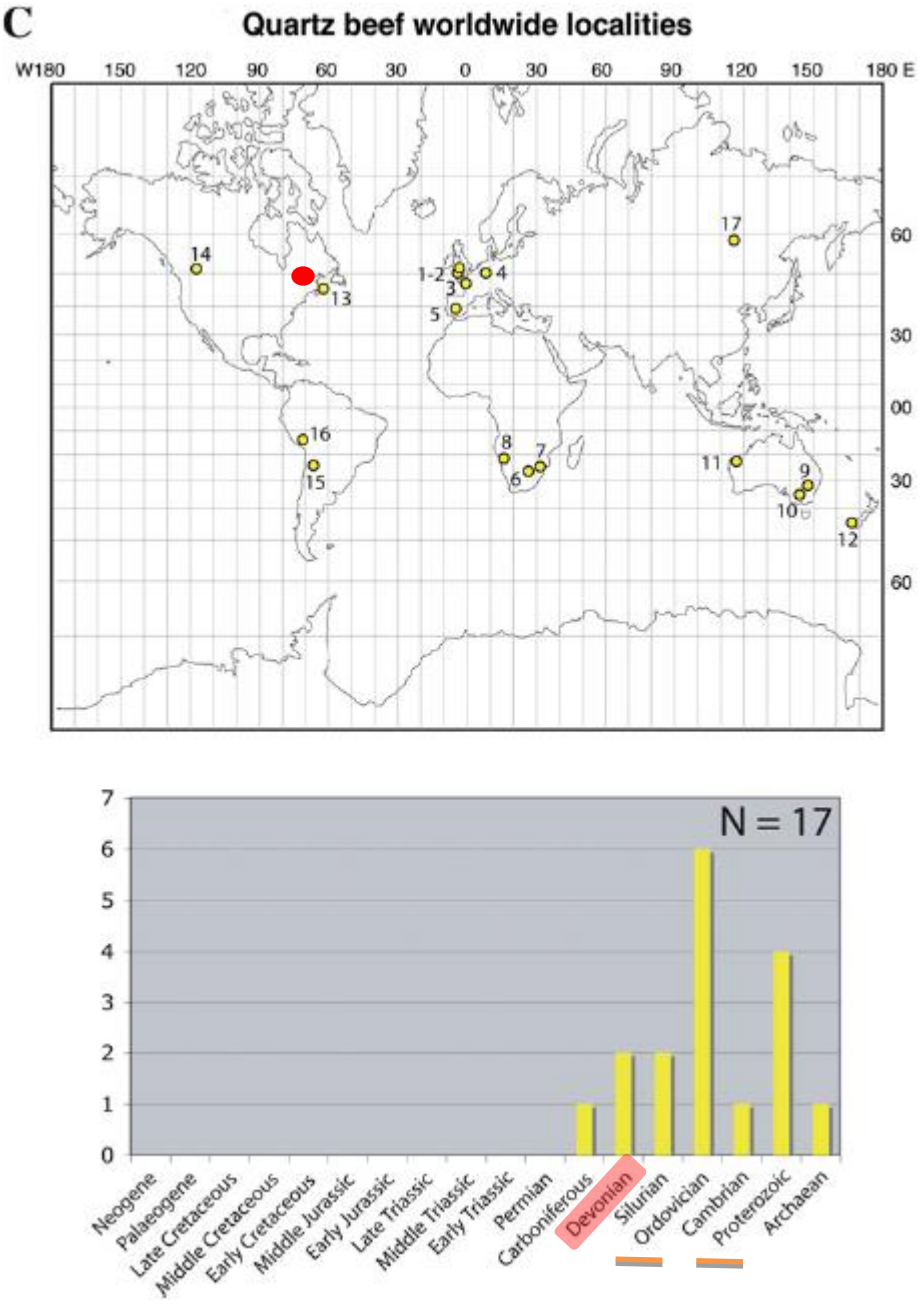

Figure 1-3 Worldwide localities (top) and histograms of stratigraphic ages of host rocks (bottom) for calcite beef (A), gypsum beef (B) and quartz beef (C). Numbers on maps refer to localities in Table 1, Cobbold et al., 2013. Locations are approximate. On histograms, beef rich shales (marked by orange bars) are: (1) Cambrian-Ordovician, (2)

Devonian-Carboniferous, (3) early Jurassic, or (4) Cretaceous to Palaeogene ages for calcite beef; Middle Triassic or Neogene, for gypsum beef; and Proterozoic or Ordovician for quartz beef. Localities of the beef studied in this work, and the ages of their hostrock are marked in red on the maps and histograms. From Figure 2, Cobbold et al., 2013.

1.2 Problem and Objectives

A comprehensive and systematic characterization of natural fractures is required in order to have a better understanding of how they may impact hydraulic fracture treatments or may control fluid flow in shale hydrocarbon reservoirs. Existing publications focus on characterizing vertical fractures (Gale et al., 2007; Gale et al., 2014 for review; Kim et al., 2015;). Publications on bed-parallel fractures are mostly based on outcrop studies in Europe and South America (Rodrigues et al., 2009; Maher et al., 2016), and describe the occurrence of this type of fracture mainly. Systematic size and spatial distribution data have not been presented in published works. However, bed-parallel fractures also likely contribute to the overall fracture network and therefore a more systematic study of them is needed.

The objective of this study is to characterize the bed-parallel fractures in three shale reservoirs; the Vaca Muerta Formation, Marcellus Formation, and Wolfcamp Formation. To achieve this, the morphology of bed-parallel fractures, their cement texture and composition are described and documented. Fracture sizes are analyzed systematically. I chose to focus on aperture data because, considering the geometry of outcrops, vertical cores and the bed-parallel fractures, the configuration means that aperture data sets are more complete. Large numbers of aperture size data collected along vertical scanlines at outcrops and from cores make bed-parallel fracture population size distribution analysis possible.

I tested several hypotheses regarding bed-parallel aperture-size distributions: 1) the aperture-size distribution may follow a power law as is common for vertical fractures or 2) they may follow a different function such as an exponential. There are also other possibilities such as the fractures may tend to have preferred sizes, or their sizes may not follow any function at all.

The location of bed-parallel fractures in the stratigraphy and any association with particular lithology is also important. Hypotheses regarding bed-parallel fracture location include: 1) Bed-parallel fractures may be more intense in organic rich layers or 2) they may form preferentially along mechanical interfaces.

1.3 GEOLOGICAL SETTING

1.3.1 Vaca Muerta Formation, Neuquén Basin

The Neuquén Basin (Figure 1-4) lies entirely onshore in western Argentina. Its western boundary is formed by frontal thrusting of the Andean range (Vergani et al., 1995). The basin's southern and eastern boundaries are at the onlapping or erosion limits of the prospective Jurassic to Cretaceous section. The basin was initiated as an intra-continental rift in Permo-Triassic times, when volcanics and vocanoclastic sediments of the Choiyoi Group were deposited unconformably over metamorphic basement (Vergani et al., 1995; Zapata et al., 2005; Howell et al., 2005). In the late Jurassic, these strata were laid down in lakes and alluvial fans (Vergani et al., 1995).

The Jurassic-Cretaceous post-rift succession was deposited in an embayment of the ocean that lay to the west. Five transgressive-regressive cycles are recognized, all of which are economically significant. Within each cycle, marine mudstone in the west grade into fluvial channel and deltaic sandstones toward the eastern and southern limit of

the basin; the Choiyoi Group is considered the provenance. Minor limestones are deposited in the west. As the environment became more restricted later in cretaceous, widespread anhydrites were deposited and the sea finally retreated to the west. The east-west dextral wrench fault system of the Dorsal de Neuquén was active during this post-rift phase, which was otherwise tectonically quiescent (Ramos, 1978; Vergani et al., 1995; Zapata, 1999; Brissón and Veiga, 1998; Cobbold and Rossello, 2003, Rojas Vera, 2014).

From the Tertiary, Andean thrusting from the west came to dominate the basin. The thrusting was most intense in the north part of the basin, generating anticlines in a thin-skinned style. To the south of the Dorsal de Neuquén, the thrusting is replaced by gentle folding. The molasses-type deposits of the Malargue Group were shed from the rising Andean chain. Major andesitic volcanism also characterized the Tertiary history if the basin and continues to the present day (Ramos, 1978; Vergani et al., 1995; Brissón and Veiga, 1998; Zapata, 2006; Rojas Vera, 2014).

In general, Neuquén Basin structural history can be considered in three stages: (1) a Triassic to Early Jurassic pre-rift and rift stage, (2) a Late Jurassic to Cretaceous subsidence stage, and (3) a Tertiary to recent modification stage punctuated by magmatic events (Kozlowski et al., 1993; Vergani et al., 1995).

Source rocks in the basin are restricted to the post-rift unit. That includes the later Jurassic bituminous mudstones of the Vaca Muerta Formation and the Mendoza Cycle, which are exceptionally rich and widespread, and are also mature for oil over the entire basin except where it thins to the east (Figure 1-4). The age span of Vaca Muerta Formation, based on ammonite studies, is between late Lower Tithonian to Lower

Valanginian (Mitchum and Uliana, 1985; Leanza, 2012). The TOC of Vaca Muerta Formation is reported to be around 1%-8% according to several references (Findlay and Benton, 1993; Leanza, 2012). It contains a high proportion of amorphous-algal kerogen. The higher TOC values are located near the base of the unit. Coeval marine nearshore siliciclastic and carbonate rocks, and fluvial units are recorded at the southeastern and eastern basin margins, displaying clinoforms that during the time of Vaca Muerta deposition prograde and interfinger with the depocentral black shales.

Five wells, and two outcrops were studied. The field area is near the basin's depocenter (Figure 1-5) where Jurassic to upper Cretaceous sedimentary strata crop out.

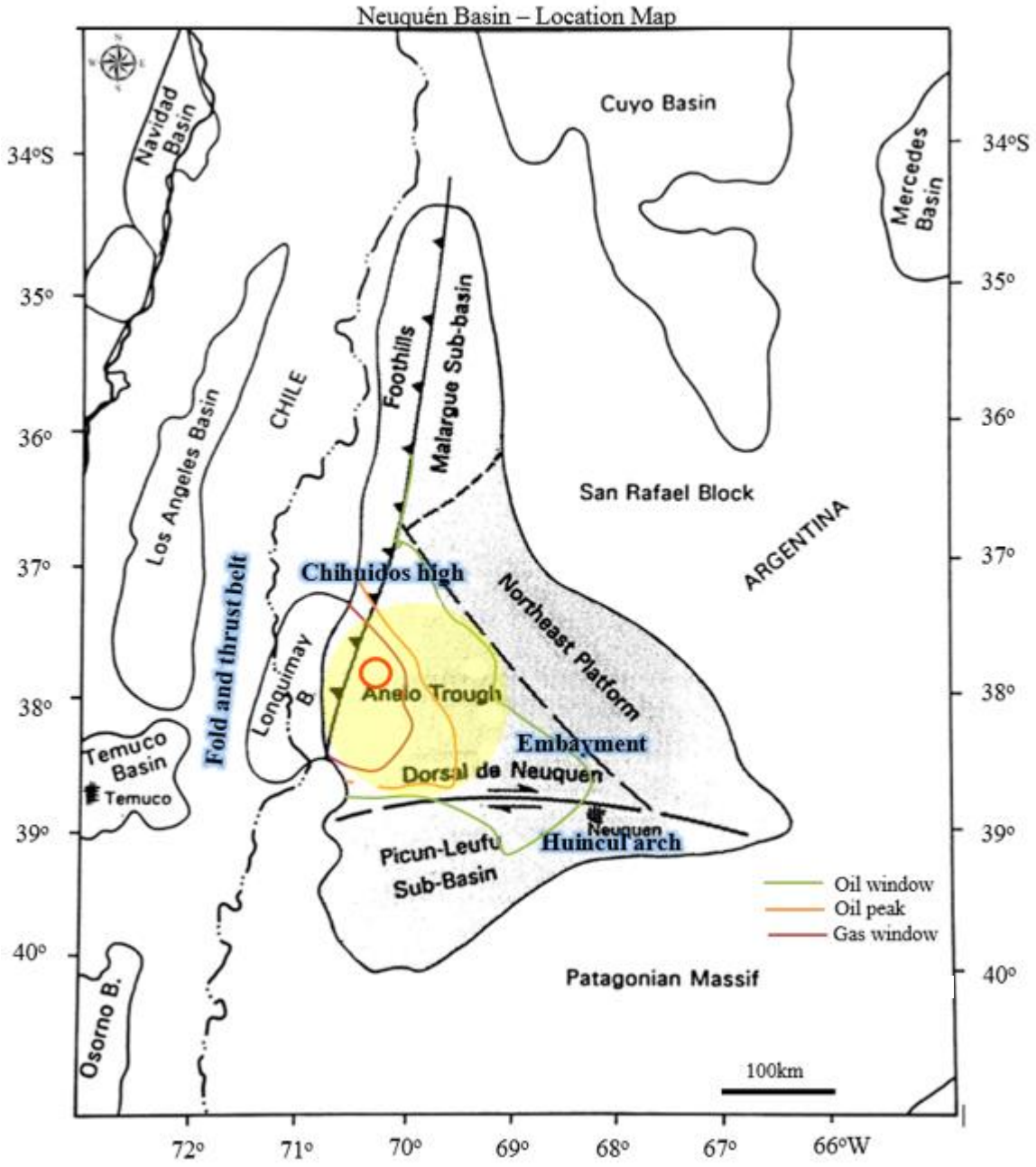

Figure 1-4 Geological provinces of Neuquén basin region. The Neuquén basin is a triangular area (solid black line). Modified from Vergani et al., 1995. Yellow shaded area indicates the approximate location of the 5 wells studied. Red circle indicates the field area. The colored lines mark the boundaries of the oil window, gas window, and the peak of oil generation projected to the ground surface.

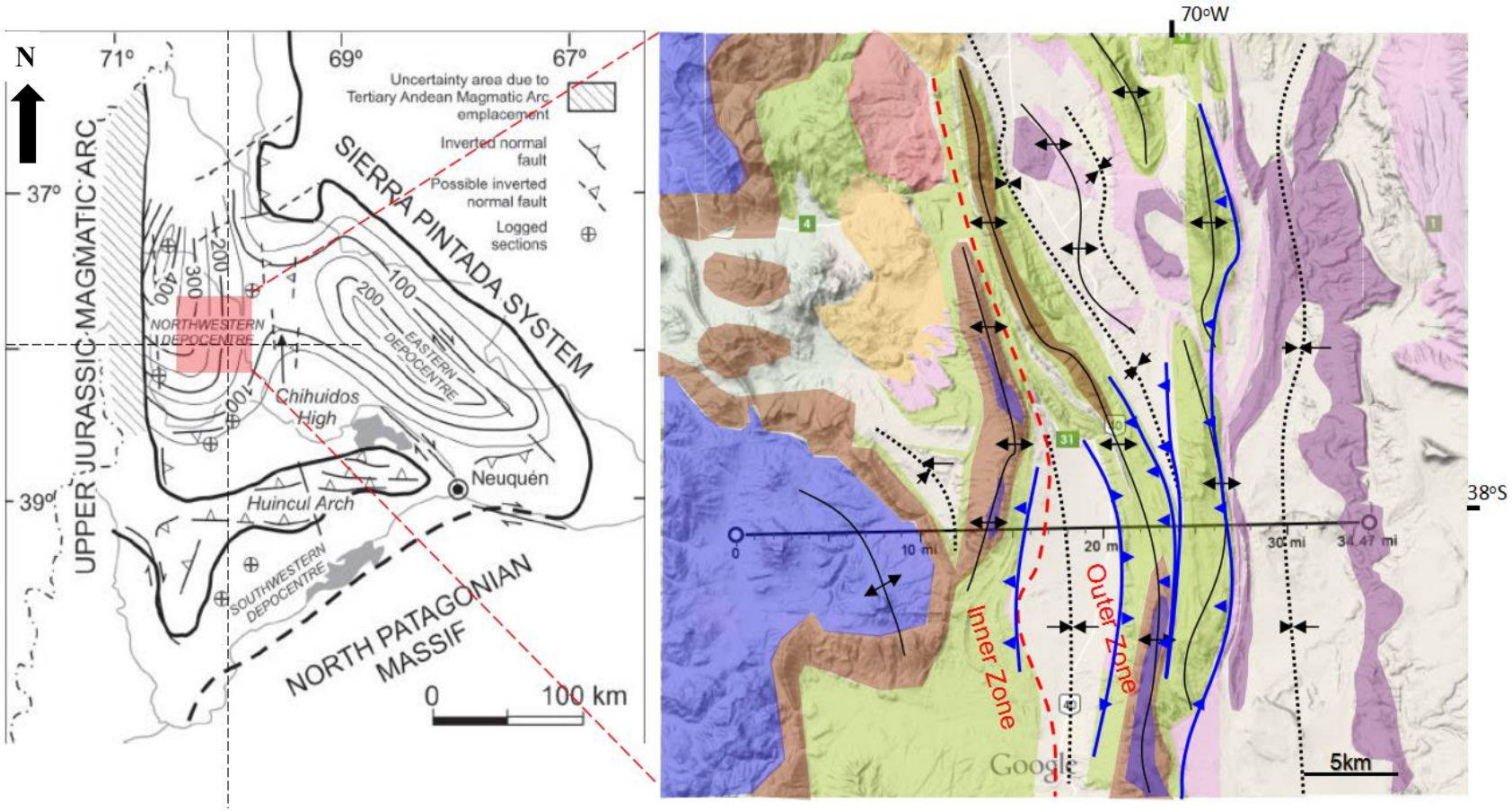

Figure 1-5 Left: Depocenters of Neuquen Basin. From Legarreta and Gulisano, 1989. Right: Geologic map of the studied field area showing the age of the rock outcrops, main fold axes and the other structures. See Figure 1-6 for color codes. (Based on Zamora et al, 2006)

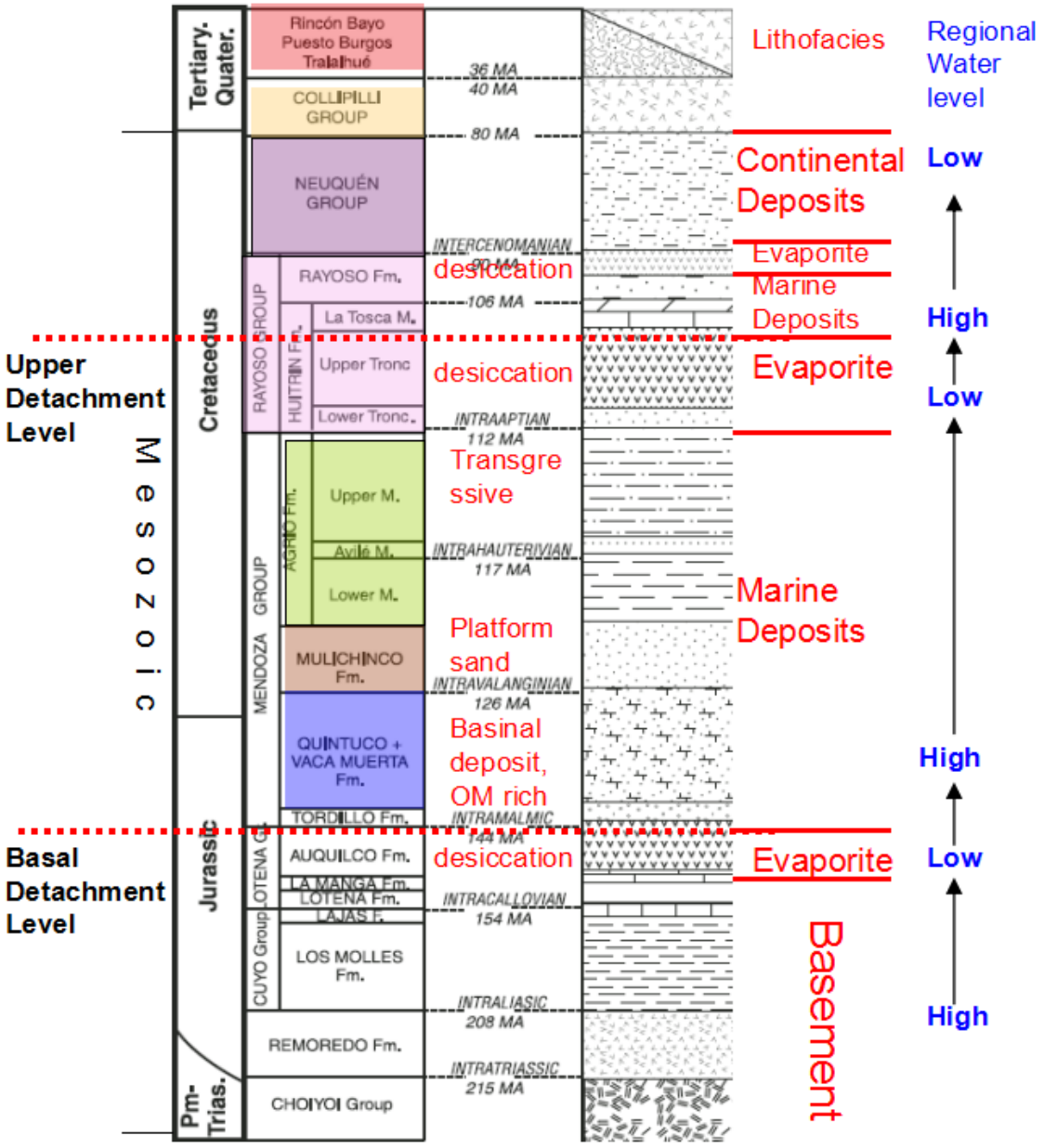

Figure 1-6 Schematic stratigraphic column showing the main stratigraphic units of the region, lithofacies, water level change and other relevant information. Modified from Brissón and Veiga (1998). Colors representing each stratigraphic unit also apply to Figure 1-5.

1.3.2 Marcellus Formation, Appalachian Basin

The Appalachian Basin is a multistage retroarc foreland basin that formed over approximately 220 million years in response to tectonic loading during four nearly continuous orogenies on the eastern margin of Laurentia (Ettensohn, 2008). From the Precambrian to the Permian, the Appalachian Basin has been through at least four cycles of continent and oceanic crustal collision, compression, mountain building and basin infill.

The breakup of Rodinia established the curving east coast of Laurentia with alternating embayments and promontories. These promontories served to localize shortening and deformation (Figure 1-7). They went through greater compression which led to greater flexural subsidence, and formed four major depocenters (Ettensohn, 1985, 1994, 2008; Ferrill and Thomas, 1988; Lash and Engelder, 2011; Lavoie, 2008).

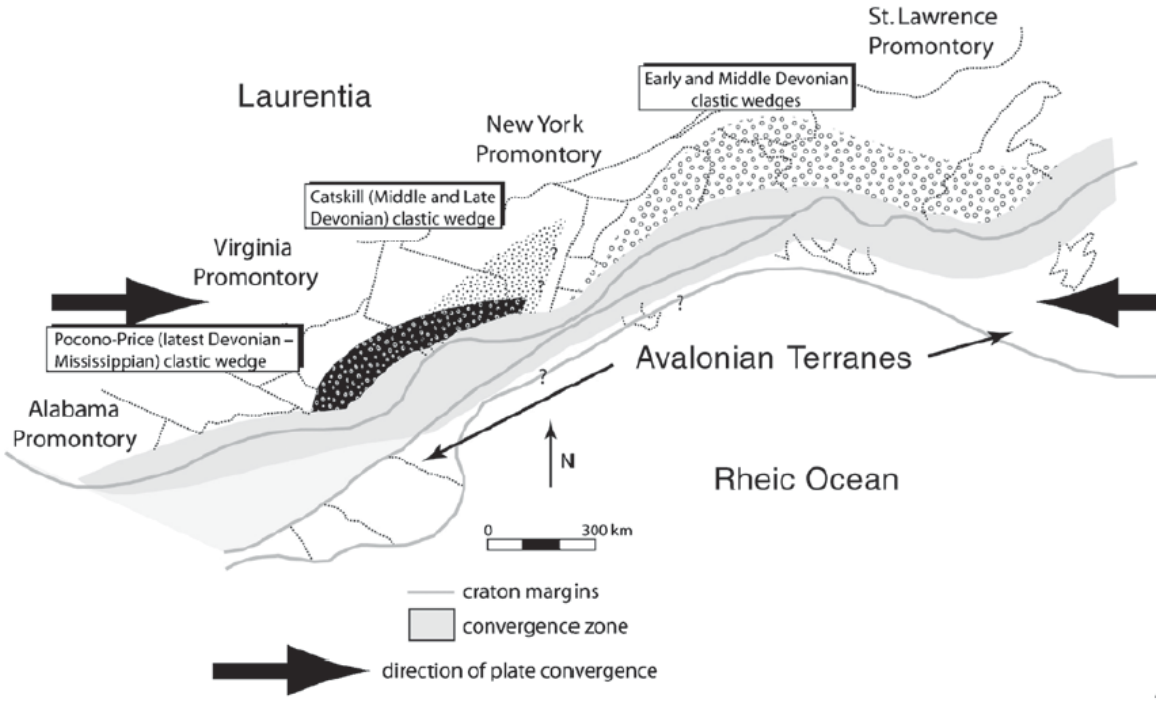

Figure 1-7 Promontories of Laurentia causing localized shortening and deformation. The gray shaded areas on the map are the depocenters generated. (Ettensohn, 1994; Ferrill and Thomas, 1988; Lash and Engelder, 2011).

The tectonic development of the Appalachian Basin can be separated into four phases. As compiled in Table 1-1.

Table 1-1 A summary of the tectonic phases and related depositional facies of Appalachian Basin. Modified from Lavoie, 2008 and Pommer, 2013.

Phase 1	**Phase 1**	**Phase 2**	**Phase 3**	**Phase 4**
Taconic Orogeny	Salinic Disturbance	Acadian Orogeny	Carboniferous Appalachian Basin	Alleghenian
Ordovician-Silurian	Silurian	Devonian	Mississippian-Pennsylvanian	Permian
Collision: Microcontinent, Magmatics arcs, Accretionary prisms	Onset: Acadian deformation	Collision: Laurentia and Avalon terrane	Quiescence: Deposit of coals	Collision: Gondwana and Laurentia
Fluvial, lacustrine, deep water and delta complex	Carbonates	Volcanic ash beds, delta complexes, carbonate sediments	Alluvial, deltaic, estuarine, and marine facies.	Deep marine facies interbedded with fluvial detritus. Thick coal bed.

The Marcellus Formation is a black, organic rich shale, deposited approximately 350 million years ago during Middle Devonian in a shallow inland seaway where the Appalachian Mountains now stand (Ettensohn, 2008; Faill, 1997). The Marcellus Formation was deposited during the onset of the Acadian orogeny, above the Onondaga

limestone. It has been hypothesized that pulses of mountain building during the Acadian created a rain shadow effect on the basin, with westerly winds unable to carry precipitation over the high mountains. This allowed fine-grained sediment to blanket the restricted basin, where it was preserved due to dysoxic or anoxic conditions on the basin floor (Ettensohn, 2008; Fichter et al., 2010). The formation extends across Southern New York into Pennsylvania, Western Maryland, Eastern Ohio West Virginia, a small portion of Kentucky and Tennessee, and into southern Ontario, Canada (Figure 1-9). The formations above the Marcellus are illustrated by figure 1-8 including their lithofacies. Marcellus and the Middle and Upper Devonian rocks above it form the Devonian Clastic Wedge. The eastern portion of the wedge is composed of fine-grained, organic-rich black shale with interbedded gray shales that contain less organic material. The western sediments are sandstone, siltstone, and shale (Harper and Kostelnik, 2010; Potter et al., 1980).

Three cores, from northeast Pennsylvania in through the Marcellus Formation are included in this thesis study.

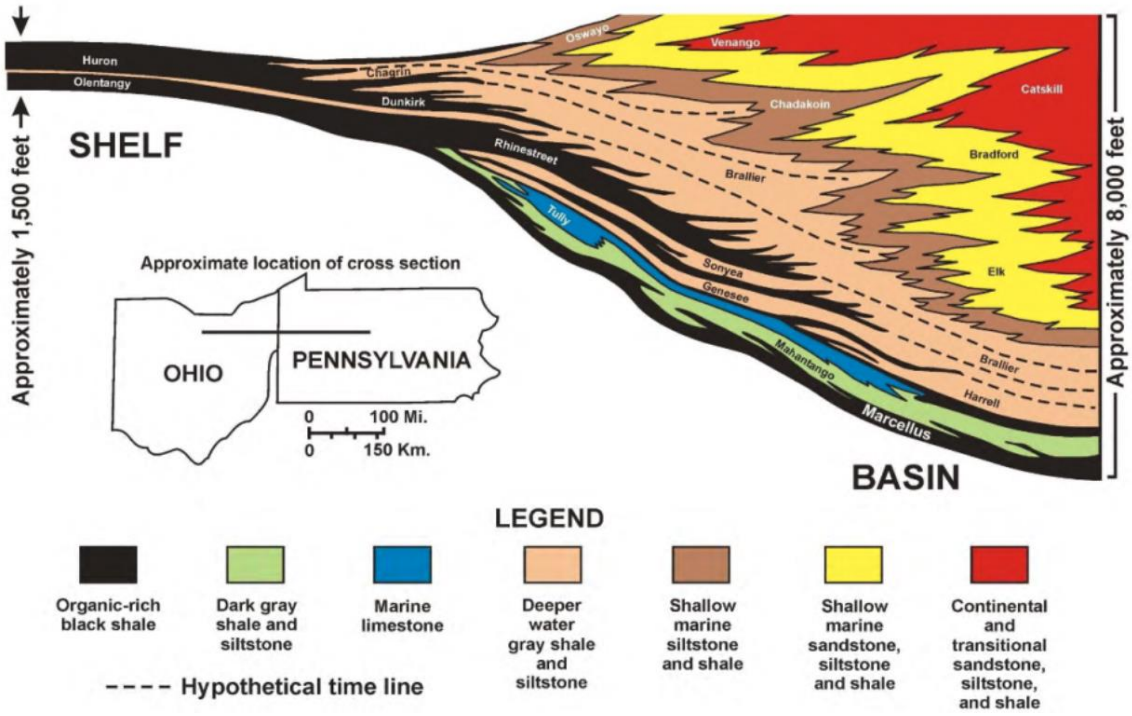

Figure 1-8 An east-west cross-section of The Devonian Clastic Wedge in the Appalachian Basin (from Harper and Kostelnik, 2010).

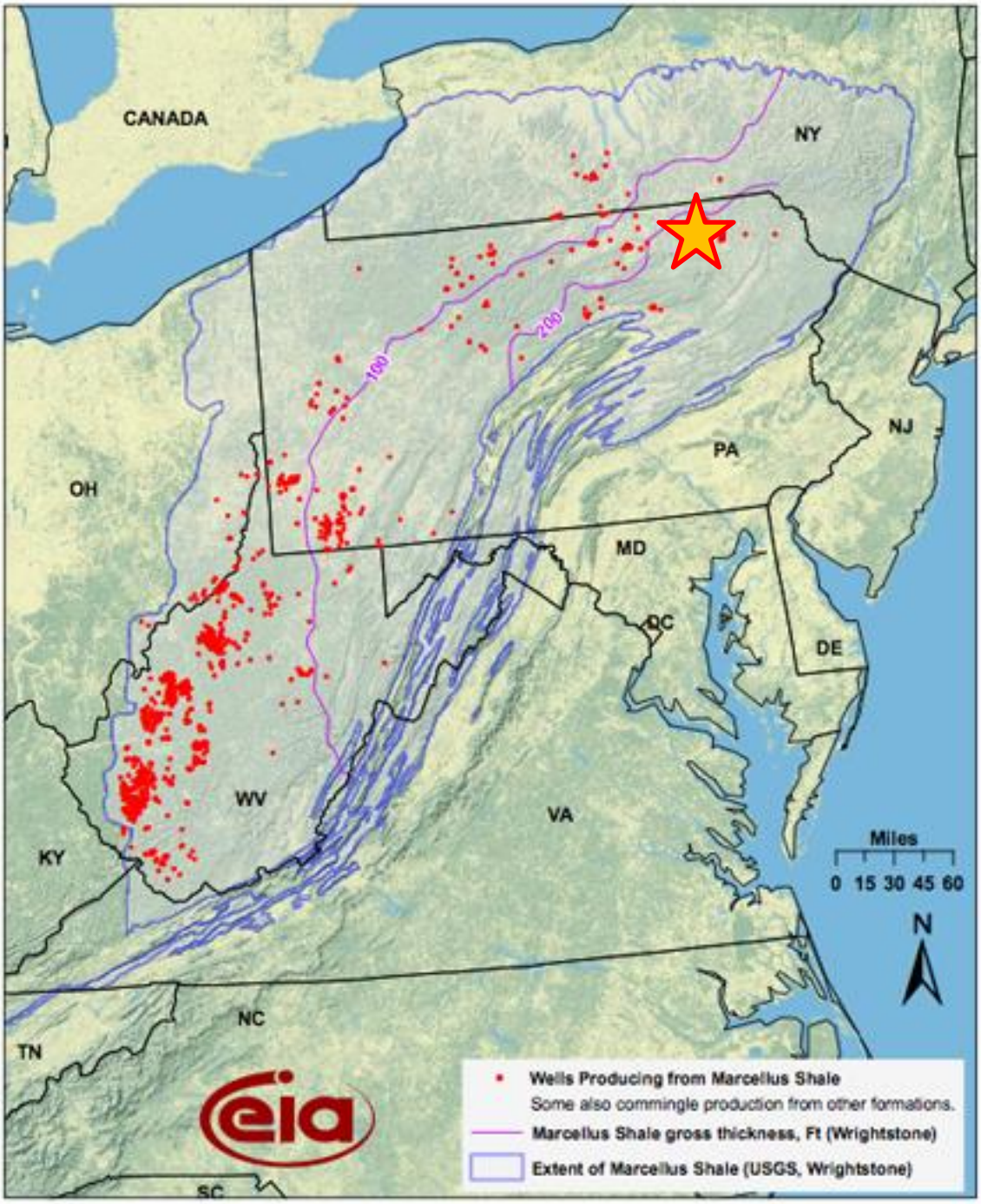

Figure 1-9 Areal extent, gross thickness and producing wells of the Marcellus Shale from US Energy Information Administration. The star indicates the approximate location of the studied wells.

1.3.3 Wolfcamp Formation, Permian Basin

The Greater Permian Basin (GPB) is one of the largest and most structurally complex regions in North America. This sedimentary basin can be divided into several sub-basins and platforms. It covers an area about 250 miles wide and 300 miles long in 52 counties in west Texas and southeast New Mexico. It contains one of the world's thickest deposits of Permian-aged rocks, and was named after the period of geologic time (Permian: 299 million to 251 million years ago) where the basin reached its maximum depth of 29,000 feet (Galley, 1958; Silver, 1969).

The evolution of the basin can be attributed to three distinct phases: (1) mass deposition (2) continental collision (3) basin filling. Before the Permian Basin was formed, this region was a broad marine area called the Tobosa Basin (Adams, 1965; Hills, 1984). During the Cambrian to Mississippian periods (541 to 323 million years ago), massive amounts of clastic sediments were deposited in this area causing it to form a depression. The basin we see today began forming in late Mississippian and early Pennsylvanian (323 to 299 million years ago) when the supercontinents Laurasia and Gondwana collided to form Pangea causing faulting and uplift. The area was covered by a seaway, and episodes of faulting, uplift, and erosion associated with the Marathon-Ouachita Orogeny as well as different rates of subsidence caused structural deformations in the Tobosa Basin that divided it into sub-basins and platforms (Ross, 1962; Adams, 1965; Hills, 1984) (Figure 1-11). The final process that created the GPB was the filling of the sub-basins with sediments. The Midland Basin, Central Basin Platform, and the Delaware basin are the three main components of the GPB that we know today (Cheney, 1940; Galley 1958; Ross, 1962).

Figure 1-10 Paleographic time sequence, from youngest to the oldest, of the evolution of the Greater Permian Basin, based on Leslie Sutton, 2014 post on Drillinginfo.com. Extracted from Deep Time Maps™ Paleogeography.

The Permian age Wolfcamp formation is an oil and gas zone found throughout the Permian Basin. The formation takes its name from the Wolfcampian epoch during which it was deposited. The Wolfcamp formation occurs at a vertical depth of 5,500-10,000 ft, with a thickness of 600-1,100 ft. It has 4%-12% porosity. Wolfcamp Formation is mostly shale, varying from almost black to gray and greenish gray. Interbedded are several layers of limestone which are cemented shell breccias, in places conglomeratic. There are also layers of calcareous sandstone. The Wolfcamp Formation comprises 92% shale, 6% limestone, and 2% calcareous conglomerate (Udden, 1917; Galley, 1958).

The western area of the GPB, the Delaware Basin, was a structural and topographical low that provided an inlet for marine water during most of the Permian. The topographic low creates larger accommodation space and the Delaware Basin is approximately 2,000 feet deeper than the Midland Basin. This is a leading factor in the stratigraphic discontinuities between the two sub-basins (Harrison, 1973; Jarvie, 2012). While the Wolfcamp formation is present in both the Midland Basin and the Delaware Basin, stratigraphy of the Permian aged strata above Wolfcamp formation is

fundamentally different (Figure 1-12). The Delaware basin sediments also experienced greater pressure and temperature during burial than their Midland Basin counterparts.

One core from the Wolfcamp in the Delaware Basin from Ward County was studied.

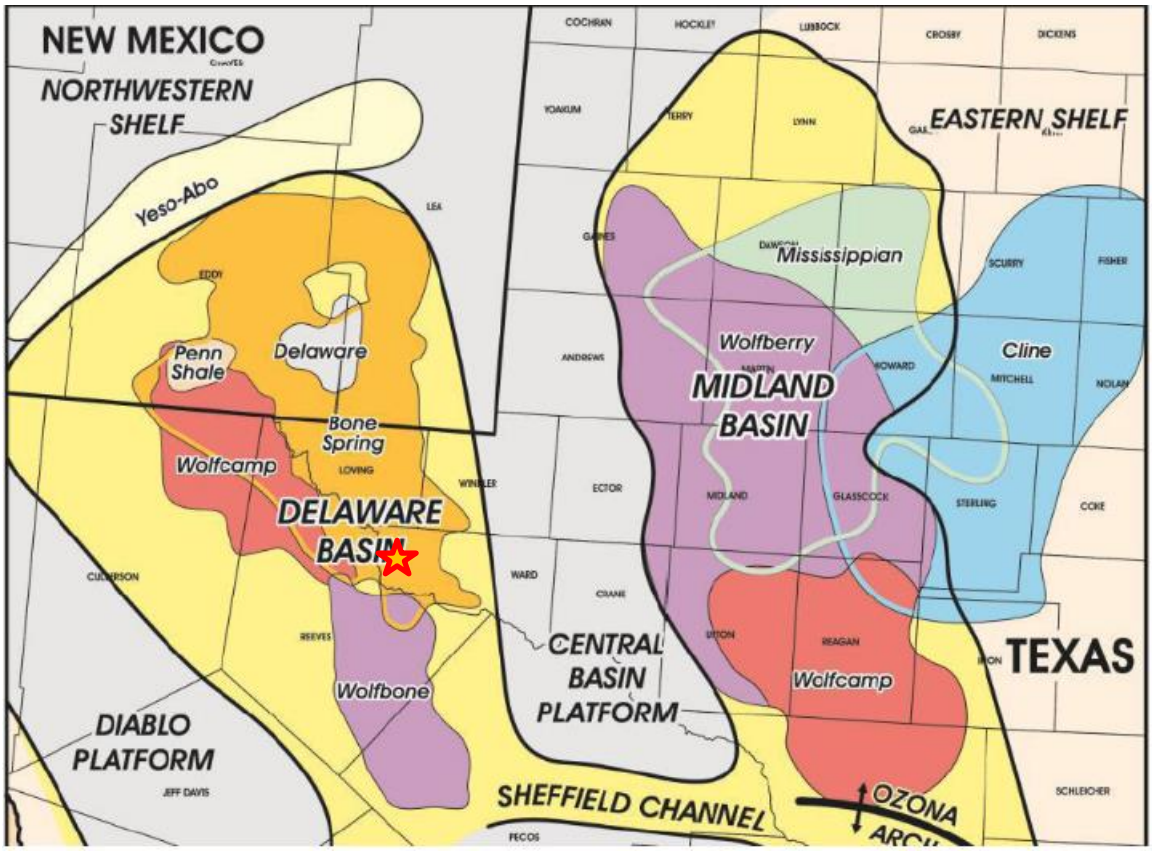

Figure 1-11 Permian Basin geological breakdown. Wolfcamp shale in red. The star indicates the approximate location of the studied well. (Source: Shale Experts, retrieved in July 2016)

Generalized stratigraphic correlation chart for the Permian Basin region

SYSTEM	SERIES/ STAGE	NORTHWEST SHELF	CENTRAL BASIN PLATFORM	MIDLAND BASIN & EASTERN SHELF	DELAWARE BASIN	VAL VERDE BASIN
PERMIAN	OCHOAN	DEWEY LAKE RUSTLER SALADO	DEWEY LAKE RUSTLER SALADO	DEWEY LAKE RUSTLER SALADO	DEWEY LAKE RUSTLER SALADO CASTILE	RUSTLER SALADO
	GUADALUPIAN	TANSILL YATES SEVEN RIVERS QUEEN GRAYBURG SAN ANDRES GLORIETA CLEAR FORK YESO WICHITA	TANSILL YATES SEVEN RIVERS QUEEN GRAYBURG SAN ANDRES GLORIETA CLEAR FORK WICHITA	TANSILL YATES SEVEN RIVERS QUEEN GRAYBURG SAN ANDRES SAN ANGELO LEONARD SPRABERRY, DEAN	DELAWARE MT GROUP BELL CANYON CHERRY CANYON BRUSHY CANYON	TANSILL YATES SEVEN RIVERS QUEEN GRAYBURG SAN ANDRES
	LEONARDIAN				BONE SPRING	LEONARD
	WOLFCAMPIAN	ABO WOLFCAMP	WOLFCAMP	WOLFCAMP	WOLFCAMP	WOLFCAMP
PENNSYLVANIAN	VIRGILIAN	CISCO	CISCO	CISCO	CISCO	CISCO
	MISSOURIAN	CANYON	CANYON	CANYON	CANYON	CANYON
	DESMOINESIAN	STRAWN	STRAWN	STRAWN	STRAWN	STRAWN
	ATOKAN	ATOKA — BEND	ATOKA — BEND	ATOKA — BEND	ATOKA — BEND	(ABSENT)
	MORROWAN	MORROW	(ABSENT)	(ABSENT ?)	MORROW	(ABSENT)
MISSISSIPPIAN	CHESTERIAN MERAMECIAN OSAGEAN KINDERHOOKIAN	CHESTER MERAMEC OSAGE KINDERHOOK WOODFORD	CHESTER MERAMEC OSAGE "BARNETT" KINDERHOOK WOODFORD	CHESTER MERAMEC OSAGE "BARNETT" KINDERHOOK WOODFORD	CHESTER MERAMEC OSAGE "BARNETT" KINDERHOOK WOODFORD	MERAMEC OSAGE "BARNETT" KINDERHOOK WOODFORD
DEVONIAN		DEVONIAN SILURIAN (UNDIFFERENTIATED)	DEVONIAN	DEVONIAN	DEVONIAN	DEVONIAN
SILURIAN			SILURIAN SHALE FUSSELMAN	SILURIAN SHALE FUSSELMAN	MIDDLE SILURIAN FUSSELMAN	MIDDLE SILURIAN FUSSELMAN
ORDOVICIAN	UPPER	MONTOYA	MONTOYA	SYLVAN MONTOYA	SYLVAN MONTOYA	SYLVAN MONTOYA
	MIDDLE	SIMPSON	SIMPSON	SIMPSON	SIMPSON	SIMPSON
	LOWER	ELLENBURGER	ELLENBURGER	ELLENBURGER	ELLENBURGER	ELLENBURGER
CAMBRIAN	UPPER	CAMBRIAN	CAMBRIAN	CAMBRIAN	CAMBRIAN	CAMBRIAN
PRECAMBRIAN						

Figure 1-12 Stratigraphy of the Permian Basin Region. From Yang and Dorobek, 1995.

Chapter 2. Bed-parallel Fractures in Core and Outcrop

I collected data from three different formations; the Vaca Muerta in the Neuquén Basin in Argentina (Figure 2.1), Marcellus in the Appalachian Basin (Fig 2.2) and the Wolfcamp in the Permian Basin, west Texas (Figure 2.3). Fracture data collected includes morphology and texture of fractures, aperture sizes, lateral extent, and vertical spacing, and where these fractures occur in the stratigraphy. Core data includes data collected from real cores and core panel scan mosaics.

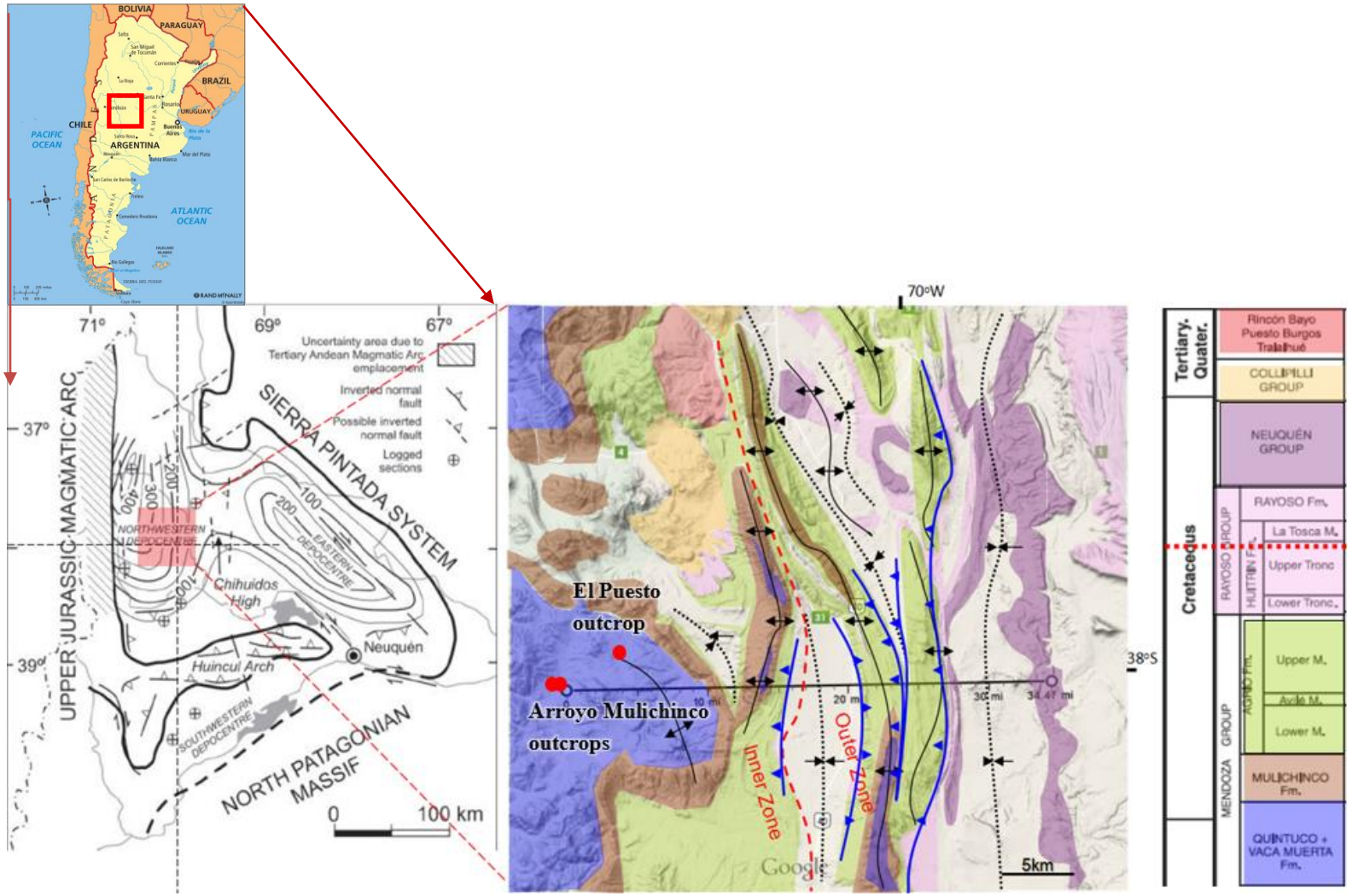

Figure 2-1 Left: Structure and depocenters of Neuquén Basin. From Legarreta and Gulisano, 1989. Right: Geologic map of the studied field region showing the rock that outcrops, main fold axes and the other structures. Three outcrops studied are marked by red dots. (Modified from Zamora et al., 2006)

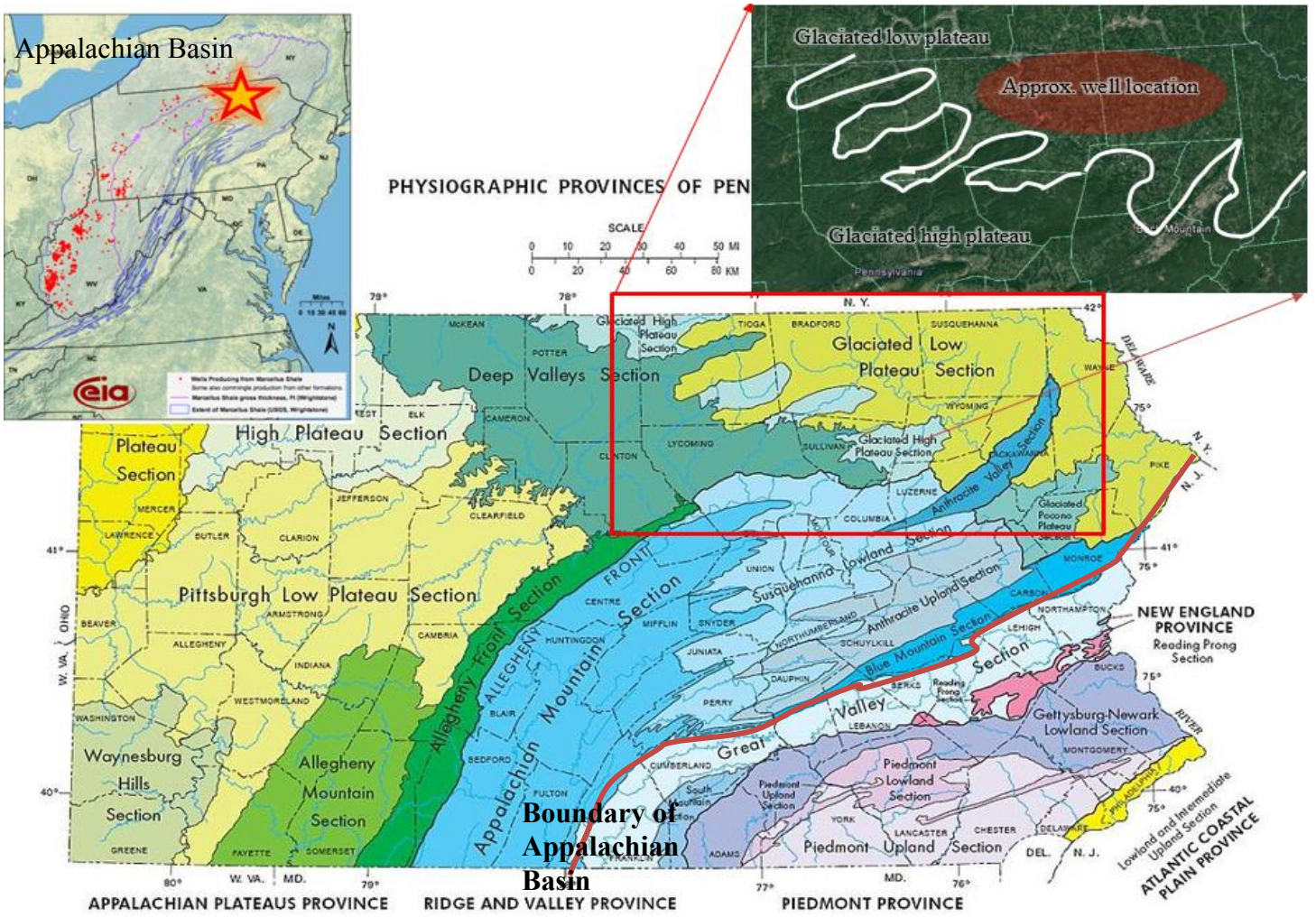

Figure 2-2 Physiographic provinces of the Appalachian Basin in Pennsylvania. Studied wells located in the glaciated low plateau in Penn. Source: US Energy Information Administration and Pennsylvania Geological Survey.

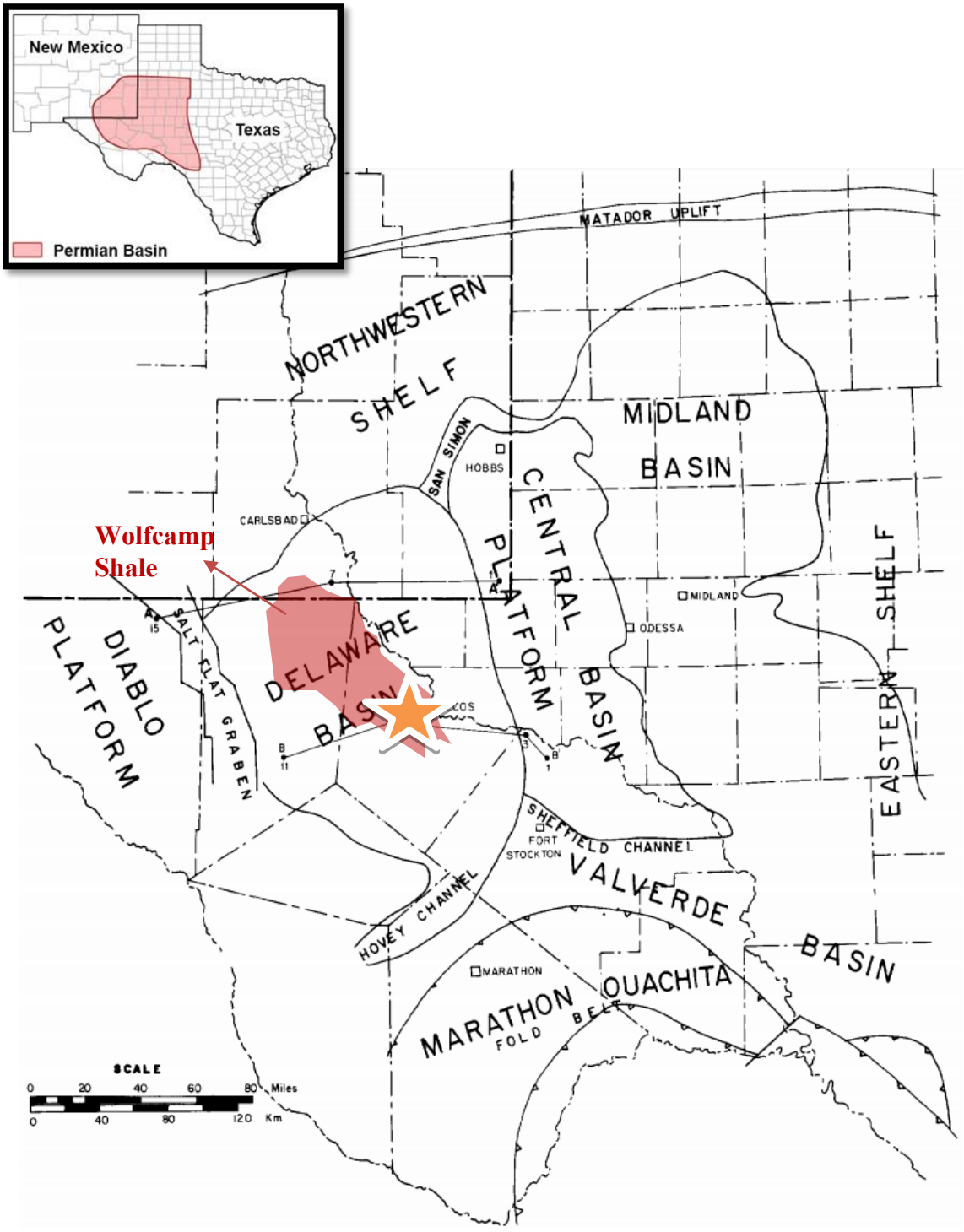

Figure 2-3 Index map showing structural provinces of Permian basin region and lines of cross sections. Red shade marks the Wolfcamp shale, yellow star indicates the approximate location of the studied well. Modified from Hills, 1984.

The studied formations and related data types collected are summarized below.

Table 2-1 Summary of studied formations and related data types collected

Studied Formation	Field Data	Core	Core Scan Images
Vaca Muerta	**Yes** (3 scanlines)	**Yes** (discontinuous core samples from 5 cores, 5 wells)	**Yes** (4 scanlines)
Marcellus	**No**	**Yes** (2 wells, continuous cores, 2 scanlines)	**No**
Wolfcamp	**No**	**Yes** (1 well, 1 continuous core, 1 scanline)	**No**

For the Vaca Muerta study I collected both outcrop and core data. The core data comprised core samples from 5 wells, and scanned images of the whole core. For the Marcellus and Wolfcamp studies I had core samples and fracture descriptions made from direct observation of the core.

The Vaca Muerta shale crops out around the northwest margin of the Neuquén Basin, Argentina (Fig. 2-1). I conducted field work at two locations informally named Arroyo Mulichinco, and El Puesto, near Loncopue, Neuquén in March, 2015, assisted by Dr. Julia Gale, and YPF geologists and geophysicists. We made general observations about the nature of the shale host rock and the fractures within it, including taking measurements of fracture attributes along vertical linear traverses (scan-lines). Fracture aperture, spacing, orientation, morphology, composition and texture of fracture fill, were recorded for each studied outcrop.

The objective of studying fractures in the field was to evaluate the possibility of using them as a guide for reservoir characterization. The rock at outcropped Vaca Muerta field area is most comparable to the Vaca Muerta #1 well. Bed-parallel fractures were

collected from core samples in all three studied formations, in order to characterize bed-parallel fractures in the subsurface. To accomplish this, cores were examined together with well-logs where available.

2.1 DATA COLLECTING PROCEDURE

The scanline method for collecting fracture data in outcrop and core is similar in approach but differs in detail. The procedures are explained in the following sections.

2.1.1 Fieldwork Methodology

Field scanline data and samples were collected from Vaca Muerta outcrops at Arroyo Mulichinco (38°01'16" S, 70°27'45" W) and El Puesto (~37º58'41" S, 70º21'42" W) locations. A total of three scanlines were set. Two scanline datasets were collected at Arroyo Mulichinco outcrop; these captured 142 bed-parallel fractures within a total scanline length of 31.04 m. The other dataset collected from the El Puesto outcrop, captured 30 bed-parallel fractures within a total scanline length of 48.46 m. The essential fracture documentation technique of this study was to measure fracture attributes along linear traverses, which are usually called scanlines. In order to collect systematic datasets, I used a measured section technique (vertical scan lines constructed normal to bedding) to capture all fractures in the section.

Fracture aperture, spacing, orientation, morphology, composition and texture of fracture fill, were recorded for bedding-parallel fractures at each place where they intersect the scanline. Mechanical-layer thicknesses of beds, lithology of the host rock and occurrence of concretions, cross-cutting relationships with vertical fractures and outcrop-scale structures including gentle folds and faults were also recorded.

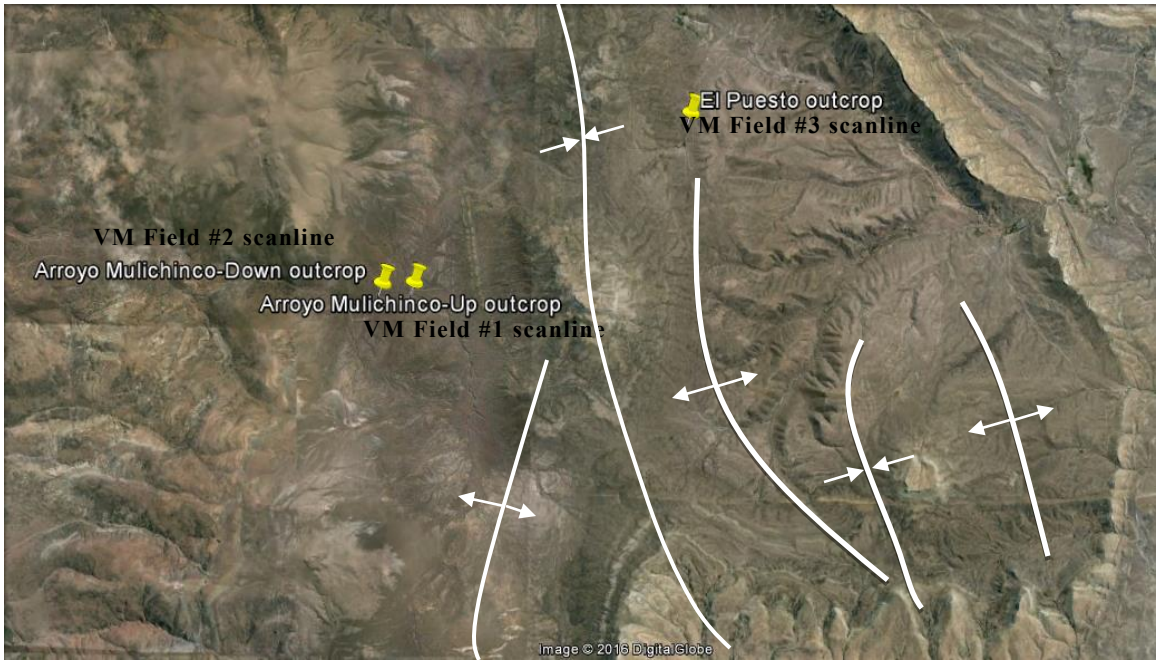

Figure 2-4 Satellite image of the field area with outcrop/scanlines locations. (Image from Google Earth, 2016)

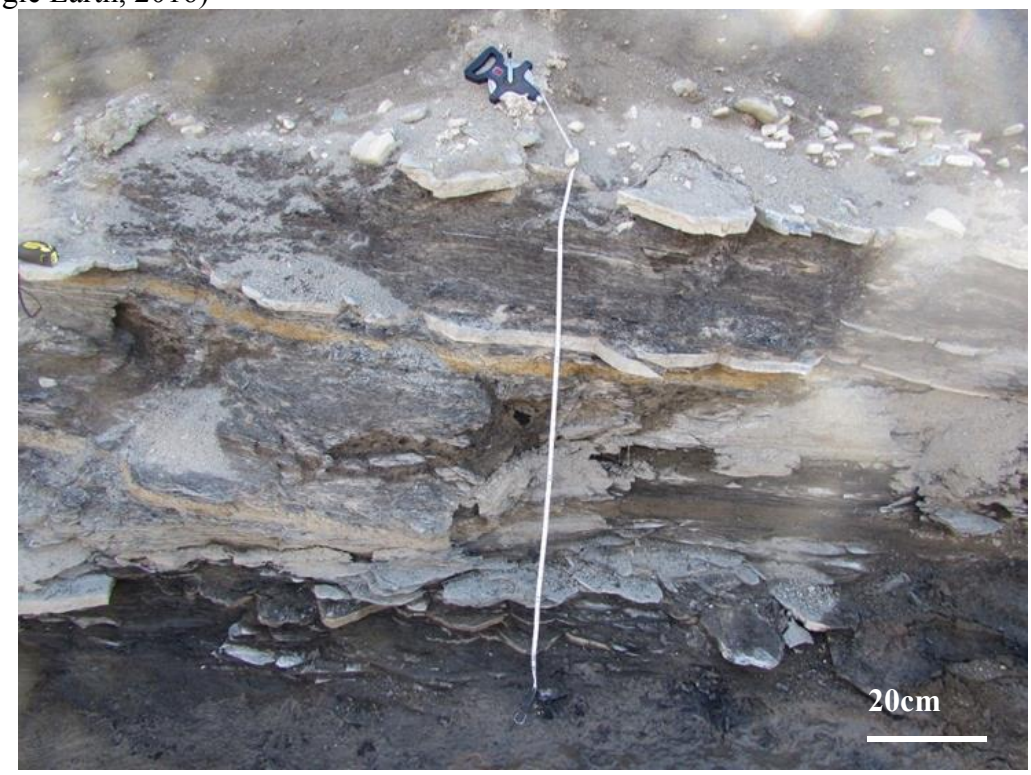

Figure 2-5 Vertical scanline setup for collection of outcrop fracture data. Each mineral cement-filled fracture is recorded where it intercepts a 1D scan line, marked by a

measuring tape was recorded. The line is constructed perpendicular to the bed-parallel fractures.

Figure 2-6 Bedding and bed-parallel fracture strike and dip were measured using a Brunton compass.

Sections were chosen from the best exposed outcrops such that the longest continuous measured section could be examined. Using a logarithmically scaled comparator, I measured the kinematic aperture for each bed-parallel fracture. The kinematic aperture is the entire opening displacement irrespective of fracture fill, at the point where the vertical scanline intersected the fracture. Using this tool with a hand lens allows documentation of fracture apertures as small as 0.05 mm (0.002 in.) on sufficiently exposed outcrops in the field (Ortega et al., 2006) (Figure 2-7). Fractures thicker than 5 mm are measured by a standard ruler. Accurate aperture measurement of these fractures is possible because they are filled by calcite cement, which gives them good visual contrast relative to the dark shale host rock.

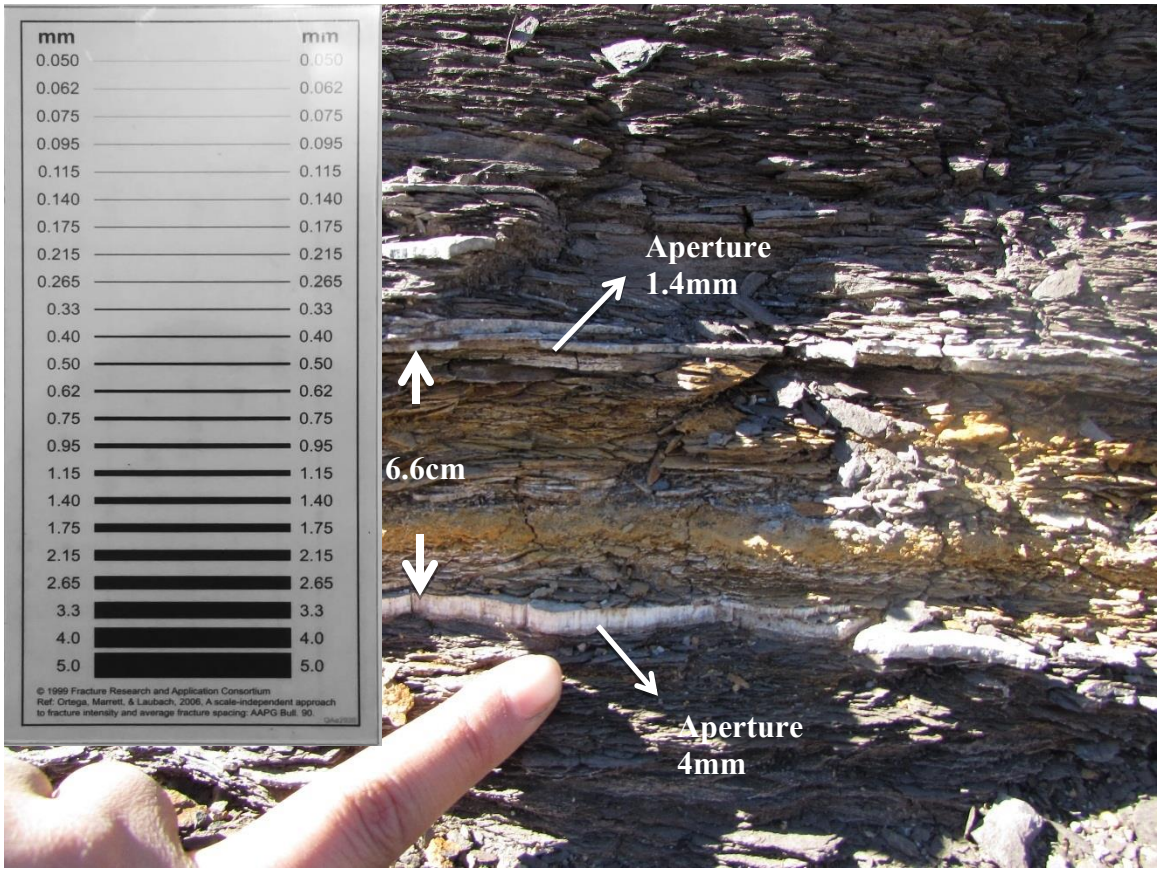

Figure 2-7 Measure bed-parallel fracture using a comparator, when aperture size < 5mm. Aperture width is 4 mm, spacing between the two neighboring fractures is 6.6 cm. Add some annotation to the figure to show the fracture width and spacing.

The spacings are the distances in between neighboring fractures along the scanline (Figure 2-6), so that a completed scanline consists of a series of fracture apertures and inter-fracture spacing, which collectively add up to the entire scanline length. In cases where fractures are not perpendicular to the scanline, both the fracture aperture and spacing may be trigonometrically corrected. However, the spacing between fractures could be overestimated if there are any fractures missed due to covered-up outcrop. I tried to clean the outcrop as much as possible to avoid possible covered fractures at each stop. Also, I set the scanlines where the bed-parallel fracture exposure was cleanest. Since the outcrops were of limited height I made several successive

sections of the scanline at different stops. I linked the sections by tracing the fracture at the top of a stop along the cliff up-section so that same fracture was now exposed in the cliff base, where exposures on one side of the river discontinued. I traced the fracture across the river to the other bank. Thus the scanlines are made up of successive sections. This method is not ideal, but was the best method given the limited height of the outcrops.

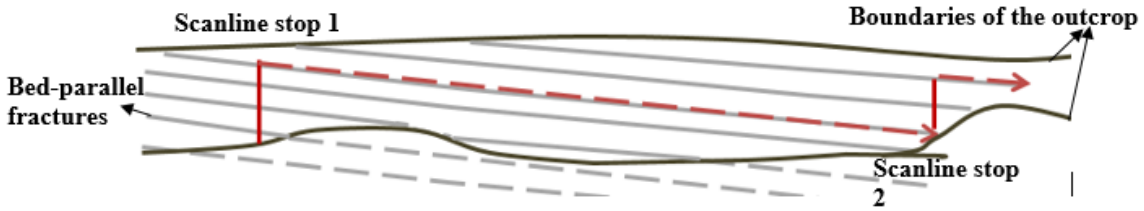

Figure 2-8 Sketch diagram illustrating the linking of scanlines.

Only filled fractures are counted in both cores and outcrop studies. It can be difficult to tell natural fractures from artifacts such as breaks due to weathering, pressure release due to outcrop uplift or bringing core to the surface, and at the small scale damage due to thin-section processing. Some fractures in outcrop can be filled with gypsum that can be derived from breakdown of pyrite in a carbonate-rich rock or, in the case of the Vaca Muerta, could be derived from the thick underlying Aulcilco evaporate. This type of cement is derived by a different mechanism than the calcite cement. The challenge with distinction between fractures and fossils also can't be ignored, since both of them can be of similar thickness, calcareous and fibrous. However, compared to bed-parallel fractures, the fossils tend to have a larger thickness/length ratio, and they are usually much more sinuous. Besides, the fossils do not have a median line with hostrock inclusions (Figure 2-9).

Figure 2-9 Fossil inoceramids can easily be confused with bed-parallel fractures

Fracture lateral extent was quantified by measuring along the fractures in two orthogonal directions, termed width and length, wherever a 3D observation could be made (Figure 2-10).

Figure 2-10 Fossil inoceramids can easily be confused with bed-parallel fractures

Fracture length, even in large exposures, can be difficult to measure objectively. In cases where the fracture is made up of linked segments, highly branched fractures, or fractures with extremely complicated morphology, it could be difficult to decide where the fracture begins and ends. To keep a constant standard, I followed the following rule when measuring bed-parallel fracture length. I first cleaned up all the covered part of the fracture to reach the maximum possible exposure of the fracture. If the fracture is not distinctively segmented, but its true extent is larger than the exposure, I measure the length and width where available and consider these the minimum dimensions. If the fracture is seemingly segmented, but with no distinctive displacement between the segments, I still consider them the same fracture with variable aperture size along the

length direction. However, if the fracture is segmented with distinctive displacement between each fragment, I consider them to be several separated fractures. Distinctive displacement is where intact rock is visible to the unaided eye between parts of the fracture. In practice, this is a few to several centimeters of rock. The width/length measurements were measured along the maximum exposure; orientations of the measurement are not constant for all fractures measured in the same outcrop and different outcrops. At Arroyo Mulichinco, length is measured along the direction of the river cut cliff (130-degree direction), width is measured across the river (40-degree direction), perpendicular to the length. At El Puesto, length is measurement along a direction of 30 degrees; no corresponding width is measurable at this outcrop due to limitation in fractures' 3D exposure.

3D exposure of bed-parallel fractures at outcrop Arroyo Mulichinco. Length is measured along the direction of the river cut cliff (measurement in this example is in the 130-degree direction), width is measured across the river (in this example along the 40-degree direction), perpendicular to the length.

A complete field scanline dataset consists of a series of aperture, width, and length measurements and inter-fracture spacing normal to bedding, together with fracture orientation. For the Vaca Muerta outcrops the scanlines crossed 43 fractures at the El Puesto location, 88 fractures in the Arroyo Mulichinco upper section, and 54 fractures in the Arroyo Mulichinco lower section. An effort was made to obtain fracture intensity data from low-fracture-intensity beds at the El Puesto outcrops facilitate comparison with other sections. Since the fracture intensity is much lower at the El Puesto location, a longer scanline was set (3 times longer than that in Arroyo Mulichinco) in order to reach a number of recorded fractures that is statistically meaningful. A short scanline was also

set at the El Puesto outcrop, higher up in the section than the main scanline at this outcrop, with only 4 fractures captured.

Bed-parallel fracture strike and dip, and fracture cement fiber orientations were measured using a Brunton compass, with a geomagnetic correction of 6 degrees to the west. Fracture morphology, composition and texture of fracture fill were noted. A hand lens was used to examine cement texture and 10% hydrochloric acid was used to test for carbonate composition.

The fractures counted in the scanline may be subject to sampling bias. The lower size limit of fractures visible in an outcrop may vary according to exposure quality and fracture-fill characteristics. Furthermore, sampling biases for measurements of fracture intensity or spacing at different scales may be different. The scale-dependent sampling bias, such as truncation and censoring artifacts will be discussed in Chapter 4.

2.1.2 Core Study Methodology

Scanline Methods

Picking cemented bed-parallel fractures from shale cores is considered a reliable data collecting method in this study. The scanline method is similar to that done in outcrops. The fracture perpendicular scanlines were positioned through the middle of the core. Cores from vertical wells are expected to have advantages in hitting the majority of bed-parallel fracture exists within its depth range, which can be a lot more efficient than sampling vertical fracture in vertical cores. Collecting bed-parallel fracture data from core and core scan images helps to achieve long scanline length in a more efficient way. These cores and core-scans were able to provide large datasets of bed-parallel fracture spacing and size distribution. Same as in the outcrop, only fractures with cement will be picked. Although we only look for filled fractures, powder abrasives used in thin-section

polishing, and evaporates formed due to shale dehydration, can be confused with cements. The challenge with distinction between fractures and fossils also can't be ignored in core studies.

Scanline data collected from direct core observation from 3 cores, 2 in the Marcellus and 1 in the Wolfcamp, were provided for analysis for this study to allow comparison with the Vaca Muerta data. These data sets had been previously collected by Dr. Julia Gale, but had not been analyzed for aperture-size distribution or spacing. Fracture apertures measured directly from cores can be as small as about 0.05 mm (0.002 in.) through use of a hand lens and comparator. Cement texture and composition descriptions are also possible with direct core observation. The description is considered more reliable than that at the outcrop, since the core cut-face is cleaner and less weathered compared to the outcrop.

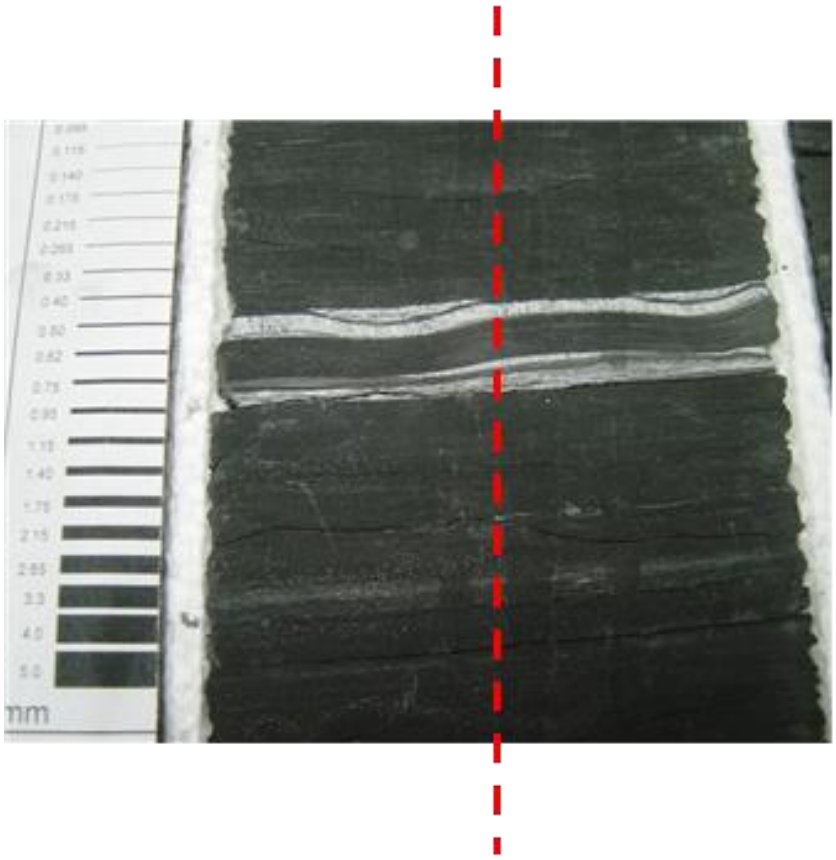

Figure 2-11 Measurement of bed-parallel fracture aperture along a vertical scanline, in a slabbed core, using a hand lens and comparator. The scanline is set through the middle of the core.

Figure 2-12 Measuring bed-parallel fracture aperture and spacing along a vertical scanline from core scan images. Scanline was set through the middle of the core.

For the Vaca Muerta cores I did not have direct access to the core and worked from scanned images of the cores (Figure 2-12). In this case measurement of apertures was restricted by the resolution of the images. A minimum aperture-size cut-off of 0.33 mm was chosen so that all fractures at or above this size could be measured and captured in the dataset. Cement texture and composition can't be known from core scan images, especially in thin fractures with <1mm aperture. I was provided with core photos or scan images from 5 Vaca Muerta cores (VM_Wells #1-#5). However, since the core photo of VM. Well #5 is of very low resolution, and is taken at an oblique angle to the core slab face, I decided not to collect scanline data from this well. Another artifact is that the core scan images are not always continuous throughout the depth range provided because individual core runs may be relatively short. The most complete core scan images set is from the VM_Well #1 from which I collected scanline data from a continuous, high resolution scan image of a total length of 73.28 m. Other wells all have missing sections

of around 0.3 m to tens of meters. Missing core will have a large influence on fracture spacing, and lead to increase numbers of spacing around or larger than 0.3m. In order to minimize the effect that missing core has on fracture spacing, I take the long missing sections (> 1m) out of the scanline, and only add up the relatively continuous parts of the mosaic to make up the whole scanline. Bias due to differences in spacing that would have been in missing core versus spacing in the measured core is possible.

A total of 7 scanline datasets was collected from 7 wells in different shale formations, including both the ones from direct core observation and those from core scan images. 4 of the 7 are from Vaca Muerta, Neuquén Basin, capturing 724 bed-parallel fractures; 2 of the 7 are from Marcellus, Appalachian Basin, capturing 129 bed-parallel fractures; and the other 1 is from Wolfcamp, Permian Basin, capturing 68 bed-parallel fractures. A total of 921 bed-parallel fractures were captured during core studies, within a total scanline length of 549.48 m, with their size and spacing data documented.

The fractures mentioned above do not include microfractures with apertures less than 0.05mm. In order to measure micro-fractures, we need to set microscanlines in thin-sections. However, collecting bed-parallel microfracture data in shale is more challenging than doing so in sandstone. Artifacts mentioned previously for outcrops cause even worse problems when studying very fine bed-parallel fractures in shale thin sections, and section damage during preparation where the core breaks along weak bedding planes is a particular problem. The result is that most thin sections contain many barren bed-parallel fractures. Cement-filled microfractures are fine, with composite morphologies and commonly vague boundaries, and their apertures size is highly variable. In addition, microfractures in general may be at a low intensity (Gale et al., 2014), and the population of fractures in a thin section may be too few to be representative. In order to get a

comprehensive dataset, I set up scanlines in thin sections made from Marcellus cores, where there are fair numbers of bed-parallel fractures within thin section scale. However, by selecting relatively high fracture-intensity samples for the analysis there is already a sampling bias. Sampling bias is discussed further in Chapter 4.

A summary of scanline datasets is listed in Table 2-2.

Table 2-2 A summary of scanline datasets.

Dataset	Scanline Length, m (Vertical scanline)	# of fractures	# of fracs/m
VM_ Well #1	73.28	340	4.64
VM_ Well #2	34.69	230	6.63
VM_ Well #3	28.00	142	5.07
VM_ Well #4	18.99	12	0.63
VM_ Arroyo Mulichinco-up	17.84	88	4.93
VM_ Arroyo Mulichinco-down	13.20	54	4.09
VM_ El Puesto	48.46	30	0.62
Marcellus Well #1	89.18	47	0.53
Marcellus Well #2	163.46	82	0.50
Wolfcamp Well #1	141.88	68	0.48
Total	628.98	1093	Ave: 2.696

Petrographic Methods

A total of 71 thin sections were analyzed using petrographic methods. 22 of the 71 thin sections were made out of selected 20 Vaca Muerta core samples from VM_ Well #1 (13 thin-sections), VM_ Well #2(2 thin-sections), VM_ Well #3 (4 thin-sections), along with 23 field samples. There were 34 thin sections from 29 samples from Marcellus well #1, #2 and #3 and 5 thin sections made from Wolfcamp Well #1 core. The thin sections do not only include the ones with bed-parallel fractures. There are also thin sections with vertical fractures, stylolite, faults, cross-cutting features, and some for hostrock lithology description.

The core pieces were first stabilized with clear epoxy so that the shale would not fall apart during cutting. The thin sections were cut perpendicular to the fractures, and were either parallel to or perpendicular to bedding. The field samples were cut across the maximum cement fiber inclination. I cut notches into the sections to mark the stratigraphic up of the sections when available. The thin sections were 30 μm thick, standard size (1”x2”) or large size (2”x3”), standard polished, with blue epoxy (there are several with colorless epoxy). The thin sections were made under low heat, to prevent the shale organic matter from being thermally altered, and also to preserve fluid inclusion integrity within the fracture cement.

The sections were examined and photographed with either a Zeiss petrographic microscope fitted with a Zeiss AxioCam digital camera or a Nikon LV100 petrographic microscope equipped with a Nikon DS-Ri1 cooled digital camera and reflected-light capabilities. Using these microscopes, observations could be made of the fracture attributes, the character of the sealing cement, and the lithology of the host rock.

Table 2-3 Brief summary of thin sections analyzed in each dataset. One slide may have both high angle and bed-parallel fractures.

Core Name	With bed-parallel fracture	With high angle fracture	Others
VM_ Well #1	9	9	3
VM_ Well #1	2	1	1
VM_ Well #1	4	0	2
VM_ Arroyo Mulichinco-up	8	0	2
VM_ Arroyo Mulichinco-down	7	0	0
VM_El Puesto	4	0	2
Marcellus Well #1	6	5	4
Marcellus Well #2	8	3	12
Marcellus Well #3	4	3	3
Wolfcamp Well #1	3	2	0

2.2 FIELD DATASETS DESCRIPTION

Three field vertical scanline datasets were collected at the field area located on the north-west of Neuquén Basin, Argentina. Field scanline datasets include Field Scanline 1-Arroyo Mulichinco-up, Field Scanline 2-Arroyo Mulichinco-down, and Field Scanline 3-El Puesto.

2.2.1 Field Scanline 1-Arroyo Mulichinco-up

Arroyo Mulichinco-up outcrop is a river cut cliff generally striking 85 degrees to 105 degrees. It is located at around 38`01.23'S, 70`27.25'W. Vaca Muerta Formation outcrops at this location. (Figure 2-13)

Numerous of bed-parallel fractures are exposed here; it is one of best outcrops in the world for bed-parallel fracture exposure. But outcrop weathering, and coverage by plants, mud and water allowed only parts of the river cut cliff to be measured systematically. When measuring the lower section of the scanline at the western end, data was collected from the southern bank of the river, which presents better exposure. At the east end of the outcrops, when measuring the upper section of the scanline, data was collected from the northern bank of the river. Structurally, the Vaca Muerta here is gently dipping, with a dip angle of 5-15 degrees towards SE (Figure 2-14). However, close to the east end of the path, next to the bridge where the road crosses Arroyo Mulichinco, there is a fold structure comprising an anticline and syncline pair. The fold is marked by thick bed-parallel fractures following the bedding, indicating that the folding is most possibly happened after the beef was formed (Figure 2-16). I measured bedding around the fold and the fold axis. The fold axis plunge and trend are oriented $4^{o}/187^{o}$ (Figure 2-15). There are also at least 4 sets of vertical fractures exposed at this location.

Thick bed-parallel fractures are exceptionally common at this outcrop, especially where the tuff is also present. The bed-parallel fractures are found at the top and bottom boundaries of the tuff and do not cut through it (Figure 2-16). The thickest fracture collected during my field work is from this location. It has an 8.7 cm aperture, close to the top of the Arroyo Mulichinco-up vertical scanline (Figure 2-17).

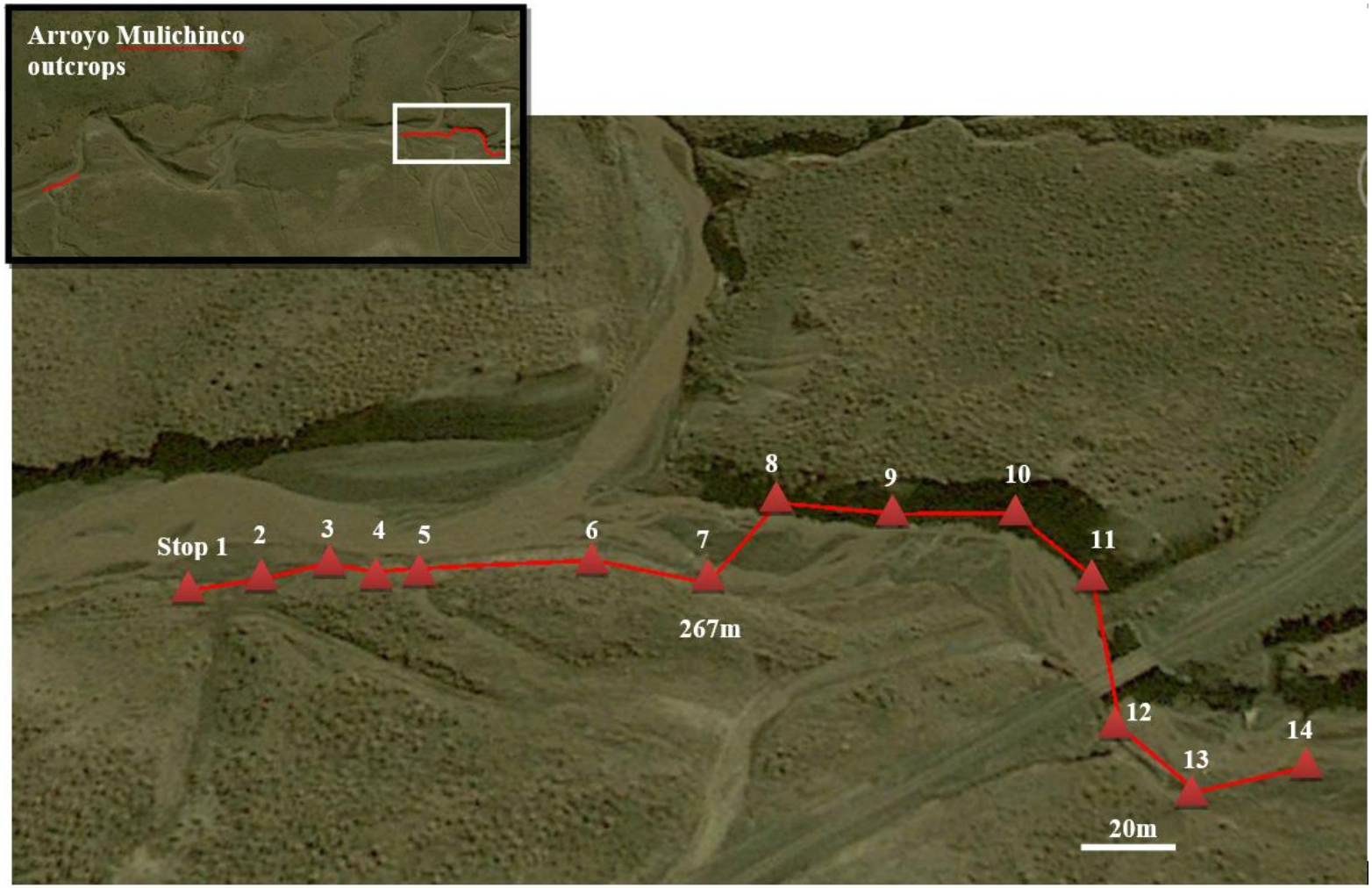

Figure 2-13 Map showing scanline 1 at Arroyo Mulichinco- up outcrop. Red line is highlighting the path taken, triangle indicates the stops at where the scanline data was collected.

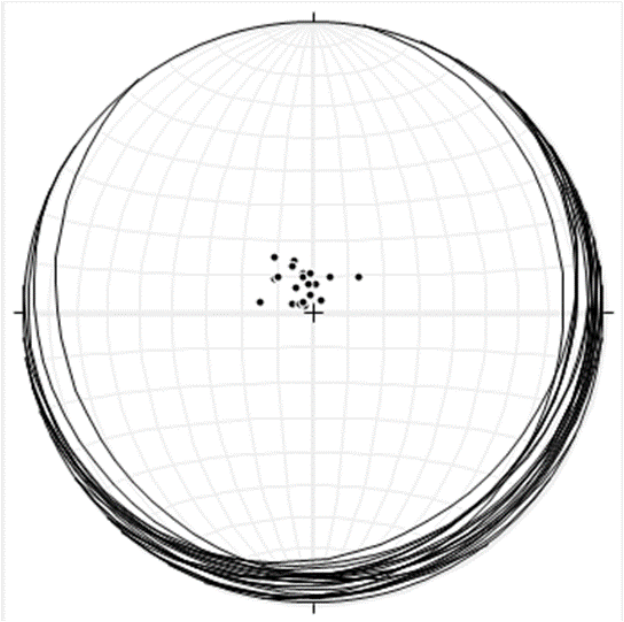

Figure 2-14 Planer and pole projectionsshows the strike and dip of bedding at Arroyo Mulichinco-up outcrop. Bedding strikes NE-SW, dipping ~10 degrees to the south.

Figure 2-15 Antiform-synform structure. Fold axis 04º/187º

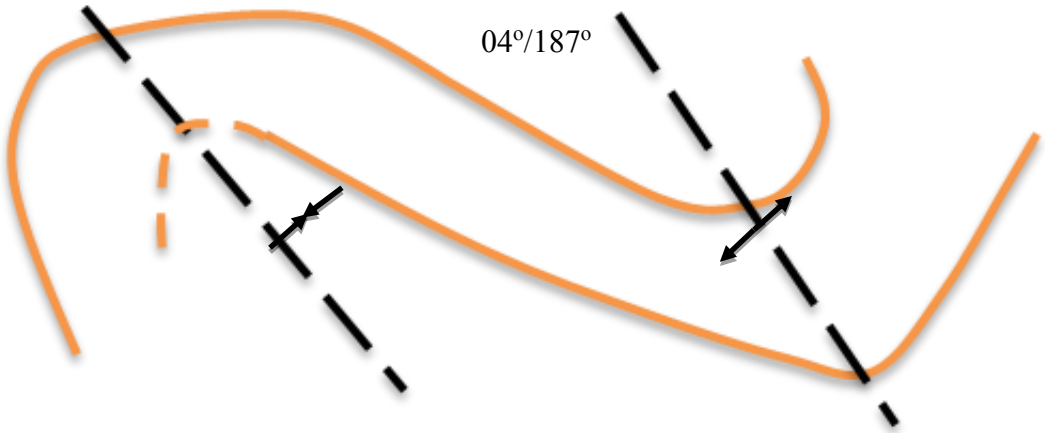

Figure 2-16 Sketched diagram illustrating the elements of the fold structure.

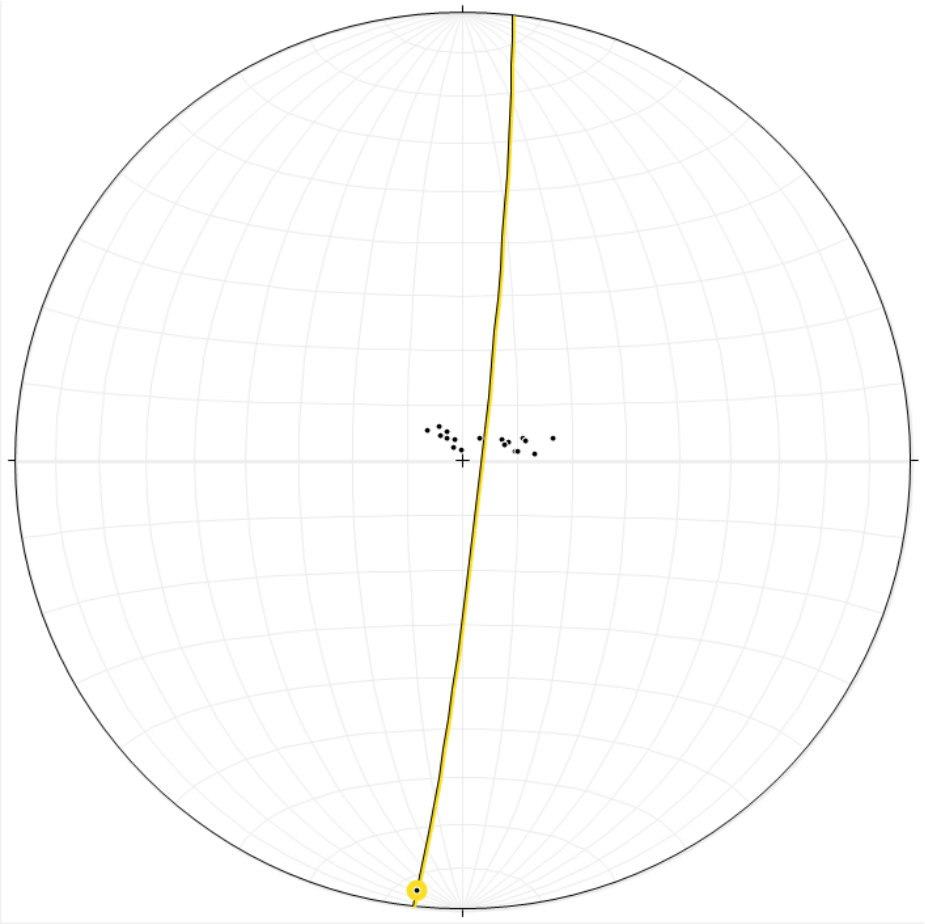

Figure 2-17 Stereogram of the fold structure. Fold axis projected as 04º/187º. Bedding was measured around the fold and the fold axis was also measured.

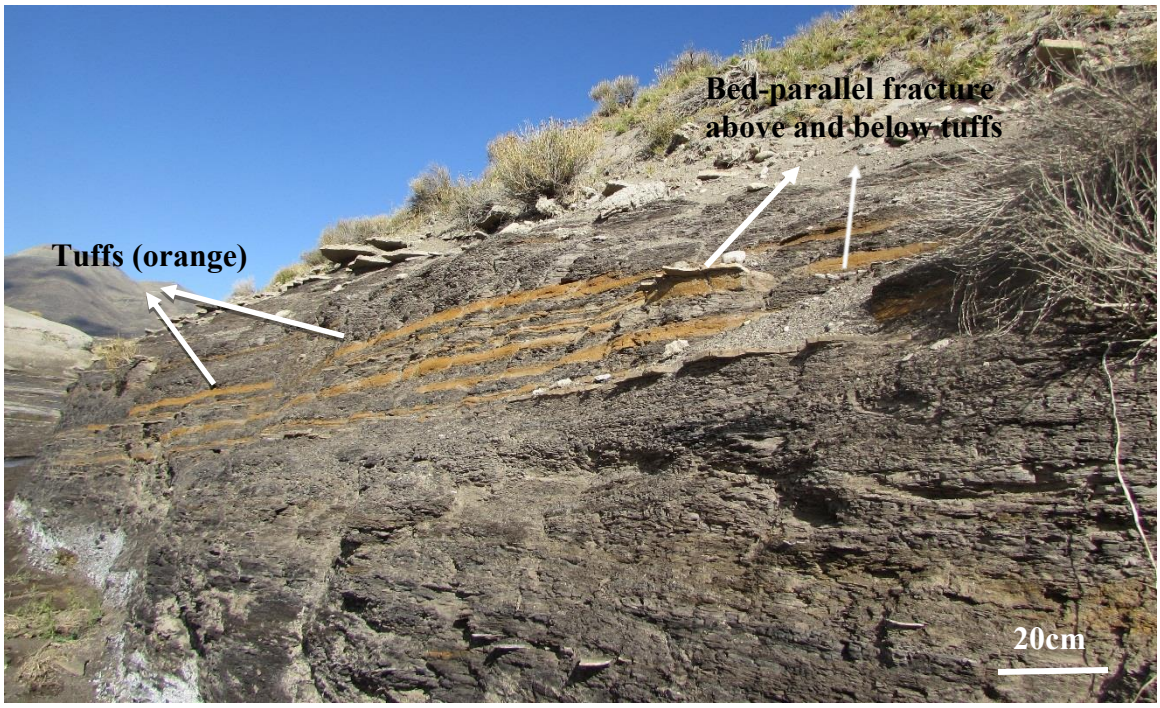

Figure 2-18 Thick bed-parallel fractures associated with tuff layers. The tuffs are weathered orange.

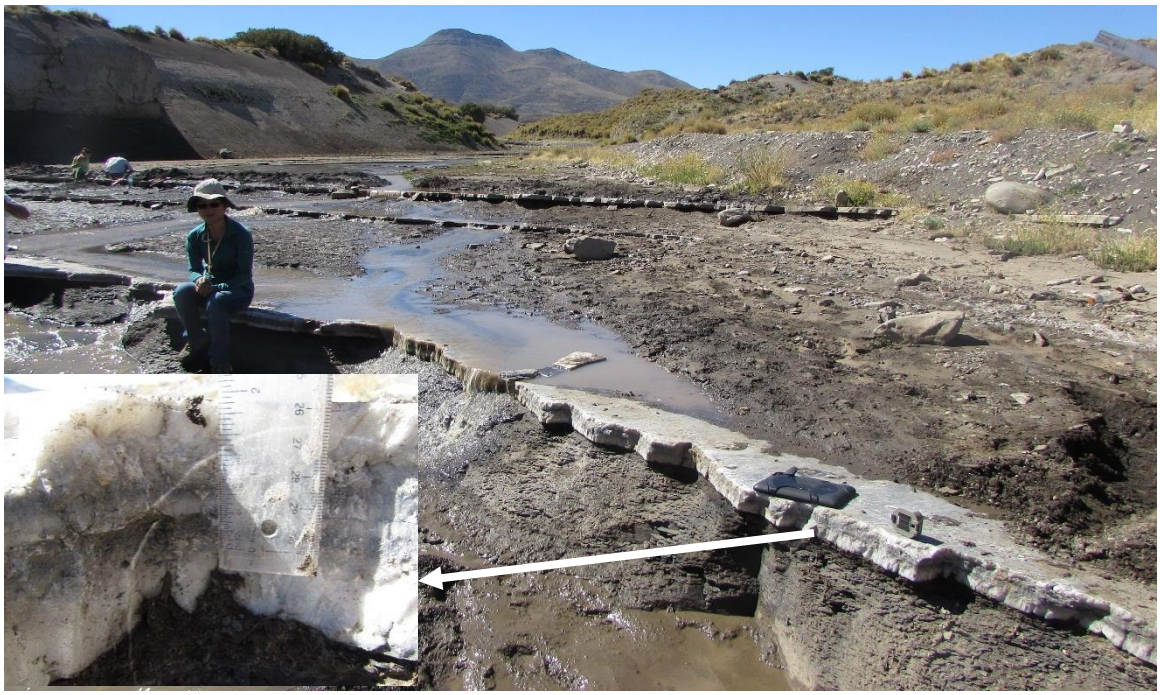
Figure 2-19 Thickest bed-parallel measured along scanline, 8.7mm aperture.

2.2.2 Field Scanline 2-Arroyo Mulichinco-down

Arroyo Mulichinco-down outcrop is also a river cut cliff generally striking 70 degrees to 90 degrees. It is located at around 38`01.16'S, 70`27.45'W. Vaca Muerta Formation outcrop at this location (Figure 2-20). The Vaca Muerta here is dipping more than at other locations, with a dip angle of 15-25 degrees (Figure 2-21). A large thrust structure lies between the two Arroyo Mulichinco outcrops (up and down outcrop). The thrust moved from the west to the east, the hanging wall is to the west of the fault plane. This structure may explain why the dips in the lower section (Arroyo Mulichinco down) are steeper than those in the upper section (Figure 2-22).

Numerous bed-parallel fractures are exposed here; the outcrop is well exposed with continuous exposure of bed-parallel fractures at the southern bank of the river (Figure 2-23). Large numbers of concretions lie between bed-parallel fractures, with the fractures curving around the concretions (Figure 2-24). This outcrop also shows great 3D exposure of many thick bed-parallel fractures. Combined with the good continuity, many fracture length and width data pairs were collected at this outcrop.

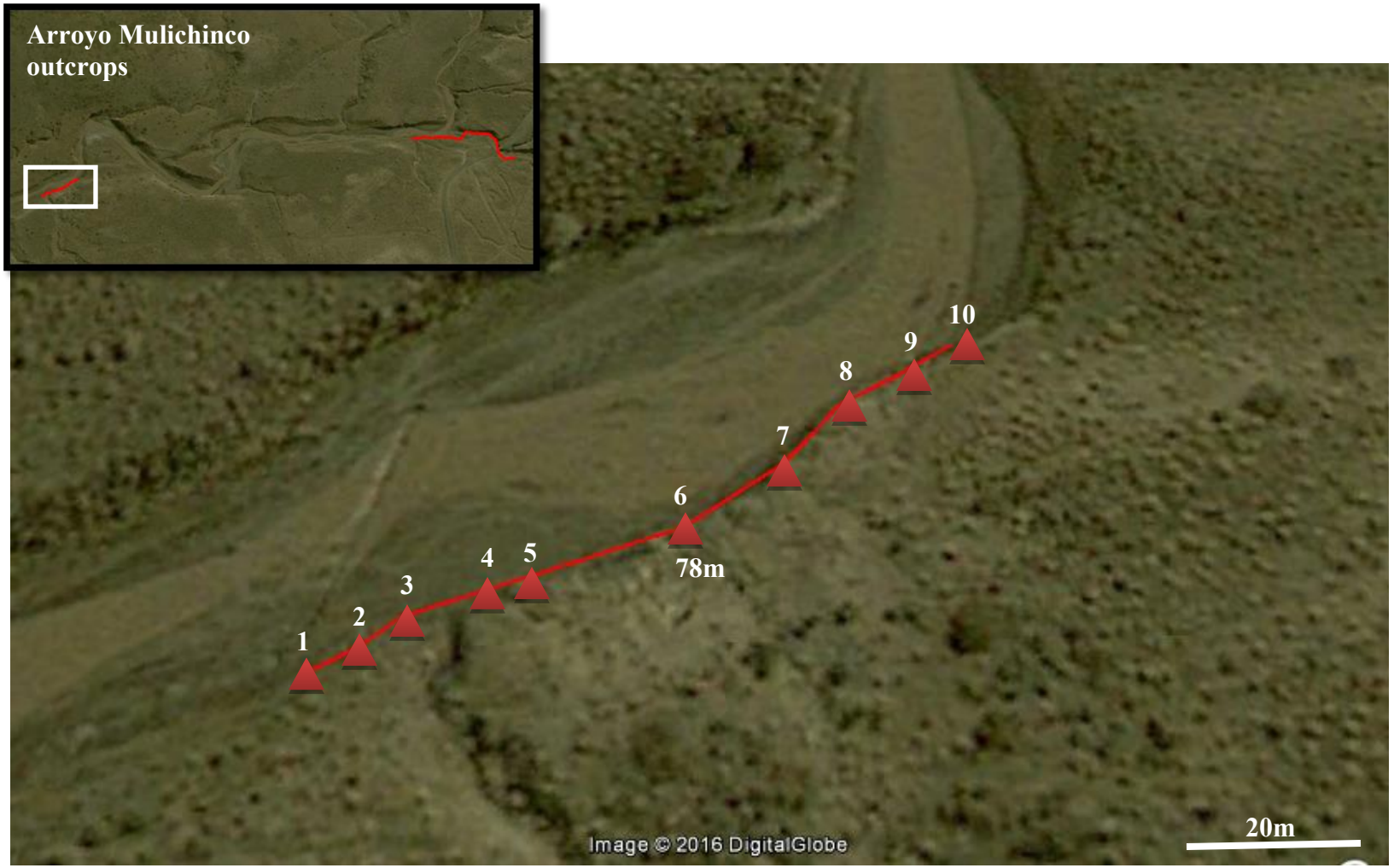

Figure 2-20 Map showing field scanline 2 at Arroyo Mulichinco-down outcrop. Red line is highlighting the path taken when collecting vertical scanline data.

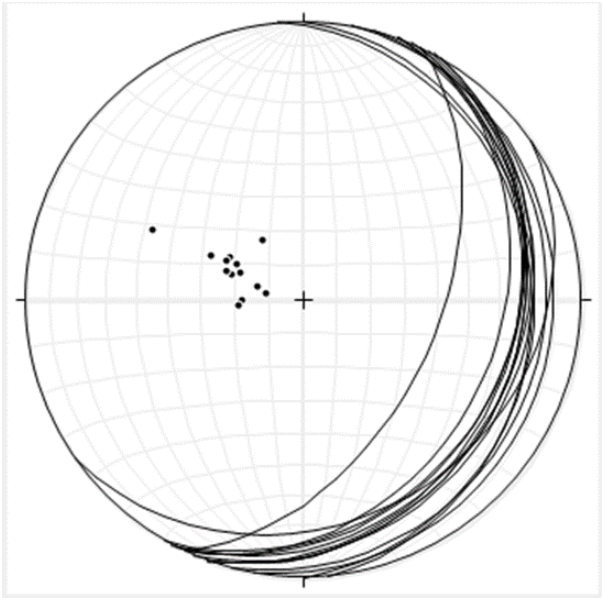

Figure 2-21 Stereonet plot shows the strike and dip of bedding at Arroyo Mulichinco-down outcrop. Bedding striking NE-SW, dipping ~20 degrees to the south

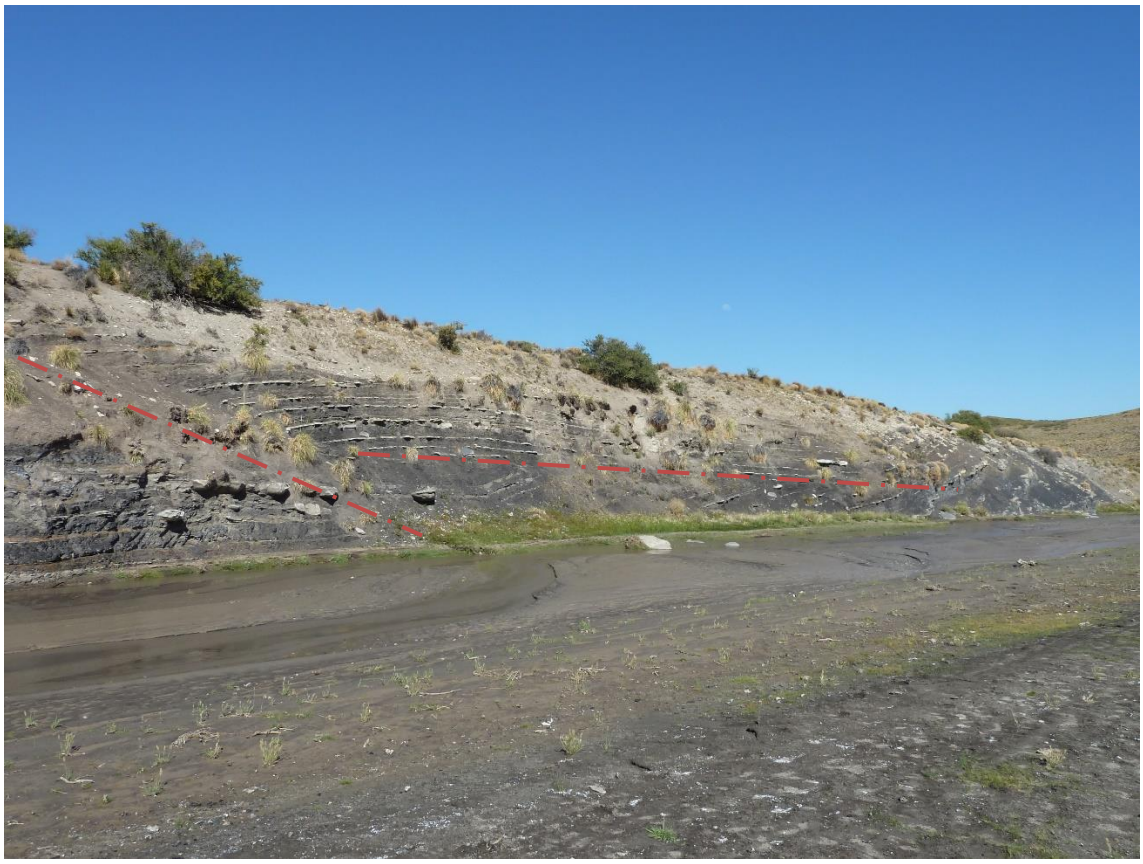

Figure 2-22 Large thrust structure that lies between Arroyo Mulichinco up and down. W-E thrusting, hanging wall at the west. This structure may explain why the dips in the lower section (Mulichinco down) are steeper than those in the upper section.

Figure 2-23 Well exposed, continuous exposure of bed-parallel fracture, both at river cut cliff and river bed.

Figure 2-24 Bed-parallel fractures curving around calcareous concretions.

2.2.3 Field Scanline 3- El Puesto

El Puesto outcrop is also a river cut cliff generally striking 280-20 degrees. The outcrop gradually turns from EW striking toward NE-SW striking. The outcrop is located at around 37º58'41" S, 70º21'42" W. Vaca Muerta Formation outcrops at this location. (Figure 2-20) Vaca Muerta here dips around 20 degrees, and strikes 200 degrees. However, the dip direction is to the north, which is the opposite to that for the Arroyo Mulichinco outcrops (Figure 2-21).

Fewer bed-parallel fractures are exposed here, compared to the previous two outcrops. However, this outcrop is dry (facilitating measurement) and well exposed with relatively continuous exposure of bed-parallel fractures (Figure 2-22). In order to capture enough bed-parallel fractures for statistically reasonable scaling work, a scanline of three times the length of the previous two was established to collect fracture attributes.

At least two sets of vertical fractures are also present and cross-cut the bed-parallel fractures. One set of the two contains thick (>1m) vertical blocky calcite veins that cut through the bed-parallel fractures.

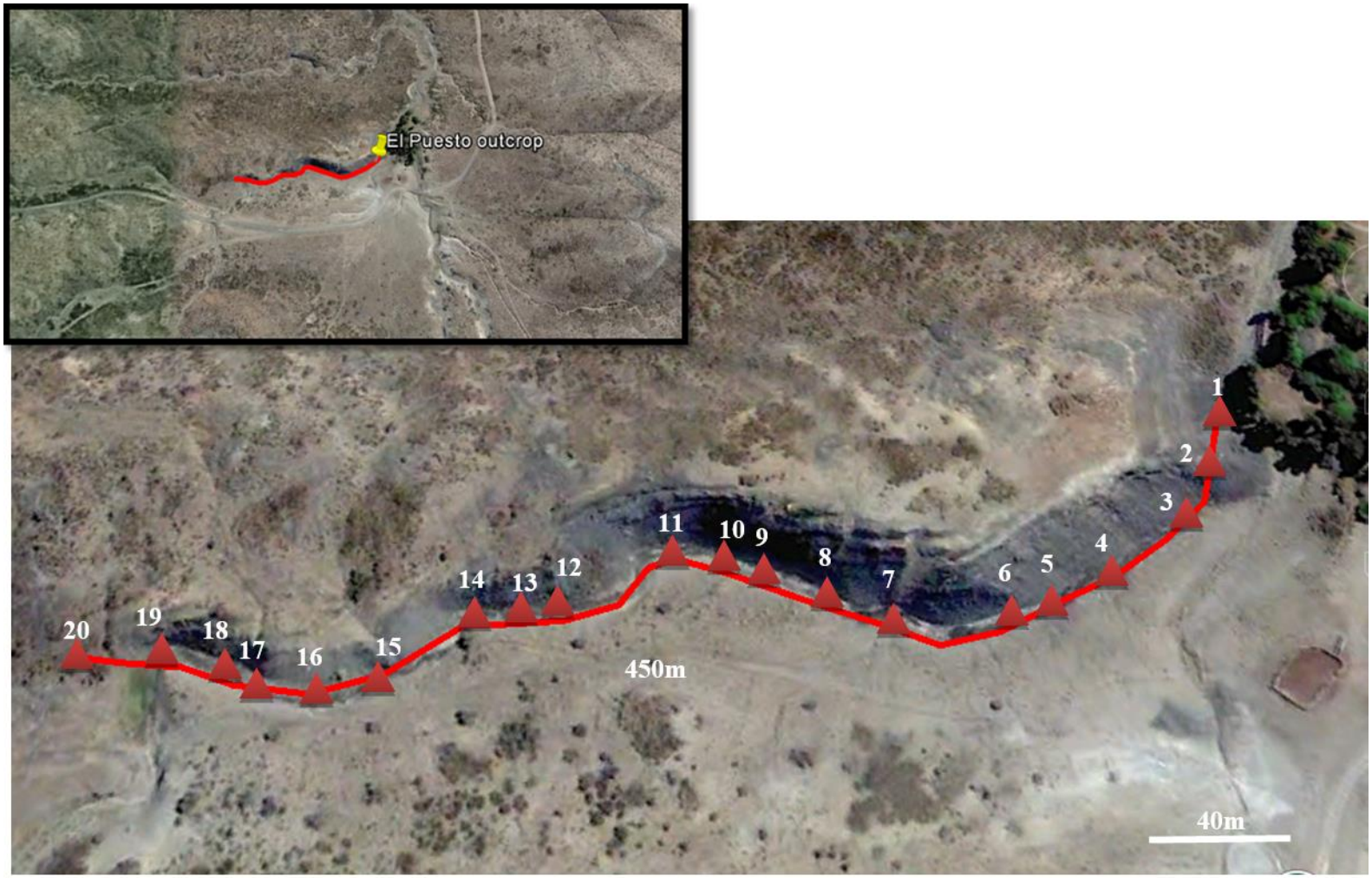

Figure 2-25 Map showing field scanline 2 at El Puesto outcrop. Red line is highlighting the path taken when collecting vertical scanline data.

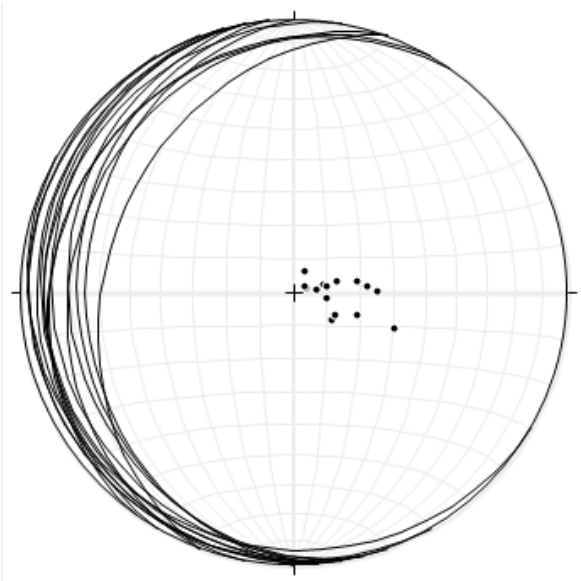

Figure 2-26 Stereonet plot shows the strike and dip of bedding at El Puesto outcrop. Bedding striking NE-SW, dipping ~10-30 degrees to the west

Figure 2-27 Well exposed, relatively continuous exposure of bed-parallel fracture at El Puesto outcrop

2.3 Observed Local Structures and Stress Direction Indication

Since it is already known that the outcrop area is rich in bed-parallel fractures, if the hypothesis is correct, the field area should be able to fulfill the proposed positive factors contribute to bed-parallel fracture generation. As addressed before, the outcropped Vaca Muerta shale is mostly black shales (Figure 2-28). The black shale looks bituminous and smells like oil, which means it has high TOC content and oil prone maturity. The black shale is also rich in fossils. The interbedded concretions and tuff layers provides large numbers of material interfaces. However, the structural elements and dominant stress direction of the field area can't be easily determined. As mentioned

in earlier in this chapter, the dip angles of beddings are very shallow, ranges from 0 º - 30º. Most of them are dipping around 10º. However, since the dipping direction of bedding at Arroyo Mulichinco and El Puesto outcrop are of around 180º different, the beds at the two outcrops are dipping toward each other (Figure 2-29). It may infer that there are at least one or more folding structures in between the two outcrops. If this is true, and with the assumption that the fold in between is a broad anticline or syncline, fold axis can be calculated based on the strikes and dips for the fold limbs. In this case, the strike and dip of the limbs are inferred by the bedding measurements from Arroyo Mulichinco and El Puesto outcrops. According to the calculation, the trend and plunge of the fold axis is 198.1º/4.1º. The strike and dip of the fold axial plane is 197º/75.5º W. It means the fold axis is plunging NE-SW with a small deviation angle of ~17º from N-S. The inter-limb angle of the fold is 159.7º.

Figure 2-28 Black shale at studied Arroyo Mulichinco outcrop. The outcropped Vaca Muerta shale is mostly black shales which looks bituminous, properly cooked and rich in fossil. Although inter-bedded with grey shale and tuff, black shale is the most abundant at both outcrops.

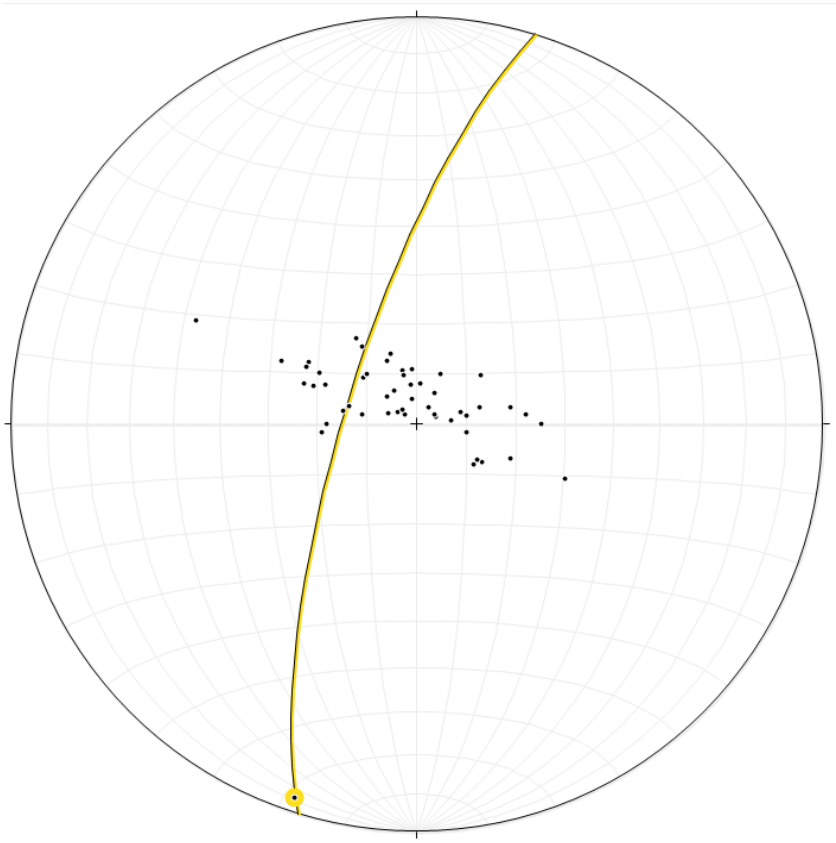

Figure 2-29 Fold axis of the bedding inferred broad fold. The black dots represent pole to bedding. The Yellow circled dot indicates the fold axis. The yellow line is marking the strike and dip of the fold axial plane. Fold axis plunging NW-SE at a very low angle.

Except for the larger-scale, inferred fold, there is a small-scale anticline-syncline combined fold structure exposed on the river bed around 100m to the west of the start point of the Arroyo Mulichinco-up section scanline. (Figure 2-15) According to the fold limbs' attributes, the trend and plunge of the fold axis is calculated to be 186.1º/4.0º. The strike and dip of the fold axial plane is 6.3º/86.6º E. It means the fold axis is plunging NE-SW with a very small deviation angle of ~6º from N-S (Figure 2-16, 2-17). The inter-limb angle of the small fold structure is 166.5º. The attributes of the small fold structure are consistent with the ones of the previous fold.

However, due to the limited outcrop exposure, and the lack of contrast layers at many parts of the outcrop, faults were rarely found. A thrust fault was found a few hundreds of meters down-stream (to the west) of the Arroyo Mulichinco outcrop. The strike of its fault plane was projected and measured as ~020o, fault plane dipping 30o-45o. in which direction. So the fault is striking NE-SW, its western block is the hanging wall. This observation is consistent with the attitude of the fold structure discussed previously. The attributes of the local folding structures and thrust fault are consistent with much larger structures such as the neighboring Loncopue Trough and Agrio fold and thrust belt. So I conclude that the direction of the dominant force applied at the studies domain is E-W compressional force.

The attributes of the local folding structures and thrust fault are consistent with much larger structures such as the neighboring Loncopue Trough and Agrio fold and thrust belt. So I conclude that the direction of the dominant force applied at the studies domain is E-W compressional force during late Jurassic to mid Cretaceous time. This is the paleostress indication from the structures observed, this is not the present day stress. From studies of fibrous veins, especially those containing oblique fibers, there is a consensus that the fibers grow incrementally, partly or totally tracking the history of relative displacement of the walls (Taber, 1918; Durney and Ramsay, 1973). It means the fibrous nature of many bed-parallel fracture fills allows them to potentially be the structural force indicator, or at least, a shear indicator. The orientation and inclination of fibers are measured from beef at both Arroyo Mulichinco and El Puesto outcrop. The rose diagram generated from trend and plunge of the beef fibers reads that the majority of fibers are plunging to the west (southwest or northwest) in general. Which indicates that the main inter-bedding shear direction is E-W. There are a few measurements showing a

more N-S shear, however, they may be a result of local shearing activities. Measurements of line feature's attributes can be highly imprecise when the line is only seen from 2D or if the line is too short. Both occasions are quite common at the outcrop.

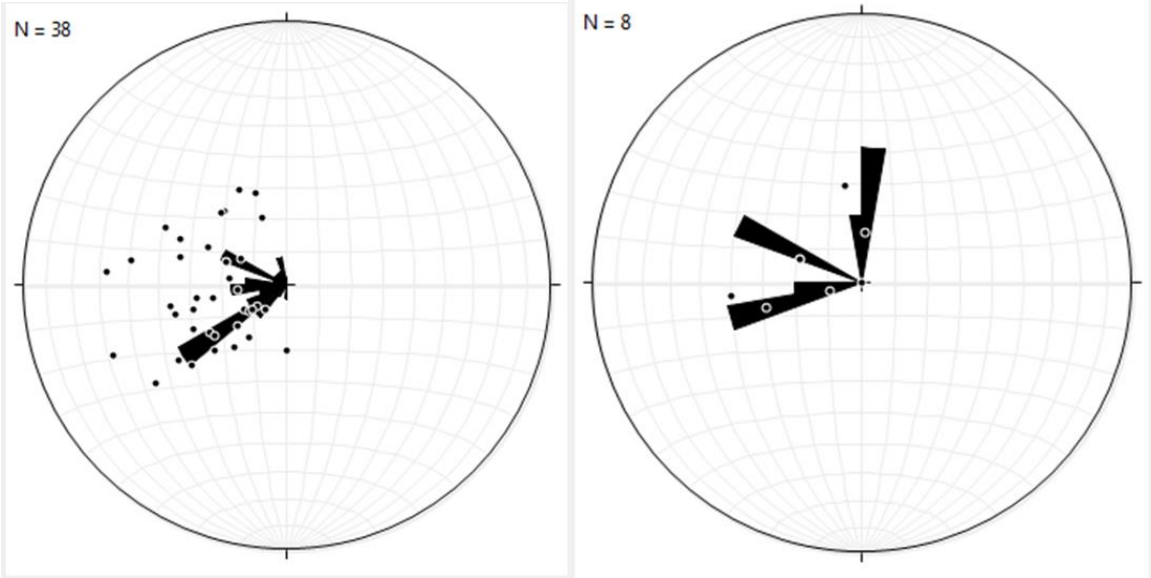

Figure 2-30 Rose diagram showing the plunging of beef cement fibers, which indicates the relative shear direction of the two fracture walls. The dominant shear direction is E-W in studied area.

Theoretically it is accepted that a context of horizontal compression, due to additional tectonic forces may be a mechanism causing bed-parallel fractures. The studied outcrop area contains multiple evidences of compressional structural activities happened around the same time of the fracture formation, and they share dominant compressional force direction. This characteristic, along with high content of black shale hostrock, and abundant material interfaces within the hostrock, make the studied area highly favorable for bed-parallel fracture to form and grow. The mechanism of generating bed-parallel fractures will be discussed in Chapter 6.

Chapter 3. Bed-parallel fracture morphology and cement texture

3.1 Core and Outcrop Observations

Preliminary examination of bed-parallel fracture examples in the literature (Rodrigues et al., 2009; Cobbold et al., 2007, 2012, 2013; Maher et al., 2016) and the outcrops and cores that you studied showed that morphology varies from simple planar to complex wavy or branched fractures. There are different mineral cements, some of which are fibrous, others can be blocky, euhedral or anhedral. The fracture size attributes include fracture lateral extent, which are the length and width of the fracture, and the fracture aperture. The aspect ratio of fracture refers to the ratio between fracture length and aperture. Fracture size distribution will be discussed in Ch 4, focusing on aperture size distribution.

The archived and/or sampled sections of seven cores from three different formations were examined and samples of fractures were obtained from the sampling half, focusing on those that contained cements. VM_ Well #1, VM_ Well #2, VM_ Well #3, Marcellus Well #1, Marcellus Well #2, Marcellus Well #3 and Wolfcamp Well #1 cores were sampled and analyzed (Table 3-1). A complete archive of photographs of sampled core is in Appendix B. Host rock composition will be discussed in detail in Chapter 5. Precise well locations are in some cases not provided as the companies providing core considered this confidential information. Individual samples may have multiple fracture types, including bed-parallel fracture along the beddings within the hostrock, short filled/partly filled fractures, and fractures associated with concretions. The fractures associated with concretions are usually bed-parallel as well and they are common in both Vaca Muerta and Marcellus cores. This type of fracture can occur at concretion margins or cut across the concretions, their morphology is often more

complex than that of the majority of bed-parallel fractures. So in this chapter, bed-parallel fractures associated with concretions will be shown and discussed separately. Vertical fractures that are not linked to or interacting with bed-parallel fractures or any other bed-parallel features are not the target of this part of the study.

Table 3-1 Core sample inventory for bed-parallel fracture morphology study. N.C = not continuous. Individual samples may have multiple fracture types. None of the cores are oriented.

Well Name	Formation	Upper Depth (m)	Lower Depth (m)	Sampled bed-parallel fracture	Sampled high angle fracture	Sampled Others
VM_ Well #1	Vaca Muerta	2415.00	2488.28	9	9	3
VM_ Well #2	Vaca Muerta	2653.00	2753.00 (N.C)	2	1	1
VM_ Well #3	Vaca Muerta	2927.00	3124.27 (N.C)	4	0	2
Marcellus Well #1	Marcellus	1900.43 (6235 ft)	1991.56 (6534 ft)	6	5	4
Marcellus Well #2	Marcellus	1983.94 (6509 ft)	2147.32 (7045 ft)	8	3	12
Marcellus Well #3	Marcellus	1915.36 (6284 ft)	2147.32 (6684ft)	4	3	3
Wolfcamp Well #1	Wolfcamp	3416.81 (11210 ft)	3560.37 (11681 ft)	3	2	0

Table 3-2 Inventory of thin-sections made out of field samples. One bed-parallel fracture may be made into two thin-sections.

Outcrop	Bed-parallel fracture	Others (hostrock)
VM_ Arroyo Mulichinco-up	8	2
VM_ Arroyo Mulichinco-down	7	0
VM_ El Puesto	4	2
Total	19	4

The VM_ Well #3 core is the shortest but contains the highest number of bedding-parallel fractures. The VM Well #2 and #3 do not have continuous cores and the total length of the core is calculated by adding up the sections available. Other cores analyzed are continuous. The Marcellus Well #1 is the longest, but it contains few bedding-parallel fractures. The VM_ Well #1 has the highest number of observed bedding parallel fractures (340 fractures). The Marcellus Well #1 is the shallowest and Wolfcamp Well #1 is the deepest, from around 6200ft to 7000ft (see Table 3-1 for depth of studied well depth sections).

For Marcellus and Wolfcamp wells, raw scanline data including fracture length, aperture and preliminary descriptions on fracture shape and cement composition were collected by Dr. Julia Gale. Raw scanline data was compiled and interpreted by me. Thin sections of Wolfcamp Well #1 were provided by Dr. Julia Gale. Core sampling of the Marcellus wells was done with the help of Dr. Julia Gale and Ms. Sara Elliott. For Vaca Muerta wells, limited numbers of core samples were provided by YPF. The core descriptions are generated from high resolution core scan images. A summary of each core including the number of fractures and depths, and preliminary descriptions of each

observed fracture can be found in Appendix B. Outcrop description and field sample collection methods were discussed in Chpater 2.

3.1.1 Bed-parallel Fracture Along the Beddings

Bedding-parallel and sub-parallel fractures such as the calcite-filled fracture shown in figure 3.1 are observed in the cores, and at the studied outcrop locations as well. Many bed-parallel fractures studied are filled with fibrous calcite cement, and have a median surface marked by inclusions of host rock. This cement type is called "*beef*" (see Chapter 1.1.1 for definition). The *beef* are usually with symmetrical or asymmetrical median line, and is the most common cement texture in all three studied formations. Except for fibrous cement, bed-parallel fractures can be cemented with blocky calcite (figure 3.2a) or other mineral cements such as sulfates, and often contain evidence of hydrocarbon flow in the form of bitumen and/or oil inclusions. Sometimes there are several phases of cement, where calcite, dolomite, gypsum, bitumen and pyrite are all present (figure 3.2 b and c). Details regarding cement composition will be discussed under section 3.2.

Table 3-3 Summary of bed-parallel fracture morphologies.

Note: Data collected from core scan panel, only sampled fractures are able to be studied in detail regarding their cement textures.					
Well Name	Formation	Sampled bed-parallel fracture	Beef	Median-line	Crack-seal texture
VM_ Well #1	Vaca Muerta	9	7	7	1
VM_ Well #2	Vaca Muerta	2	1	1	0
VM_ Well #3	Vaca Muerta	4	3	3	0
Note: Data collected from direct observation of core and outcrop.					
Name	Formation	Observed bed-parallel fracture	Beef	Segmented/ branched	Crack-seal
Marcellus Well #1	Marcellus	82	43	15	4
Marcellus Well #2	Marcellus	48	26	2	0
Marcellus Well #3	Marcellus	4	2	1	0
Wolfcamp Well #1	Wolfcamp	68	33	18 of 33 with median line, lacking other attributes	
Arroyo Mulichinco-up	Vaca Muerta	88	60	No systematic data	
Arroyo Mulichinco-down	Vaca Muerta	54	44		
El Puesto	Vaca Muerta	30	24	No systematic data	

In both core and outcrop examples, bedding-parallel fractures are sometimes show crack-seal texture (Laubach at al., 2004). The fracture cement records successive increments of cracking and sealing with cement marked by “inclusion trails” parallel to the fracture walls. Crack-seal textures in bed-parallel fractures is not as common as that in the vertical fractures. In terms of geometry, planar or lens-shaped fractures, and

complex, branching geometries, are all found (figure 3.3a, b and c). Branched or segmented morphologies are common in both thick and thin bed-parallel fractures.

I also observed low angle, non-planar fractures in core that contain slickensides along their surfaces. These are commonly in brecciated shear zones and their surfaces tend to have somewhat polished surfaces and with or without cement fill (figure 3.4a and b). This type of fracture records reverse shear along shallow-angle small-scale faults. Vertical fractures with slickensides are also observed (figure 3.4 c).

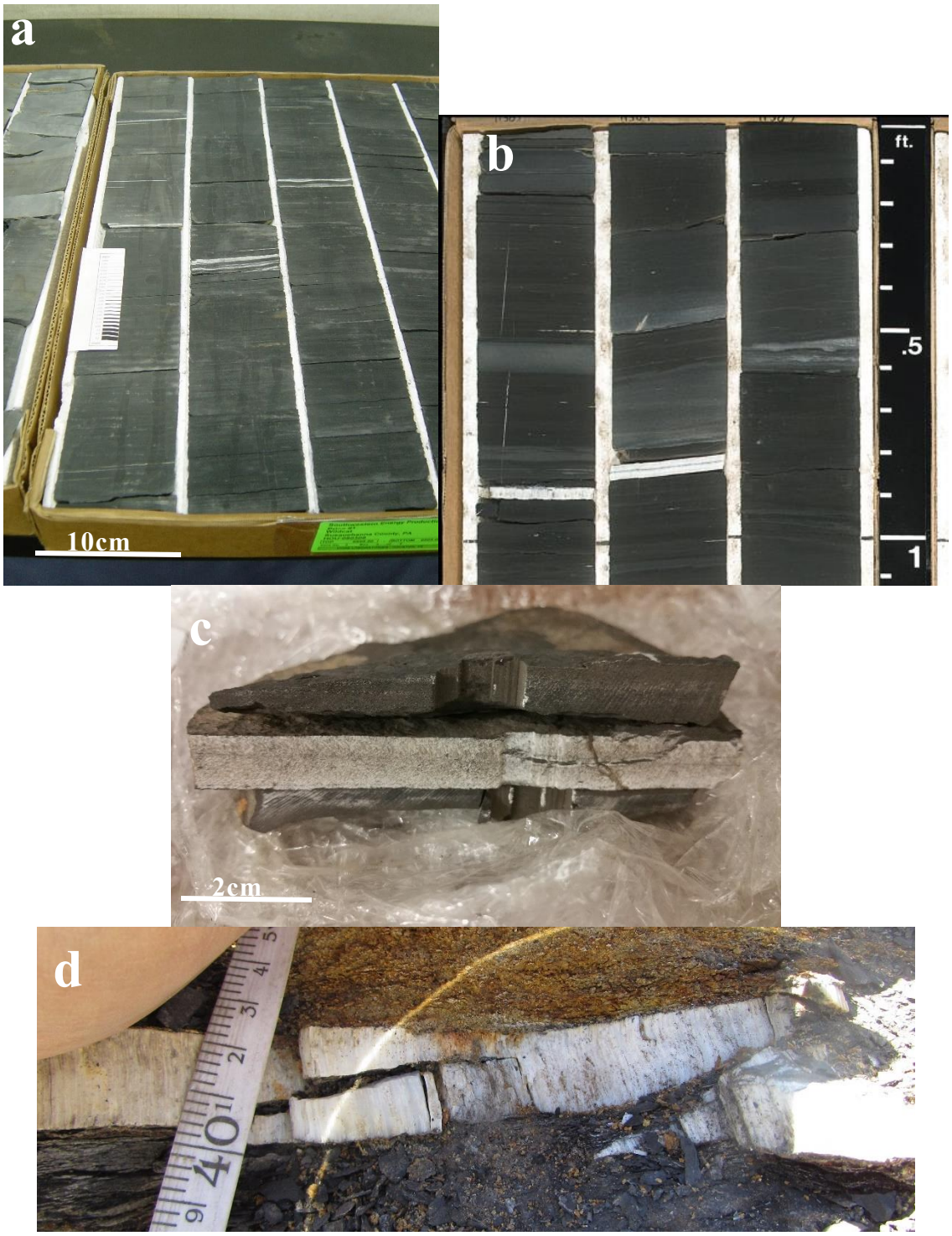

Figure 3-1 Examples of horizontal, bedding parallel fractures in the a) Marcellus core; b) Wolfcamp core; c) Vaca Muerta core; d) Vaca Muerta outcrop

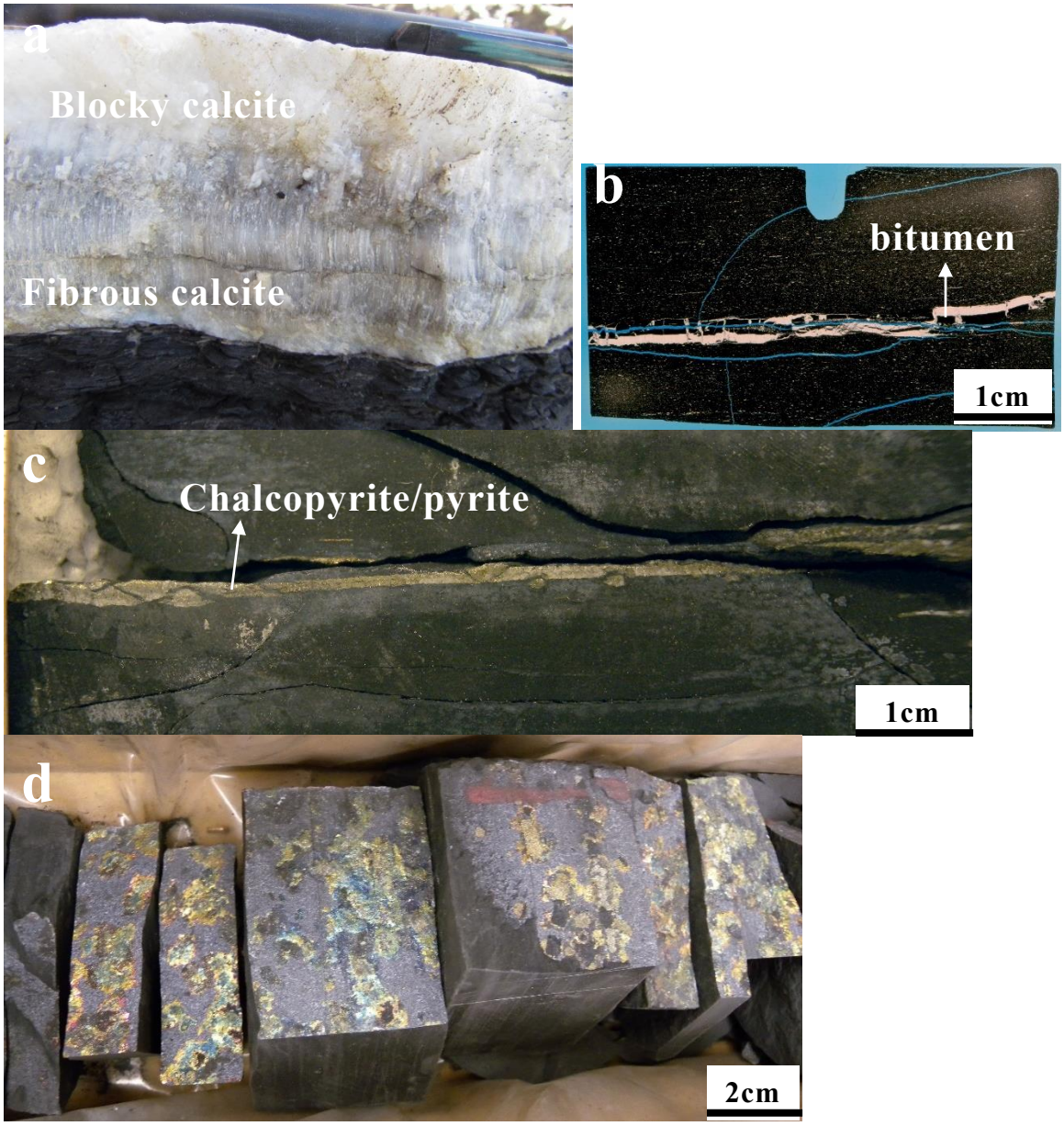

Figure 3-2 Example of common cement types observed at core/outcrop sample scale: a) Fibrous calcite cement of bed-parallel fracture. The cement near fracture wall shows blocky texture; b) Bed-parallel fracture with Calcite and Bitumen fill; c) pyrite filled bed-parallel fracture; d) Vertical fracture with Chalcopyrite-Bornite fill.

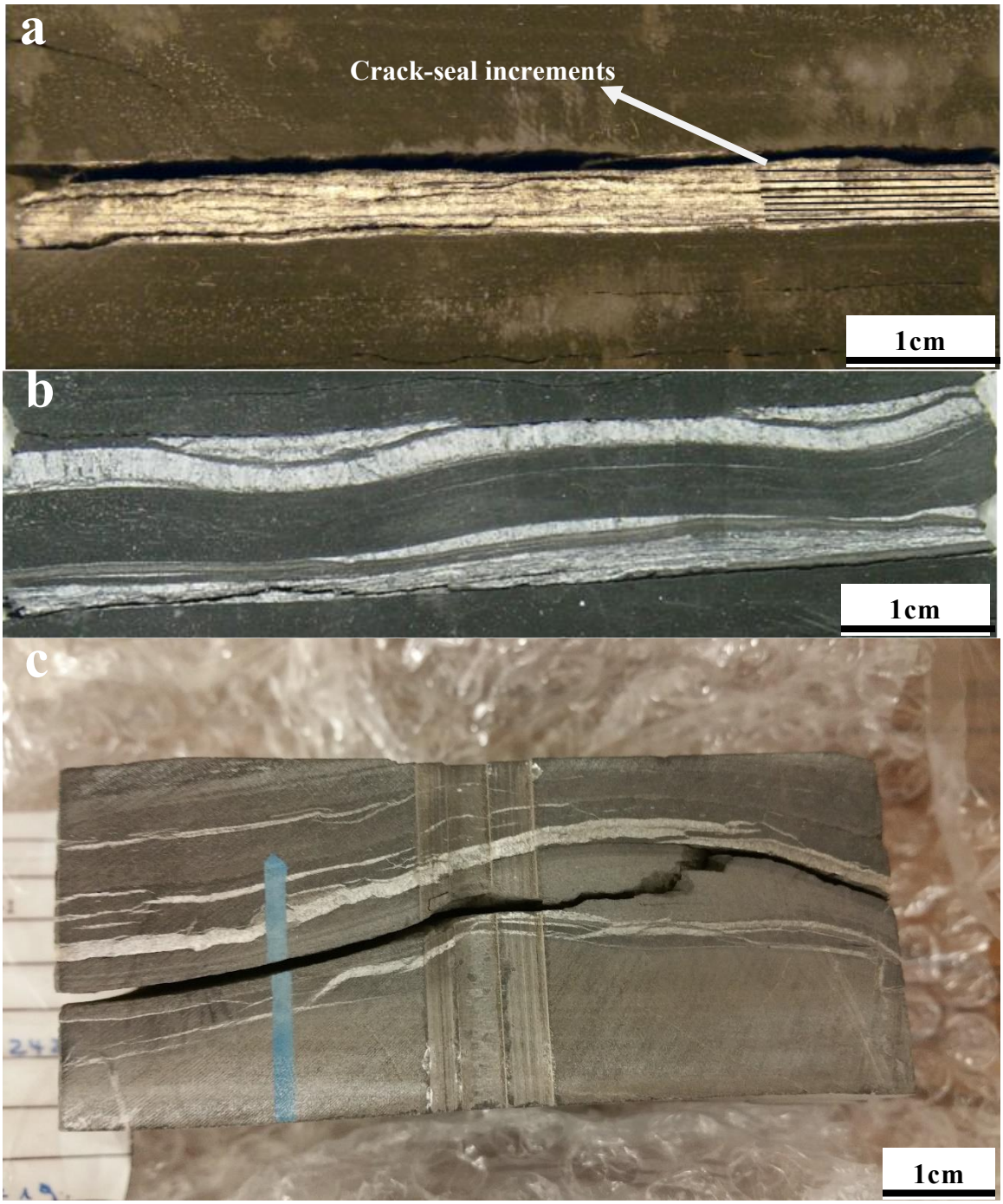

Figure 3-3 Typical bed-parallel geometry: a) Planar bed-parallel fracture with crack-seal cement texture, “inclusion trails” parallel to the fracture walls marked by black lines; b) Wavy and lens-shaped bed-parallel fractures, can be candidates of the new kinematic indicator proposed by Ukar, 2016 ; c) Branching/linking bed-parallel fractures.

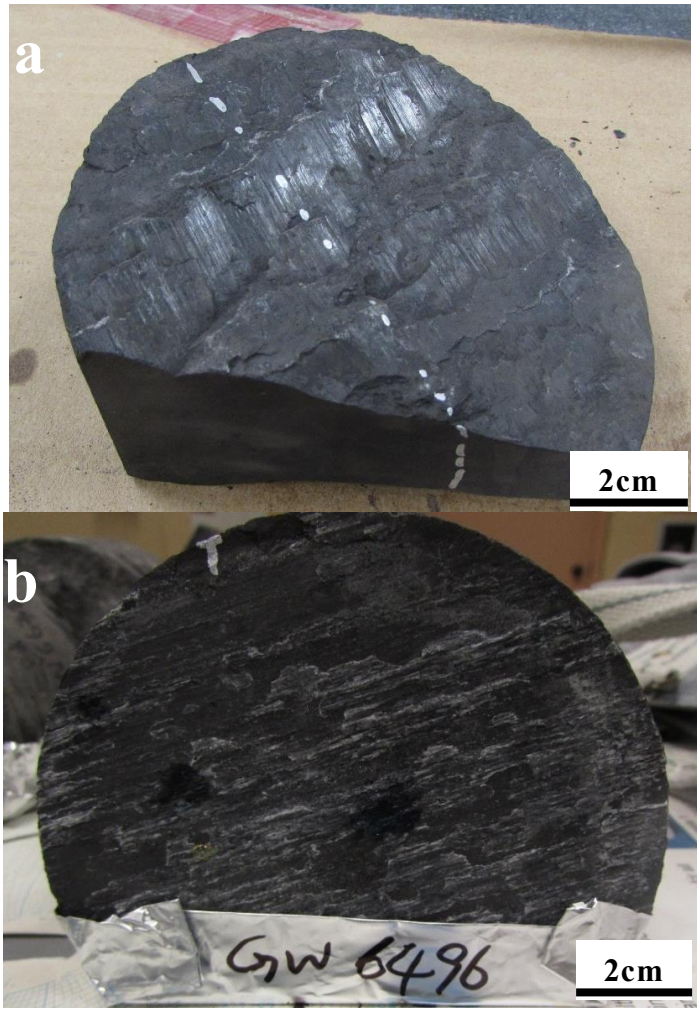
a
2cm
b
GW 6496
2cm

Figure 3-4 Fractures contain slickensides: a) low angle, non-planar fractures without cement; b) low angle thin fracture with calcite cement c) Vertical fracture with chalcopyrite/pyrite cement.

3.1.2 Fractures Around Concretion Margins

Fractures associated with carbonate or pyrite concretions are preserved in various complex pattern within the cores that are irregular and sinuous (figures 3.5a and b). The lower part of the Vaca Muerta Fm (Arroyo Mulichinco-Down outcrop) is rich in calcareous concretions (figure 3.5c). These concretions tend to be axisymmetric, oblate or spherical, so that the minor axis is perpendicular to bedding (Rodrigues, 2009). However, irregular shapes also occur. The diameter of concretions in the field is between 6 cm and a 1 m or more. Beef may occur immediately below or immediately above the concretion (figure 3.5c). The beef follows the deflections in bedding around the concretion. In general, the thickness of the beef tends to remain constant around the concretions. Concretions observed in cores are around 2-10 cm in diameter, and share similar shape with those in the field. Fractures within the concretions can preserve porosity and, though unlikely to contribute to increased porosity with hydraulic fracturing, could provide information on the fluid interactions and the structural diagenesis of the system as a whole.

A significant percentage of bed-parallel fractures are associated with concretions, either within or around the concretion. A statistical study of this type of fracture is in Chapter 5.

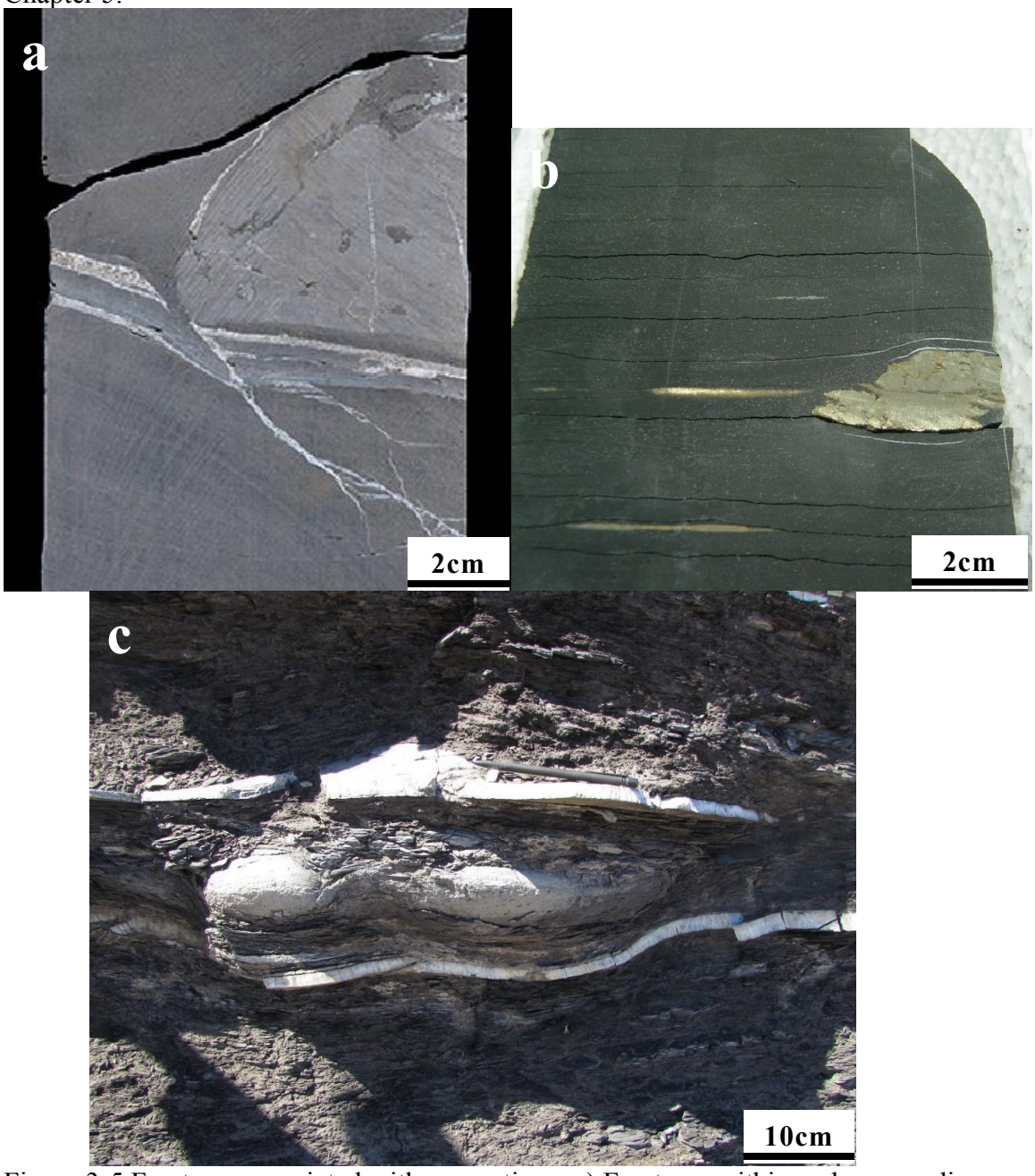

Figure 3-5 Fractures associated with concretions: a) Fractures within and surrounding concretion. Bed-parallel fracture offset at concretion boundary; b) Fracture around pyrite

concretion; c) Thick bed-parallel fracture around big calcareous concretion observed at Arroyo Mulichinco outcrop.

3.1.3 Other Morphologies

Filled to partially filled, short en-echelon or high-angle bed-bounded fractures are commonly observed in all cores (figure 3.6 and 3.7). These fractures frequently preserve porosity and potentially contribute to fluid flow and are vertically limited by stratigraphic changes or by bed-parallel fractures. Fracture fill is commonly size dependent so that some fractures in a set are filled while others in the same set are open. Fractures with complex morphologies usually have a wide range of aspect ratio. These fractures take different orientations and are likely to have different origins. Vertical or high angle fractures are not bed-parallel and are not the target of this study, but are documented here for completeness sake.

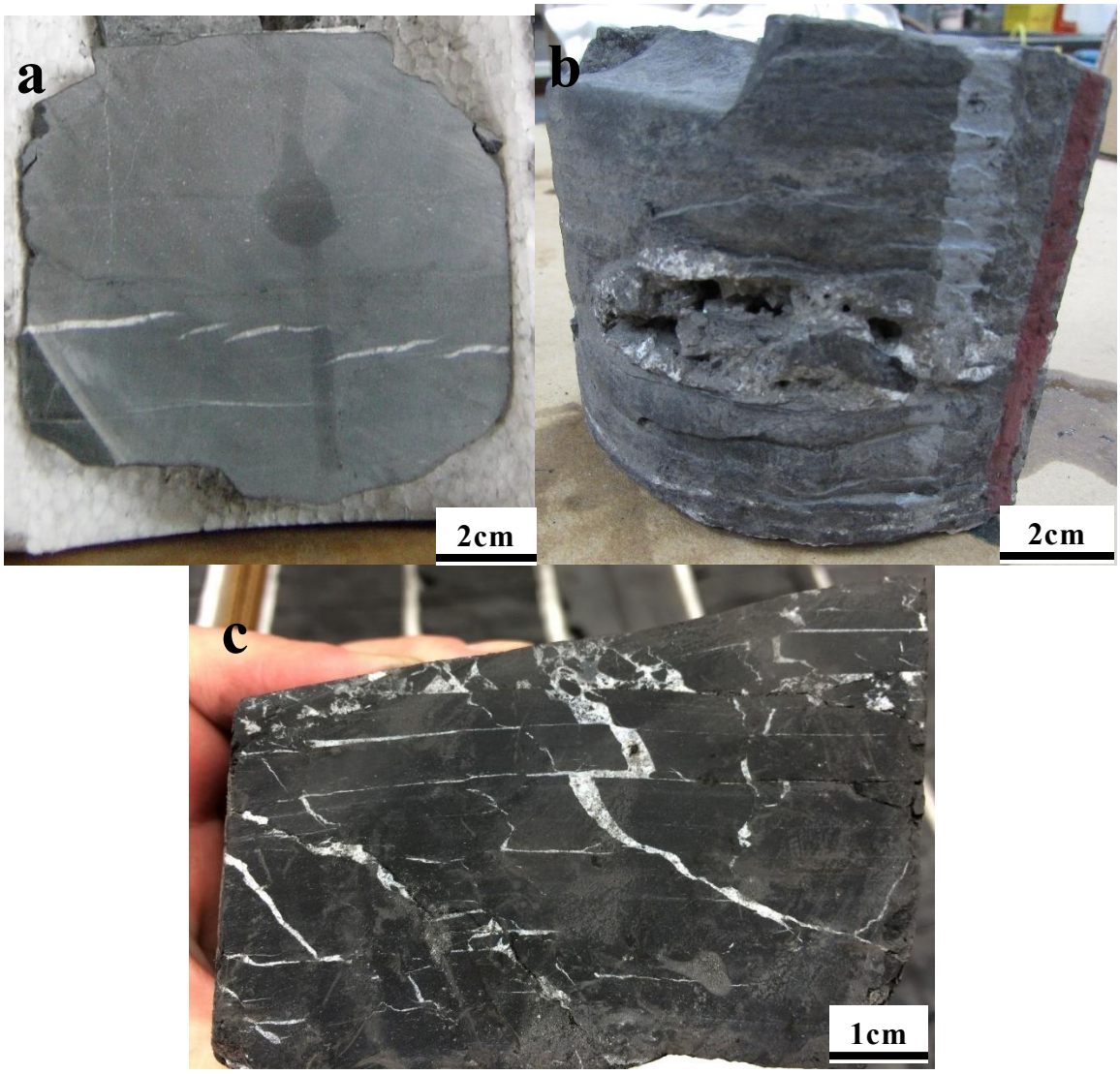

Figure 3-6 Example of filled to partially filled fractures: a) low-angle short filled en-echelon system; b) Low-angle fracture with large preserved porosity, partially filled with euhedral calcite crystal; c) Brecciated zone with a network of bed-parallel fractures, low-angle fractures and high-angle fractures. Offset within high-angle fracture indicates lateral shear. Minor porosity may be preserved.

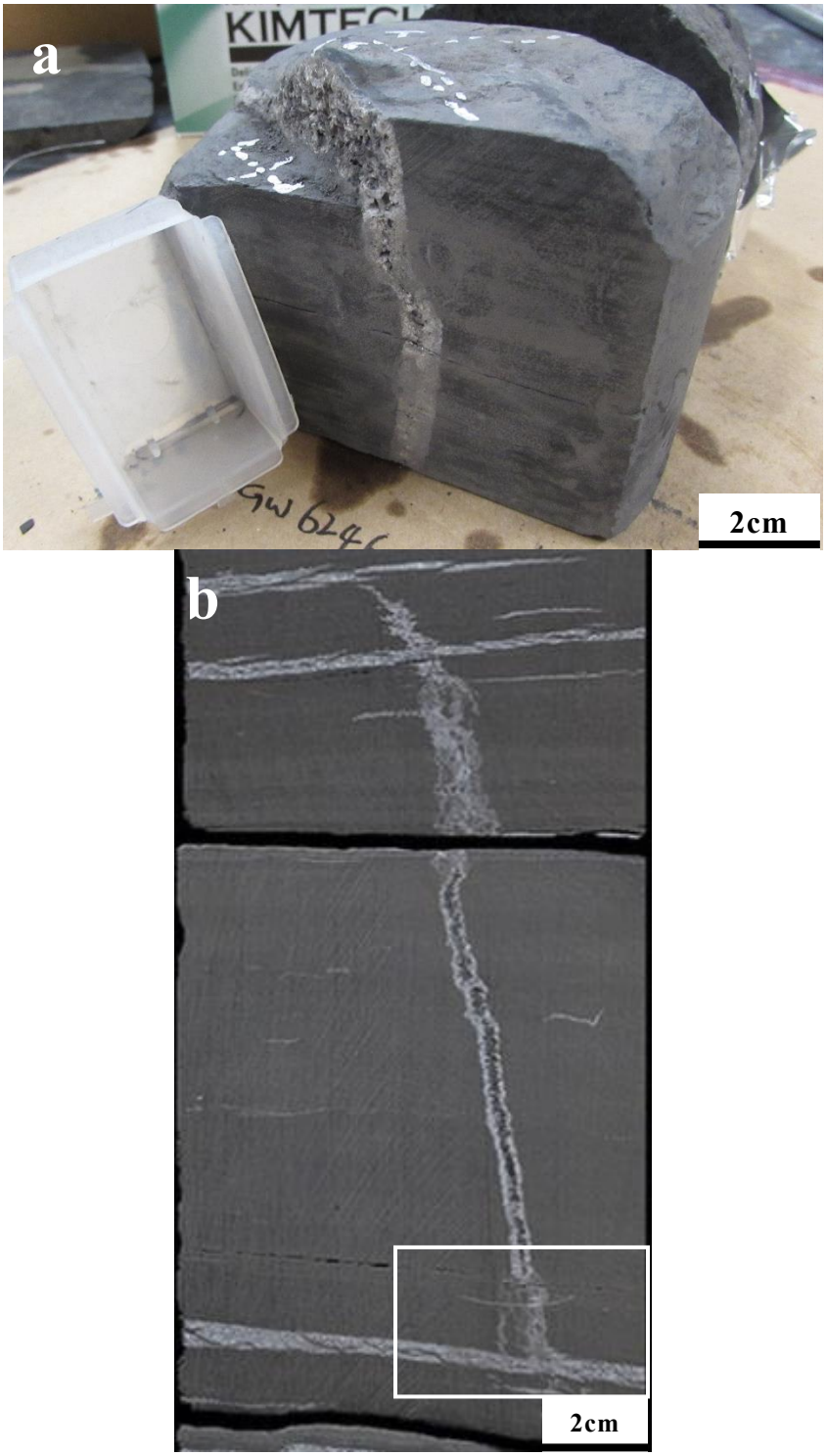

Figure 3-7 Vertical partially filled fractures: a) vertical fracture partially filled with euhedral calcite crystal; b) vertical, bed-parallel fracture bounded vertical fracture.

Observed from the bottom part of the sample, where the vertical fracture intersects the bed-parallel fracture, we can tell that the bed-parallel fracture formed earlier than the vertical fracture. The vertical fracture grow towards the bed-parallel fracture, curved near the latter's margin and stopped there. Fracture is partially filled by blocky calcite crystal coated by bitumen. The bitumen coat may help preserving porosity within the fracture.

3.2 PETROGRAPHIC AND MICROBEAM ANALYSIS

A complete archive of photographs of sampled core and scanned thin sections can be found in Appendix A. A total of 88 thin sections from the cores are included in the study. There are 19 thin sections of bed-parallel fractures sampled from three outcrops. All thin sections capturing bed-parallel fractures were made perpendicular to bedding. Field bed-parallel fracture samples were cut parallel to the major axes of the calcite fibers. The purpose of the petrographic study was to observe and describe bed-parallel fracture shape and cement texture in detail, and to identify fracture cement composition and the internal structure of typical bed-parallel veins. Under a light microscope, the cement composition and texture is identified based on the cement minerals' optical properties. Scanning Electron Microscope (SEM), Energy Dispersed Spectrometry (EDS), Electron Microprobe were also used to help identify the mineral and chemical composition of the cement, especially where mineral identification was not possible under the light microscope (for example for variations in elemental composition for a given mineral, or for very small grains). Cathodoluminescence (CL) was used to analyze the texture of fracture cement and compare to that of the fossils, which can be confused with thin planar bed-parallel fractures with fibrous cement.

3.2.1 Bedding-Parallel Fractures: Internal Structure

Typically, thick (>5mm aperture) bed-parallel fractures with fibrous cement (beef) have different zones within the cement; inner zones and outer zones (Rodrigues,

2009). Between the inner zones is a median suture, which carries inclusions of wall rock and that is usually dark shale. The outer zones are next to the fracture wall. The inner zones are usually darker in color compared to the outer zone (figure 3.8). The fibers are usually perpendicular (or nearly perpendicular) to bedding in inner zones, but oblique to bedding in outer zones (figure 3.9). In the outer zones, the fibers vary in orientation. There can be several outer zones marked by an abrupt change in fiber orientation and apparent plunge. The dip direction of fibers at different sides of the median line can be the same or opposite (figure 3.9 and figure 3.10c).

In thin section, the fibers consist predominantly of calcite. Occasional gypsum (3.9), dolomite (3.12), chalcopyrite/pyrite/bornite (3.11), quartz (3.11) and barite/Celestine (3.12, 3.13) appear to be replacements. The fibers of calcite are single crystals and appear to have grown in optical continuity within each zone, and in rare cases, across zones. Typically, the calcite fibers have a large aspect ratio of length to width. The width of the fibers can be tens of times larger at the outer zone than that in the inter zone, if the cement does not turn blocky at the outer zone. The sides of the fibers are smooth, indicating a lack of growth competition with neighboring fibers.

The median suture lies between the inner zones, but it is rarely the geometric middle surface of the vein (figure 3.10a and b). The beef can be highly asymmetrical that the median suture may be quite close to the fracture wall. The median suture can be quite faint with just a thin trace of hostrock inclusions, or it can be pretty fat. The median suture may be offset by vertical shear, or it can just branch out and end up developing into two or more separate beefs.

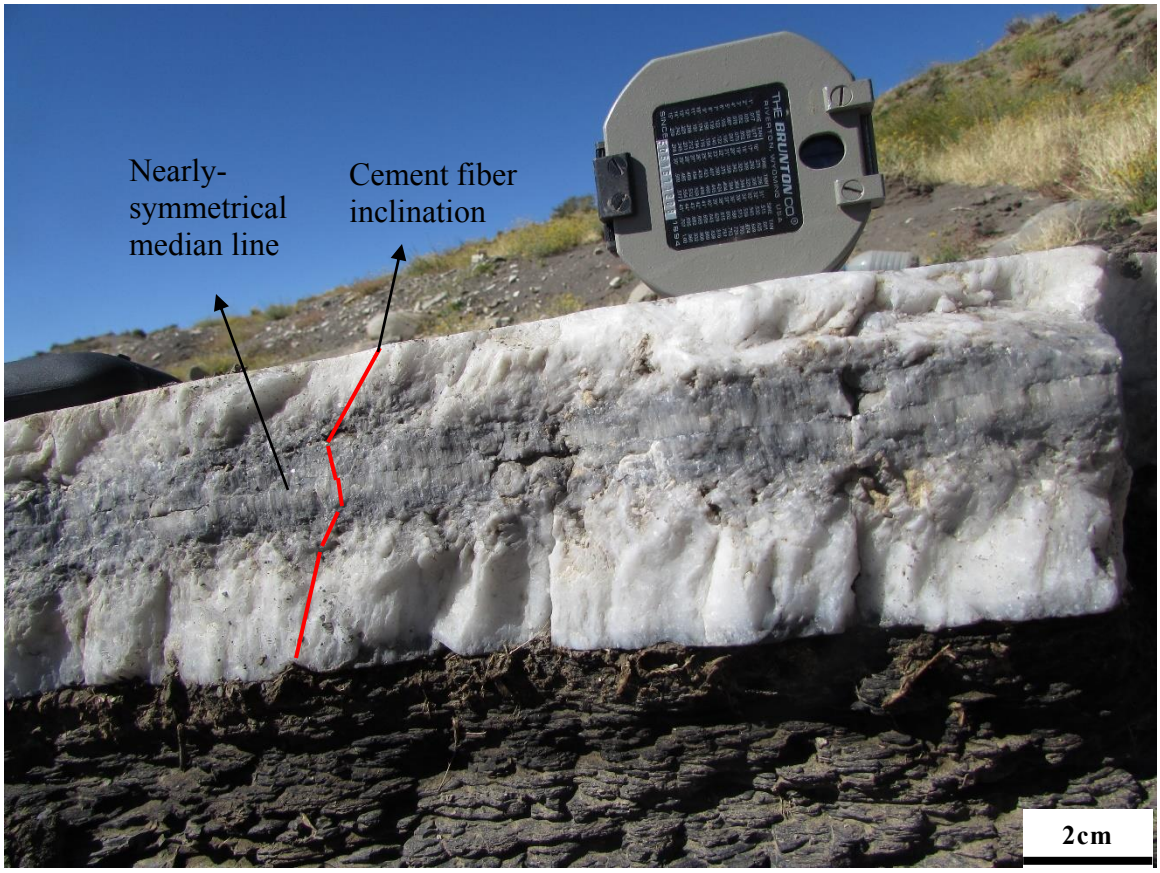

Figure 3-8 Bed-parallel fracture at outcrop. According to Rodrigues, 2009, the darker zones in the middle is called the inner zones, the whiter zones closer to the fracture wall are called the outer zones.

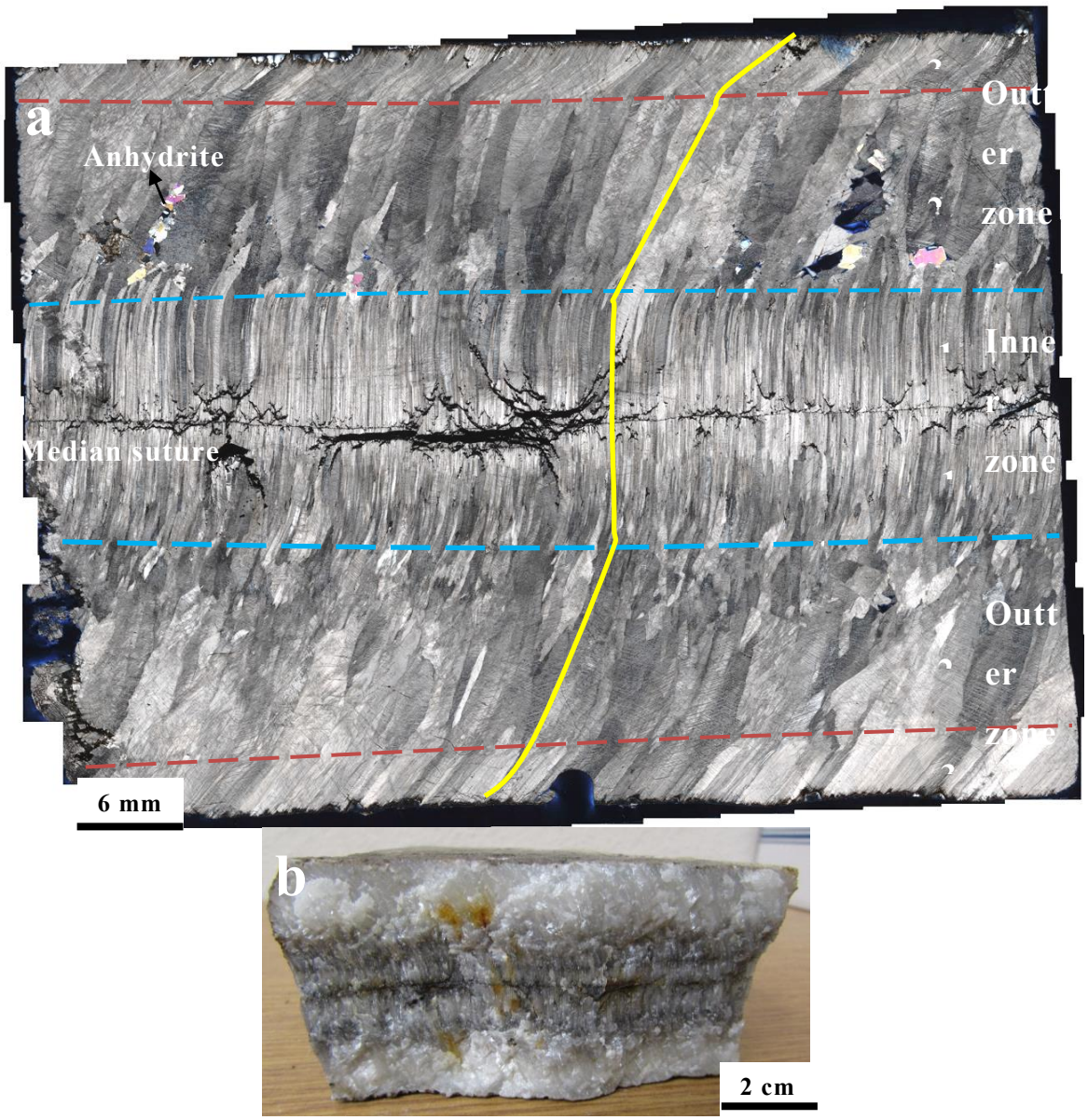

Figure 3-9 Internal structure of beef, Vaca Muerta Arroyo Mulichinco-up outcrop. Sample QWVM_M7. GPS location 038º 01.222'S, 070º 27.198'W. (a) In thin section, under polarized light. Calcite fibrous cement. Minor anhydrite replacement. Cement can be divided into 2 major zones with 3 generations of growth. In inner zones (grey), fibers are perpendicular to bedding. Some of the fibers increase in width away from suture, whereas others thin or disappear. In outer zones (white), fibers are thick and oblique to bedding. Fibers in the same generation of growth share similar plunge. The plunge of the fibers in each generation of growth is similar. Fibers are tilting toward the same apparent direction. (b) QWVM_M7 as hand specimen, Beef is parallel to bedding in Vaca Muerta Fm. Dark median line is observed between the grey inner zone, which is sandwiched between the white outer zone.

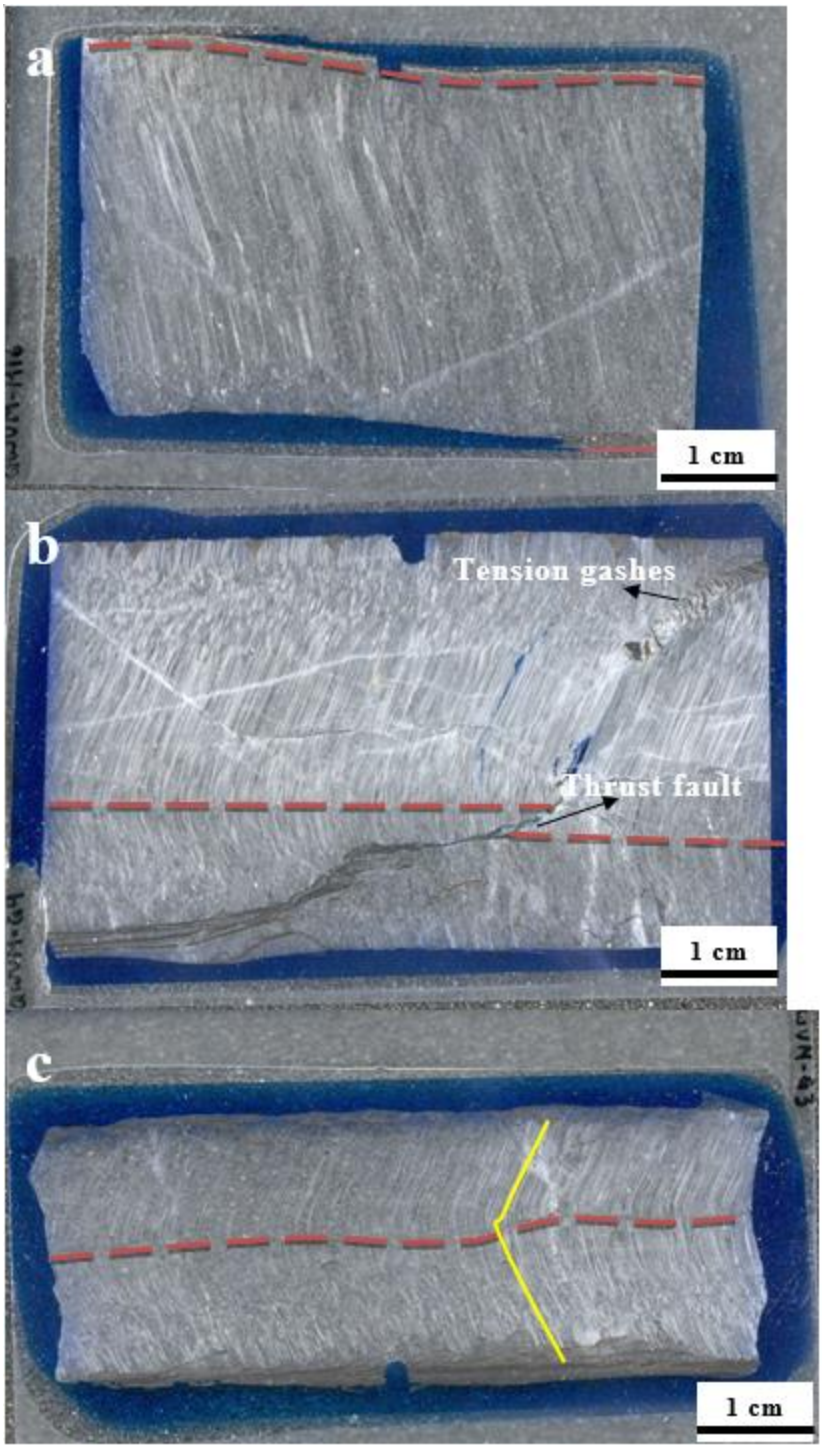

Figure 3-10 The median suture rarely the geometric middle surface of the vein, example from Vaca Muerta formation; a) sample QWVM_M16. Beef is highly asymmetrical that the median suture is quite close to the fracture wall; b) sample QWVM_G9. Asymmetrical beef, the median suture is offset by vertical shear. The shear surface is

marked by hostrock inclusions. Thrust fault and tension gashes can be identified from this thinsection; c) sample QWVM_G3. Beef with fish-bone cement texture. Fibers from different sides of the median line are dipping the opposite direction.

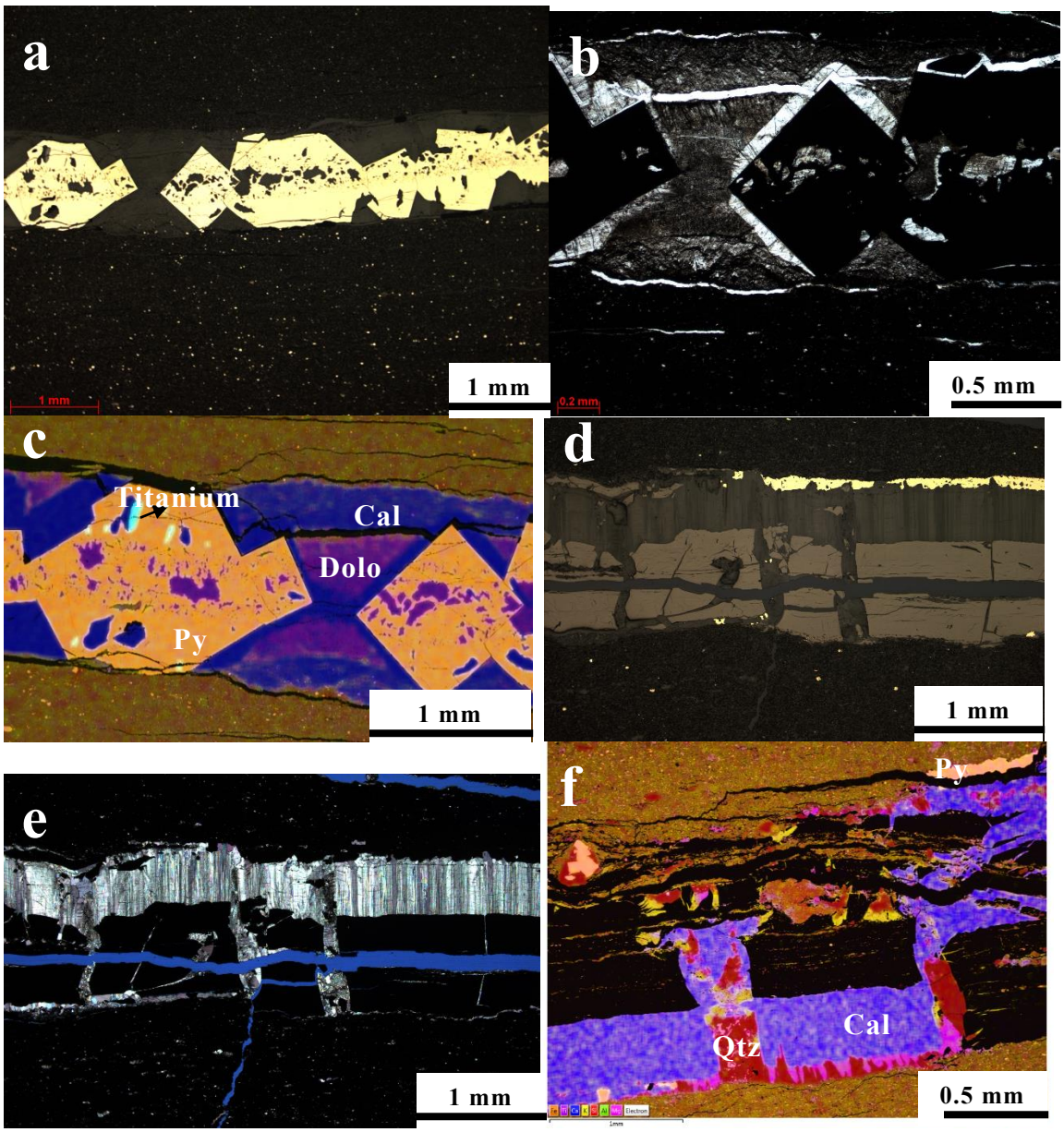

Figure 3-11 Bed-parallel fractures with multiple phases of cements, examples from Marcellus formation; a), b) and c) Sample Pr6579 under reflected light, transmitted light and EDS. Bed parallel fracture filled with calcite, dolomite, euhedral pyrite and assessor titanium. Stress shadow indicated by inclusion-free fibrous calcite around the pyrite crystal; d), e) and f) Sample Pr6704a under reflected light, transmitted light and EDS. Cements include calcite, quartz, pyrite and minor dolomite. In sample Pr6704a, pyrite

form replacement texture at the margin of the vein. In sample Pr6579, euhedral pyrite form along the median line indicates long period of time of fracture opening and cement precipitation.

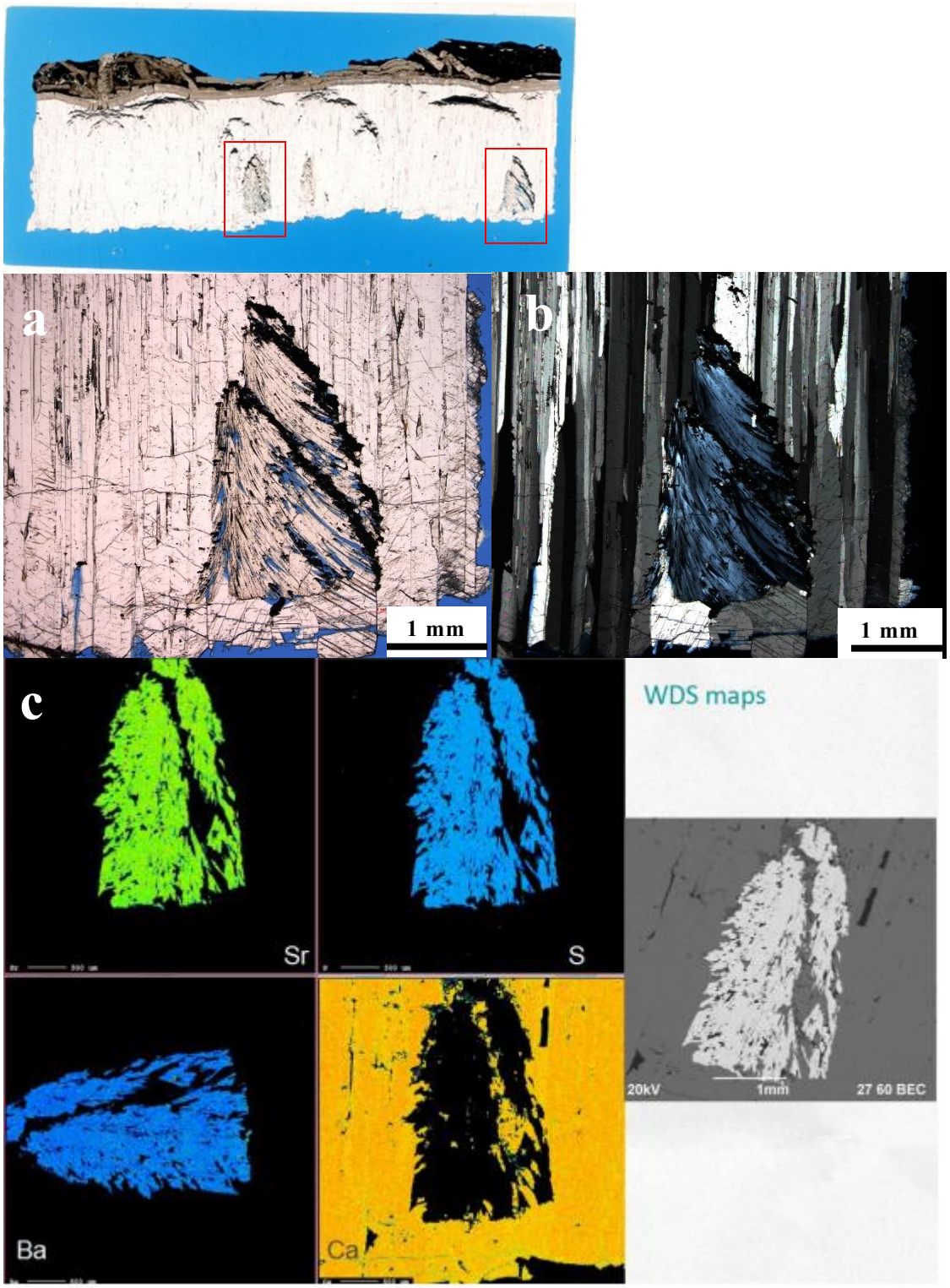

Figure 3-12 Celestine (Sr-BaSO4) cone with host rock (Shale) inclusion. Sample Wolfcamp W11301.9. Solid solution between BaSO4 and SrSO4. Both Ba2+ and Sr2+

have high ionic potentials (the ratio of charge to ionic radius) and can be readily accommodated in aqueous solution as hydrated divalent cations. Natural barite and celestine rarely exist as completely pure end-member phases; there is a wide variation in Sr/Ba and the incorporation of other cations; a) Celestine cone under transmitted light; b) under cross polarized light; c) WDS maps of Celestine cone, sounded by fibrous calcite bed-parallel fracture cement.

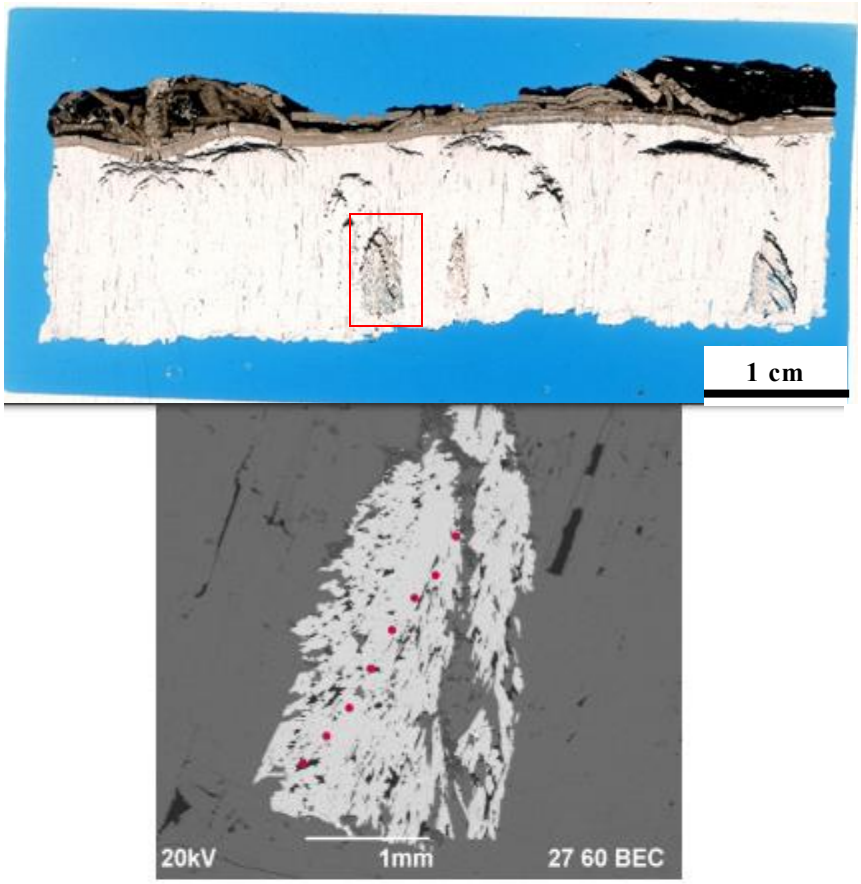

ELEM:	S	Sr	Ba	O	SUM
19	16.391	32.923	17.676	32.608	99.598
20	16.330	34.213	16.371	32.601	99.516
21	16.360	33.687	16.974	32.620	99.641
22	16.149	31.641	19.431	32.216	99.437
23	16.235	32.280	18.546	32.359	99.421
24	16.272	31.300	19.168	32.307	99.047
25	16.078	31.402	18.918	32.007	98.405
26	16.066	31.351	19.258	32.020	98.695
AVER:	16.235	32.349	18.293	32.342	99.220
%RSD:	.77	3.52	6.29	.78	

Figure 3-13 Barite/Celestine cone EPMA point analysis result in Elemental Weight Percents. According to Microprobe analysis, the ratio of S/O kept decreasing along fibers

while Sr/Ba is not showing any trend. However, the result shows once Sr increase, Ba decrease.

Other Notable Observations

When two bed-parallel fractures are growing toward each other, it is common that they "see" and curve towards each other, sometimes linking together (figure 3.14). This morphology is the result of the interaction of the growing fractures with the stress fields at the tips.

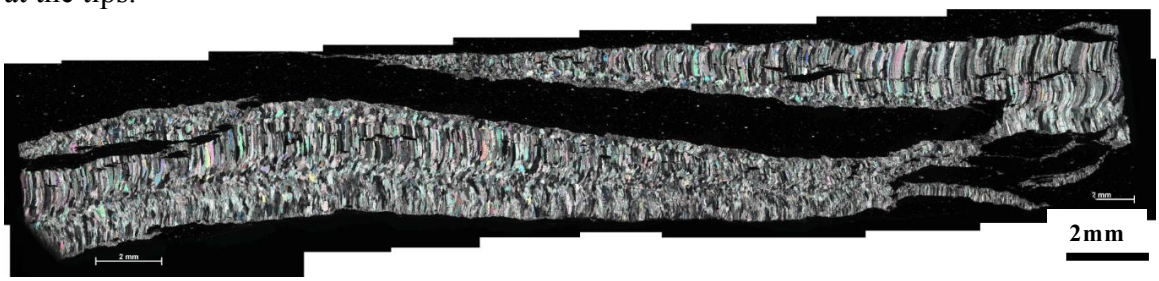

Figure 3-14 Two fractures grew in opposite directions, getting closer and curving toward each other before they met and linked together.

In the Vaca Muerta beef, imprints of monotoid bivalves (Damborenea & Leanza 2004, Rodrigues 2009) and ammonites are common at the outer surfaces of the veins (figure 3.16a). The imprint may be either an inner mold or an outer mold. In thin section, the original shell is visible at the suture and has overgrowths of calcite fibers (figure 3.15b). However, the fibers are not in optical and textural continuity with the original shell. The association of fossils with bed-parallel fractures indicates that fossils embedded in shale can act as a preferred surface of cement precipitation.

Vertical fractures can terminate at the bed-parallel fractures. In such case, relative timing of bed-parallel and vertical fractures can be determined. Figure 3.7 is an example of bed-parallel fracture bounded vertical fracture at core scale. Figure 3.16 is an example of vertical fracture terminate at bed-parallel fracture at thin section scale. Just abrupt change in hostrock lithology, the bed-parallel fracture can be considered a strong layer within the hostrock that cause vertical mechanical heterogeneity. In this thinsection the

thick vertical fractures are bounded by dolomite later above and bed-parallel fracture below. If the energy of vertical fracture is not strong enough to make it penetrate through the pre-existing bed-parallel fracture, then the vertical fracture will stop at bed-parallel fracture surface.

Another observation from figure 3.16 is that, the mechanical properties of hostrock has great influence on the generation of vertical fractures. At upper part of the thin section, there are interlayered dolomite and shale. In most cases, fractures are more likely to form within rigid layer (dolomite) compared to soft layers (shale) next to it. However, in this thin section, vertical fractures preferentially formed within the shale layer rather than the dolomite layer. This observation may indicate that the mechanism forming vertical fractures in shale is different from that in other types of rock. It may have something to do with the loss of water within shale under mild compression. The loss of water deceases the volume of shale and cause fracturing, while dolomite remains unreformed. Of course, if the compressional force is too large and it exceeds the strong dolomite layer's yield strength, vertical fracture will be generated within dolomite layer as well.

Although most bed-parallel fractures in this study have fibrous calcite cements, especially the ones with >5mm aperture. However, there are thick bed-parallel fractures that has blocky fracture cement. Figure 3.17 is an example of a bed-parallel fracture with around 5mm aperture and has blocky calcite cement. Blocky calcite cement indicates enough open space between fracture walls, enough diagenetic fluid flow through the fracture, and enough time for precipitation. The crack-seal texture observed within the blocky calcite cement records several opening event after the cement was precipitated. Blocky fracture cement is also typically found in brecciated zone. Intense deformation lead to brecciating of the hostrock, which means quick opening of large spaces within the

hostrock. If the void space remained available and there was enough fluid flow brings in the chemicals after that, blocky fracture cements could be formed (figure 3.18).

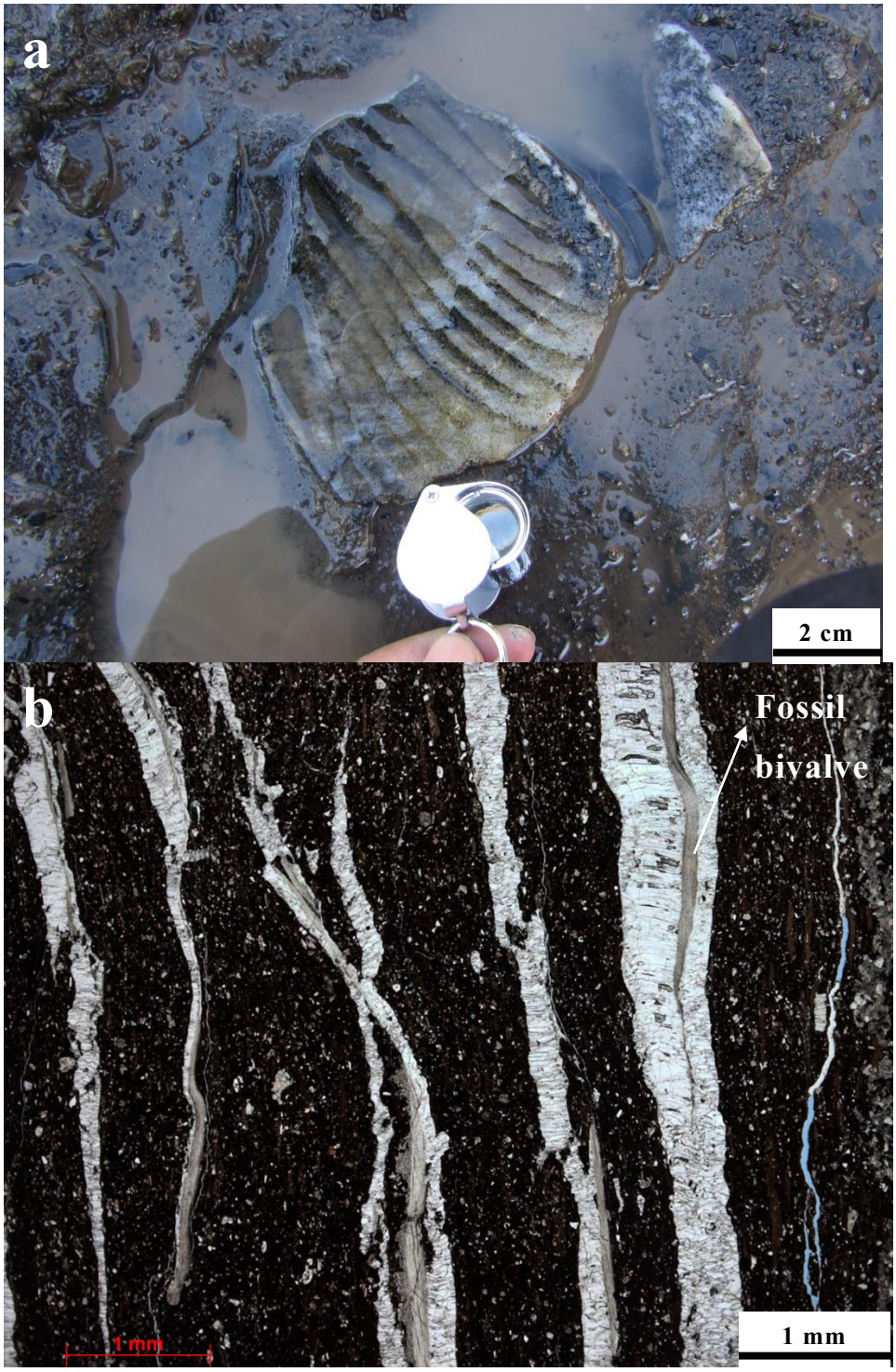

Figure 3-15 Bed-parallel fractures associated with fossils, example from Vaca Muerta 1-9-M; a) imprint of bivalves at the outer surfaces of the veins; b) original shell is visible at the suture and has overgrowths of calcite fibers.

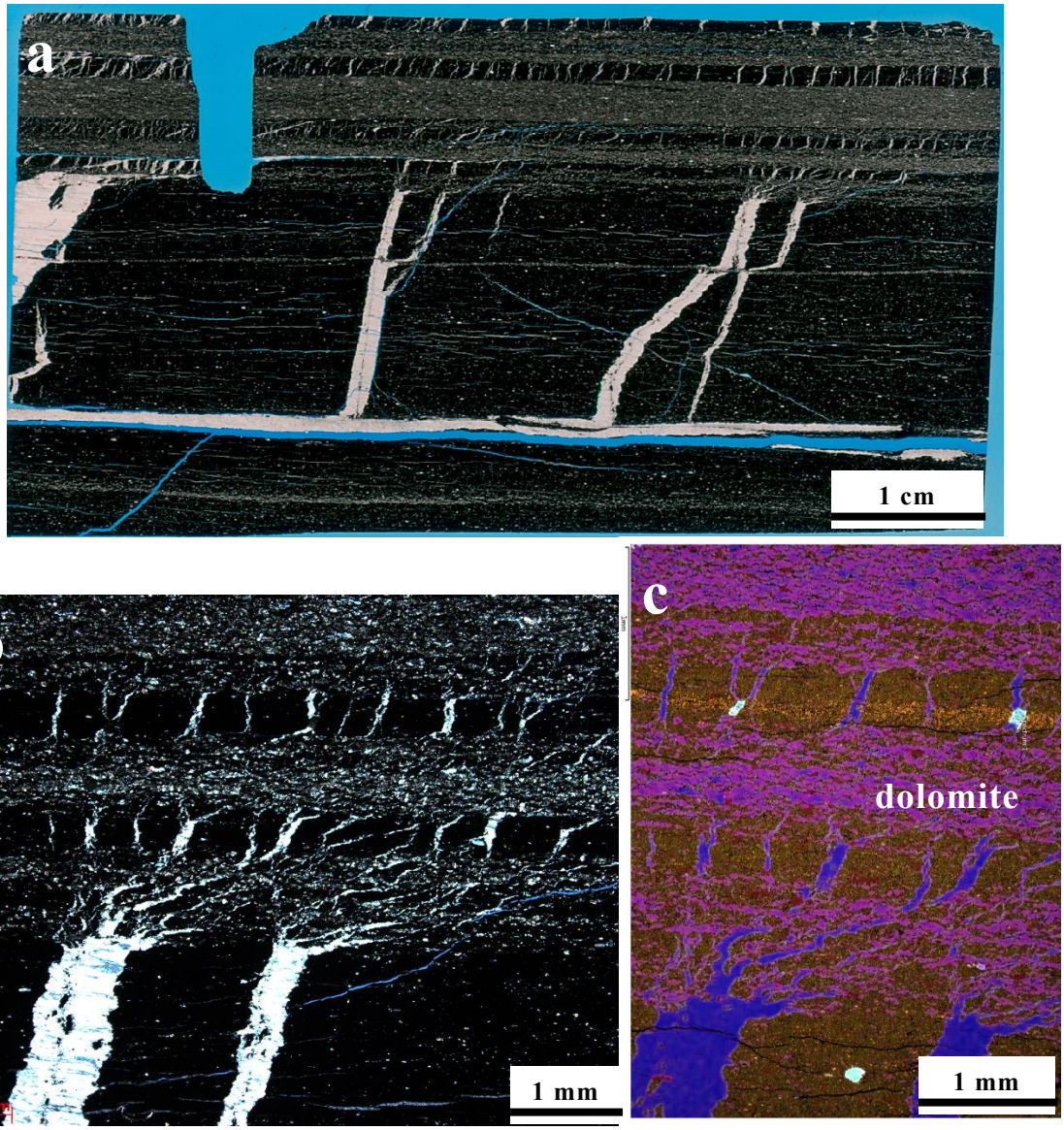

Figure 3-16 Example of vertical fracture terminate at bed-parallel fracture at thinsection scale, exampled from Marcellus fromation; a) Thick vertical fractures is bounded by dolomite later above and bed-parallel fracture below. At upper part of the thinsection, there are interlayered dolomite and shale; b) and c) in this thinsection, vertical fractures preferentially formed within the shale layer rather than the dolomite layer.

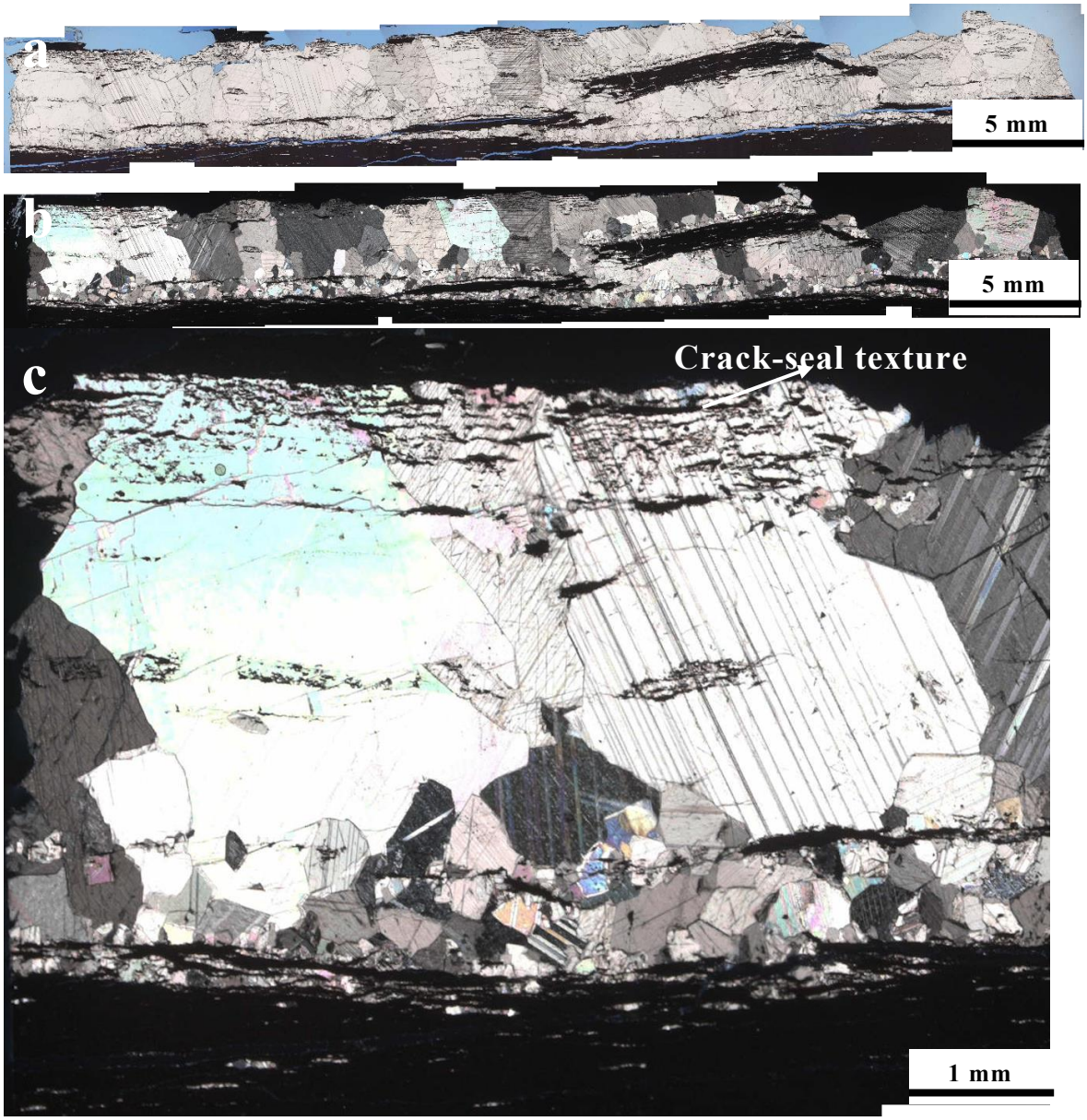

Figure 3-17 Marcellus formation, GW6512a. Example of a bed-parallel fracture with around 5mm aperture and has blocky calcite cement. The crack-seal texture records several opening event after the blocky calcite cement was precipitated.

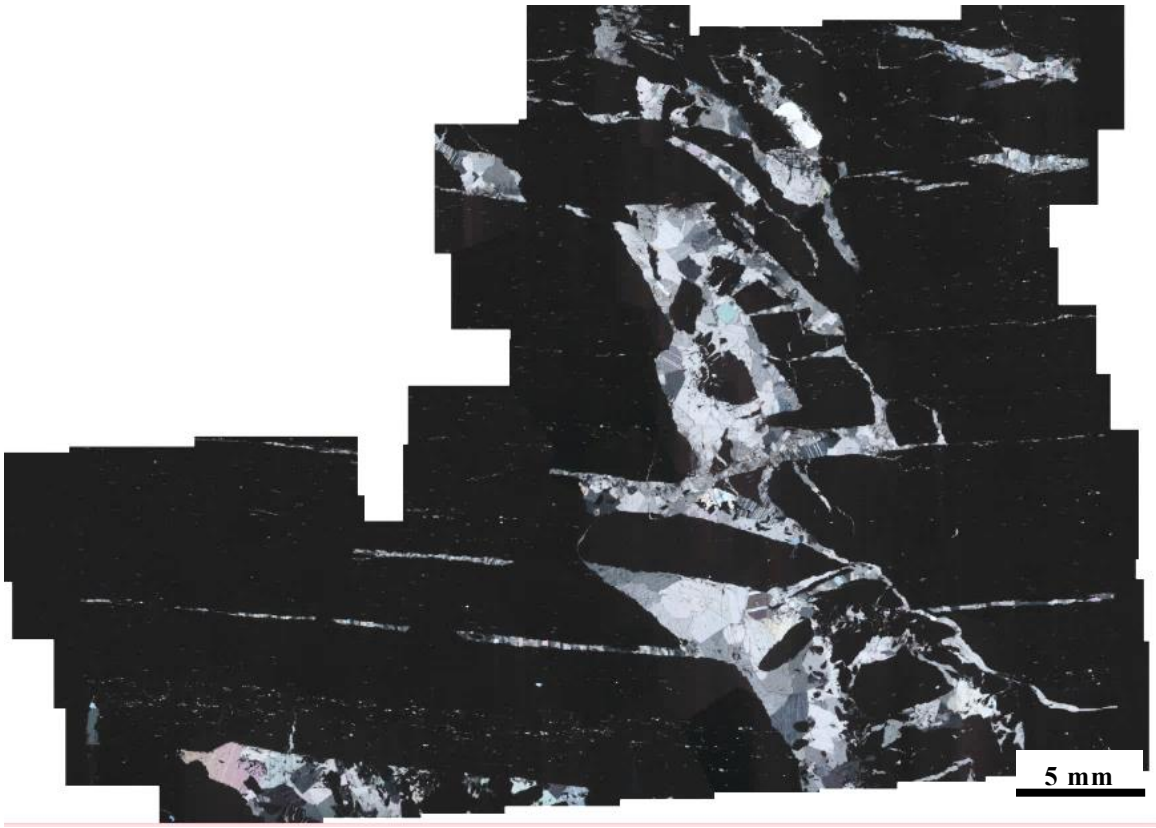

Figure 3-18 Blocky fracture cement found in brecciated zone. Intense deformation lead to brecciating of the hostrock. Quick opening of large spaces within the hostrock, fluid flow and enough time for cement precipitation lead to blocky fracture cements in the brecciated zone.

Chapter 4. Bed-parallel Fracture Size Distribution: Interpreting size scaling curves

This chapter is about presenting and interpreting bed-parallel fracture-size distribution data measured along 1D vertical scanlines (chapter 2). Different from previous research, my study focuses on the size scaling of bed-parallel fractures in shale, including aperture size and fracture length scaling. Aperture-length relationship is also discussed in this chapter. Most size-scaling studies have been done on vertical fractures in sandstones (Marrett et al 1999, Bonnet, 2001, Gillespie et al 2001, Deschamps et al. 2007, Schultz et al. 2008, Hooker et al. 2009, Hooker et al. 2012) and carbonates (Marrett et al. 1999; Ortega et al. 2006,). There are a few published data sets for vertical fractures in shale (Gale et al., 2014). However, there is nothing published for bed-parallel fracture size distribution. Therefore, the aim of my work is to study the size scaling of bed-parallel fractures. In this chapter, I will compare the results of my study with the published data for vertical fractures.

Here are some hypotheses we want to test regarding bed-parallel fracture aperture size distribution. Aperture size distribution may follow a power-law as is common for vertical fractures. Alternatively, they may follow a different function such as exponential. Other possibilities include that the fractures tend to have preferred sizes, or they do not follow any function at all. To test these hypotheses, robust datasets were collected from Vaca Muerta Formation, Marcellus Formation, and Wolfcamp Formation.

4.1 Introducing fracture size and intensity curves

Fracture intensity in this study refers to linear intensity of fractures. It describes a spatial abundance of fractures. Fracture intensity (F) in this study is most commonly

determined from one-dimensional observation domains (i.e., scan lines) by dividing the number of fractures (N) by the total length (L) of the scanline:

$$F = N/L \qquad \text{(Eq.4-1)}$$

Direct field/core measurements N/L along a straight line give unbiased estimates of fracture linear intensity (Figure 4-1). Ortega et al., 2006 proposed a scale independent approach to fracture intensity and average spacing measurement, which makes use of fracture size distributions, and allows more meaningful comparisons between different locations. It also allows both macro- and micro- fractures in subsurface samples to be used for fracture-intensity measurement. According to Ortega et al., cumulative-frequency fracture-size distributions provide a measure of fracture intensity (or average spacing) that explicitly accounts for fracture size and permits a comparison of data collected at different locations and/or observation scales. Traditional methods (e.g., Bogdonov, 1947; Ladeira and Price, 1981; Narr and Suppe, 1991; Wu and Pollard, 1995; Narr, 1996; Schopfer et al., 2011) of fracture-intensity measurement are inadequate because they ignore the wide spectrum of fracture sizes found in many fracture systems and the consequent scale dependence of fracture intensity. It is a common flaw shared by all previous empirical investigations. The scanline datasets collected for this study are from three general sources: measurement from outcrops, direct measurement from core, and measurement from core images. Each of the sources allows datasets to be collected at different scales of observation or levels of resolution. Following the method proposed by Ortega et al 2006 makes the study of cumulative-frequency fracture-size distributions has significant advantages over the traditional method that do not account for size.

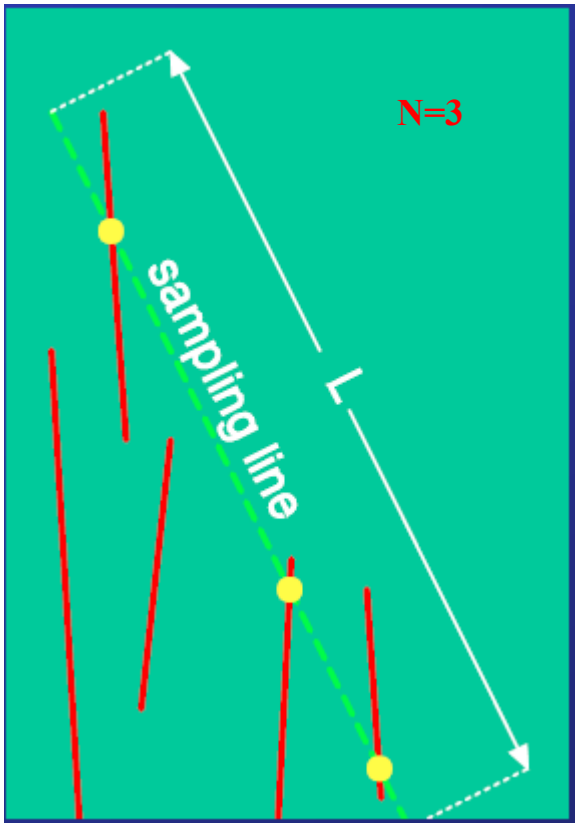

Figure 4-1 The illustration of measuring fracture linear intensity(F). F=N/L.

Using cumulative frequency fracture-size distributions with normalized fracture intensity effectively quantifies fracture intensity for detection thresholds corresponding to all fracture sizes considered. It makes the scaling work makes more sense because common thresholds of fracture size can be enforced for counting in different locations, and source of data. This method is equally applicable to any cumulative size distribution.

Following the method proposed by Ortega et al., 2006, cumulative-frequency fracture-size distributions plots were generated by: firstly, number the sorted fracture sizes from large to small, with maybe several fractures sharing the same size; then simplify the list by eliminating all fractures having the same size (given the resolution of measurements), except for the one with the largest cumulative number; lastly, normalize the cumulative numbers by the length of the scan line. This method will generate

estimates of the number of fractures of a certain size or larger per unit length of the scanline, which is called cumulative frequency of a certain fracture size along the scanline. Lastly, we plot cumulative frequency versus fracture size to provide a graphical display of the distribution. Both axes are in logarithmic scales.

Table 4-1 Example scanline data table.

Example scanline dataset		Scanline length: 25.54 m		
aperture (mm)	spacing (m)	Aperture sizes (mm)	cumulative number	cumulative frequency
0.14	0.088	10	1	0.039154268
3.3	1.134	5	2	0.078308536
1.4	0.268	3.3	3	0.117462803
1.8	1.128	2.65	4	0.156617071
5	3.993	1.8	5	0.195771339
0.39	2.027	1.75	6	0.234925607
0.05	2.454	1.4	7	0.274079875
0.4	0.655	1.15	8	0.313234143
2.65	0.838	0.75	10	0.391542678
0.75	8.778	0.5	11	0.430696946
1.75	0.091	0.4	13	0.509005482
0.095	0.030	0.39	14	0.548159749
0.14	0.012	0.14	16	0.626468285
0.05	0.018	0.095	17	0.665622553
0.05	0.003	0.05	20	0.783085356
0.4	0.003			
1.15	0.055			
0.75	0.091			
0.5	3.603			
10	0.238			
total				
30.765	25.509			

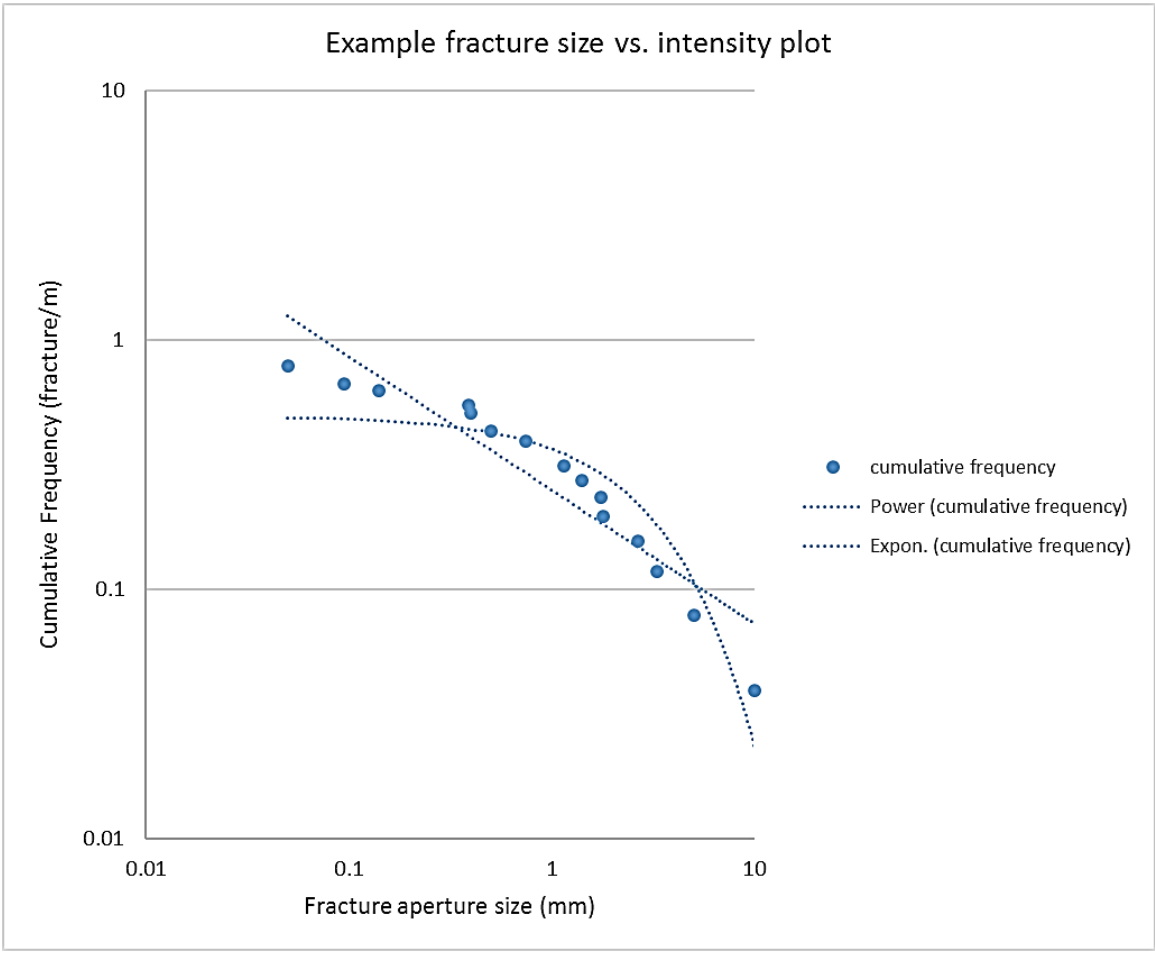

Figure 4-2 Example of fracture size vs. cumulative frequency plot (aperture size scaling curve).

Although fracture-size frequency curve has limits of scale (Hooker 2012), fracture-size distributions may still be adequately modeled using simple mathematical laws, such as power law or exponential laws. Parameters of the best fit model for the distribution can be observed from the plots (e.g., coefficient and exponent of the power law, as determined by regression).

4.2 SIZE DISTRIBUTION EQUATIONS, AND RELATED IMPORTANT PARAMETERS

Many vertical opening-mode fracture systems and fault systems in sandstones, carbonates, shale, and other lithologies show an organization of fracture sizes such that

their cumulative size distribution can be described by a simple power-law relationship (Gudmundson, 1987; Wong et al., 1989; Heffer and Bevan, 1990; Barton and Zoback, 1992; Gillespie et al., 1993; Hatton et al., 1994; Sanderson et al., 1994; Belfield and Sovich, 1995; Clark et al., 1995, Gross and Engelder, 1995; Johnson and McCaffrey, 1996; Marrett et al 1999; Ortega and Marrett, 2000; Bonnet et al., 2001, Ortega, 2002, Ortega at al., 2006, Hooker, 2012, Gale et al., 2014). A power-law of the form:

$$F = aX^{-b} \qquad \text{(Eq. 4-2)}$$

best describes the aperture size distribution in these examples. F is cumulative frequency, X is fracture size (aperture size in specific), a and b are empirical parameters which are constants referred to as the coefficient and exponent of the fracture aperture distribution, respectively, and vary with the size of the observation domain. So power-law size distributions can be considered as scale-invariant. The exponent *b* is also commonly called the fractal dimension of the distribution. The coefficient *a* is a measure of the abundance of fractures in the observation domain. (Ortega, 2002). In nature, fracture sizes have upper and lower limits, which places limits on the power-law scale range that is valid. Theoretical and geological considerations may provide limits to actual fracture size. However, there has been little attempt in the literature to evaluate naturally occurring upper and lower cutoffs to observed power law distributions. Moreover, the limited previous attempts are all made on vertical fractures, not bed-parallel fractures. It is now generally recognized that resolution and finite size effects on a power law population can also result in distributions that appear to be exponential or lognormal in real life (Bonnet et al., 2001, Hooker, 2012). However, as mentioned earlier, although much work has done on vertical fracture and fault systems in various geologic media, there is no published study discusses associated physical processes generating power law distribution of bed-parallel fractures in shale.

Similar to vertical fracture aperture size distribution, cumulative fracture-length distributions are similarly best described by power laws:

$$N = hl^{-e} \qquad \text{(Eq. 4-3)}$$

where l is the fracture length, and h and e are the coefficient and exponent of the power-law distribution.

In contrast to a power-law or scale-invariant size distribution, characteristic size distributions imply that fractures are common within a limited size range and rare outside this range. According to what was summarized by Bonnet et al., 2001, exponential law is a characteristic size distribution that has been used to describe the size of discontinuities in continental rocks (Cruden, 1977; Hudson and Priest, 1979, 1983; Priest and Hudson, 1981; Nur, 1982, Deschamps et al., 2007) and in the vicinity of mid-oceanic ridges (Carbotte and McDonald, 1994; Cowie et al., 1993b). The distribution is given by

$$F = c \exp^{(-dX)} \qquad \text{(Eq. 4-4)}$$

where c is a constant and d is a parameter reflects the physical thickness of a sedimentary layer or brittle crust, or spontaneous feedback processes during fracture growth. The physical processes resulting this distribution can be that the fracture growth results from a uniform stress distribution, and propagation of fractures can be compared to a Poisson process. Numerical simulations performed by Cowie et al. (1995) and experimental results of Bonnet (1997) have shown that exponential distributions of fracture length are also associated with the early stages of deformation, when fracture nucleation dominates over growth and coalescence processes. (Bonnet et al., 2001) Just like for the power law, the exponential law is found applicable to describing high-angle fractures, cracks, joints, and faults, but not yet considered applicable to bed-parallel fractures in shale media.

Other Characteristic size distributions that have been used to describe the size distributions of natural fractures include gamma distribution (Bonnet et al., 2001), normal size distributions (e.g., Abramowitz and Stegun, 1965), and log-normal distributions (Abramowitz and Stegun, 1965). Hooker et al., 2014 showed a table summarizing common equations documented for fracture-size distributions (Table 4-1).

All these relationships were first derived theoretically by many scientists, but high-quality fracture data sets are required to test the validity of these theoretical relationships. The second part of this chapter shows a new robust scanline dataset collected from outcrop and core, and discusses best fit fracture size scaling functions.

Table 4-2 Common equations documented for fracture-size distributions (from Hooker at al., 2014)

Equation type	Cumulative distribution function equation	Documented fracture-size or slip-magnitude distribution examples
Normal	$F = \frac{1}{2}\left[1 + erf\left(\frac{X-\mu}{\sqrt{2\sigma}}\right)\right]$	
Log-normal	$F = \frac{1}{2}\left[1 + erf\left(\frac{\ln X-\mu}{\sqrt{2\sigma}}\right)\right]$	Gillespie et al., 2001 Philipp, 2008 Larsen et al., 2010 Hooker et al., 2012
Power law	$F = aX^{-b}$	Gudmundsson, 1987 Wong et al., 1989 Marrett and Allmendinger, 1992 Sanderson et al., 1994 Clark et al., 1995 McCaffrey and Johnston, 1996 Marrett, 1997 Bohnenstiehl and Kleinrock, 1999 Marrett et al., 1999 Ortega et al., 2006 Guerriero et al., 2010 Hooker et al., 2011, 2012 Le Garzic et al., 2011
Exponential	$F = ce^{-dX}$	Nur, 1982 Deschamps et al., 2007
Gamma law	$F = aX^{-b}e^{-dX}$	Kagan, 1997 Sornette and Sornette, 1999

Note: Normal distribution equation is not documented but is included because it was tested in this study.
F—fracture cumulative frequency; *X*—fracture size; *erf*—error function; μ—average; σ—standard deviation; *a*, *b*, *c*, *d*—best-fitting variables.

4.3 Bed Parallel Fracture Size Distribution-New Datasets

4.3.1 Aperture size distributions

In this section, I will show the result of aperture size scaling. Fracture size distributions showing fracture cumulative frequency vs. aperture size were plotted for all ten scanline datasets.

Table 4-3 Basic information of 10 plotted datasets.

Core/Well #	Scanline Length (m)	# of fracs	Data Source
VM_Well #1	73.28	340	Core scan image
VM_Well #2	34.69	230	Core scan image
VM_Well #3	28.00	142	Core scan image
VM-Well #4	18.99	12	Core scan image
VM_Field #1	17.84	88	Field observation
VM_Field #2	13.20	54	Field observation
VM_Field #3	48.46	30	Field observation
Marcellus Well #1	89.18	47	Core observation
Marcellus Well #2	163.46	82	Core observation
Wolfcamp Well #1	141.88	68	Core observation
Total	628.98	1093	

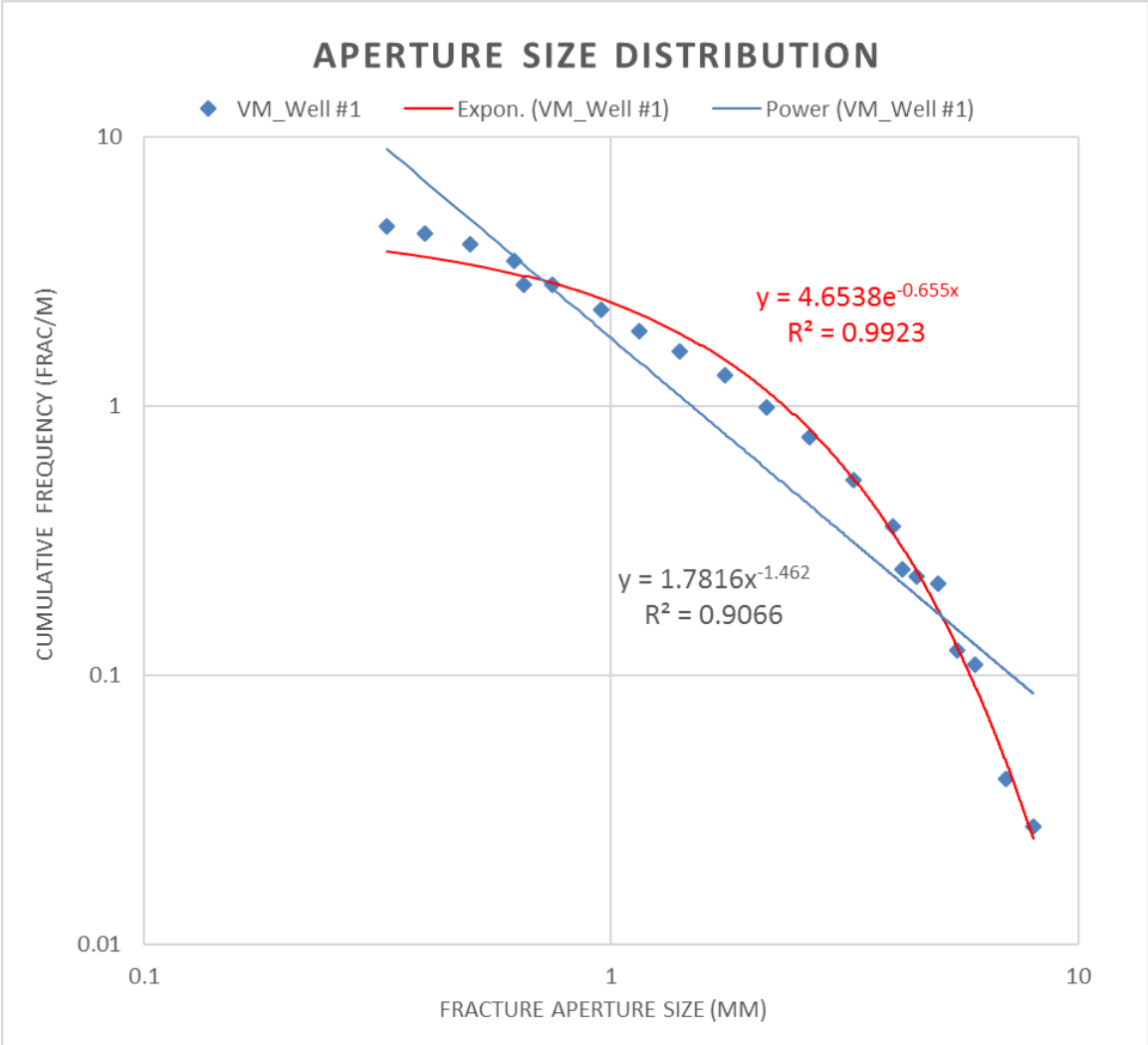

Figure 4-3 Bed-parallel fracture aperture size distribution plot (scaling curve) of VM_Well #1.

This is an aperture size distribution plot of a Vaca Muerta core dataset. It contains 340 fracture apertures within a scanline length of about 73 m. Data was collected from core panel images. The horizontal axis is fracture aperture size in mm and the vertical axis represents the cumulative frequency of fractures as fracture per meter (normalized to scanline length). Both axes are logarithmic scales so the plot shows the relative number of small and large fractures. From the plot, I assess the aperture size population, comparing all different sizes, form large to small. Trend lines were fitted to the data

points in each dataset. A power law function is marked in blue, an exponential law function is marked in red. Both fit functions and their correlation coefficient are also presented on the plots. Correlation coefficient indicates how well the data points fit the assumed function.

More aperture size distribution plots are shown below:

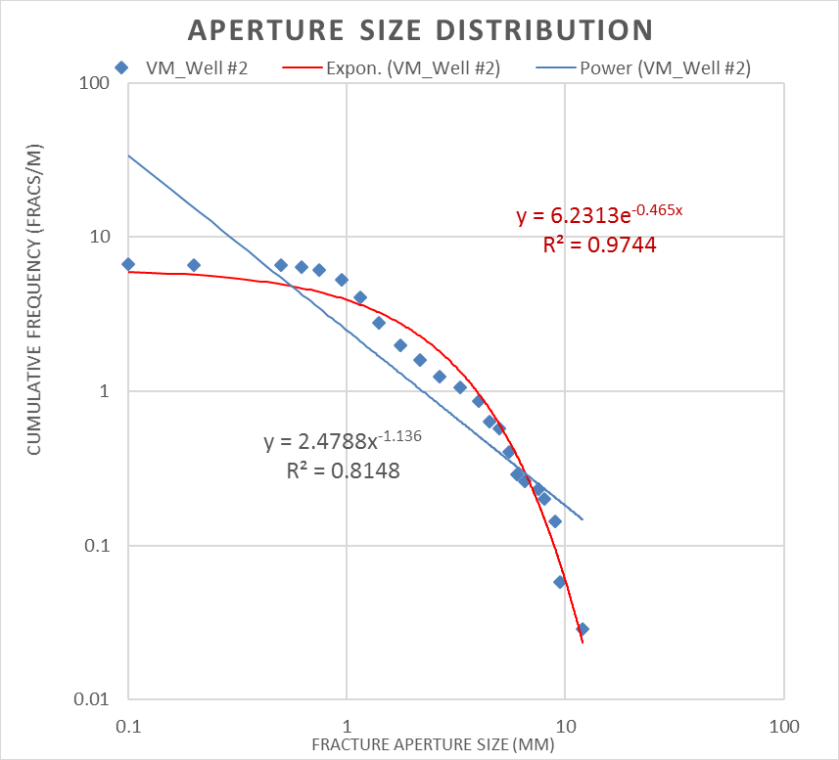

Figure 4-4 Bed-parallel fracture aperture size distribution plot (scaling curve) of VM_Well #2.

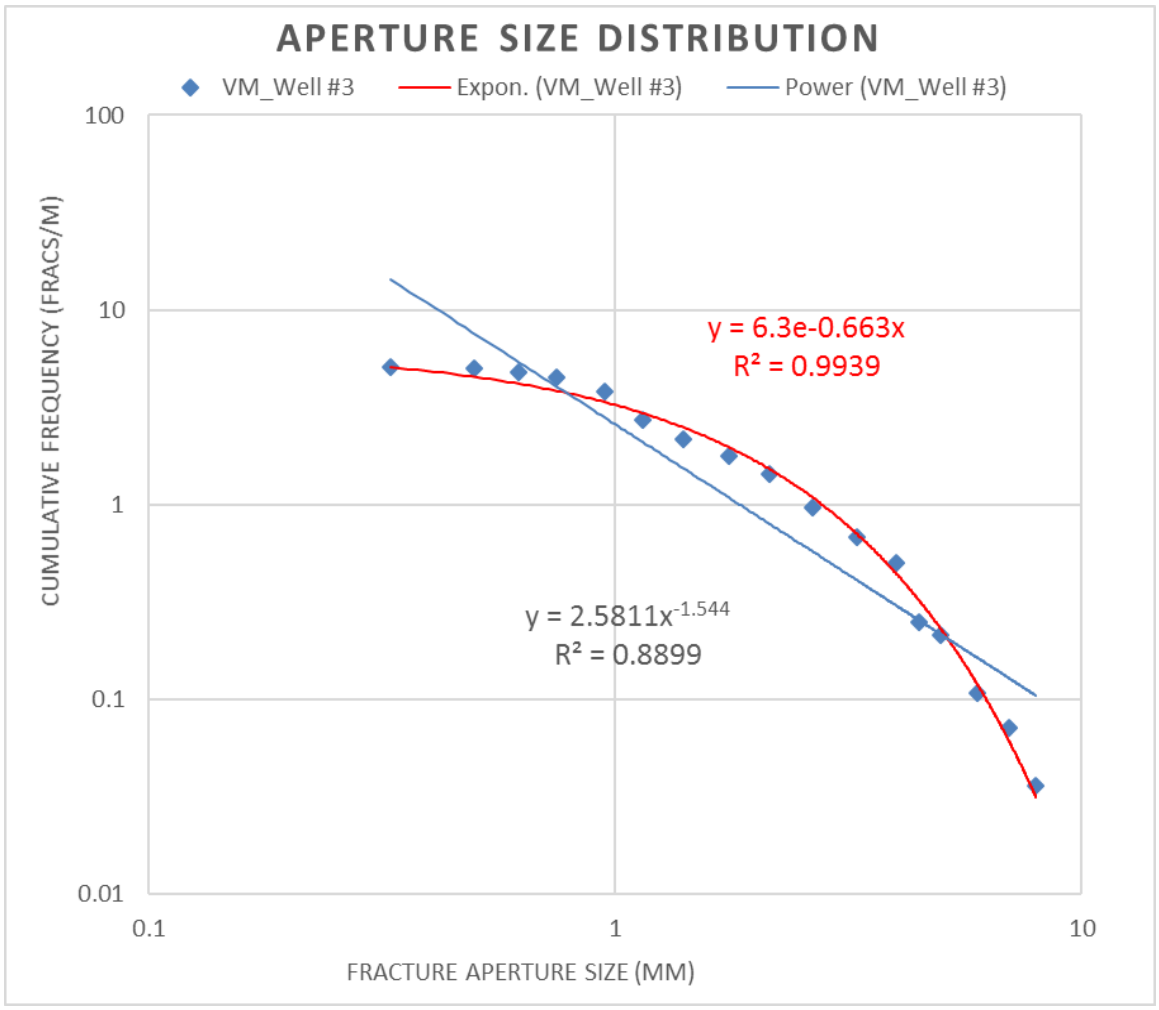

Figure 4-5 Bed-parallel fracture aperture size distribution plot (scaling curve) of VM_Well #3.

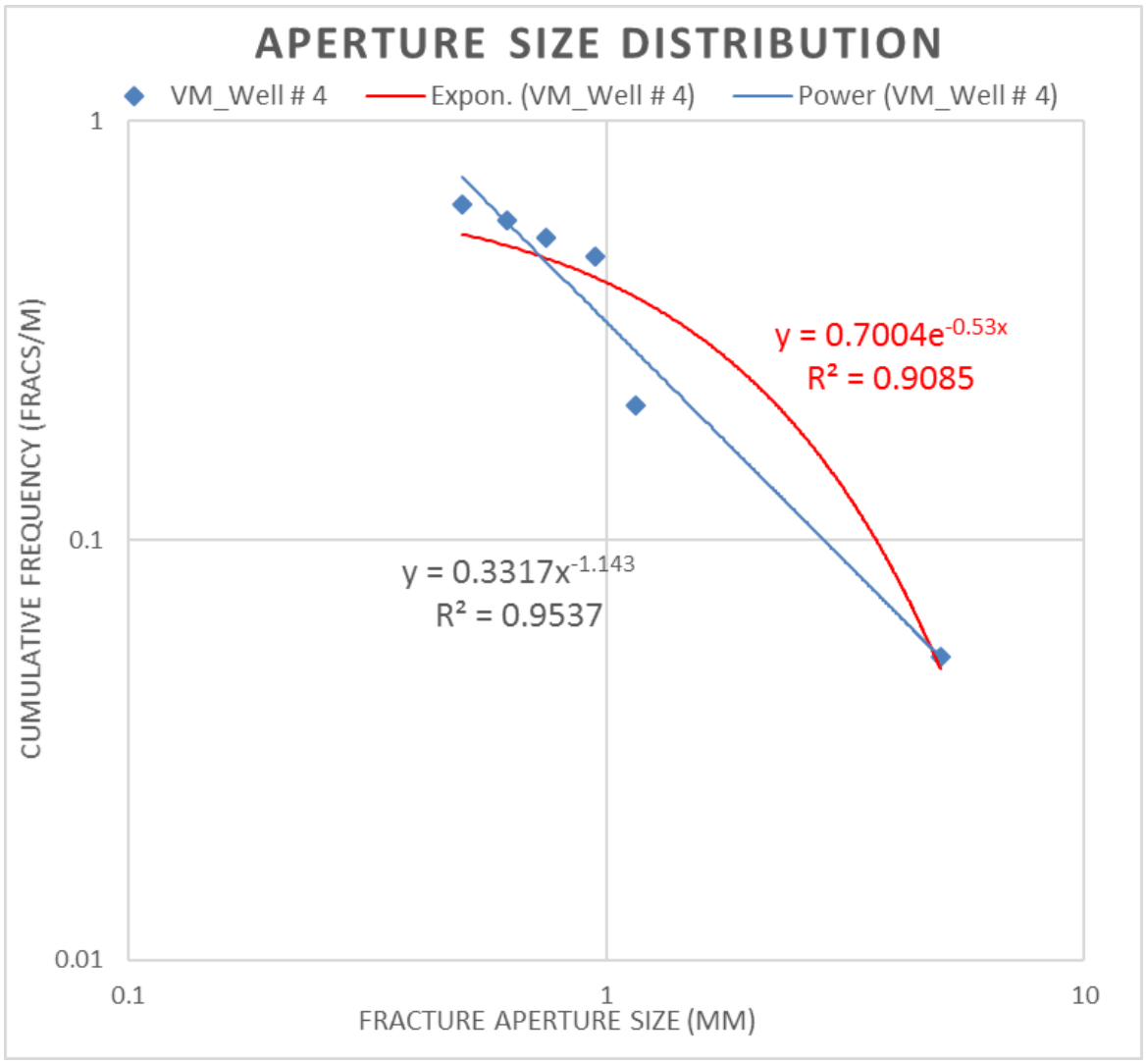

Figure 4-6 Bed-parallel fracture aperture size distribution plot (scaling curve) of VM_Well #4.

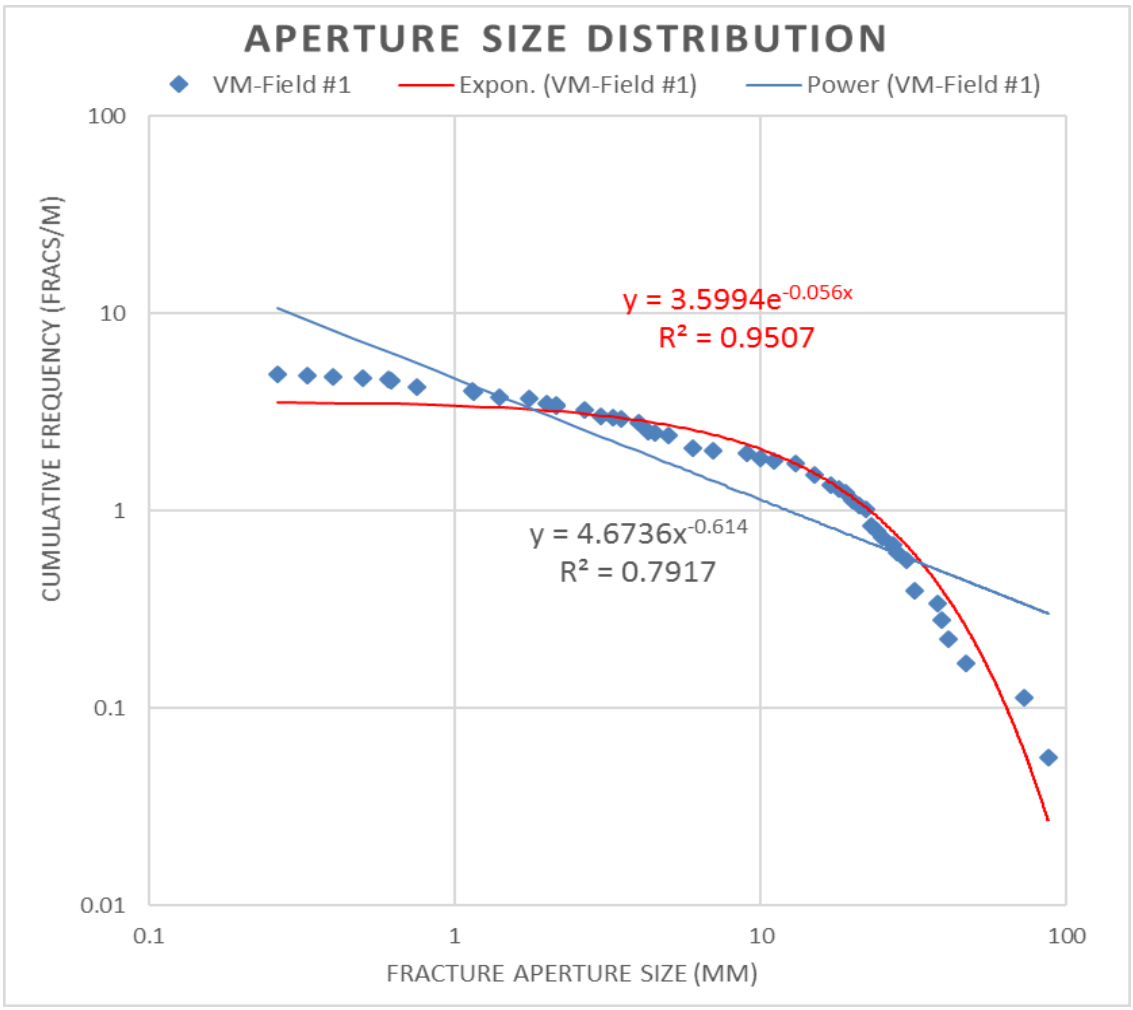

Figure 4-7 Bed-parallel fracture aperture size distribution plot (scaling curve) of VM_Field #1.

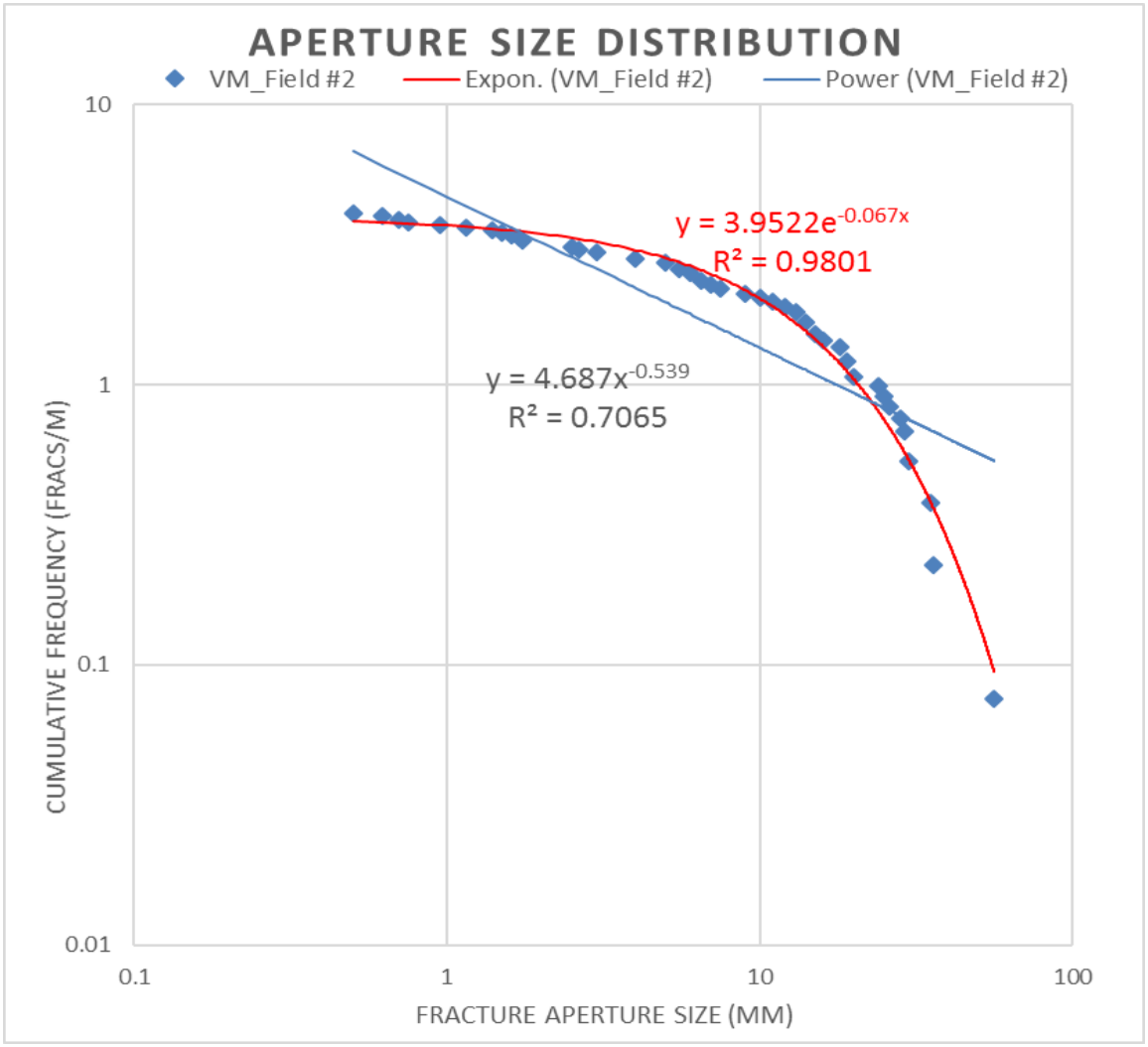

Figure 4-8 Bed-parallel fracture aperture size distribution plot (scaling curve) of VM_Field #2.

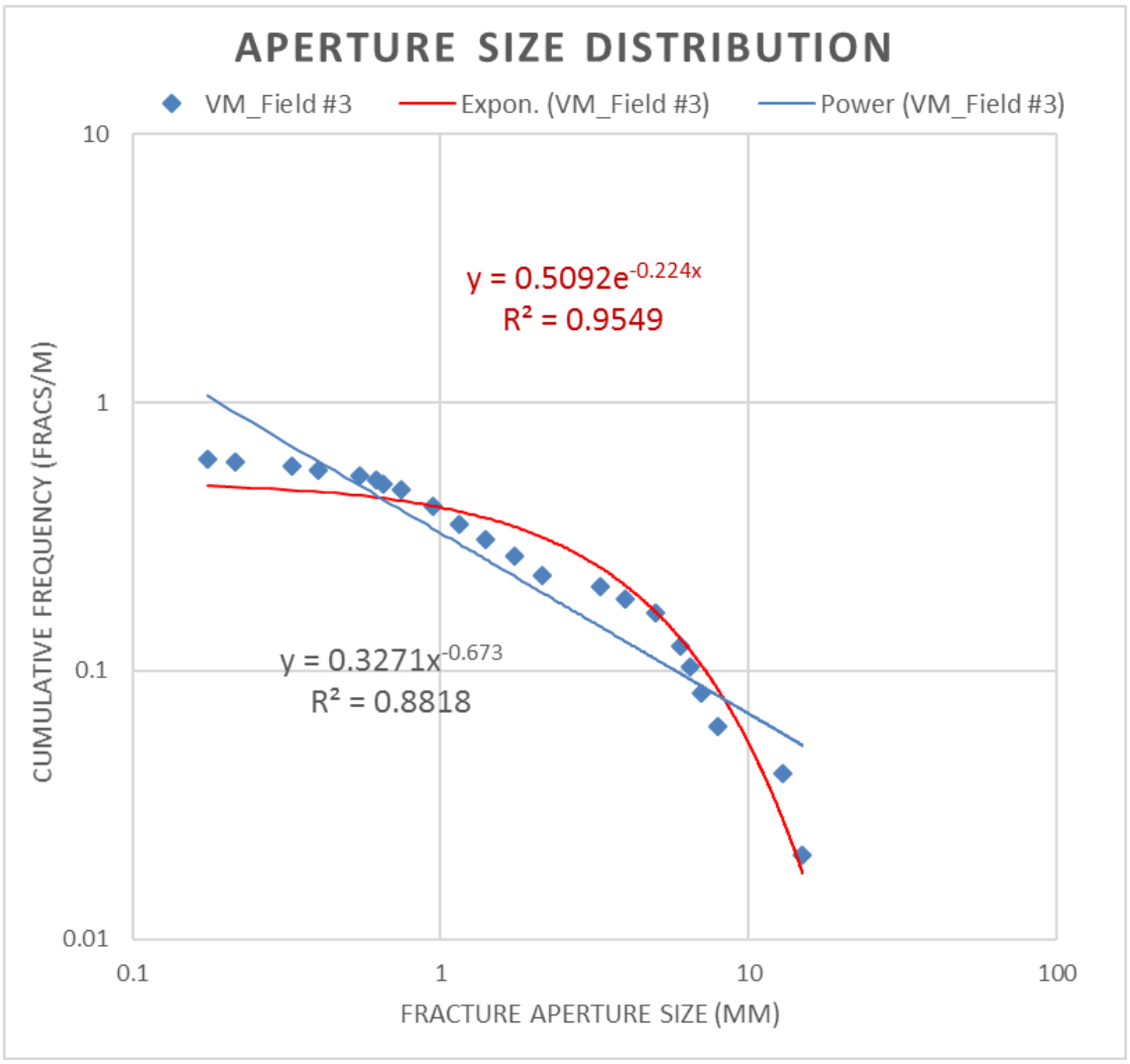

Figure 4-9 Bed-parallel fracture aperture size distribution plot (scaling curve) of VM_Field #3.

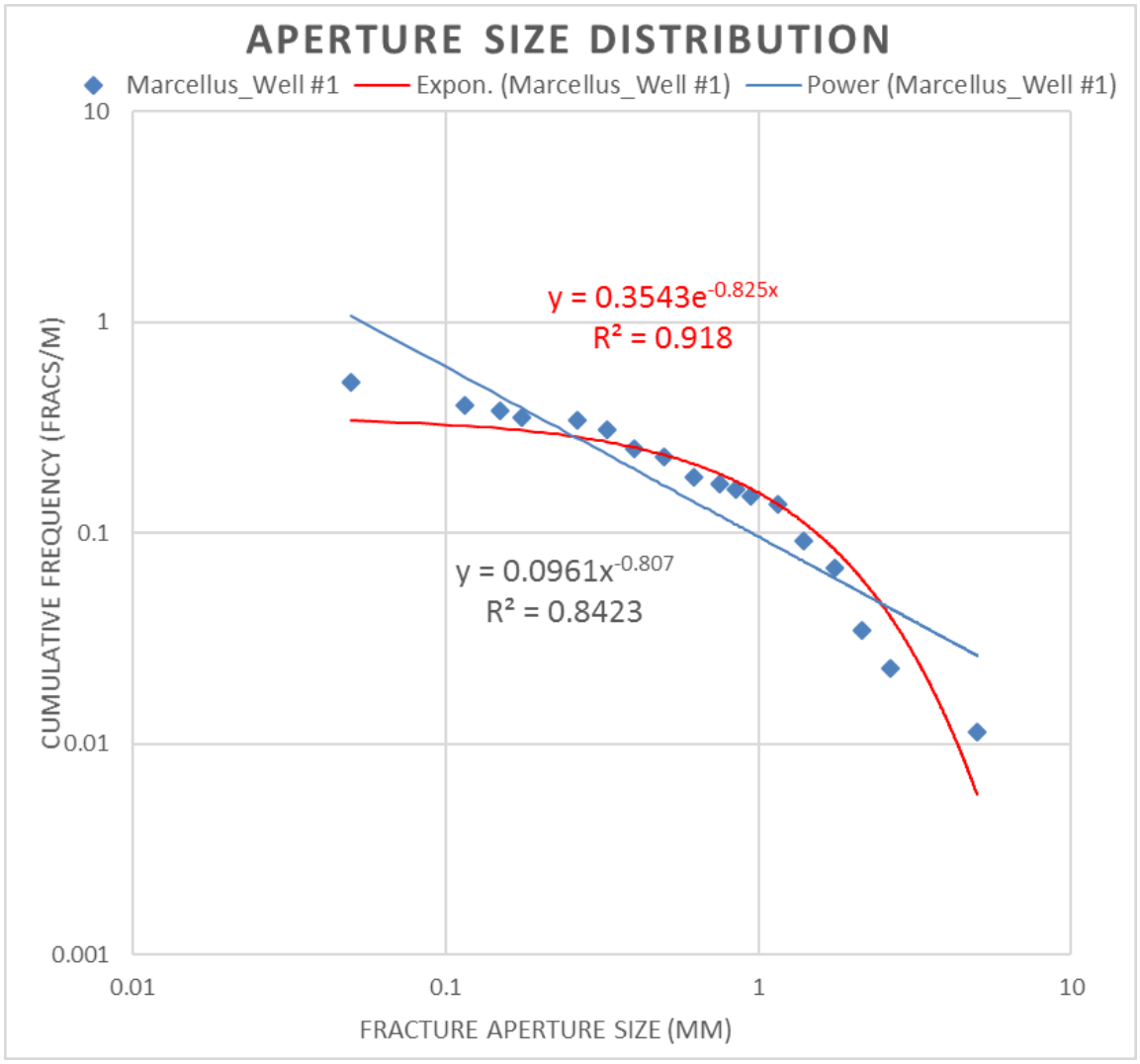

Figure 4-10 Bed-parallel fracture aperture size distribution plot (scaling curve) of Marcellus_Well #1.

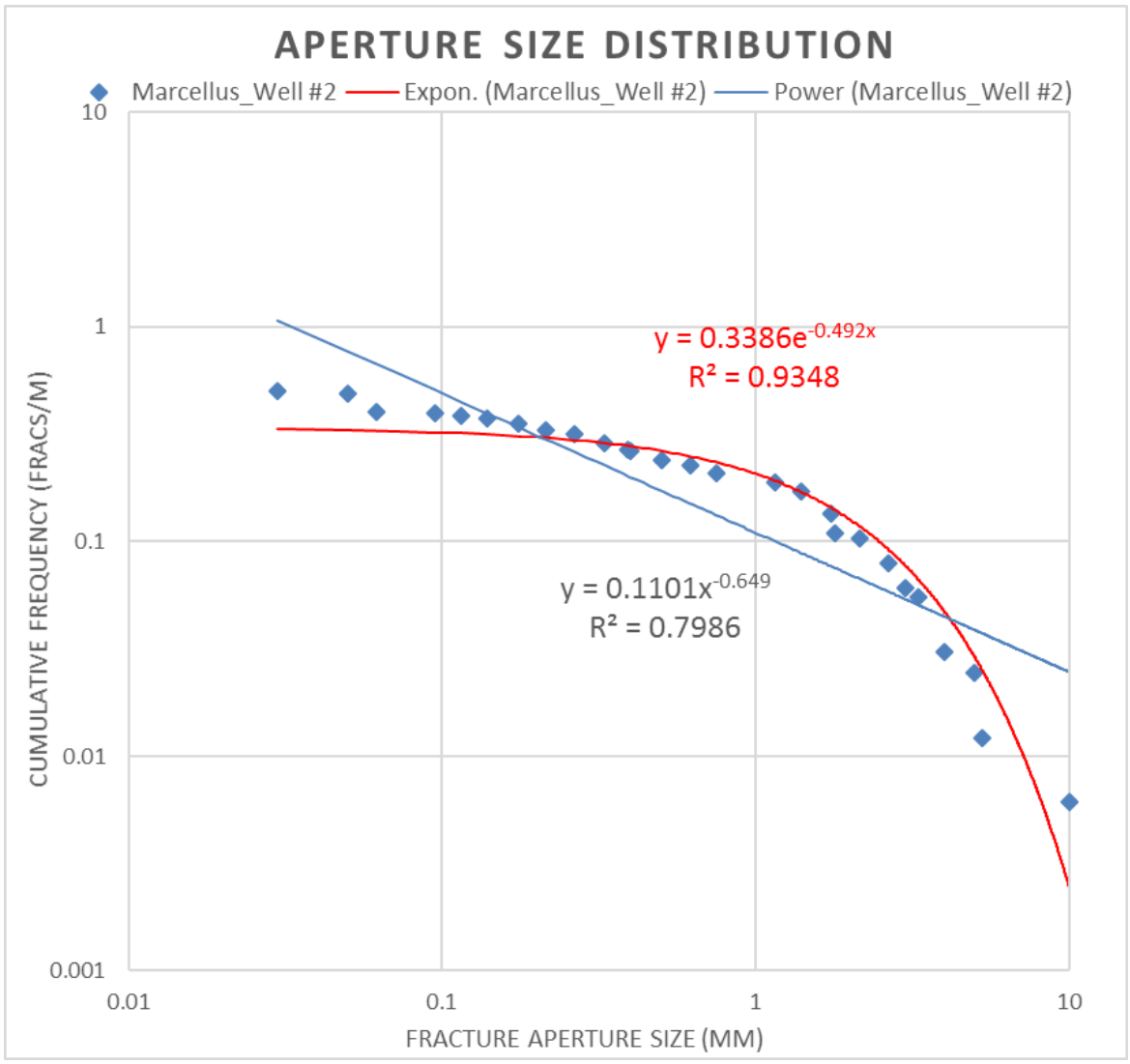

Figure 4-11 Bed-parallel fracture aperture size distribution plot (scaling curve) of Marcellus_Well #2.

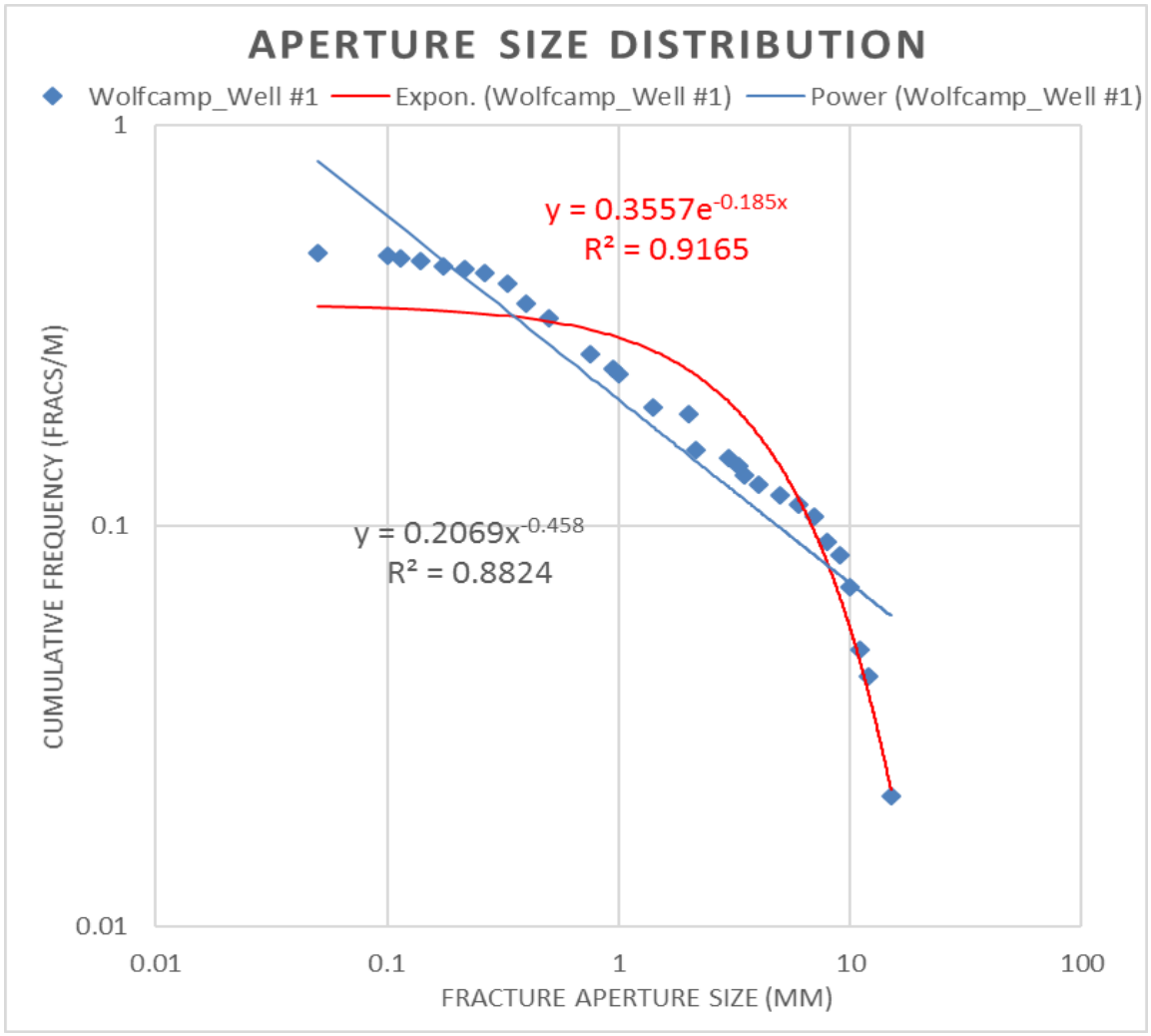

Figure 4-12 Bed-parallel fracture aperture size distribution plot (scaling curve) of Wolfcamp_Well #1.

The fracture aperture sizes within the datasets range between 0.05mm and 87mm. The small-size end of this range is near the resolution of the comparator (details in Chapter 2), and close to the smallest width of fractures which can be identified under the help of hand lens. However, it is not necessarily true that the fracture sets observed contain narrower, unmeasurable fractures. I address whether the dataset might include the smallest extant fracture sizes in this chapter. The large size end of this range is showing a reliable fracture intensity. Larger fractures could be present (Cobbold at al., 2013), but

the sets studied feature a multi cm-scale maximum observed fracture aperture size which is consistent with previous studies.

The majority of fracture aperture size distributions obtained from cores, core scan images, and by direct observation from core were modeled by negative exponential functions (Table 4-4), with a high correlation coefficient of above 0.9.

Table 4-4 Summary of scanline results. R2 values for each of the 2 tested equation types are listed. VM= Vaca Muerta. (?)= two models both show R2>0.9.

Core/Well #	# of fracs	Best Fit Model (N.E. or P.L)	Best Fit Equation	Correlation Coefficient (R^2)	2nd best fit Model	Correlation Coefficient (R^2)
VM_Well #1	340	N.E.(?)	$y = 4.6538e^{-0.655x}$	0.9923	P.L.	0.9065
VM_Well #2	230	N.E.	$y = 6.2313e^{-0.465x}$	0.9744	P.L.	0.8148
VM_Well #3	142	N.E.	$y = 6.3e^{-0.663x}$	0.9939	P.L.	0.8899
VM-Well #4	12	P.L. (?)	$y = 0.3317x^{-1.143}$	0.9537	N.E.	0.9086
VM_Field #1	88	N.E.	$y = 3.5994e^{-0.056x}$	0.9507	P.L.	0.7917
VM_Field #2	54	N.E.	$y = 3.9522e^{-0.067x}$	0.9801	P.L.	0.7065
VM_Field #3	30	N.E.	$y = 0.5092e^{-0.224x}$	0.9549	P.L.	0.8818
Marcellus Well #1	47	N.E.	$y = 0.3543e^{-0.825x}$	0.918	P.L.	0.8423
Marcellus Well #2	82	N.E.	$y = 0.3386e^{-0.492x}$	0.9348	P.L.	0.7986
Wolfcamp Well #1	68	N.E.	$y = 0.3557e^{-0.185x}$	0.9165	P.L.	0.8825
Total	1093	N.E.				

Of 10 fracture size datasets, 9 are best fit by negative exponential equations. And they all have a correlation coefficient of above 0.9, which means these data fit the

function really well; i.e. the results are signficant. Although VM_Well#4 best fits a power law, it has a fracture population of only 12, which makes the result questionable.

Among the 3 formations, the Vaca Muerta has the highest fracture intensity, or fractures per unit length. The Marcellus has the lowest intensity, with the Wolfcamp in between (Figure 4.13). The aperture size distribution profiles can be divided into 3 groups shown by the colored shading in figure 4-14. In the middle group, 3 Vaca Muerta datasets collected from cores are grouped together. These data sets have a large number of small fractures but are lacking thick ones. The Vaca Muerta field datasets 1 and 2 group together at the upper-most part of this plot, showing a similar intensity of thin fractures as the previous group, however the intensity of thick fractures is significantly larger. The third group has a similar intensity of large fractures to the middle group, but fewer thin fractures. Although it is beyond the scope of this study, knowing what is different about the field area that generates so many thick bed-parallel fractures may have implications for how we would use the outcrop data to inform reservoir studies.

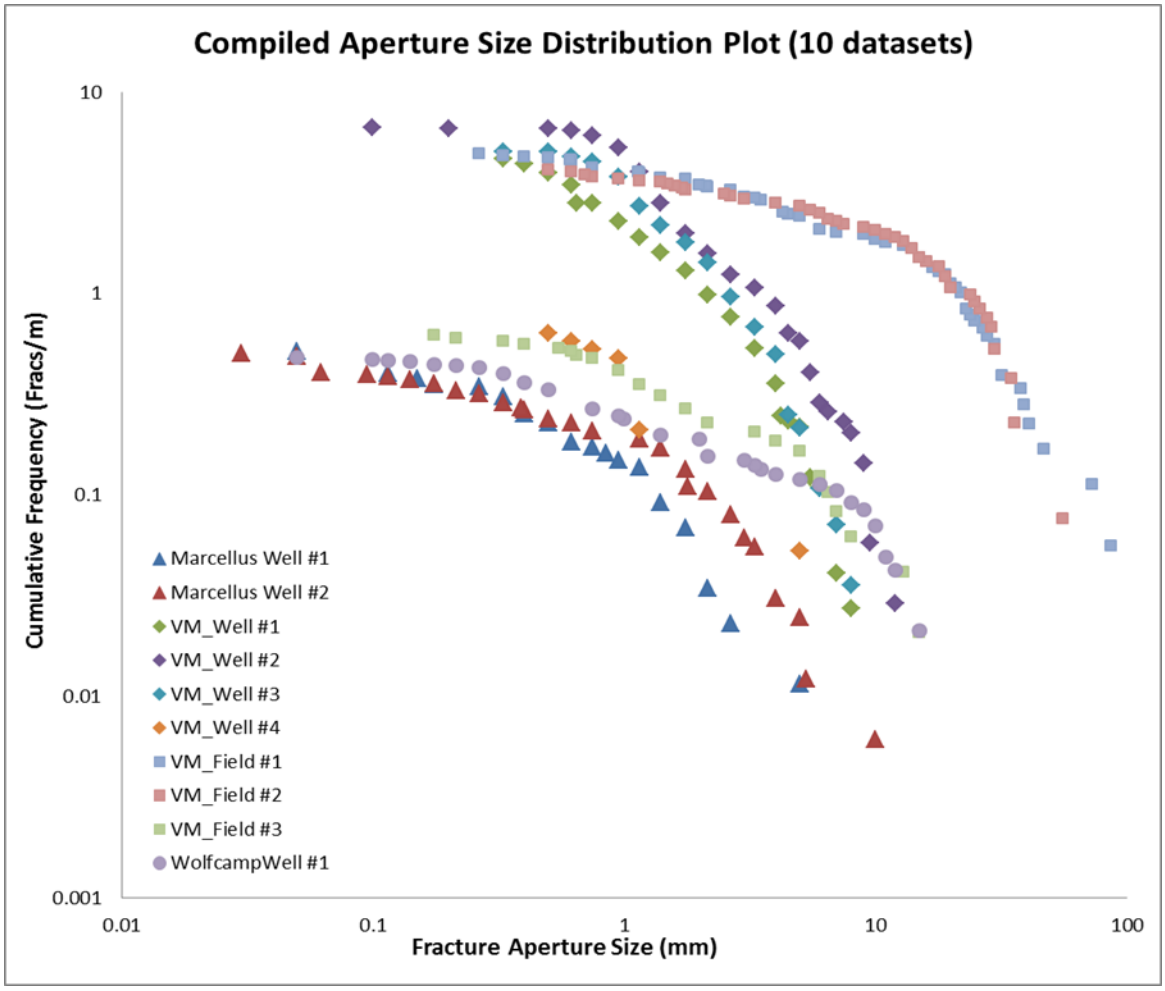

Figure 4-13 Compiled aperture size distribution plots showing all 10 datasets.

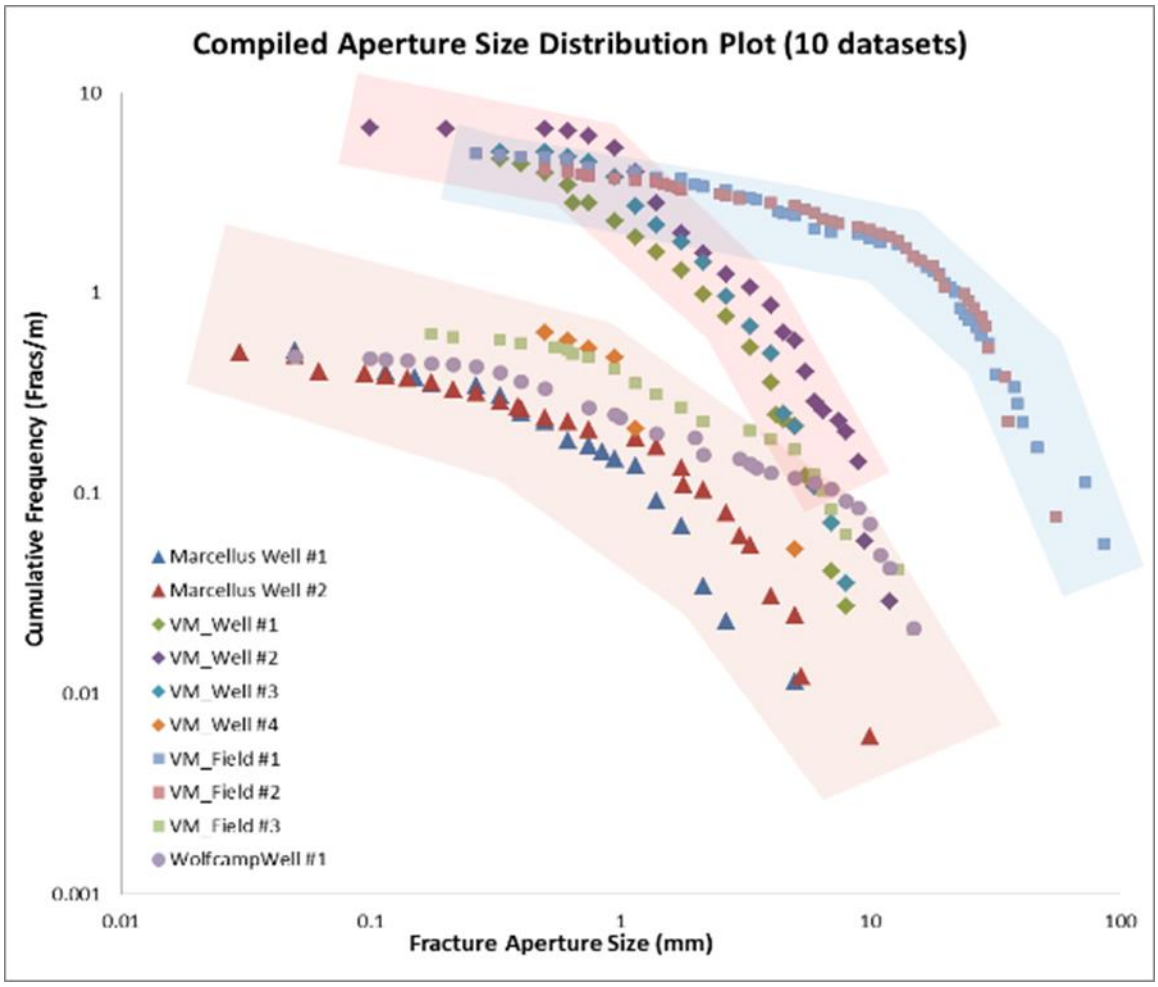

Figure 4-14 Compiled aperture size distribution plots showing all 10 datasets. Aperture size distribution curves divided into 3 groups, marked by colored shading.

4.3.2 Length Distribution

Fracture length distributions are more problematic than aperture distributions because identification of the tips of fractures can be difficult wherever two or more fractures connect. Many of the data points represent minimum measurable lengths. The length depends on the size of the outcrop or is limited by the scale of core. Where meaningful true lengths can be measured, determination of fracture length can be based on a set of geometric criteria to assure interpretation consistency, which is described in Chapter 2. The method and criteria are at best a simplistic solution to this complicated

problem, which requires a comprehensive understanding of the complex fracture system geometry and related configurations.

Length distributions were obtained only from the two Vaca Muerta outcrop datasets with statistical adequate number of length measurements. Compared to aperture measurements, the length measurement is more heavily affected by truncation and censoring artifacts (discussed later in this chapter). For many thick fractures, we only have its minimum length recorded, which could be much shorter than its real length. This can lead to the length curve's downward deviation from ideal power-law distribution on the longer fracture end. On the short fracture end, the roll-off could be a result of the under-sampling of short fractures intersect the vertical scanline. The shorter the fracture is, the smaller the chance of intersecting the scanline it has. The two-dimensional sampling yields a best-fit power-law distribution of VM Field #1 dataset with rolled-off ends (Figure 4-15). The VM Field #2 fracture length data statistically fits best with negative exponential curve. However, the length distribution of this dataset may also be considered best described by power-law with rolled-off ends, just like what happened with VM_Field #1. If considered best fit to power law, the power-law exponent of both datasets is around 0.42.

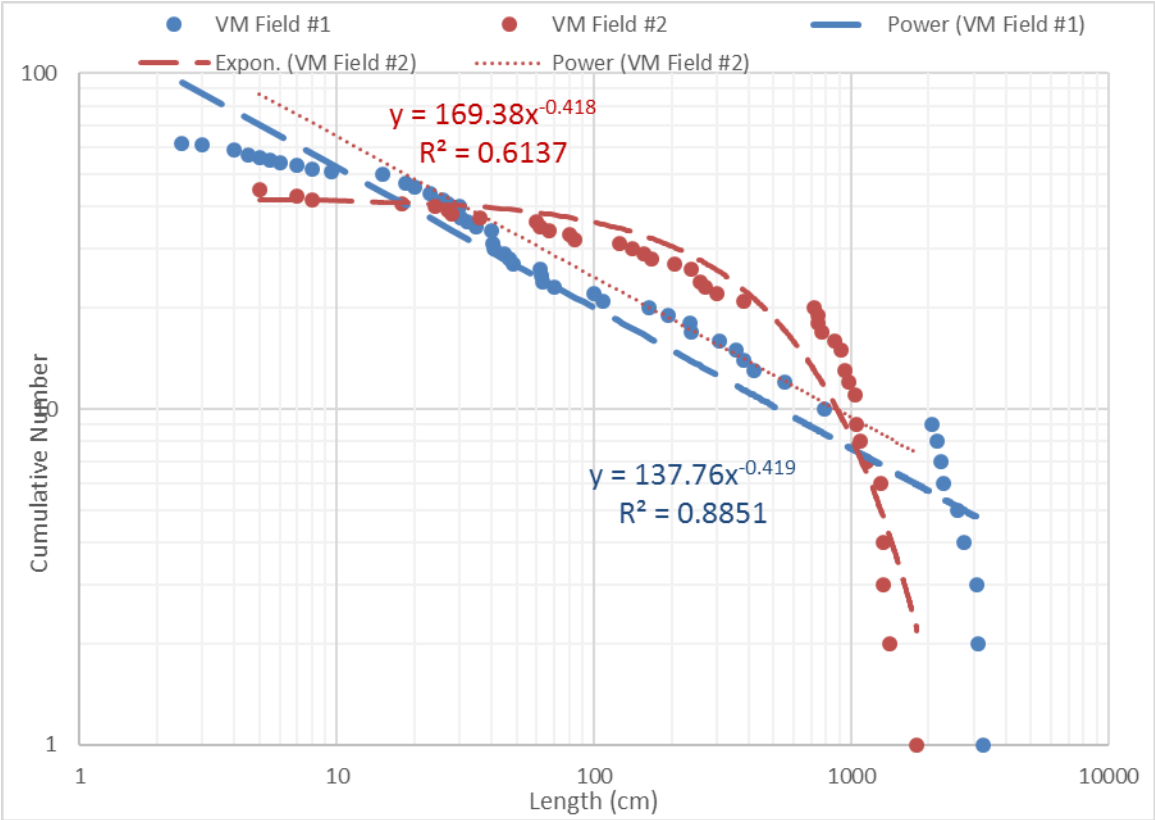

Figure 4-15 Length distribution of VM Field #1 dataset and VM Field #2 dataset.

4.3.3 Aperture-length relationship

In this part of the study, the relationship between bed-parallel fracture aperture and length are analyzed based on two field datasets from Vaca Muerta Arroyo Mulichinco outcrop.

Previous theoretical predictions published by Klimczak et al. (2010) suggests that displacement/aperture–length data from faults, joints, veins, igneous dikes, shear deformation bands, and compaction bands define two groups. The first group, having a power-law scaling relation with a slope of b=1 comprises faults and shear (non-compactional or non-dilational) deformation bands. These shearing mode structures, having shearing strains that predominate over volumetric strains across them, grow under conditions of constant driving stress. The second group, having a power-law scaling

relation with a slope of b=0.5 comprises joints, veins, igneous dikes, cataclastic deformation bands, and compaction bands. These opening- and closing-mode structures grow under conditions of constant fracture toughness. Volumetric changes accommodated by grain fragmentation, are associated with scaling of predominantly dilational and compactional structures with an exponent of b=0.5.

No prediction was made on bed-parallel fractures in shale. So in my study, the aperture-length data is considered best fit to power-law scaling relationship. Under this assumption, the power law exponent b can be determined based on the two field datasets, and be compared to Klimczak et al. 2010.

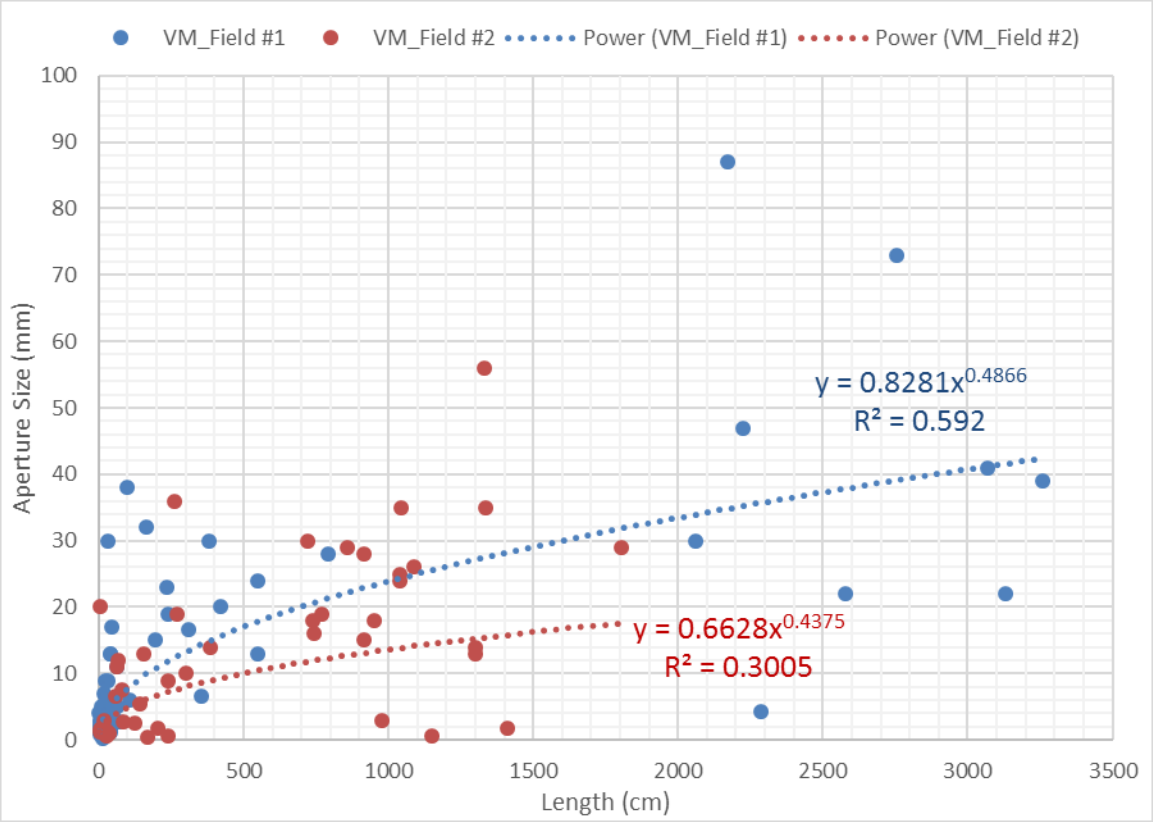

Figure 4-16 Aperture-length plot of VM field #1 and #2 datasets. Aperture-length plots of the data collected show high scatter, suggests that aperture and length are positively correlated and follow a power law of exponent close to 0.5.

Figure 4-16, although the aperture-length plots of the data collected show high scatter, suggests that aperture and length are positively correlated and follow a power law of exponent close to 0.5 (0.44-0.49). This result implies that the bed-parallel fractures should be considered an opening mode structures accommodate significant changes in volume across them and is controlled by constant fracture toughness (Klimczak et al. 2010, Schultz et al 2008). This finding may help with exploring the mechanics of these structures in relation to their displacement–length scaling characteristics.

However, in this study, the aperture size was measured where the fracture intersecting the scanline. Previous studies on aperture-length relationship (Moros, 1999; Schultz et al., 2008) showed that the majority of fractures studied are characterized by locally variable apertures, this is consistent with field and core observations. So the aperture size data used to compare with fracture length may not necessarily be the maximum aperture size. In terms of fracture length, there is evidence from both microscopic and macroscopic scale indicating that most bed-parallel fractures observed in part reflect growth by connection between individual fractures that initially grew independently and ultimately linked to make a larger fracture. These factors bring complexity studying bed-parallel fracture aperture-length relationship.

4.4 Sampling and Topologic Artifacts

4.4.1 Facing challenges due to hostrock and configuration

Most work on this aspect of fracture population statistics has been done for fracture length. In the study of bed-parallel fractures in shale, fracture-length determinations are fraught with uncertainty. As with sandstone, most of the uncertainty arises from the difficulties of clearly defining what is a through-going fracture where fractures branch or intersect (Ortega and Marrett, 2000). In the field, the length of the

fracture is usually not fully exposed, and the direction of measurement is highly dependent on the lateral extent of the outcrop. Statistically adequate number of bed-parallel fractures and their aperture size can be better collected from vertical cores. However, due to the limited diameter of the core, bed-parallel fracture length data can hardly be collected from core studies. In this study, I chose to focus on aperture data because considering the geometry of outcrops, vertical cores and the bed-parallel fractures, the configuration means that aperture data sets are more complete. The fracture length was measured to its maximum exposure in the field. The fracture length data, which may not be as good as aperture data, are used for preliminary fracture length scaling and aperture-length relationship studies.

Studies of fracture aperture distributions are less common in the literature compared to length-distribution, perhaps because of the lack of appropriate tools for effective fracture-aperture measurement in the field. It is even harder to collect aperture size data of bed-parallel fracture in shale than in other host rocks, considering the low resistivity of carbonate vain and shale outcrop to weathering, and the physical and chemical changes happen with the core as it is unloaded and dehydrated. It can be difficult to tell natural fractures from artifacts such as breaks due to pressure release and thin-section processing. Although we only look for filled fractures, powder abrasives used in thin-section polishing, and evaporites formed due to shale dehydration, can be confused with cement. We may also get confused telling fibrous bed-parallel fracture and fossils apart. As mentioned in Chapter 2, to measure micro-fractures, we need to set micro scanlines. However, collecting microfracture data in shale is harder than in sandstone. Artifacts described above are usually being a bigger problem in shale, compared to that of sandstone. What's more, based on my observation in cores and outcrops, the bed-parallel fractures in shale have a lower intensity compared to vertical

fractures, especially to the ones within sandstone matrix. There also lack micro- bedding parallel fractures. So population of bed-parallel fractures in a thin section may be too few to be representative.

With properly collected fracture size data at hand, from both the field and the core, reasonable interpretation of the distribution can be challenging using the traditional approach. Since the fracture aperture size and can range through around five orders of magnitude, which makes the non-scale dependent approach not well applicable. Besides, fracture-size distributions commonly show deviations from an ideal power law in the small and large fracture-size parts of the distribution. Deviations from power-law behavior can be explained by consideration of sampling and topologic and statistical artifacts, which can be assessed from patterns of fracture size distributions. These artifacts need to be understood and minimized before scaling methods are put into meaningful use.

4.4.2 Truncation and censoring artifacts

Dershowitz 2000 and Ortega et al., 2006 identify a series of artifacts including truncation artifacts, censoring artifacts, topologic artifacts, mechanical boundary effect, orientation bias and undersampling of large/small fractures. The truncation and censoring artifacts are mainly considered artifacts arising during collecting scanline data for fracture size scaling in this study.

Truncation artifacts have been described as deviations of small fractures from the scaling shown by larger fractures of a population (Baecher and Lanney, 1978; Barton and Zoback, 1992; Pickering et al., 1995). When fracture sizes measured are near the limits of resolution of the observation tool, such as a comparator, variable sample completeness can cause truncation artifacts. The small-size end of a size distribution curve affected by

truncation artifacts typically result in a convex-upward scaling curve that decreases in slope with decreasing fracture size. This artifact affects aperture size data the most. Truncation artifacts can be minimized by artificially imposing a minimum cut-off limit size for fracture measurement. If any fractures below the minimum cut off are all count towards the minimum size, then it may cause a spike of the minimum sized fractures. So in this study, I did not count the fractures aperture measurement below minimum cut-off into the aperture size scaling curve. Their spacing was measured for spatial distribution analysis only.

Censoring artifacts (Baecher and Lanney, 1978; Laslett, 1982; Barton and Zoback, 1992; Pickering et al., 1995) have been best described for fracture-length distributions obtained from map view. Censoring occurs where some or all of the largest fractures in a population are incompletely sampled, or only minimum estimates of their sizes can be made. In this study, censoring of fracture-length measurements is result from fractures with its length beyond the limits of outcrop exposure and the scale of the core, so their true length cannot be determined. Censoring of fracture-aperture measurements can happen in core-based studies because of an incomplete core recovery or missing cores. So there may have some of the largest fracture apertures missed. At where outcrop scanline is continuous and the exposure is good, censoring artifacts are not considered a big problem. Censoring disproportionately affects data from the largest fractures because the probability of censoring is proportional to fracture size (Ortega et al., 2006). Censoring effects on a fracture-size distribution typically show a convex-upward curve that increases in slope with increasing fracture size.

4.4.3 Interpreting scaling curves affected by artifacts

As a result of truncation and censoring artifacts, the shape of aperture size distribution curves may not represent the true scaling law of the dataset. Instead of being reproduced by simple negative exponential function, the curve may have a power-law backbone and curving down ends. Or perhaps there are different behaviors at different scales. There are indeed more than one interpretations. My interpretation represents the simplest, common fit that applies to all. And there really are no other datasets like this that are already published.

Hooker et al., 2014 addressed interpretations of concave-downwards scaling curves among the small and large fracture sizes. As discussed in earlier in this chapter, the small-fracture end of the size distribution can be expected to show truncation bias, in the form of a concave downwards curve. This bias assumes correct measurement of fracture size but incomplete fracture detection, and thus should represent only underestimations of fracture frequency.

Figure 4-12 shows a representative curve that could be interpreted as a power-law backbone with roll-offs at both large and small fracture ends (Wolfcamp_Well #1). The data was collected from direct observation of cores. However, considering the data collecting processes, the roll-off at the small fracture end is considered real since no hundreds of 0.5mm and smaller fractures could possibly be missed when measured from core. In outcrop we might miss some because of the weathered surface, but in slabbed core we would be able to see and collect them.

However, a power-law backbone may not always be found in datasets collected from direct observation from core. Figure 4-11 is showing a dataset collected Mercellus_Well #2, however, it shows a good fit to exponential curve when aperture size >0.175mm. When aperture size<0.175mm, the data points lie between the projected

power-law and exponential-law curve. It means more small aperture fractures were collected than predicted by exponential-law. Actually this shape is found in most of the datasets. Figure 4-3 and 4-7 shows similar patterns for datasets collected from the outcrop (VM_Field #1) and from core scan images (VM_Well #1). The upward deviation from ideal exponential-law size distributions may result from inclusion in the dataset of features which are not actually microscopic fractures related to the large-fracture population. (Hooker et al., 2014) For example, fossils, gypsum fill due to weathering, and filled fissile as a result of coring and handling may be miscounted as bed-parallel fractures. Besides, when collecting thin fractures from core scan images, the scratches, silt layers, fossils or other linear features may be misinterpreted as natural fractures. These misidentifies can contribute to a higher intensity of small fractures.

Fracture size data also typically deviate down from best-fit power-law equations at the large-size end of the data distribution. It means compare to ideal power-law distribution, the number of large aperture fractures collected is fewer. (Figure 4-12) It is often due to inadequately sampled large size fractures along a not long enough scanline. However, since the bed-parallel fracture data was collected along continuous vertical scanlines at least tens of meters, which is more than 200 times of the thickest bed-parallel fractures collected, the censoring artifacts should be negligible. So the roll-off on the large aperture fracture end of the curve is considered real.

There may be different behaviors at different scales. Use Marcellus_Well #2 as an example. In figure 4-17, two power-law functions are applied to describe behaviors of aperture size population among small and large fractures. As shown in Figure 4-11, the Marcellus_Well#2 dataset shows a best fit to negative exponential function with a correlation coefficient of around 0.93. However, when fit to two power-law functions,

correlation coefficient of both are above 0.96, and the upward deviation of data points from exponential curve at the small aperture end can no longer be seen.

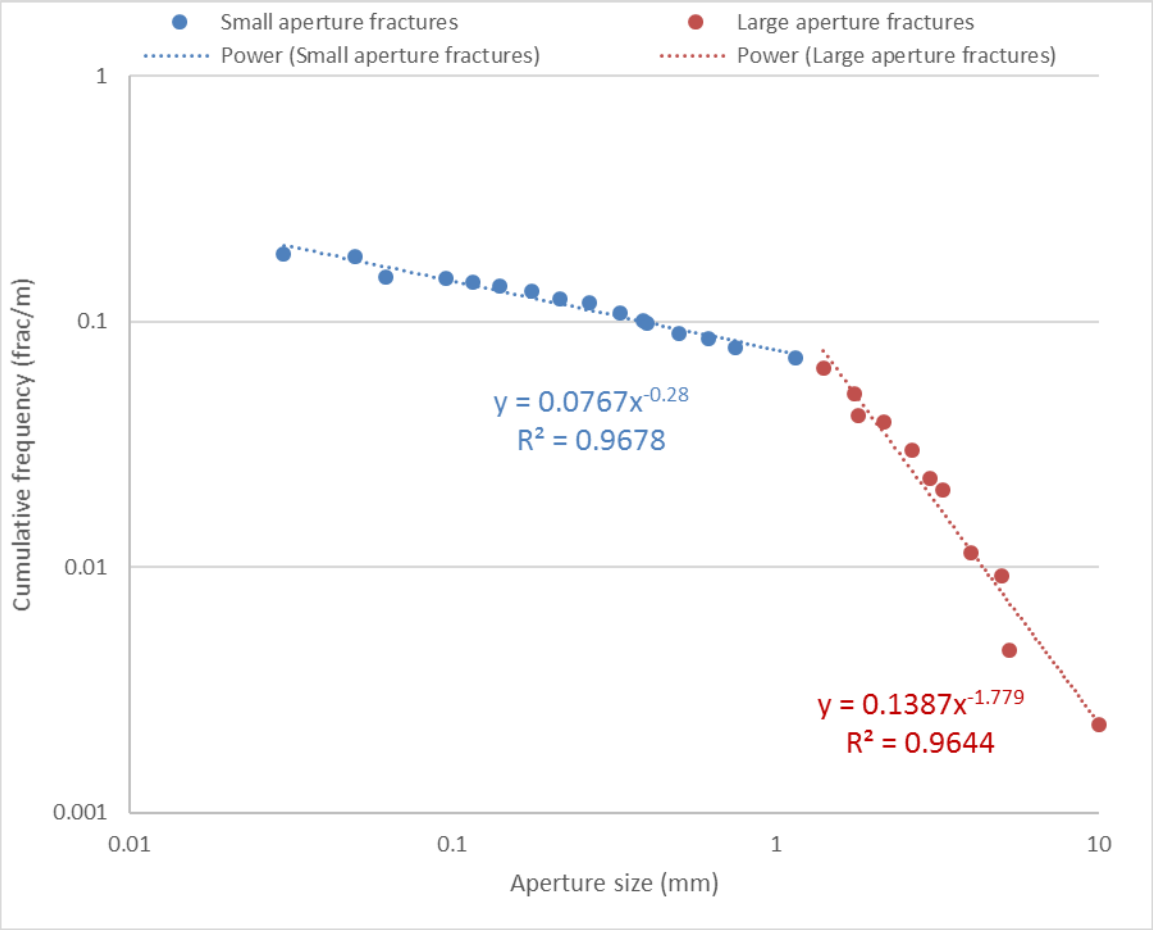

Figure 4-17 Two power-law functions are applied to describe the aperture size distribution of Marcellus well #2 data.

Chapter 5. Bed-parallel fracture spatial organization and possible lithologic controls

Many previous studies examined how geologic parameters control variations in fracture intensity (Nelson, 1985; Handin et al., 1963; Handin et al., 1963; Sinclair, 1980; Das Gupta, 1978; Proce 1966; Friedman, 1969; Friedman, 1972; Bogdonov, 1947., Marrett, 1999; Ortega, 2002; Ortega, 2006, Lash, 2011 etc.) with the goal of using known stratigraphic characteristics and mechanics of sedimentary successions to predict subsurface natural fractures. The stratigraphic characteristics used can be sedimentary facies, content of specific mineral/minerals, bed thickness, and stacking patterns. These analyses may help to determine which stratigraphic parameters exert the strongest control on fracture intensity distribution, the nature of this control, and finally a predictable pattern of fracture intensity distribution. Understanding of the aperture-size scaling and location of bed-parallel fractures may contribute to improved modeling of both natural and hydraulic fracture networks. Being able to predict fracture network may, on the other hand, also be important for quantifying the mechanical behavior of fractured rock masses. However, such an approach has shortcomings in terms of only considering present day observed fracture stratigraphy, which can be constantly changing through the history of basin evaluation, sedimentation and deformation (Laubach, 2009).

However, almost all previous studies are about how vertical fracture distribution is controlled by stratigraphic characteristics. There are no other systematic robust published datasets focusing on bed-parallel fractures. Fracture characterization, no matter for vertical or horizontal fractures, is challenging mainly because of sampling problems. Chapter 2 and chapter 4 of this work addressed the challenges in sampling and how that may affect the datasets collected and the interpretation. Datasets for this part of the study were collected from the Vaca Muerta formation and the Marcellus formation along

vertical scanlines perpendicular to bedding at outcrops and in vertical cores and provide statistically adequate data for spatial organization analysis.

In this chapter, I explore the lithologic characteristics of the hostrock (shale) that may control the spatial distribution of bed-parallel fractures. I investigated whether the location of bed-parallel fractures is related to lithology and lithology change within the host rock, and whether the bed-parallel fractures occur more often in certain lithologies, or show any clustering. Improved understanding of these controls may indicate mechanism of growth.

This Chapter presents data on bed-parallel fracture location, spacing and host rock lithology, and examines whether fractures and lithology are correlated.

Two hypotheses were tested:

1) Bed-parallel fracture intensity is higher in more organic rich layers. This hypothesis is proposed on the basis that generation of bed-parallel fractures in the Vaca Muerta Formation has been linked to fluid overpressuring due to hydrocarbon generation in high TOC shales.

2) Bed-parallel fractures preferentially develop at weak mechanical interfaces within the host rock. Material interfaces at lithological boundaries or around the margins of concretions may allow fracture growth, due to reduced bed-parallel strength. Other host rock characteristics other than TOC that show up to be related to high fracture intensity.

5.1 Location, Stratigraphy and Structural Context

As covered in Chapter 1, the Neuquén Basin (Figure 5-1) lies entirely onshore in western Argentina. Its western boundary is formed by the frontal thrusting of the Andean range. On the east and southeast the basin is boarded by the Colorado basin and north

Patagonian Massif. The sedimentary sequence exceeds 7000m in thickness, comprising complex continental and marine sequences of the late Triassic to early Cenozoic strata (Mariano et, al., 2013). In Neuquén Basin, Permo-Triassic rifting took place on north-south and northwest-southeast normal faults, and these faults influence later structural development. The east-west dextral transpression along the Dorsal de Neuquén wrench system occurred episodically through the Jurassic and Cretaceous, generating many potential structural traps. The remainder of the basin was characterized by gentle extension with dip slip activity on normal faults. The Andean thrusting in Tertiary time was concentrated in the northern two thirds of the basin, generating anticlines in a thin-skinned type. Detailed descriptions of sedimentary successions, tectonic activities and deformation histories of the basin are available from literatures such as Vergani et, al., 1995; Ramos et al., 2005; Rojas Vera, 2013; Sagasti 2001, and Leanza, 2009.

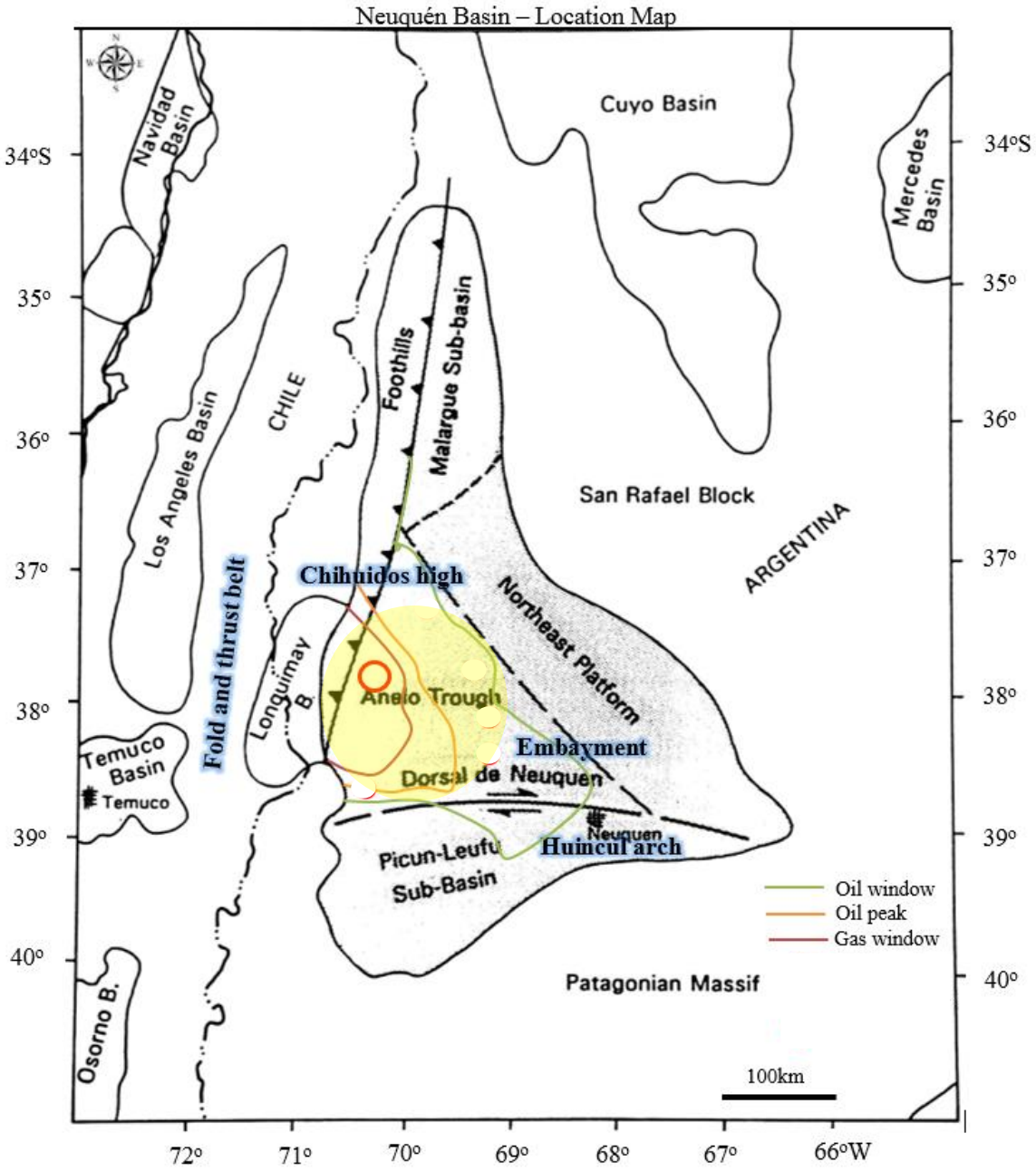

Figure 5-1 Location of study area on a map of the geological provinces of Neuquén basin region. Neuquén basin is a triangular area marked by solid black line. Modified from Vergani et, al., 1995. Yellow shaded area indicates the approximate location of the sampled 5 wells. Data from 3 out of 5 wells are selected for fracture spatial distribution analysis. Red circle indicats the field area. The colored lines are marking the boundaries of oil window, gas window, and the peak of oil generation projected to the ground surface.

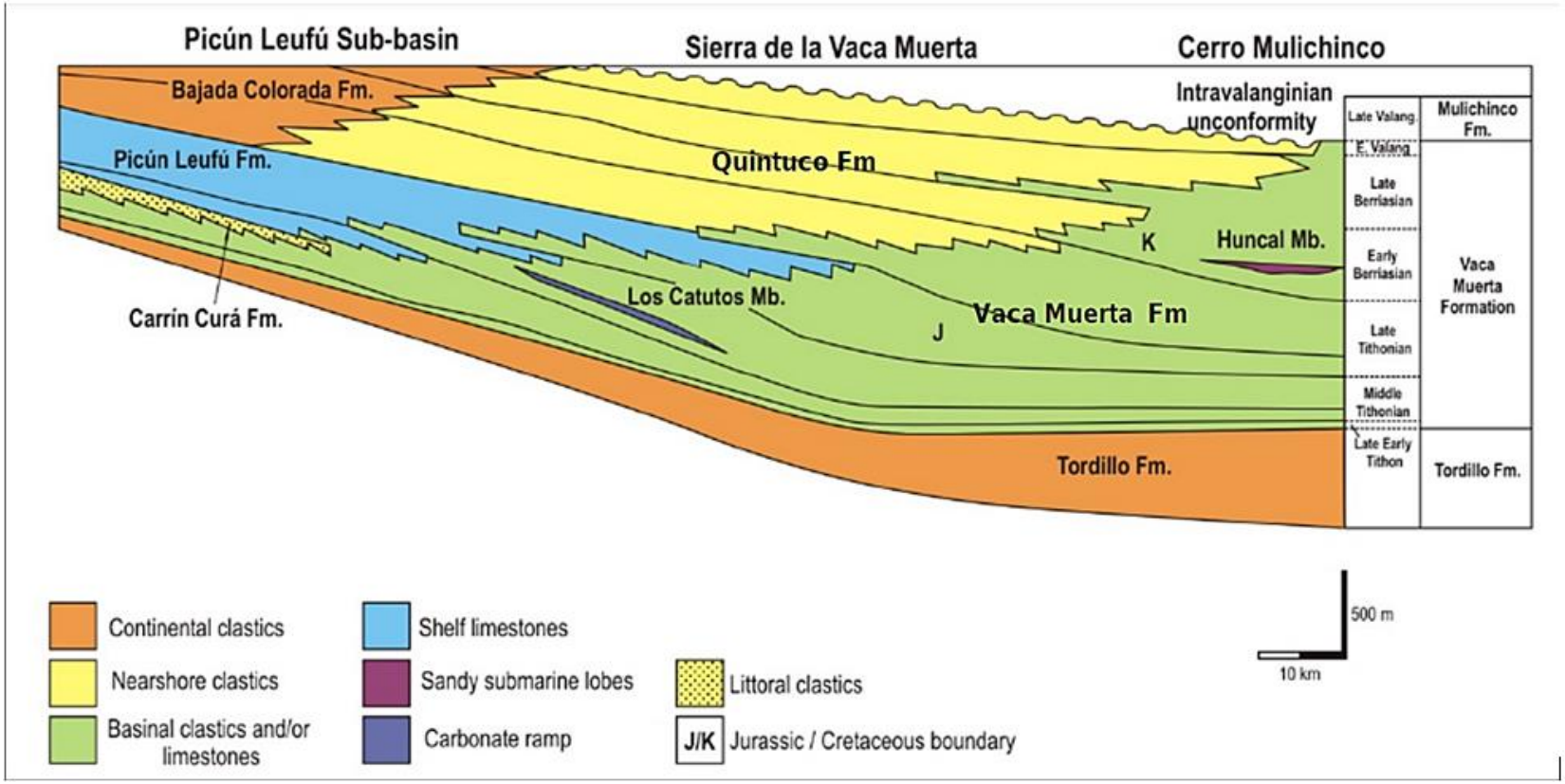

Figure 5-2 Schematic cross section of Vaca Muerta Fm. and neighboring formations in the western part of the Neuquén basin. Modified from Leanza, 1973; Gulisano et al., 1984 and Leanza, 2011.

The Vaca Muerta The Vaca Muerta formation consists of highly bituminous shales, with TOCs of 2-8% (Leanza, 2012). The organic-rich facies developed in a backarc marine embayment, under anoxic conditions, in tune with the Jurassic-Cretaceous changes of eustasy (Mitchun and Vliana, 1985). It is a rich, oil-prone black shale and the most important source rock in the basin. Except in the east, the Vaca Muerta formation is everywhere mature for oil generation (Figure 5-1).

Previous studies tell that the Vaca Muerta formation displays cyclic sedimentation, with rhythmical alternation of black shales, grey shales, marls and siltstones, with bioclastic mudstones, wachestones, packstones, floatstones and rudstones. (Kietzmann et al., 2008) The facies mentioned above may not all have been observed in this study, but in general my observation matches that of Kietzmann's at Arroyo Mulichinco and El Puesto outcrops, and in the wells. These cyclic lithology changes provide material interfaces, which may provide mechanical heterogeneity within the host rock. Besides, at both outcrops, the volcanic Tuff layers (Figure 5-4) and bed-parallel aligned calcareous concretions (Figure 5-3) interbedded with black or grey shales. They can also provide candidates of mechanical interfaces, along which bed-parallel fractures may tend to occur.

Excellent outcrops of the Vaca Muerta formation are found at the Arroyo Mulichinco and El Puesto localities, close to the town of Loncopue (see Chapter 2 for details). The river-cut cliffs and shallow water river-bed are fairly well preserved outcrops which provide an ideal opportunity to collect fracture attributes and study lithological controls on fracture intensity. The 3 wells used in this study are in the oil window. The Vaca Muerta #1 well is considered a good subsurface analogue to the outcrop while other studied wells may not be as comparable toward the outcrop. Vaca Muerta well #1 is also the well from which I have the most comprehensive and complete

dataset. Although the well and outcrop may not share all host rock characteristics, I was able to find most features of interest at outcrop in cores as well, such as black and grey shales, fossils, tuff layers and concretions.

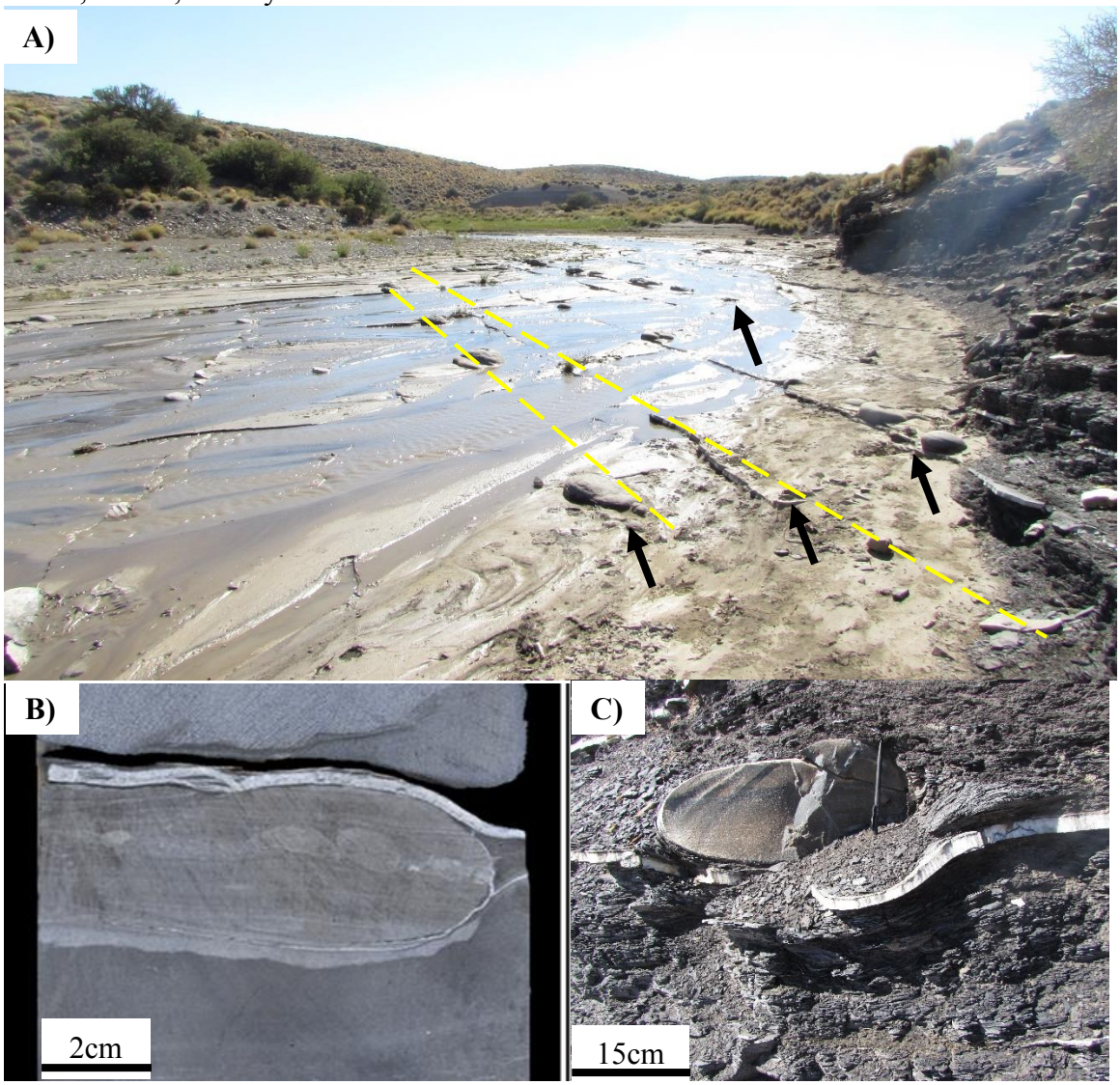

Figure 5-3 A) Aligned large concretions seen at reverbed and river-cut cliff. The concretions aligned parallel to the bedding, marked by dashed lines and arrows. Approx. width of the river is 30m; B) Bed-parallel fracture associated with concretion observed from core #1. C) Fibrous bed-parallel fracture formed along the concretion observed at outcrop.

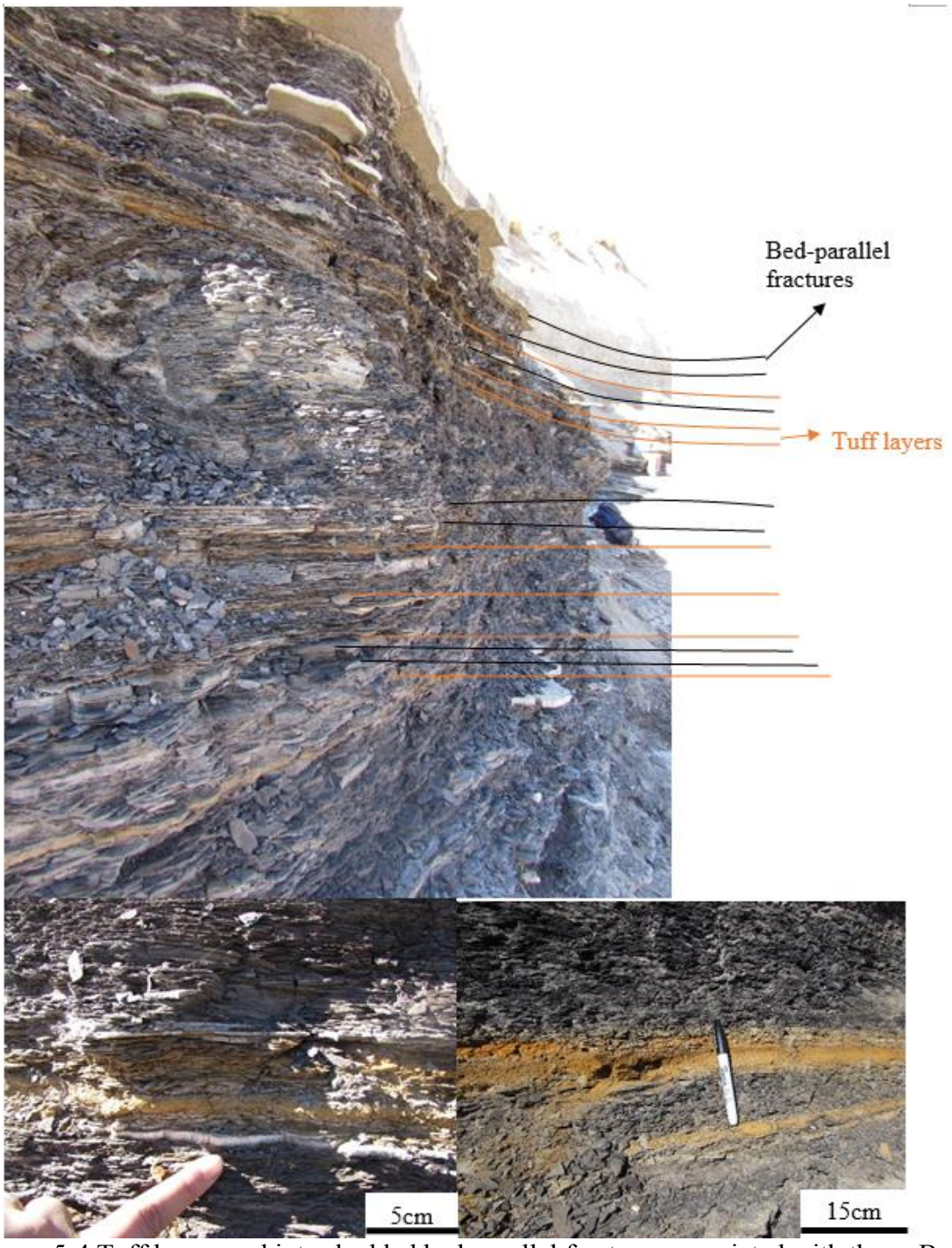

Figure 5-4 Tuff layers and inter-bedded bed-parallel fractures associated with them. Bed-parallel fractures tend to occur along the margins of tuff layers what is common in this outcrop area. Shale and tuff layers have different mechanical property so that the margin of the tuff layers can be considered as a surface of mechanical heterogeneity along which the bed-parallel fractures formed preferentially.

5.2 CORE STUDY – CORRELATION BETWEEN HOSTROCK LITHOLOGICAL CHARACTERISTICS AND HIGH FRACTURE INTENSITY

5.2.1 High fracture intensity and Organic richness

In this part of study, I investigated a possible correlation between fracture intensity and organic richness. Bed-parallel fracture aperture size and spacing data measured from core scan images (see Chapter 2), were converted into a text file and imported into software that can generate a fracture intensity curve along a scanline (CorrCount software developed by Dr. Randall Marrett, 2015). The fracture intensity curve can be used to visualize the variation in intensity with depth. The fracture intensity dataset generated by the software can be imported through Petrel （2013） to become a fracture intensity log, which can then be put side by side by other logs. In this case, GR (Gamma Ray), TOC (Total Organic Carbon)-kerogen log, and Lab TOC measurements are considered a proxy of TOC content of shale (Figure 5-5).

TOC-Kerogen is the amount of TOC based on kerogen volume. It is estimated from GR, sonic, density, neutron and NMR well log data (Gonzales et al., 2013). Lab TOC was measured from core samples, and displayed as a log in the same composite plot (Figure 5-5, second track). The logs, except for fracture intensity log, were provided by YPF. Figure 5-5 shows one of the studied Vaca Muerta wells- VM well #1. Lab-TOC spikes match with 4 major fracture intensity peaks. TOC-KER is also a good match to fracture intensity, but generally not as well matched as lab TOC. Correlation of fracture intensity with TOC supports the hypothesis that bed-parallel fractures are more intense in organic rich layers.

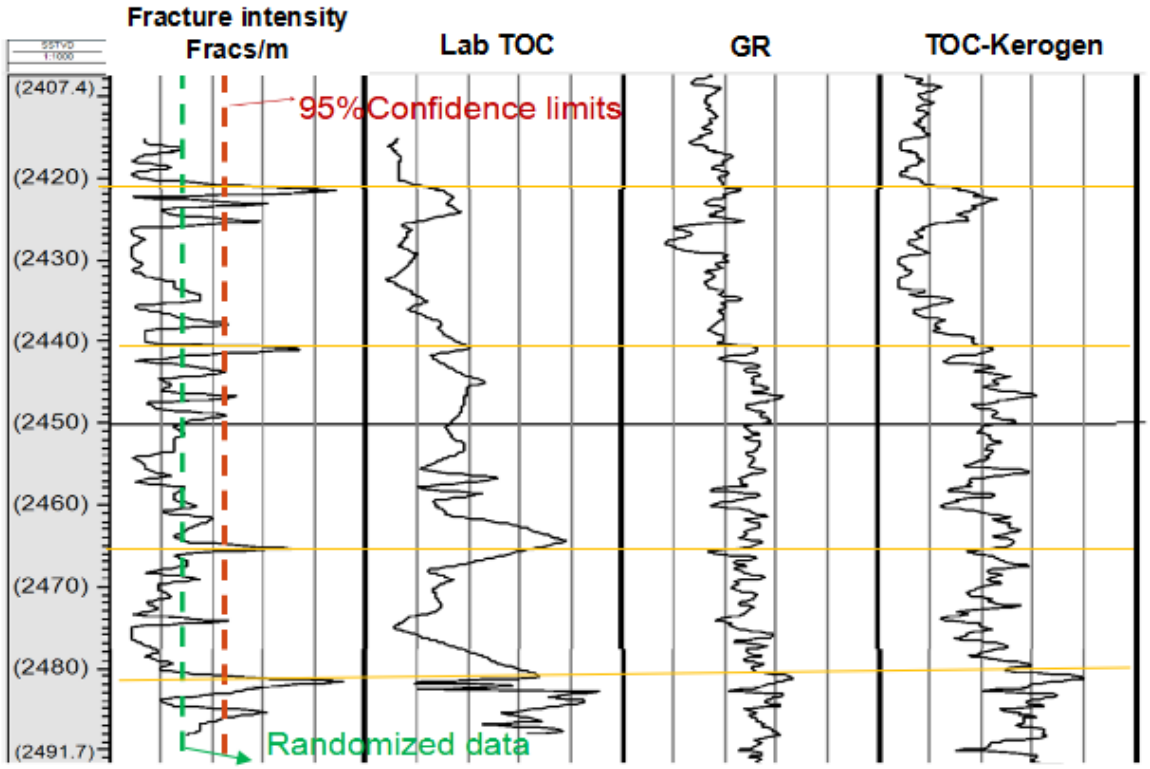

Figure 5-5 Well log correlation between the peaks of fracture intensity and organic richness. Lab-TOC spikes match with 4 major fracture intensity peaks. The 4 fracture intensity peaks are above the 95% confidence limits for a random distribution of fractures, which indicates that the fractures are more clustered than would be the case for a random distribution.

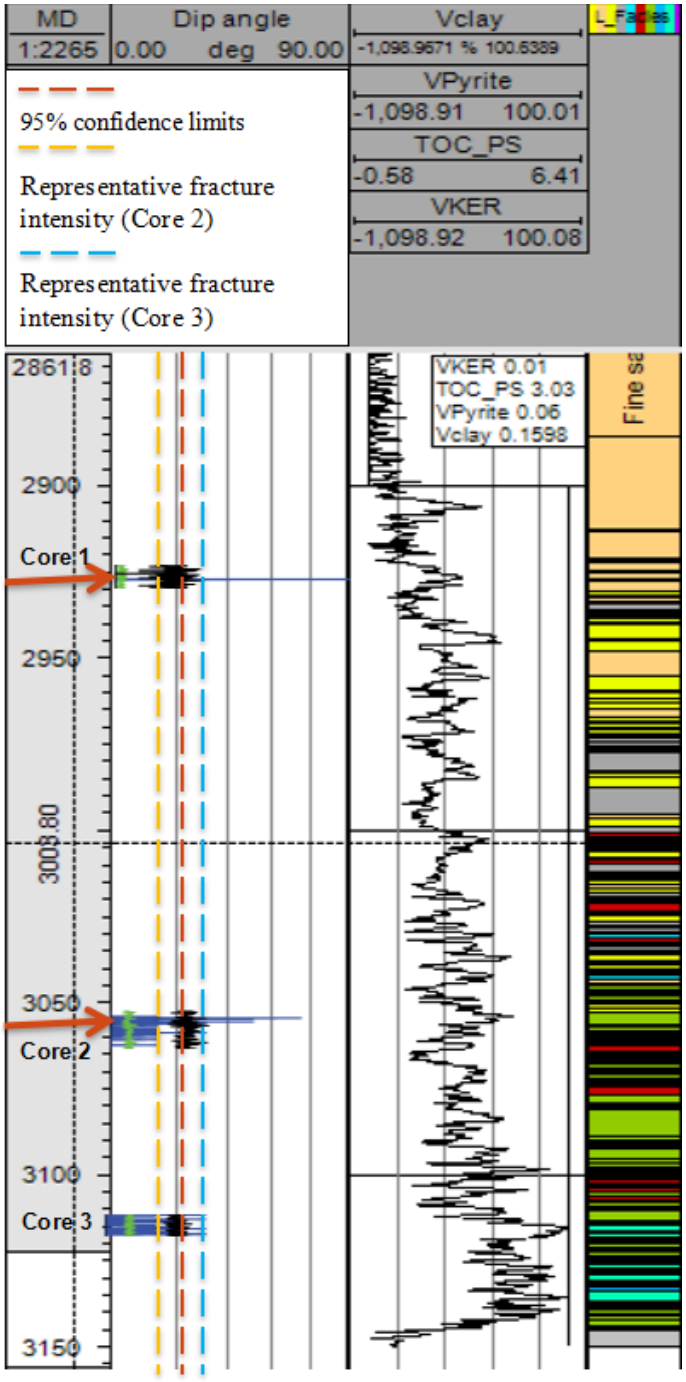

Figure 5-6 Well log correlation between the peaks of fracture intensity (left column, in blue) and organic richness. Fracture intensity peaks (pointed out by red arrow, above the 95% confidence limits) match local maximum organic content. Compared to core 2, core 3 in general has a higher organic content. Although there are no exceptionally high fracture intensity peaks within core 3, the fracture intensity in this core is generally higher than that of core 2.

Figure 5-11 shows another example where fracture intensity peaks match local maximum organic content. There are three short cores from the Vaca Muerta Well #3. Lacking long, continuous core and lab TOC measurement, data quality from this well is not as good as that from the VM Well #1. The well log-intensity correlation still shows fracture intensity peaks (pointed out by red arrow, above the 95% confidence limits) match local maximum organic content within core 1 and core 2. Another finding is that although there are no exceptionally high fracture intensity peaks within core 3, the fracture intensity in this core is generally higher than that of core 2. Core 3 has multiple smaller peaks, but they are all above the 95% confidence limits. So actually core 3 can be considered rich in bed-parallel fractures. Compared to core 2, core 3 in general has a higher organic content. The two findings from Vaca Muerta Well #3 support the hypothesis that bed-parallel fractures tend to be more intense in organic rich layers.

We need to be careful drawing the conclusion that bed-parallel fractures are usually more intense in well-log indicated organic-rich layers. In the Vaca Muerta well #2 the bed-parallel fracture intensity (Figure 5-7, left column, shown in blue) does not show a strong correlation with the TOC-kerogen log. At some depths, high TOC correlates to high intensity but this is not always the case. For example, at around 2436m depth, the fracture intensity peak does not overlap with the local high of TOC. For this well, lab TOC measurements were not available.

Near the bottom of the depth column in Vaca Muerta well #2, at around 2750 m depth, TOC content increases, and the left color column indicates an abrupt change from organic rich shale to organic rich carbonate (may be marl). Although no core is provided below 2750m, it is clear that the highest spike of fracture intensity occurs at the abrupt lithology change. This relationship is consistent with the hypothesis that bed-parallel fractures develop preferentially at mechanical interfaces.

On the basis of observations in these three wells, it appears that bed-parallel fractures correlate with higher TOC in some locations but not in others, and that in one case, a large lithological change coincides with a peak in fracture intensity. There is no one-to-one relationship, however, and the coincidence in location between fractures and other properties may not indicate a causal relationship. We can say that the results do not falsify either hypothesis, but neither do they fully support either one. It is likely, therefore, that more than one factor controls the location of bed-parallel fractures in the Vaca Muerta reservoir rocks sampled by the wells in the study.

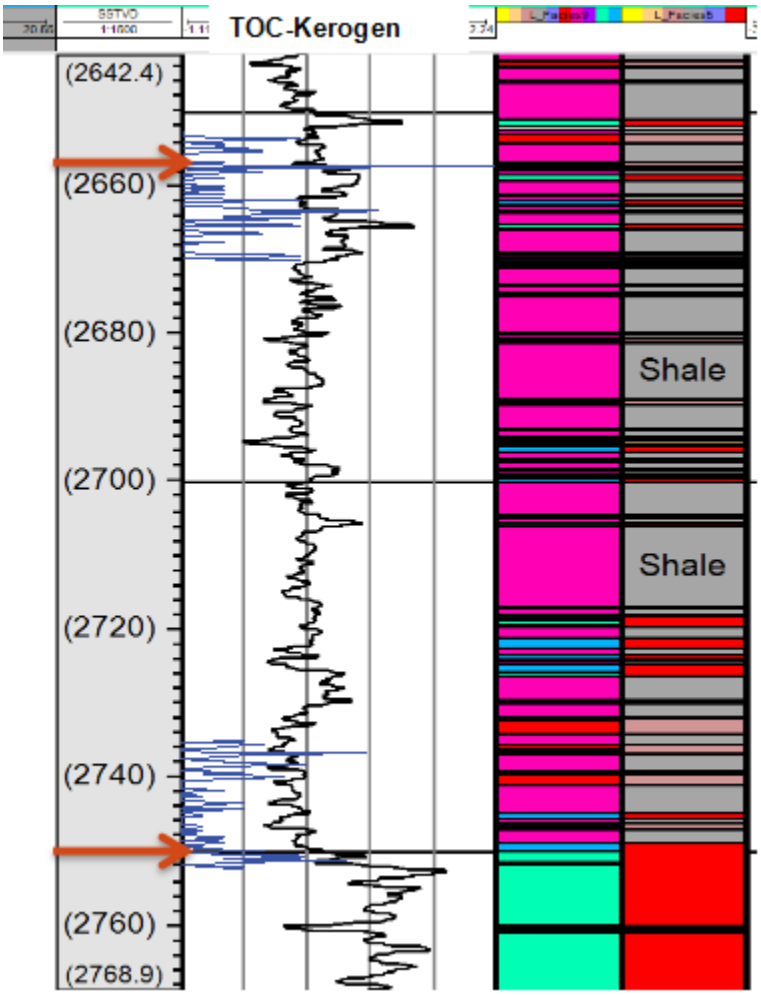

Figure 5-7 The bed-parallel fractures intensity (left column, shown in blue) in this well is not showing strong correlation with TOC-kerogen log. The highest spike of fracture intensity happens right at where the abrupt lithology change is (~2750m).

5.2.2 Shale lithology and fracture intensity

A variety of shale lithologies are present in Vaca Muerta Formation. Vaca Muerta formation displays cyclic sedimentation, with rhythmical alternation of black shales, grey shales, marls and siltstones, with bioclastic mudstones, wackestones, and packstones. A common approach for studying the relationship between fracture intensity and sedimentary facies is to build a lithology column and compare fracture intensity with the different rock types. This approach could not be used for all the datasets for this study

because: 1) identification and description of shale lithologies in logs is not always consistent from well to well, and is challenging to compare to outcrops (2) VM wells #2 and #3 have several short cores so that the lithology coverage within the studied depth range is limited. Instead, I chose to analyze the VM well #1 only.

The VM well #1, has 90 m of continuous core, a full set of well-log data including lab TOC, and I was able to examine several core samples from different depths from both fracture-rich and fracture-barren locations. These samples were made into thin sections for petrographic study. I used the mudstone classification proposed by Milliken (2014) for general classification and lithology description of the samples. This tripartite compositional classification of fine-grained rocks effectively assigns fine-grained rock to one of the three classes: Tarl, Sarl and Carl. The grain assemblages that define these classes follow contrasting and predictable diagenetic pathways that have significant implications for the evolution of bulk rock properties. Thus, as Milliken (2014) states, assigning a fine-grained rock to one of these classes is an important first step for predicting for predicting properties that might affect fracture generation and growth. My main purpose of doing lithology description and classification is to see if the hostrock (shale) at fracture rich positions share any similarities. Likewise for the host rock from where there are no bed-parallel fractures. I also want to compare the two groups of lithologies to determine if there are differences that can explain the fracture intensity variability.

13 thin sections were made out of the VM well #1 core samples. Table 5-1 summarizes basic information of these thin sections, such as their depth, bed-parallel fracture intensity, and other features within the sample. Photos of core samples and thin sections are documented in Appendix B.

Table 5-1 Summary table of Vaca Muerta well #1 thinsections.

No.	Sample #	Depth (m)	Features (b=Bed-parallel fracture; v=vertical fracture)	Bed-parallel Fracture
1	1-7-M	2427.2-2427.27	v	rare
2	1-9-M	2424.84-2424.81	b	common
3	1-19-M	2415.06-2415.11	v	rare
4	2-7-M	2445.05-2445.02	b, v	common
5	3-2-M	2468.79-2468.73	b, v	common
6	3-3-M	2467.74-2467.71	b, v	common
7	3-5-M	2465.29-2465.18	b, v	common
8	3-16-M	2454.29-2454.23	v	rare
9	3-18-M	2452.77-2452.74	b	common
10	4-6-M	2482.83	b	common
11	4-7-Ma	2481.82-2482.0	v	common
12	4-7-Mb		b, v	
13	4-4-M	2484.56-2484.51	b	common

A Field sample from the thick-beef rich area at Arroyo Mulichinco (#14), and a sample from the relatively beef-barren outcrop at El Puesto (#15), were also analyzed.

As a result of petrographic analysis, 6 representative lithologies were identified in the VM Well #1.

Table 5-2 Examples of typical lithology in VM Well #1.

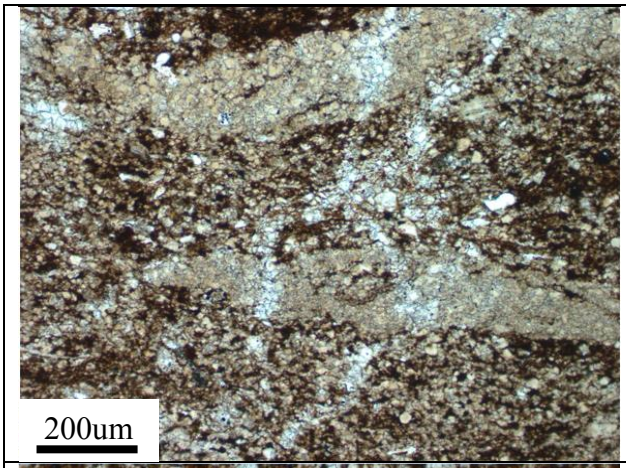	Dolomite replaced carbonate mud, with calcareous pellets. Sample 1-7-M, plane light. (Carl)
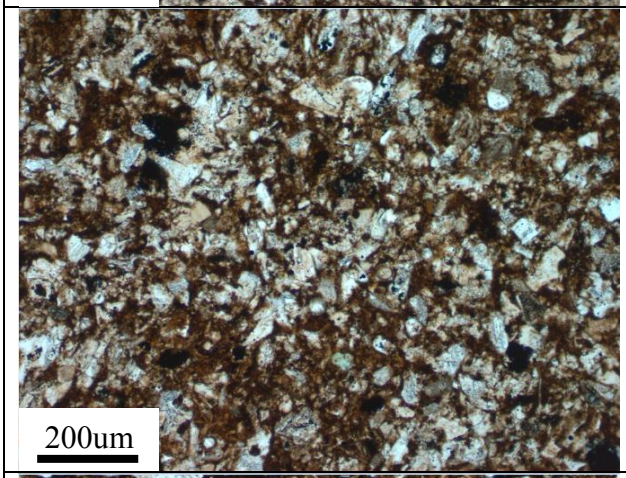	Silt - feldspar– clay mixture. Minor calcite component. Sample 1-19-M, plane light. (Tarl)
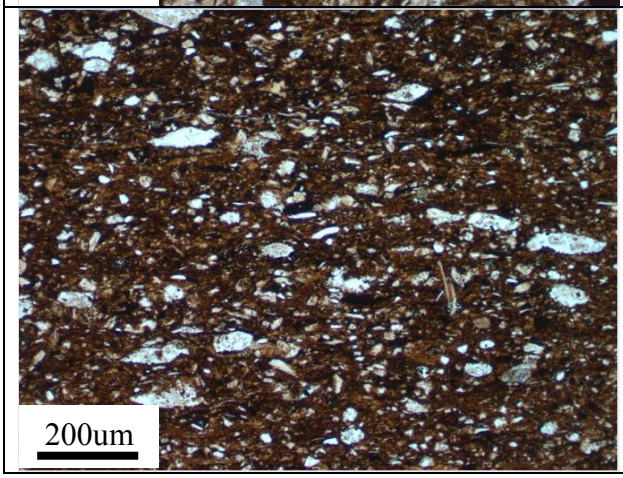	Clay rich, silt bearing. Detrital feldspar and carbonates. Have some diagenetic carbonates, but low in content. Sample 3-16-M, plane light. (Tarl)

Table 5-2 continued

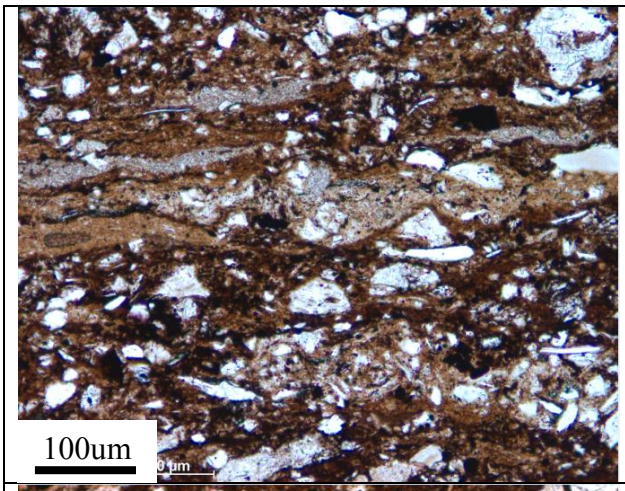	Pellets and aggregations everywhere. Pellets are calcareous mud or clay rich. Silt and fine sand bearing. Sample 1-9-M, plane light. (Carl)
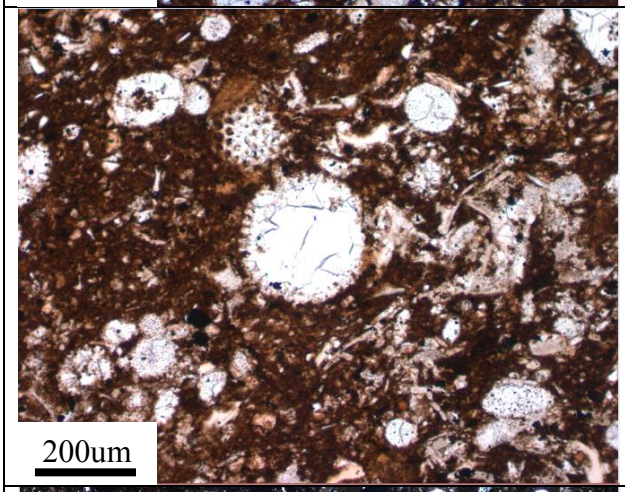	Quartz-replaced sponge spicules and radiolarians. Silt-bearing, clay-rich mudstone. Sample 3-2-M, plane light. (Sarl)
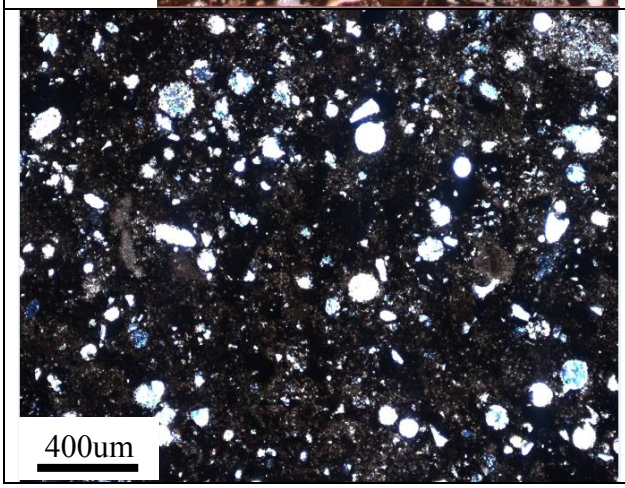	Calcite replaced radiolarians. With pellets. Silt-bearing, clay-rich mudstone. Field sample from beef-rich Arroyo Mulichinco outcrop, XPL. (Carl)

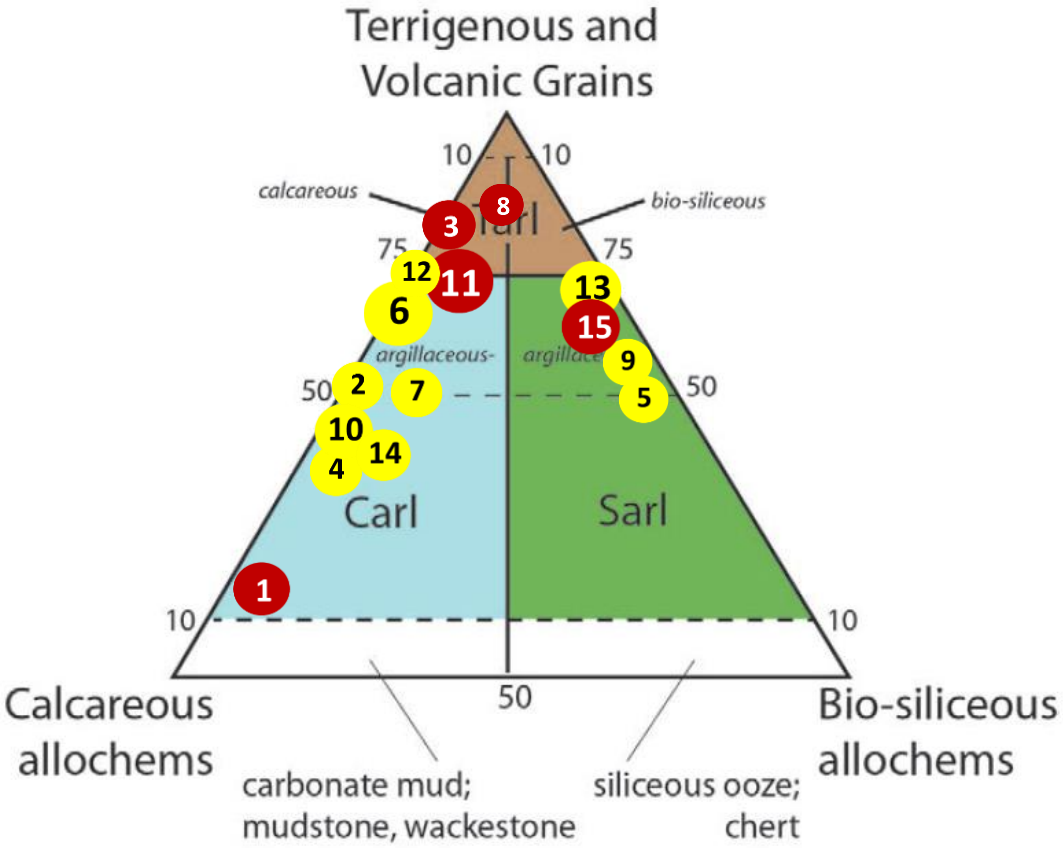

Figure 5-8 Classification of the 13 core samples and 2 field samples using Milliken mudrock classification. (Milliken, 2014) Red spots represents fracture barren lithology and yellow spots represents fracture rich lithology.

Figure 5-8 shows the classification of the 13 core samples and 2 field samples. Since the classification is performed without extensive help of SEM and XRD, the size of the dots on the diagram indicate an estimate of uncertainty. Uncertainty can also come from low magnification of image, and the dark field of view if the shale has an exceptionally low transparency.

Most samples contain glass shards and feldspar as a minor component, which brings majority of analyses to the upper half of the diagram. It is highly notable that except for sample 1, all other four host rocks barren in bed-parallel fractures plot within or near the edge of the Tarl class. It means that the host rocks with higher content of terrigenous components, such as quartz, feldspar, detrital calcite and clay, and lithic

fragments, tend to be less favored by bed-parallel fracture generation. Sample 1 is almost purely dolomitized calcareous mud. Its mechanical property could be highly different from rest of the samples. For example, the rock can be highly homogeneous and strong after dolomite replacement, which can be the reason why bed-parallel fractures do not form within this lithology.

The rock hosting high intensity bed-parallel fractures tend to fall into the classes of Carl and Sarl. In this well, Carl is more abundant. The environments forming Carl and Sarl are most likely to be marine, whereas the Tarl is formed in a dryer environment with less organic matter involved. Bed-parallel fractures are thought to favor host rocks with higher TOC content, so they are expected to be fewer in the Tarl facies. The prediction is consistent with the observation from core. This finding supports the hypothesis that the bed-parallel fractures tend to have a higher intensity in higher TOC shales.

5.2.3 Fracture occurrence and material interfaces

Another control of fracture spatial organization may be weak mechanical interfaces within the hostrock. Material interfaces may be a candidate of mechanical interfaces. Figure 5-9 is a photo showing examples of material interfaces considered in this study. Material interfaces considered include abrupt lithology change, and concretion margins. Abrupt color change or competence change of the core are used as proxy of lithology change.

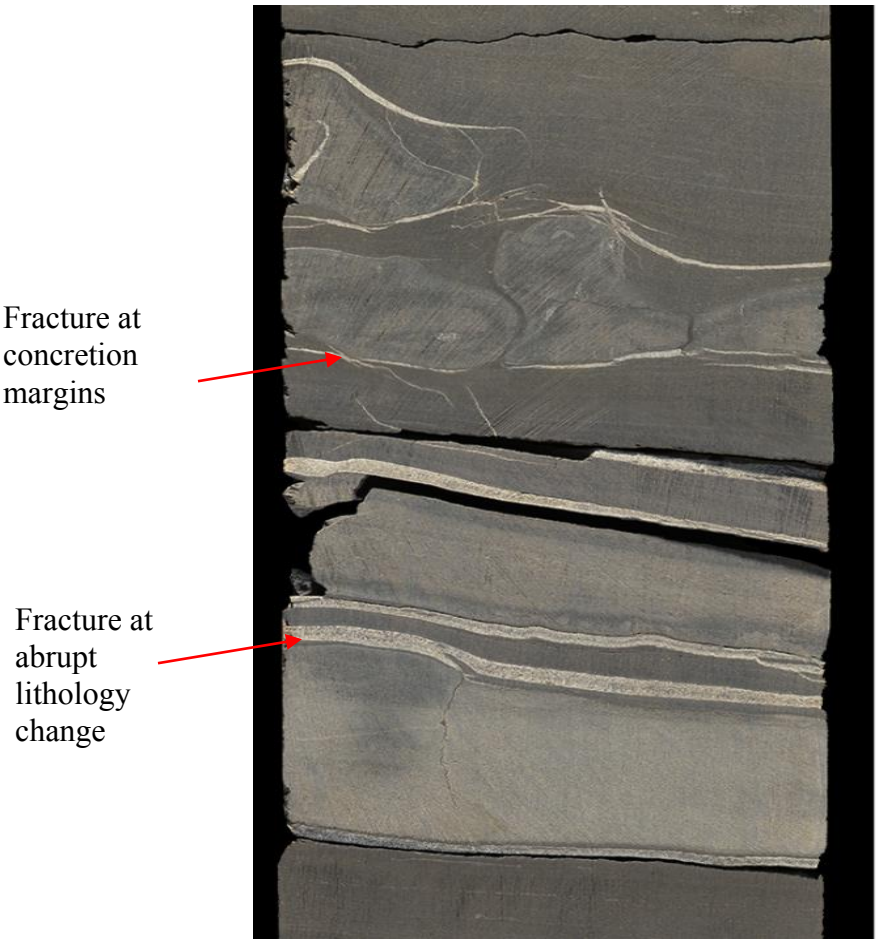

Figure 5-9 A photograph of Vaca Muerta core showing bed-parallel fractures along interfaces. Material interfaces considered in this study include abrupt lithology change, and concretion margins. Upper half of the photo shows fracture associated with concretions. Lower half of the photo is an example of fracture formed along abrupt lithology change (material interfaces).

I quantified the percentage of bed-parallel fractures that occur at material interfaces (Table 5-3). To perform a more detailed analysis, I further separated the two types of material interfaces out in the table. Based on the calculation, 25-30% of the bed-parallel fractures occur at material interfaces. These interfaces may allow fracture growth, due to reduced bed-parallel strength. Then I looked into the question the other way around, trying to see the percentage of material interfaces with fracture occurrence. The result turns out to be around 65-75% of material interfaces have bed-parallel

fractures associated with it. This finding supports the hypothesis that bed-parallel fracture form preferentially along mechanical interfaces.

It may be too early to draw a conclusion that bed-parallel fracture form preferentially along mechanical interfaces. Most interfaces host fractures but not all fractures occur at interfaces, so that there is likely a combination of factors controls fracture location. It may be possible to surmise that with all other factors being equal, successions with multiple lithology changes are more prone to hosting bed-parallel fractures than more homogeneous successions. Gaining a comprehensive understanding of how all the potential controlling factors affects the distribution of bed-parallel fractures is beyond the scope of this study.

Table 5-3 Result of the quantification of the percentage of bed-parallel fractures occur at material interfaces, and the percentage of material interfaces have bed-parallel fractures.

		Occurrence			% of material interfaces with fracture occurrence
wells	Total # of fractures	At material interfaces	At lithology change	At concretion	
Vaca Muerta well #1	341	105 (30.7%)	35	71	64%
Vaca Muerta well #2	229	55(24.0%)	44	11	76%
Vaca Muerta well #3	142	44(30.9%)	44	N/A	70%

5.3 CONCLUSIONS

In this chapter, two hypotheses regarding the spatial organization were tested: 1) Bed-parallel fractures tend to be more intense in organic rich layers, on the basis that bed-parallel fractures in the Vaca Muerta are generated as a result of fluid overpressure due to hydrocarbon generation in high TOC shales; 2) Bed-parallel fractures form preferentially along mechanical interfaces within host rock such as abrupt lithology changes and concretions. These interfaces may allow fracture growth, due to reduced bed-parallel strength.

To find the correlation between host rock lithological characteristics and high fracture intensity, core data from 3 Vaca Muerta wells are used. In VM well #1, lab-TOC spikes match with 4 major fracture intensity peaks. TOC-KER is also a good match to fracture intensity, but generally not as well matched as lab TOC. Correlation of fracture intensity with TOC supports the hypothesis that bed-parallel fractures are more intense in organic rich layers.

The Vaca Muerta Well #3 core sample includes three short cores from one well. Lacking long, continuous core and lab TOC measurement, data from this well is not of good quality. But still, the well log-intensity correlation still shows fracture intensity peaks match local maximum organic content within short core 1 and short core 2. Another finding is that although there are no exceptionally high fracture intensity peaks within core 3, the fracture intensity in his core is generally higher than that of core 2. The reason for that might be, compare to core 2, core 3 in general has a higher organic content which act as a stimulating factor. The two findings from Vaca Muerta Well #3 also supports the hypothesis that bed-parallel fractures tend to be more intense in organic rich layers.

However, we need to be careful drawing the conclusion that bed-parallel fractures are usually more intense in well-log indicated organic-rich layers. Vaca Muerta well #2 shows a bed-parallel fractures intensity that is not having strong correlation with TOC-kerogen log. At some depth high TOC correlate to high intensity but not always the case.

After plotting all 15 samples on the ternary diagram, it showed up that the rock hosting high intensity bed-parallel fractures tend to fall into the class of Carl and Sarl. In this well, Carl is more abundant. It is not hard to predict that the Tarl facies will have less TOC content. Bed-parallel fractures are thought to favor hostrock with higher TOC content, so they are expected to be fewer in Tarl facies. The prediction is consistent with the observation from core. This finding supports the hypothesis that the bed-parallel fractures tent to be have a higher intensity in high TOC shales.

In the last part of the chapter, I present the result of analyzing the relationship between fracture occurrence and material interfaces. Based on the calculation, 25-30% of the bed-parallel fractures occur at material interfaces. Moreover, around 65-75% of material interfaces have bed-parallel fractures associated with it. It may be too early to draw a conclusion that bed-parallel fracture form preferentially along mechanical interfaces. However, based on the results from this study people may expect to see bed-parallel fracture occur where there is a material interface, if other requirements are all met.

Chapter 6. Discussion

The objective of this study is to characterize the bed-parallel fractures in Vaca Muerta Formation, Marcellus Formation, and Wolfcamp Formation. To achieve this, the morphology of bed-parallel fractures, their cement texture and composition are described and documented. The central hypotheses I tested regarding bed-parallel aperture size distribution is that the aperture size distribution may follow a power-law as is common for vertical fractures or they may follow a different function or other scaling patterns. Hypotheses regarding bed-parallel fracture spatial organization are that bed-parallel fractures may be more intense in organic rich layers or they may form preferentially along mechanical interfaces. As concluded in Chapter 4, bed-parallel fracture aperture size distribution tends to follow negative exponential function, and this type of fracture. In Chapter 5, result of studied bed-parallel fracture spatial distribution from Vaca Muerta formation shows that 25-30% of the bed-parallel fractures occur at material interfaces. Moreover, around 65-75% of material interfaces have bed-parallel fractures associated with it. It may be too early to draw a conclusion that bed-parallel fracture form preferentially along mechanical interfaces. However, based on the results from this study people may expect to see bed-parallel fracture occur where there is a material interface, if other ingredients such as compressional force, high-TOC hostrock, are all met. The study on bed-parallel fracture morphology, size scaling and spatial organization may lead to a better understanding of the driving mechanism and the nature of growth of bed-parallel fractures.

6.1 Mechanism of Bedding Parallel Fracture Generation

The mechanisms developing bed-parallel fractures are still under discussion, and there is no published or widely accepted distribution law/pattern. However, there are

proposed and widely thought causes of bed-parallel fractures from previous studies. A question that has arisen frequently in discussions is whether the opening of a beef vein is due to an internal agent, such as force of crystallization, or to an external agent, such as tectonic stress or pore fluid pressure. Cobbold et. al., 2013 states that possible causes of bed-parallel fractures are either (1) force of crystallization, or (2) seepage forces, due to fluid overpressure. For layers that form at depths of several km, fluid overpressure is the more likely cause. Cobbold et. al. listed a series of theoretical and experimental evidences supporting both the internal and external forces to be the dominant cause. For example, Keulen et al. (2001) did experiments on the hydration of anhydrite and succeeded in measuring a pressure of crystallization of as much as 11 MPa, equivalent to the vertical stress resulting from an overburden of 450-600 m. However, they did not manage to reproduce fibrous veins. External agents are harder to address. In a purely lithostatic situation, where a sedimentary basin is subject to no forces except those of gravity, the greatest effective stress should be vertical and the least effective stress should be horizontal (Sibson, 2003). On this basis, beef should not form in lithostatic basins containing isotropic rock. On the contrary, necessary conditions for the formation of bed-parallel tensile fractures would seem to be, either (i) a context of horizontal compression, due to additional tectonic forces, or (ii) a high susceptibility to fracturing along bedding, in other words, an anisotropy of tensile strength (Cosgrove 1995, 2001; Lash & Engelder 2005). Hydraulic fracturing of rock due to overpressure has been identified as one potential mechanism for the opening of horizontal fractures (Hilgers and Urai, 2002; Hillier and Cosgrove, 2002; Shearman et al., 1972), with seepage of pore fluids possibly causing the greatest effective stress to become horizontal as opposed to vertical (Cobbold and Rodrigues, 2007). According to Cobbold and Rodrigues (2007), the seepage forces of upward fluid flow counteract the weight of the rock, and even surpass it, generating a

tensile effective stress. Others propose that fibrous bedding-parallel fractures do not require fluid motion or increased fluid pressure, but rather form in a dilatant manner late in the diagenesis of the rock due to crystal growth in groundwater flow (Marshall, 1982). In fact, according to Wiltschko and Morse (2001), the term "crack-seal" is a misnomer in some cases, since cracking and precipitation are interactive and likely simultaneous (this view was disputed, however, by Laubach et al., 2004). Wiltschko and Morse (2001) attribute the growth of sealed fractures due to supersaturation at pressure solution locations followed by crystal pressure growth independent of increased pore fluid pressure. The samples of my study are from famous producing shale sources rocks in basins with complex structural deformation histories, so a combination of mechanical compaction and overpressure caused by hydrocarbon generation may plausibly be the initiating forces causing bed-parallel fractures. Evidence discussed below supports the combined mechanism mentioned above.

6.1.1 Evidence for Dilatancy

The horizontal bed-parallel fracture possesses features characteristic of dilatant veins, specifically antitaxial fibrous veins (Ramsay and Huber, 1983). These include: (1) the vein filling is of a crystal species that is uncommon or absent in the wall rock of the vein, (2) fibrous mineral habits perpendicular to the veinlet walls, (3) median sutures or median lines, (4) crystallographic continuity within a mineral across the vein, from median line to fracture wall, (5) mineral bands parallel to fracture walls and mirrored on either side of the median line, (6) linear shards of wall rock parallel to fracture walls, although not necessarily along the median line, and (7) trails of wall-rock shards across the filled fracture from wall to wall (Jowett, 1987; Rodrigues, 2009) (Figure 6.1, 6.2). Antitaxial veins are defined by Ramsay and Huber (1983) as being compositionally

different from the host rock (e.g., calcite veins in shale) and not in crystallographic continuity with the wall rock, whereas syntaxial veins are similar in composition (e.g., quartz veins in quartzite) and often show crystallographic continuity with wall-rock grains. Although similar in appearance, they differ in formation. Antitaxial veins grow by accreting material along the vein-wall contacts in a series of crack-seal cycles (Ramsay 1980), whereas syntaxial veins grow from one center along the median line. The shard trails across most of the studied bed-parallel fractures demonstrate that dilation occurred along the fracture walls and not along the median line (i.e., the central fill was formed first, and the outer bands last). For symmetrical bed-parallel fractures then, the crack-generating mechanism must act along both contacts more or less equally, though not necessarily simultaneously.

Most of the fibrous cement tend to have fatter fibers toward the fracture wall, which is another indication of antiaxial growth of fracture cement fibrous. Fracture opening creates enough space along fracture wall that enables the fibrous cement to precipitate overgrowth on existing fibrous fracture cement. Less competitive mineral growth during later stage cement generation results in fatter cement fibrous close to present day fracture walls (Figure 6.2).

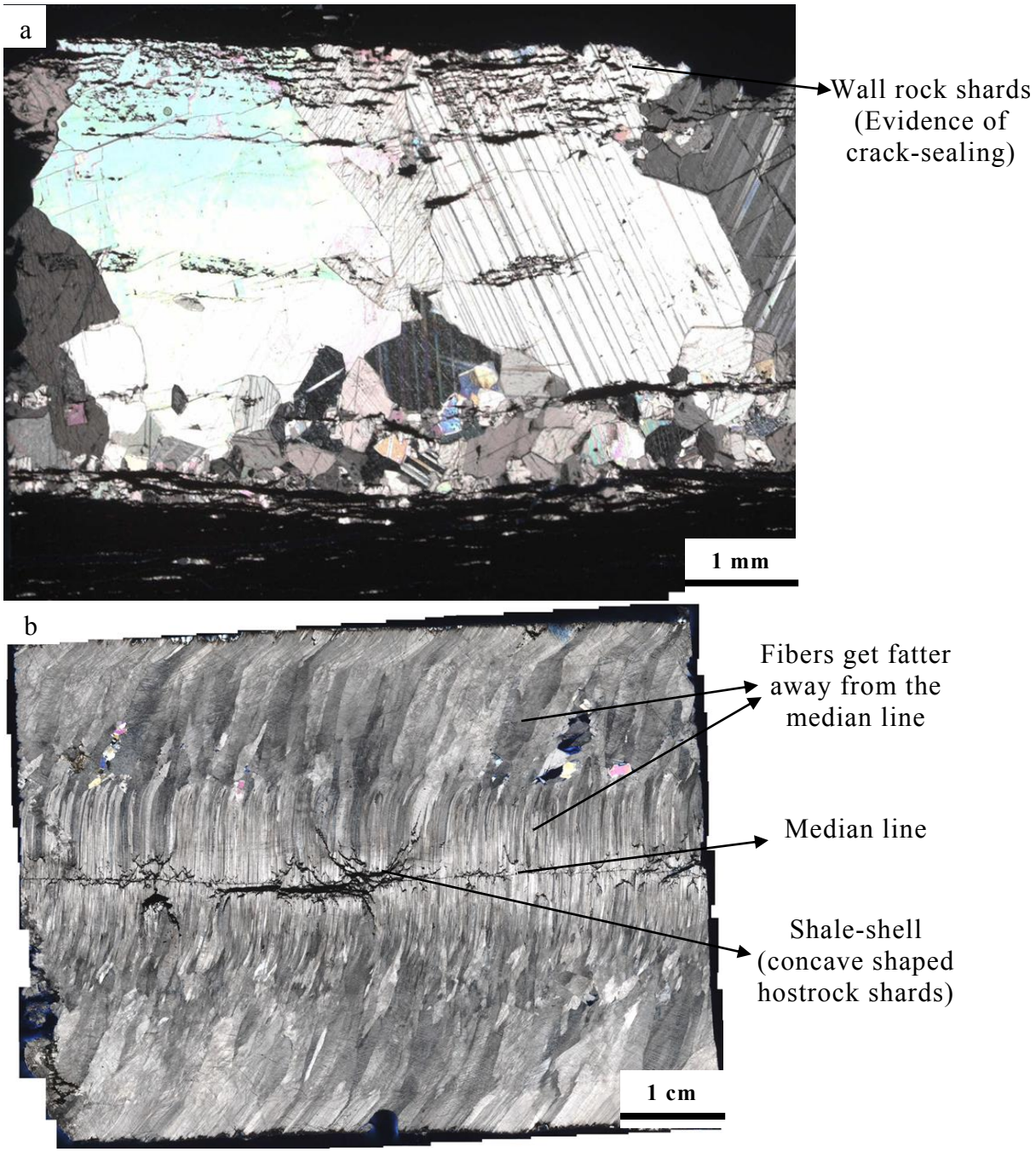

Figure 6-1 a) Linear shards of wall rock parallel to fracture walls, although not necessarily along the median line, indicating cycles of crack-sealing; b) Typical symmetrical fibrous calcite cement. Fibers perpendicular to fracture wall were formed due to fracture opening with no shear. The wider oblique fibers closer to fracture wall were formed as a result of both fracture opening and lateral shear.

Crack-Seal Mechanism

The median line of an antitaxial veinlet is formed when the central mineral band infills and seals the initial crack from wall to wall (Figure 6.2a). Increase of pore pressure opens a new crack between either wall and the vein-fill material, and more mineral fills this new crack as pressure is leaked (Jowett, 1987). Shard trails can be used to approximate the amount of opening during each crack-seal cycle. If a wall shard were formed at each cracking, the spacing between fragments in the trail represents the width of each crack. However, since there could be several episodes which did not break off pieces of wall rock, the spacing better represents the maximum width of the crack at any one time. In figure 6.2b. the irregular shards are spaced 50- 200 microns apart, and the number of shards indicates that a minimum of 9 crack-seal cycles were necessary to form the bed-parallel vein, assuming that the fracture wall at the bottom represents the first crack-seal cycle. As a general observation, trails of shards often appear to emanate from lithologic units in the wall rock, which are coarser than usual, leaving concave-shaped depressions where shards were broken off (Jowett, 1987).

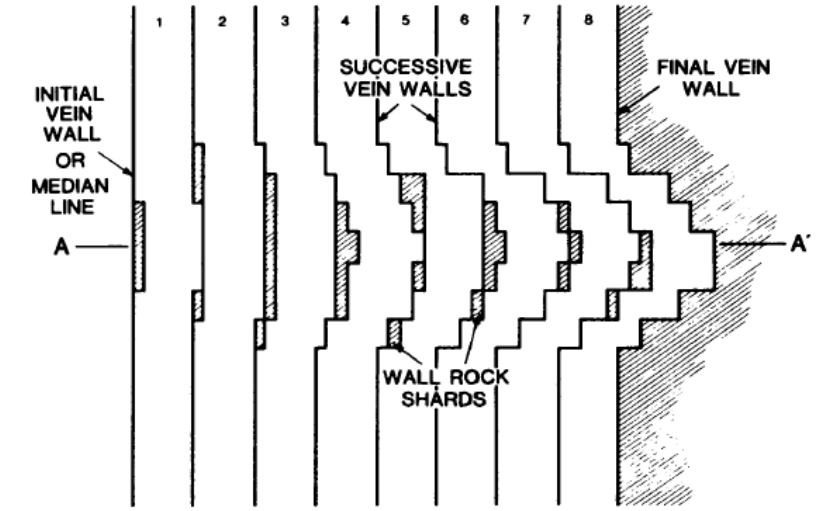

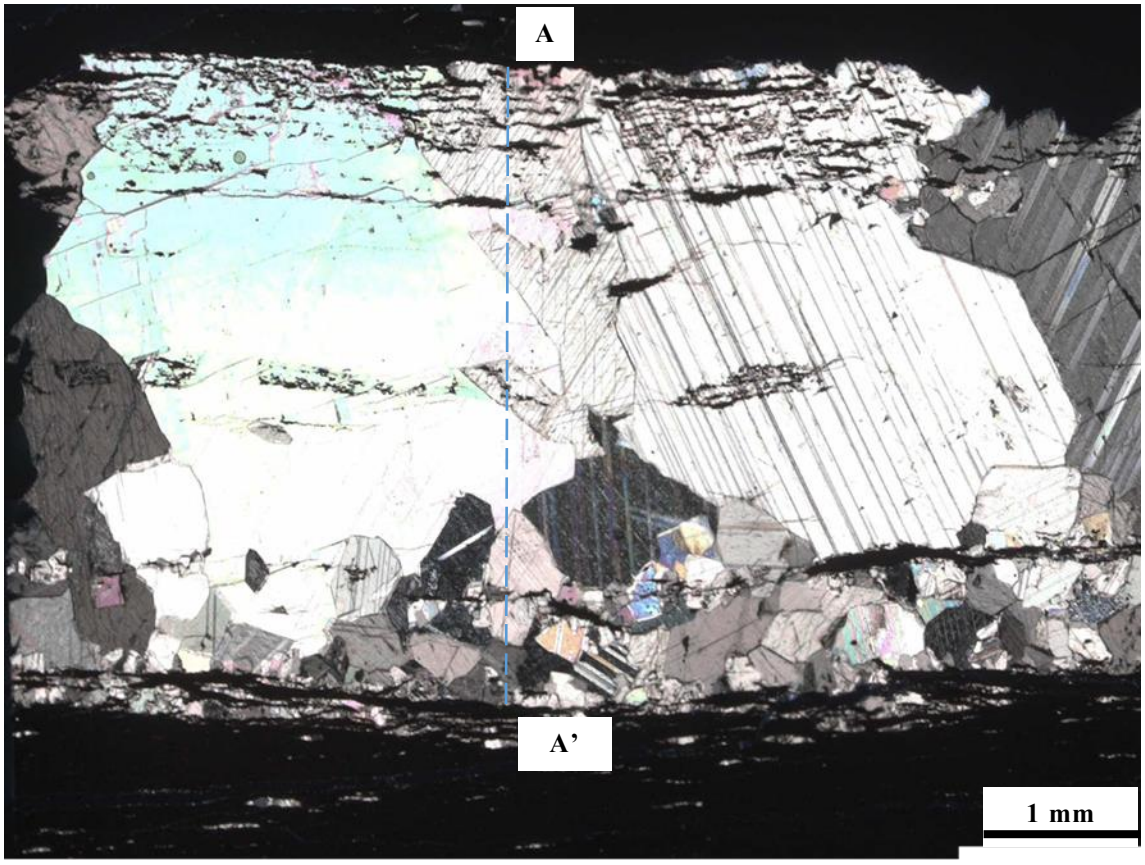

Figure 6-2 a) Schematic diagram of the formation of a trail of wall rock shards from the median line, where the rock first cracked, to the final veinlet wall in a series of crack-seal cycles. The trail along section A-A' in this figure suggests six cycles whereas eight actually occurred; b) The trail along A-A' in b) could be formed in a minimum of nine crack-seal cycles.

6.1.2 Evidence of Shear and in Relation with Local Structure

Curved fibers of calcite can record shear with bending of the individual fibers of calcite, however this is not always the case, as curved fibers do not necessarily track opening (Cox, 1987) (figure 6.2). Still, the local and regional stress directions may still have an effect on the orientation of fibers within bed-parallel fracture cement. As mentioned in previous Chapters, the studied outcrop area contains multiple evidences of compressional structural activities, including s thrust fault between the up and lower section of Vaca Muerta Arroyo Mulichinco outcrop, and an antiform-synform structure near the top of the Arroyo Mulichinco-up section outcrop. These structures are expected to be happened around the same time of the fracture formation, and they share dominant compressional force direction.

The attribute of the thrust fault plane was projected as $20^o/30^o$. Therefore, the fault is striking NE-SW; its western fault block is hanging. The direction of compressional force is WN-ES, close to E-W direction. This observation is consistent with the attitude of the fold structure around 100m to the west of the start point of the Arroyo Mulichinco-up section scanline. The trend and plunge of the fold axis is $186.1^o/4.0^o$. The strike and dip of the fold axial plane is $6.3^o/86.6^o$ E. The fold axis is plunging NE-SW with a very small deviation angle of around 6^o from N-S, indicating a E-W compressional force. The rose diagram with the attributes of cement fibers from Arroyo Mulichinco outcrops indicates that the majority of fibers are plunging to the west (southwest or northwest) in general (Figure 6.3). It means that the main inter-bedding shear direction is E-W. The shear direction indicated by the inclination of cement fibers is consistent with that of the local structures. Therefore, we may conclude that the fibrous nature of many bed-parallel fracture fills allows them to potentially be the structural force indicator, or at least, a shear indicator.

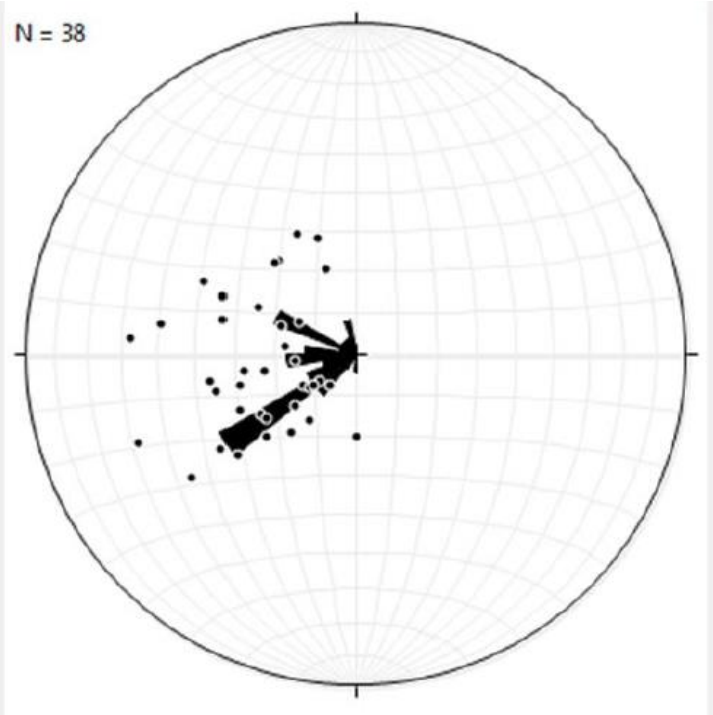

Figure 6-3 Rose diagram showing the plunging of beef cement fibers, which indicates the relative shear direction of the two fracture walls. The dominant shear direction is E-W in studied area indicated by inclination of cement fibers.

6.1.3 Petroleum Expulsion and Pore Pressure Increase

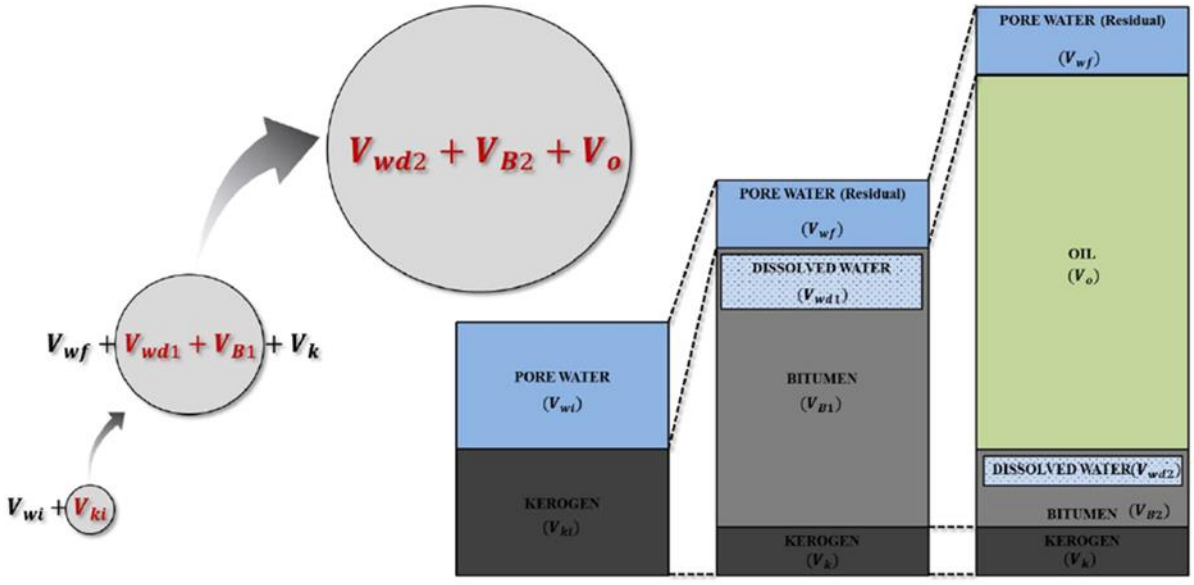

Figure 6-4 Full stages of oil generation and volume expansion (not to scale): Kerogen – bitumen - oil (from Al Duhailan, 2014)

$V_P(P_i) = V_{P_i} = Pore\ volume\ at\ initial\ pressure, before\ kerogen - to - bitumen\ conversion$
$V_P(P) = V_P = Pore\ volume\ at\ increased\ pressure, after\ kerogen - to - bitumen\ conversion$
$V_{wi} = Volumetric\ water\ content\ before\ kerogen - to - bitumen\ conversion$
$V_{wf} = Volumetric\ water\ content\ after\ kerogen - to - bitumen\ conversion$
$V_{wd1} = Volumetric\ dissolved\ water\ content\ in\ bitumen\ after\ kerogen - to - bitumen\ conversion$
$V_{ki} = Volumetric\ Kerogen\ content\ before\ kerogen - to - bitumen\ conversion$
$V_k = Volumetric\ Kerogen\ content\ after\ kerogen - to - bitumen\ conversion$
$V_{B1} = Volumetric\ bitumen\ generated\ after\ kerogen - to - bitumen\ conversion$

Mass Balance Approach:

$$V_P(P_i) = V_P(P)$$

$$V_{P_i} = V_P$$

$$V_k = V_{ki} - FV_{ki}$$

$$V_{B1} = F\left(\frac{\rho_k}{\rho_B}\right)V_{ki} \qquad \left(\frac{\rho_k}{\rho_B} = D_{kB}\right)$$

$$V_{wf} = V_{wi} - V_{wd1}$$

$F = Converted\ fraction\ of\ Kerogen$
$\rho_k = Density\ of\ Kerogen$
$\rho_B = Density\ of\ Bitumen$
$D_{kB} = Kerogen - Bitumen\ density\ ratio$

Figure 6-5 Mass balance approach estimating volume expansion of shale during Kerogen-Bitumen-Oil conversion. From Al Duhailan, 2014.

During the primary migration process within these extremely low-permeability rocks, petroleum is expelled, causing a volume expansion followed by a significant increase in pressure (Figure. 6.4). Based on the mass balance (Figure. 6.5), with 100% of kerogen converted to bitumen, only 4% volume expansion occurs. However, conversion of 100% of the generated bitumen to oil can cause as much as 30% volume expansion to the original volumetric kerogen content in the rock (Al Duhailan, 2014). Consequently, the force of petroleum expulsion is initiated, driving fluids to migrate initially along pressure-induced, bedding-parallel fractures until reaching near-vertical fractures. This

volume expansion, which has been invoked as a mechanism to increase pressures and fracture, has been documented by several authors (Momper, 1978; Meissner, 1978; Swarbrick and Osborne, 1998). Utilizing the concept of poroelastic deformation and the role of pressure in fracturing (Secor, 1965; Engelder and Lacazette, 1990), conditions that may drive horizontal, layer-parallel crack propagation were highlighted by Lash and Engelder (2005).

Al Duhailan (2014) derived two equations modelling the increase in pressure due to kerogen-bitumen-oil conversion, by using the mass balance approach and compressibility relationship with volume expansion and pressure increase. The increase in pore pressure due to petroleum expulsion is calculated based on the equation from Al Duhailan (2014) (Figure 6.6, Figure 6.7). The governing equations he proposed for pressure increase are derived with the consideration of the full stages of oil generation (kerogen-to-bitumen-to-oil). It is an extension based on the work of Berg and Gangi (1999).

During kerogen-bitumen conversion, the volumetric ratio term VR includes the organic richness, porosity and density of the rock:

$$\Delta P_{kB} = \frac{F(D_{kB}-1)}{V_R\left(\frac{3(1-2v)}{E}+C_w\right)+F(D_{kB}C_O-C_k)+\left(\frac{3(1-2v)}{E}+C_k\right)}$$

$F = Converted\ fraction\ of\ Kerogen$

$D_{kB} = Kerogen - Bitumen\ density\ ratio$

$E = Young's\ modulus$

$v = Poisson's\ ratio$

$V_R = \frac{V_{wi}[D_{kr}+a(TOC)(1-\phi)(1-D_{kr})]}{a(TOC)(1-\phi)\times 100}$ (Vernik, 1994)

$V_{wi} = \frac{\phi}{Specific\ gravity \times(1-\phi)}$ (Rieke and Chilingrian, 1974)

$a = transformation\ coefficient\ to\ organic\ matter \approx 1.3$ (Vernik, 1994)

$TOC = Totla\ Organci\ Content$

$\phi = matrix\ porosity$

$D_{kr} = Kerogen - rock\ density$

$C_w, C_O\ and\ C_k = water, oil\ and\ kerogen\ compressabilities$

$V_R = \frac{V_{wi}[D_{kr}+a(TOC)(1-\phi)(1-D_{kr})]}{a(TOC)(1-\phi)\times 100}$ (Vernik, 1994)

$V_{wi} = \frac{\phi}{Specific\ gravity \times(1-\phi)}$ (Rieke and Chilingrian, 1974)

$a = transformation\ coefficient\ to\ organic\ matter \approx 1.3$ (Vernik, 1994)

$TOC = Totla\ Organci\ Content$

$\phi = matrix\ porosity$

$D_{kr} = Kerogen - rock\ density$

Figure 6-6 The governing equations for pressure increase are derived with the consideration of hydrocarbon generation, taking various of source rock properties into account. It is used for modelling the increase in pressure due to kerogen-bitumen-oil conversion,

To study the role of organic richness and porosity of the rock during kerogen-bitumen conversion, a comparison of rich (25% TOC), lean (2.5% TOC), high porosity (30%) and low porosity (5%) was performed. The TOC and porosity range is set to be larger than what is reasonable for natural shale, for the purpose of showing significant difference in the amount of pressure increase under different scenarios. Other inputs used in the analysis is listed in Table. 6.1. Then I put in real parameters from Vaca Muerta Formation, a formation considered to be rich in bed-parallel fractures, to estimate the increase in pressure due to kerogen-bitumen conversion.

Table 6-1 Inputs used in the analysis of pressure increase regarding organic richness and porosity of the rock during Kerogen-bitumen conversion.

Controlling Factors	**Organic Richness (TOC)**		**Real Shale (Vaca Muerta)**
	Rich 25%	**Lean 2.5%**	**TOC 6%**
Vw% for 5% porosity	2.35	2.35	2.35
Vw% for 30% porosity	19.13	19.13	
Vkr % in 5% porosity	45.47	5.61	13.00
Vkr % in 30% porosity	35.47	4.16	
VR for 5% porosity	0.05	0.42	0.18
VR for 30% porosity	0.54	4.59	
DKB	1.09	1.09	1.09
Dkr	0.54	0.54	0.54
Cw (1/psi)	2.8×10^-8	2.8×10^-8	2.8×10^-8
Ck (1/psi)	1.0×10^-5	1.0×10^-5	1.0×10^-5
CB (1/psi)	1.5×10^-5	1.5×10^-5	1.5×10^-5
E (psi)	2.4×10^6	2.4×10^6	2.4×10^6
v	0.20	0.20	0.20
a	1.30	1.30	1.30

During bitumen-oil conversion, oil generation becomes live where the dissolved water in bitumen acts as a source of hydrogen. Therefore, compressibility of the

generated products, the solubility of water in bitumen (Xw%) plays a role in controlling pressure increase. In this model, TOC is set to be 25%, I compared the increase of pressure between the solubility of water in bitumen is 15% (hydrous condition) and 0% (anhydrous condition). Other inputs are listed in Table 6.2.

$$\Delta P_{BO} = \frac{F\left[D_{Bo}\left(\frac{x_w}{1-x_w}+1\right)-\left(\frac{x_w}{1-x_w}-1\right)\right]}{\left(\frac{x_w}{1-x_w}\right)\left(\frac{3(1-2v)}{E}+C_w-FC_w+FD_{Bo}C_o\right)+F(D_{Bo}C_O-C_B)+\left(\frac{3(1-2v)}{E}+C_B\right)}$$

$F = Converted\ fraction\ of\ Kerogen$

$D_{kB} = Kerogen - Bitumen\ density\ ratio$

$D_{Bo} = Bitumen - Oil\ density\ ratio$

$x_w = Solubility\ of\ water\ in\ bitumen$

$E = Young's\ modulus$

$v = Poisson's\ ratio$

$C_w, C_O\ and\ C_B = water, oil\ and\ bitumen\ compressabilities$

Figure 6-7 Pressure increase due to bitumen-oil conversion. From Al Duhailan, 2014.

Table 6-2 Inputs used for modelling pressure increase during bitumen-oil conversion

Controlling Factors	**Role of Water**	
	Hydrous	**Anhydrous**
TOC	25	25
Vw% for 5% porosity	2.35	0
Vkr % in 5% porosity	45.47	45.47
VR for 5% porosity	0.05	0
DKB	1.09	1.09
DBO	1.38	1.39
Dkr	0.54	0.54
Cw (1/psi)	2.8×10^-8	0
Ck (1/psi)	1.0×10^-5	1.0×10^-5
CB (1/psi)	1.5×10^-5	1.5×10^-5
CO (1/psi)	2.0×10^-5	6.0×10^-5
Xw (%)	15	0
E (psi)	2.4×10^6	2.4×10^6
v	0.20	0.20
a	1.30	1.30

According to the result of modelling pressure increase during Kerogen-Bitumen conversion, high TOC and Low porosity are positive factor for pressure increase (Figure 6.8). With low porosity (5%) and high TOC (25%), a maximum pressure increase of around 5200 Psi (35.85 MPa) can be reached with a conversion fraction of 100%. When putting real parameters from Vaca Muerta Formation in the model (6% TOC, 5% porosity), a maximum pressure increase of around 4500 Psi (31.03 MPa) can be reached with a conversion fraction of 100% (Figure 6.9).

For the pressure increase during bitumen to oil conversion, the results show that there is a significant increase in pressure in the hydrous case compared to the anhydrous in the process of bitumen to oil conversion. Pressure increase in the hydrous case (e.g. xw=15 %) can reach as much as three times the pressure increase in the anhydrous (e.g. xw=0%) (Figure 6.10). Volatile oil has been generated in anhydrous pyrolysis (Lewan

and Roy, 2011), which should have much higher compressibility than the oil generated in hydrous pyrolysis. This resulted in a higher pressure increase due to volume expansion in the hydrous scenario.

By combining the influence of the TOC content and porosity of shale, the presence of water, hydrocarbon product compressibility, tens of MPa of overpressure within shale can be achieved. This amount of overpressure may make the induced fractures happen as a result of petroleum expulsion in organic rich shale. High TOC and low porosity shale, hydrous condition during bitumen-oil conversion are positive factor for pressure increase. However, the impact of more factors, such as rock tensile strength, compressional force and seepage force should also be considered when discussion the possibilities of generating bed-parallel fractures in shale.

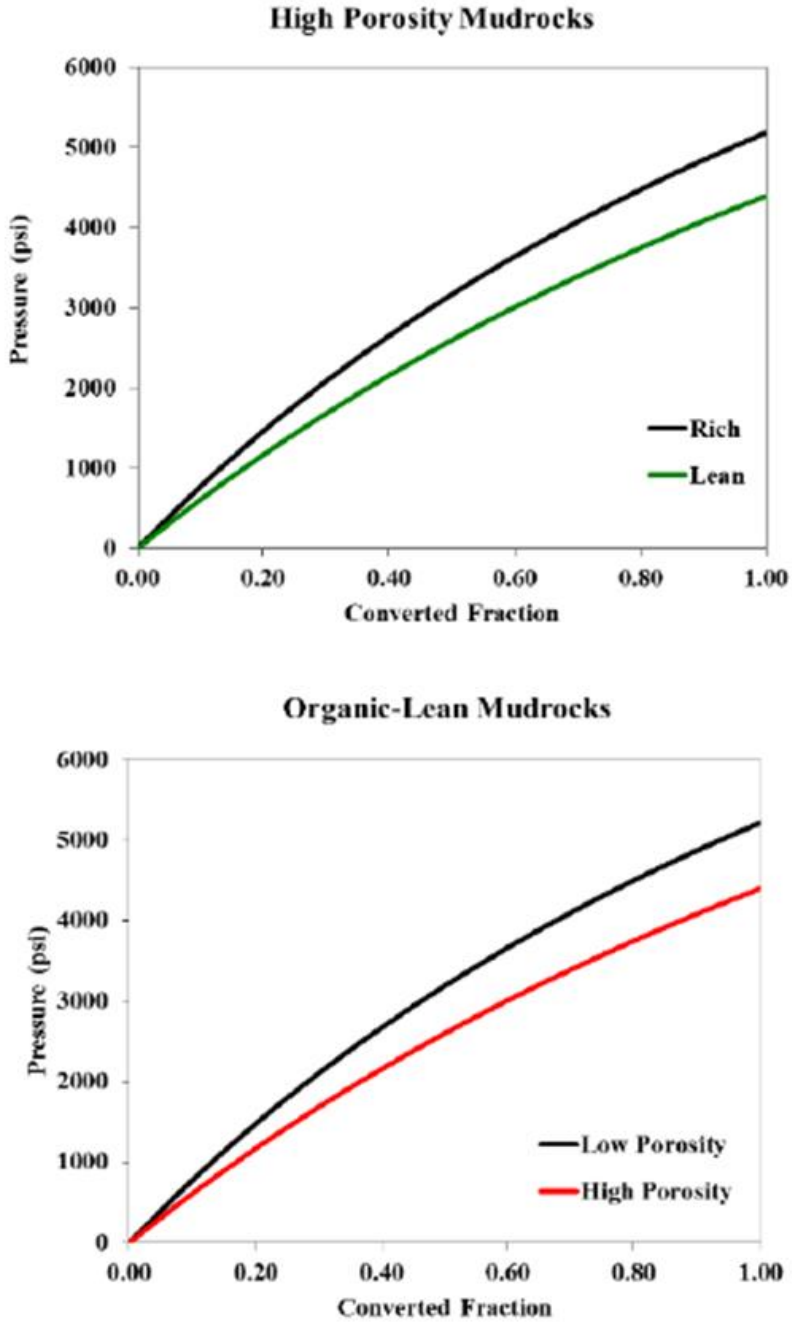

Figure 6-8 Result of modelling pressure increase during Kerogen-Bitumen conversion. Comparison between rich (25% TOC), lean (2.5% TOC), high porosity (30%) and low porosity (5%).

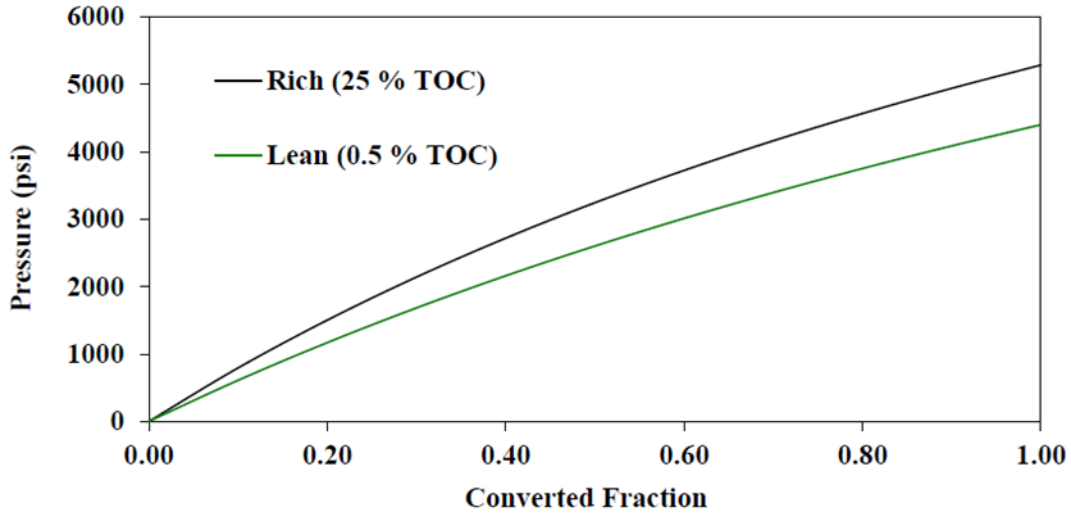

Figure 6-9 Modelled Vaca Muerta shale pressure increase vs. conversion fraction. TOC 6%, porosity 10%.

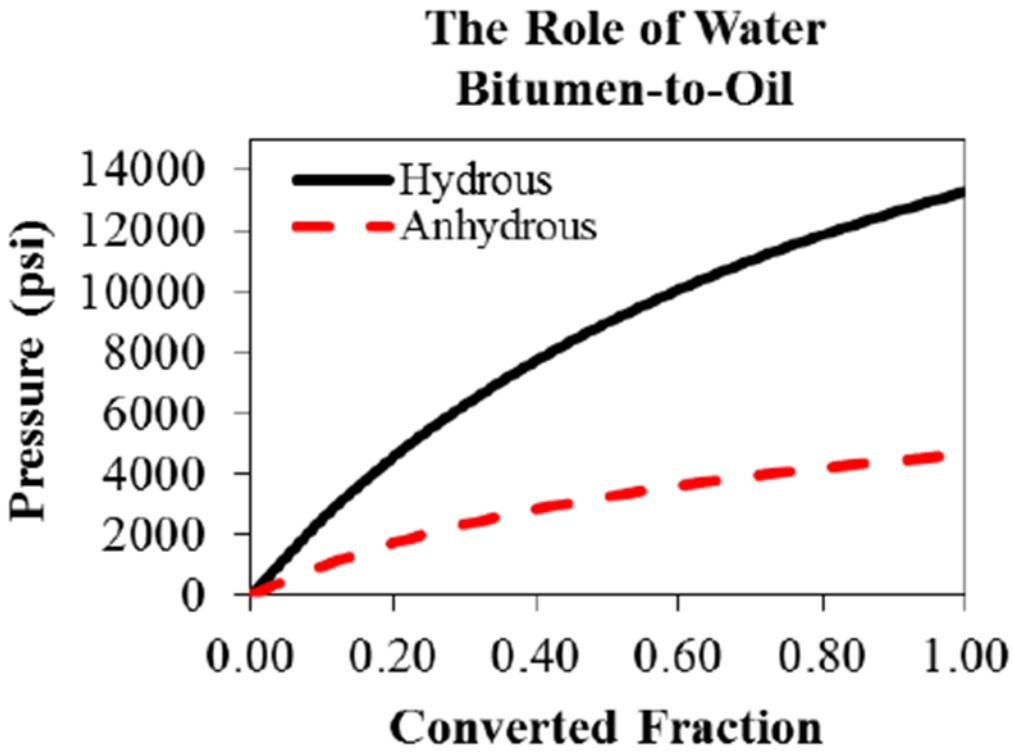

Figure 6-10 Comparison between the increase in pressure in hydrous and anhydrous condition during bitumen oil conversion (Xw 15% vs. Xw 0%).

6.1.4 Shale Overpressure, Tensile Strength and Seepage Forces Generates Parallel Fracturing

To study the genesis of bed-parallel hydraulic fracturing, we need to answer the question: whether the increase in pressure solely due to petroleum expulsion can cause bed-parallel tensile hydraulic fracturing in homogeneous shale. It is a base case with the effects of external forces and mechanical heterogeneity eliminated. If bed-parallel tensile fracture can be generated in the base case, then we expect under compressional external forces, or with weak bed-parallel material interfaces, this type of fractures can also be generated.

Taking Vaca Muerta Formation as an example. The increased pore pressure, shale tensile strength and depth/overburden are put into a brief physical model of bed-parallel fracturing. From 6.1.2, we consider pressure increase during kerogen-bitumen conversion is around 31 MPa. Pressure increase during bitumen-oil conversion is hard to estimate since there are two scenarios (hydrous and anhydrous), and the bitumen-oil conversion fraction is unknown. Considering that abundant bitumen is observed in Vaca Muerta hostrock, in this model the total increase of pore pressure during Kerogen-bitumen-oil conversion is estimated to be 50 MPa (~20MPa pressure increase during Bitumen-Oil conversion), which means in this model, under hydrous scenario, the bitumen conversion ratio is around 15%; under anhydrous scenario, the bitumen conversion is around 35%. The pore pressure increase input here is a conservative number, actual pressure increase can be much larger if there were water involved in bitumen-oil conversion or if the conversion percentage is larger than 35%. The original pore pressure within the organic rich shale before hydrocarbon generation is considered following the oil gradient. Maximum depth of burial of Vaca Muerta Formation in the studied area is around 3500m-5500m (Rodrigues, 2009). Hydrostatic gradient is 10 MPa/km, lithostatic gradient

is 22 MPa/km, oil gradient is 8 MPa/km. Tensile strength of organic rich shale is 9.5 MPa (Eseme et al, 2007), and it is smaller than that of the organic lean shale, which can be around 13 MPa to 30 MPa. The seepage force is hard to determine as well, according to Cobbold 2007, the seepage force counteracts overburden and may be able to lift overburden on its own in extreme cases. In this model, it is considered that the water pressure and oil pressure are the same at the bottom of the formation (5500m). Equations and inputs used to generate the pressure-depth plot is listed in Table 6-3. The pressure-depth plot of the shale formation is shown in Figure 6.11.

Table 6-3 Equation and major inputs used in generating the pressure-depth plot.

Dependent variables	Equations	Independent variables
Overburden (MPa)	$\sigma_v = \int_o^z \rho_b(z)gdz$, u= ρgz	ρ g=22 MPa/km, z=depth
Hydrostatic pressure	u'= ρ'gz	ρ'g=10 MPa/km, z=depth
Pore pressure before hydrocarbon generation	U= ρ"gz	ρ" g=8 MPa/km, z=depth
Pore pressure after oil generation	U'= U+U"	U"=pressure increase after hydrocarbon generation according to the pressure generation model ~50MPa
Bed-parallel fracturing stress	P=u+ $\sigma_{tensile}$	$\sigma_{tensile}$ =9.5 MPa
Seepage force (σ_Δ)	Estimated according to experiments (Cobbold 2007) counteracts overburden and may be able to lift overburden on its own in extreme cases.	
Shale tensile strength ($\sigma_{tensile}$)	Estimated according to experiments (Eseme et al, 2007), counteracts breaks within shale.	

The simulated pressure-depth plot (Figure 6.11) illustrates the pore pressure within the Vaca Muerta formation after oil and gas generation, put it side by side with the bed-parallel fracturing stress of the shale hostrock, to determine whether it is possible to

generate bed-parallel fractures within the shale. The horizontal axis of the plot is the pressure/stress in MPa, and vertical axis is the depth in km. The blue and brown lines show the overburden and hydrostatic stress with depth. The yellow line shows the pore pressure if the formation is charged with oil (do not take into any conversion in to account), and is considered the original state of pore pressure within the organic rich shale before kerogens in its pores started to convert. The red solid line is the pore pressure after kerogen-bitumen-oil generation. The red dashed line is the estimated pore pressure taking the seepage force into account, it is around 15 MPa to the right of the solid red line. The solid purple line indicates the bed-parallel fracturing stress. It is the overburden stress plus the tensile stress of the organic rich shale, so this line shows the minimum stress needed to lift the overburden and break the shale. The dashed purple line is the bed-parallel fracturing stress when bed-parallel heterogeneity (planes of weakness within shale) is taken into consideration.

Toward the top of the modeled Vaca Muerta shale Formation, the effective stress of the rock is getting smaller. At around 4500m deep, the pore pressure after kerogen-oil conversion exceeds the overburden stress. However, considering the effect of tensile strength of the rock, without seepage force, bed-parallel tensile hydraulic fracturing can barely happen at the very top of the formation (~3700m deep).

If we put seepage force into consideration, since it counteracts the overburden, the line of pore pressure and the bed-parallel fracturing line intersects at around 5100m, which means a bed-parallel tensile effective stress can be generated at a larger depth. When the pore press exceeds the bed-parallel fracturing stress, or in other words, bed-parallel tensile effective stress exceeds the tensile strength of the rock, bed-parallel tensile hydraulic fracturing will be generated. In this case, with seepage force, one can

expect a higher possibility to find bed-parallel fracture in Vaca Muerta, even if the over-pressuring solely due to Kerogen-oil conversion is less intense as modeled.

Another process should be considered when discussing bed-parallel fracturing is that, the fracturing may happen not only when shale is deeply buried and being cooked. It can happen because of uplifting and unloading of the shale, at later stage in its burial history. Unloading decreases the overburden stress, causing even larger effective tensile stress within the low permeability rock. These are all discussed with the assumptions that there is no influence of external forces and the mechanical heterogeneity of shale is negligible. If bed-parallel tensile fracture can be generated in the base case (effects of external forces and mechanical heterogeneity eliminated), then we expect under compressional external forces, or with weak bed-parallel material interfaces, this type of fractures may be generated more easily, or at a larger depth.

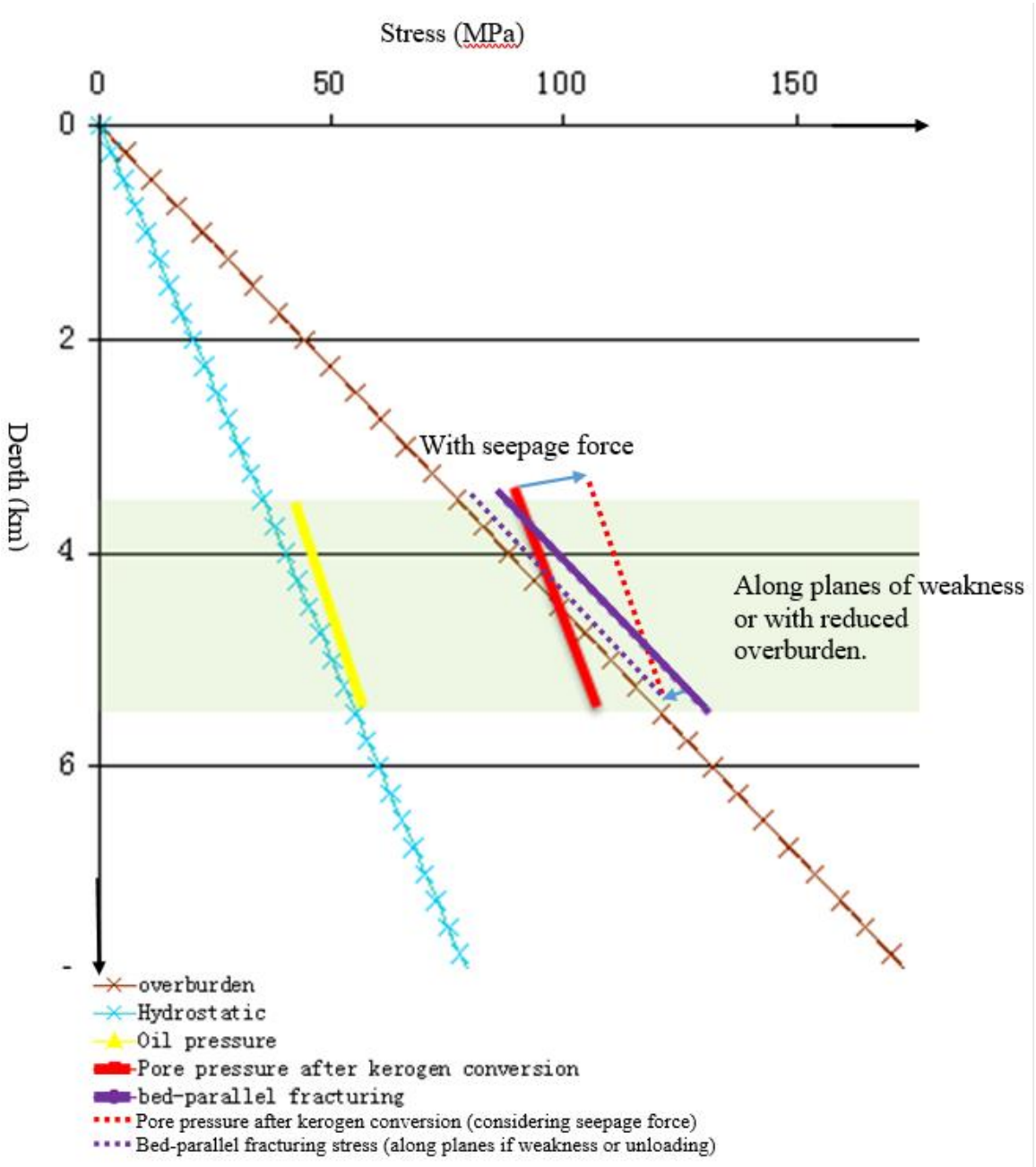

Figure 6-11 Pressure-depth plot of Vaca Muerta formation (3500m-5500m). Increased pore pressure due to hydrocarbon generation, and pressure needed to initiate bed-parallel fracturing are also plotted. Vaca Muerta is marked by color shade. Tensile effective pressure may exceed bed-parallel fracturing envelope at a larger depth, due to seepage force, or due to decreased rock bed-parallel tensile strength marked by planes of mechanical weakness.

Chapter 7. Conclusions

Bedding-parallel fractures that are filled with mineral cement are common in shale but are not ubiquitous. Their presence may impact fluid flow in hydrocarbon reservoirs, and may also influence the propagation of hydraulic fractures, which are needed to stimulate production in shale. Bed-parallel from Vaca Muerta, Marcellus and Wolfcamp Formations were collected and analyzed. Basic knowledge such as the fractures' morphology, relationship between fracture sizes and their cumulative frequency, and the location of fractures in the stratigraphy are necessary before we can better understand the potential impact of this type of fracture.

Bedding-parallel and sub-parallel fractures are observed infrequently in the cores, and at the studied outcrop locations as well. Bed-parallel fractures studied are commonly antiaxially filled with fibrous calcite cement, and have a median surface marked by inclusions of host rock. This cement type is called "beef" and occurs in all three studied formations. Bed-parallel fractures can also be cemented with blocky calcite or other mineral cements. In the studied samples, there can be several phases of cements, where calcite, dolomite, gypsum, bitumen and pyrite are all present. Typical bed-parallel geometry includes planar, wavy/lens-shaped, and branching/linking geometries. Bed-parallel fracture may follow the deflections in bedding around the concretion. They may also be short en-echelon or are interacting with high-angle bed-bounded fractures. Crack-seal texture of cement can be used to approximate the amount of opening during each crack-seal cycle, and the inclination of cement fibers may be used as a local shear indicator.

I plotted the bed-parallel fracture aperture size population, to see that if the bed-parallel fracture size distribution follows a distribution function, such as power law or

exponential law. Nine out of ten datasets show best fit to negative exponential equations with a high correlation coefficient of above 0.9. Among the three formations, the Vaca Muerta has the highest fracture intensity. The Marcellus has the lowest intensity, with the Wolfcamp in between. Length distributions were obtained from the two Vaca Muerta outcrop datasets. The length distribution could be interpreted as best-fitting either power law with rolled-off ends or negative exponential function.

I looked at bed-parallel fractures' location within stratigraphy from cores and well-logs from Vaca Muerta, to test the hypotheses that bed-parallel fractures tend to be more intense in organic rich layers. As a result, log lab-TOC and TOC-KER spikes match with four major fracture intensity peaks which supports the hypothesis that bed-parallel fractures are more intense in organic rich layers. However, we need to be careful drawing the conclusion that bed-parallel fractures are usually more intense in well-log indicated organic-rich layers, since there are also examples showing at some depth high TOC correlate to high intensity but not always the case.

Hostrock (shale) lithology description and classification is performed to analyze the possible relationship between shale lithology and fracture intensity. Hostrock was classified based on the tripartite compositional classification of fine-grained rocks proposed by Dr. Kitty Milliken. After plotting all 15 samples on the ternary diagram, it showed up that the rock hosting high intensity bed-parallel fractures tend to fall into the class of intrabasional organic-rich Carl and Sarl.

In order to rest the hypothesis that bed-parallel fracture form preferentially along mechanical interfaces within host rock, I analyzed the relationship between fracture occurrence and material interfaces. 25-30% of the bed-parallel fractures occur at material interface and around 65-75% of material interfaces have bed-parallel fractures associated with it. It may be too early to draw a conclusion that bed-parallel fracture form

preferentially along mechanical interfaces. However, based on the results from this study people may expect to see bed-parallel fracture occur where there is a material interface, if other the hostrock in high in TOC, had been under lateral compression, and properly cooked. This combination can lead to high effective tensile stress that lifts the overburden and exceeds the tensile strength of hostrock, thus is critical in the genesis of pressure induced bed-parallel fractures as a result of petroleum expulsion in organic rich shale.

APPENDICES

Appendix A: Field Samples

Appendix A is a photographic summary of the outcrop locations. Samples collected and selected to be processed are listed in Table 1, together with brief descriptions. Each selected sample has a section with images of the hand sample, images of the chip after cutting and the remaining rock if any, and scanned image of the thinsections.

Table 1 Field samples selected, processed and analyzed.

Vaca Muerta outcrop sample list				
fiber orientation is after beeding rotated to horizontal			**N.O.= not oriented**	
Several blackshale hostrock sample collected because we want to make sure to have at least one blackshale sample survive the travel.				
name	attitude	fiber orientation	notes	Beef at scanline=beef collected very near scanline
Arroyo Mulichinco - Up				
QWVMM01	124/4 S		Grey shale, beef-rich, for hostrock lithology, stop 1	
QWVMM05	41/3 S	340/50	beef at scanline, tilted/curve fibers w/ medianline, stop 6	
QWVMM06	75/10 S	256/70	beef at scanline, tilted/curve fibers w/ medianline, stop 7	
QWVMM07	30/4.5 S	293/65	beef at scanline, tilted/curve fibers w/ medianline, stop 10	
QWVMM08	320/9 S	270/70	beef at scanline, tilted/curve fibers w/ medianline, stop 10	
QWVMM09	45/14 S	206/60	beef at scanline, tilted/ curve fibers w/ medianline, stop 12	
QWVMM10	N.O.		Black shale with tuff layers miixed, beef-rich for hostrock lithology, Stop 12	
QWVMM13	81/8 S	255/60	Beef from stop 14, curved fibers w/ medianline	
QWVMM14	85/11 S	270/57	Another beef from stop 14, curved fibers w/ medianline	
Arroyo Mulichinco - Down				
QWVMM15	23/20 S	230/65	beef at scanline, fishbone texture, stop 1	
QWVMM16	20/22 S	250/55	beef at scanline, tilted/curve fibers w/ medianline, stop 3	
QWVMM18	10/11 S	280/70	beef at scanline, tilted/curved fiber w/median line, at top of stop 6	
QWVMM19	30/ 25 S	159/75(-50)	beef at scanline, fishbone texture, stop 6	
QWVMM20	15/14 S	278/45	beef at scanline, tilted/curved fiber w/median line, at top of stop 7	
QWVMM21	20/24 S		beef at scanline, tilted/curved fiber w/median line, near concretion, at top of stop 8	
QWVMM22	27/25 S	286/55	beef at scanline, tilted/curved fiber w/median line, near concretion, at top of stop 9	
El Puesto				
QWVMG01	165/9		Shale from beef-barren part of puesto outcrop, for hostrock lithology	
QWVMG02	170/10 S	309/72	fibrous beef from beef-rich part of puesto outcrop	
QWVMG03	120/7 S	304/53(-63)	fibrous beef from beef-rich part of puesto outcrop	
QWVMG04	150/4 S	300/55 and 85/65	fibrous beef from beef-rich part of puesto outcrop	
QWVMG05	N.O.		Blackshale from beef-rich part of puesto outcrop, for hostrock lithology	
QWVMG06	165/13 S	249/55 and 330/-52	top beef at puesto scanline, fibrous beef from beef-rich part of puesto outcrop	

QWVMM01

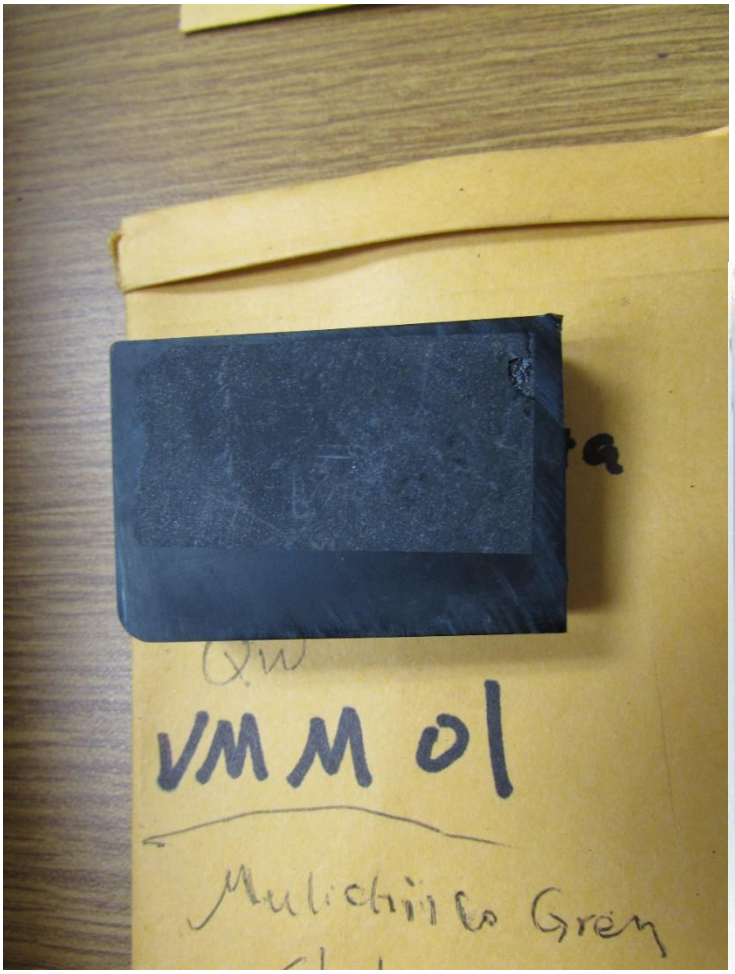

QWVMM05

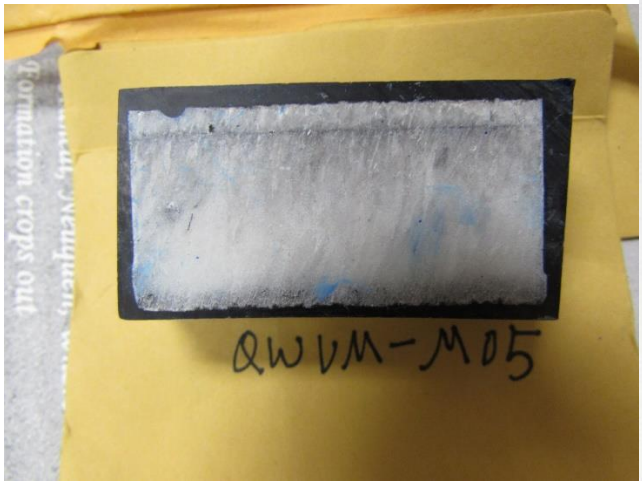

QWVMM06

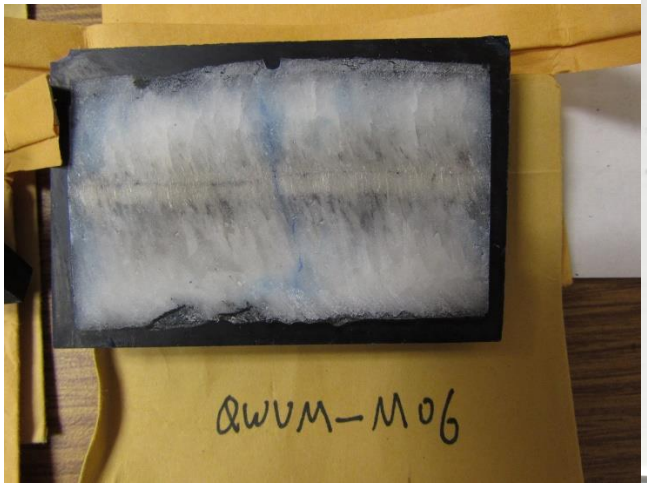

QWVMM07

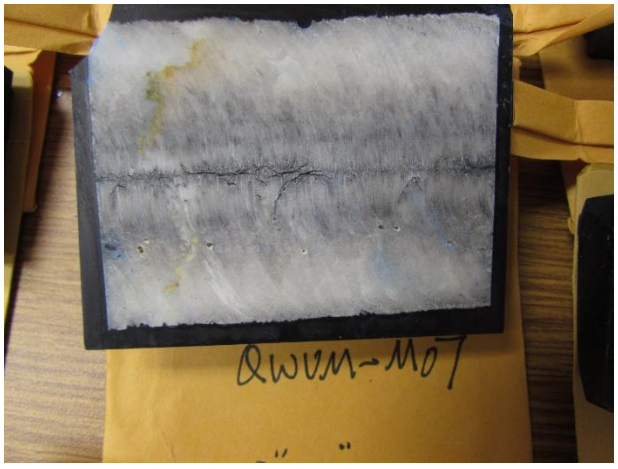

QWVMM08

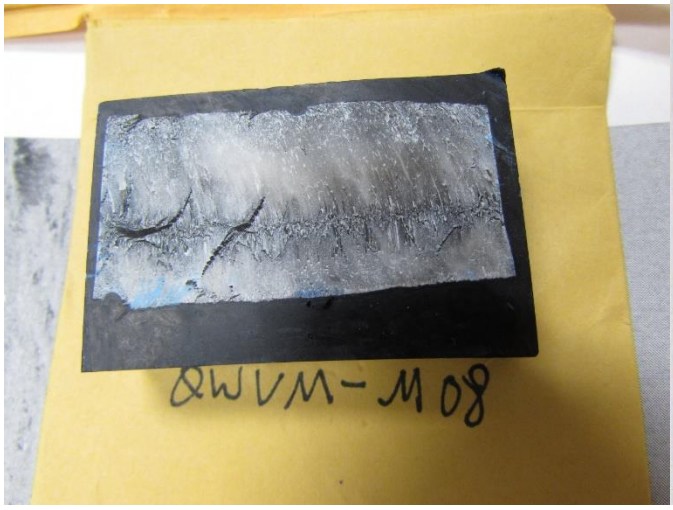

QWVMM09

QWVMM10

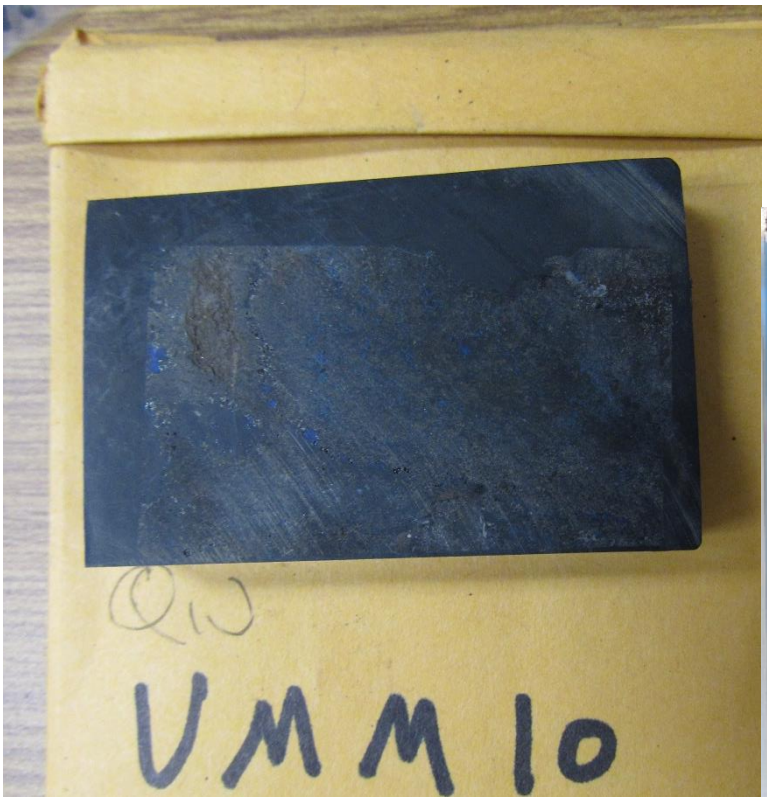

QWVMM13

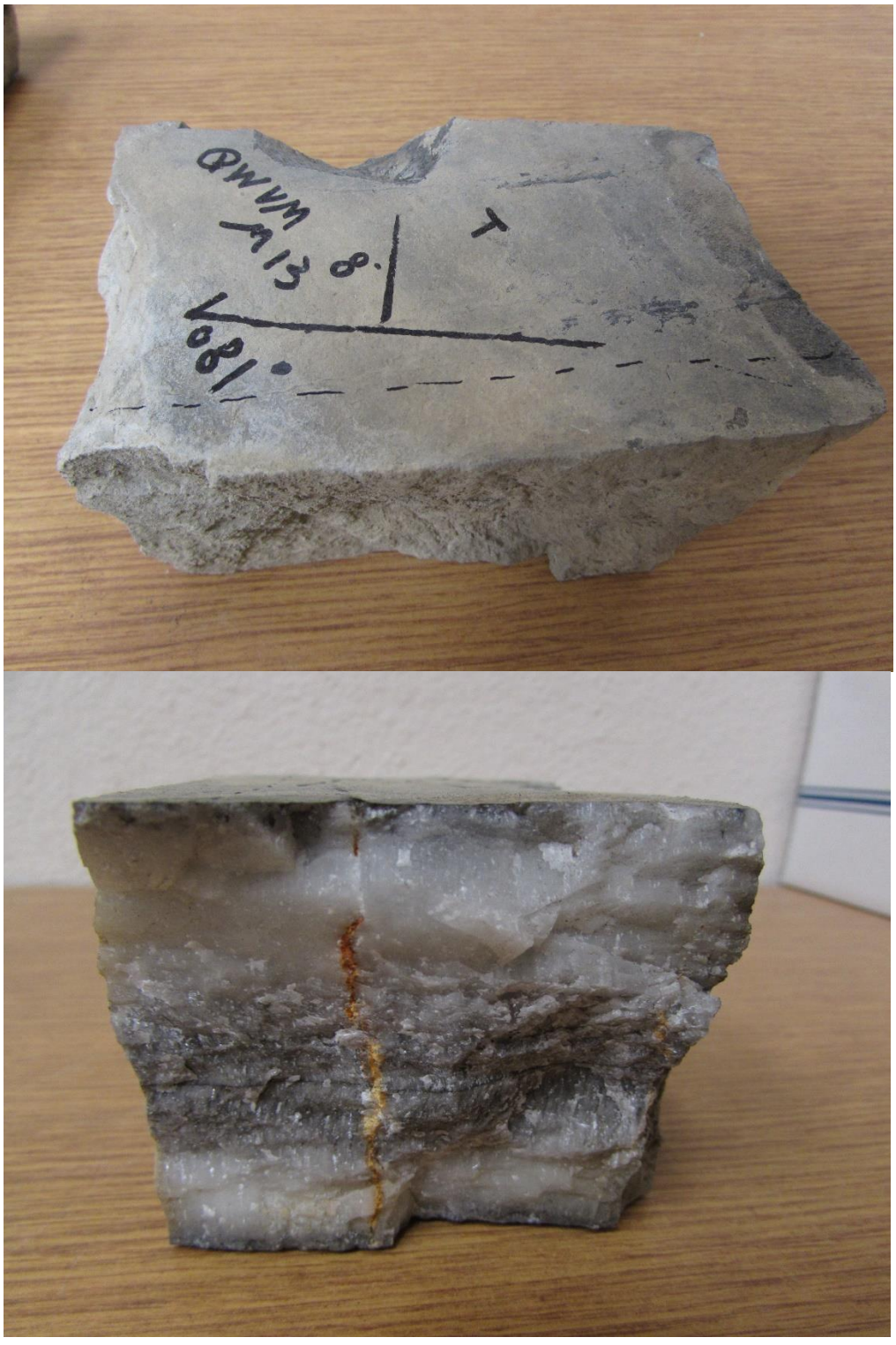

QWVMM13a

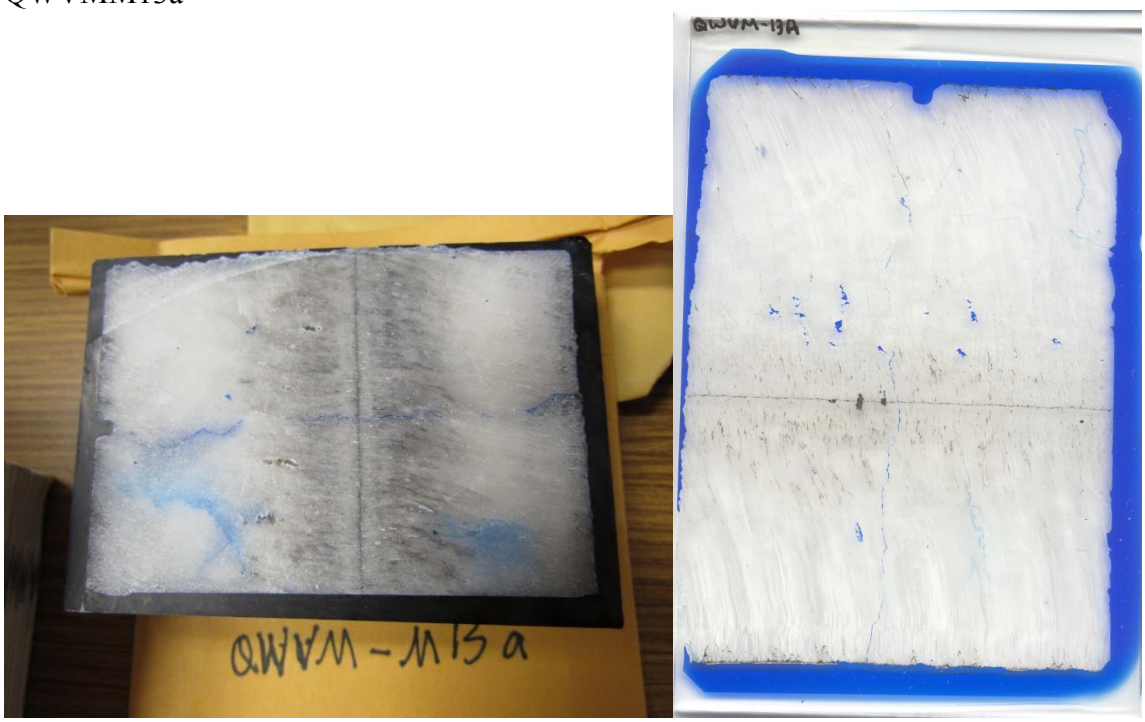

QWVMM13b

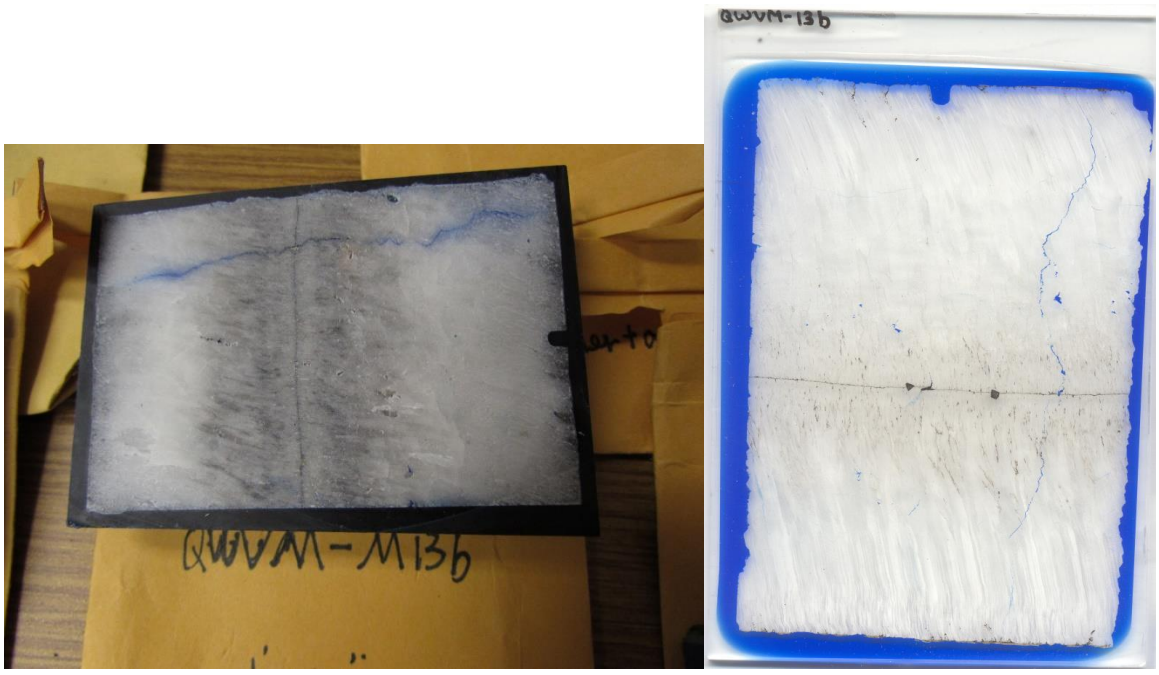

QWVMM14

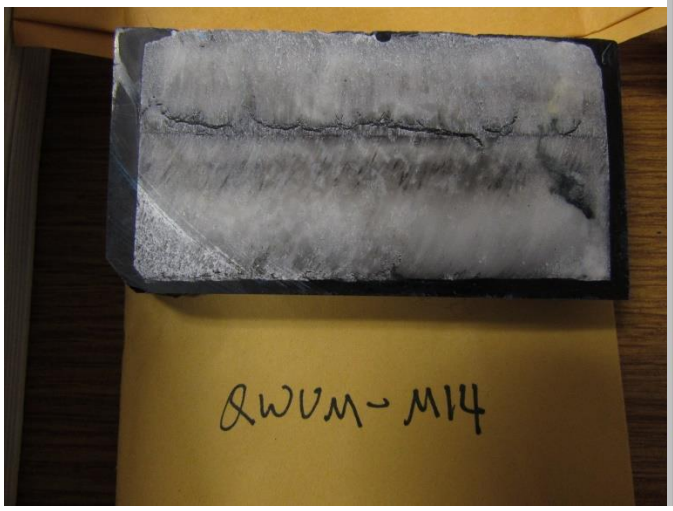

QWVMM15

QWVMM16

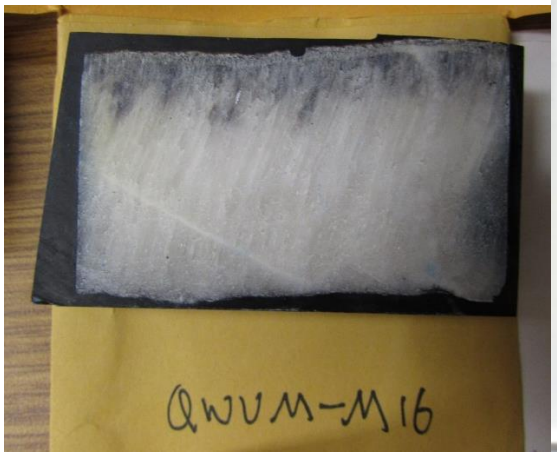

QWVMM18

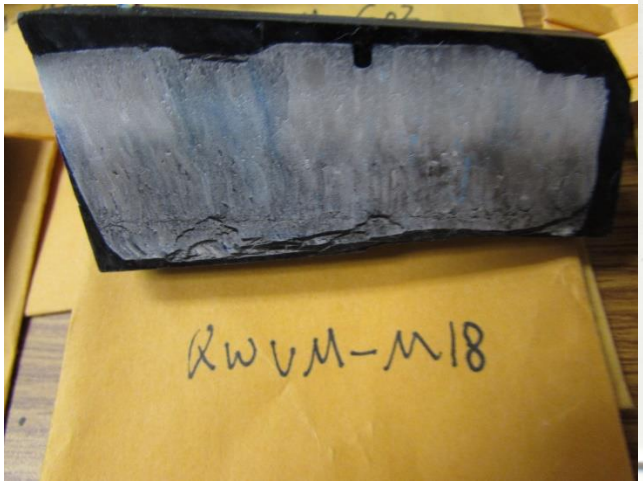

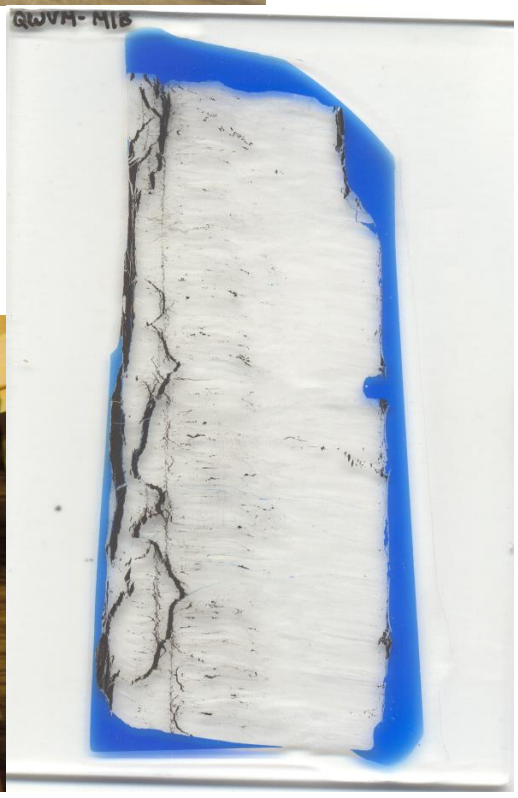

QWVMM19

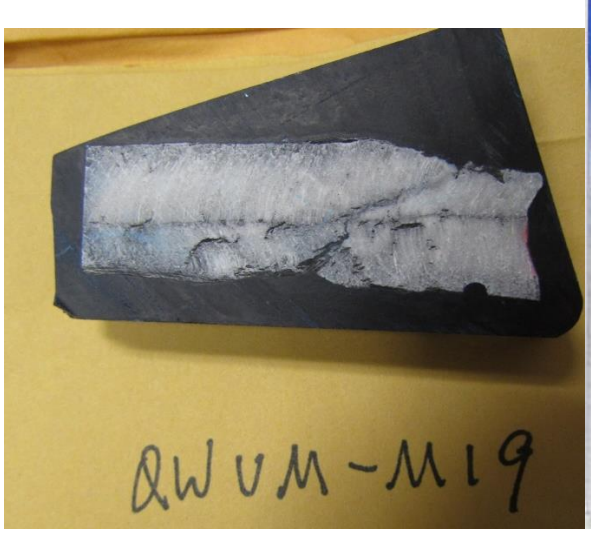

QWVMM20

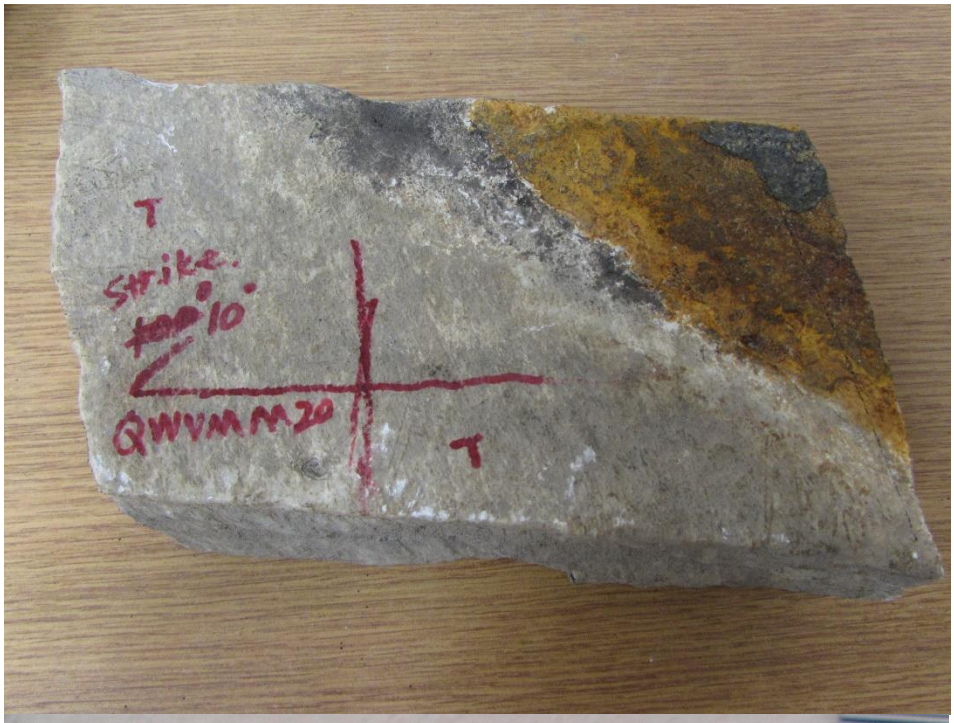
T
Strike.
10°
QWVMM20
T

QWVMM20a

QWVMM20b

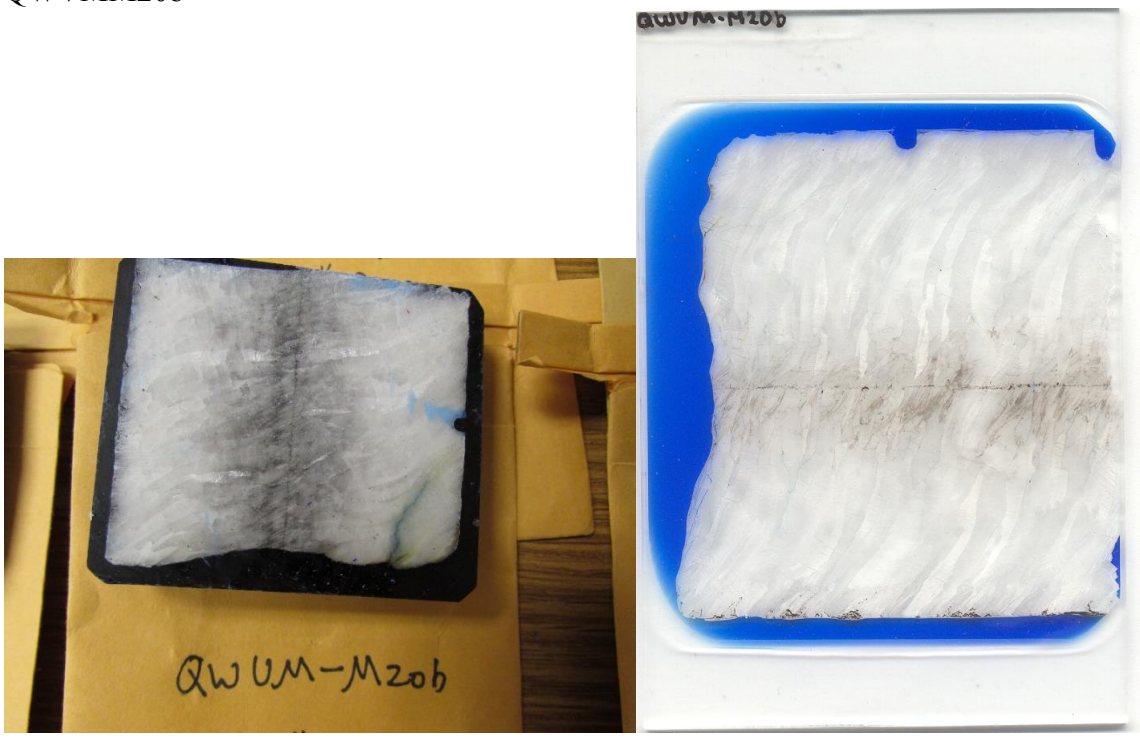

QWVMM22

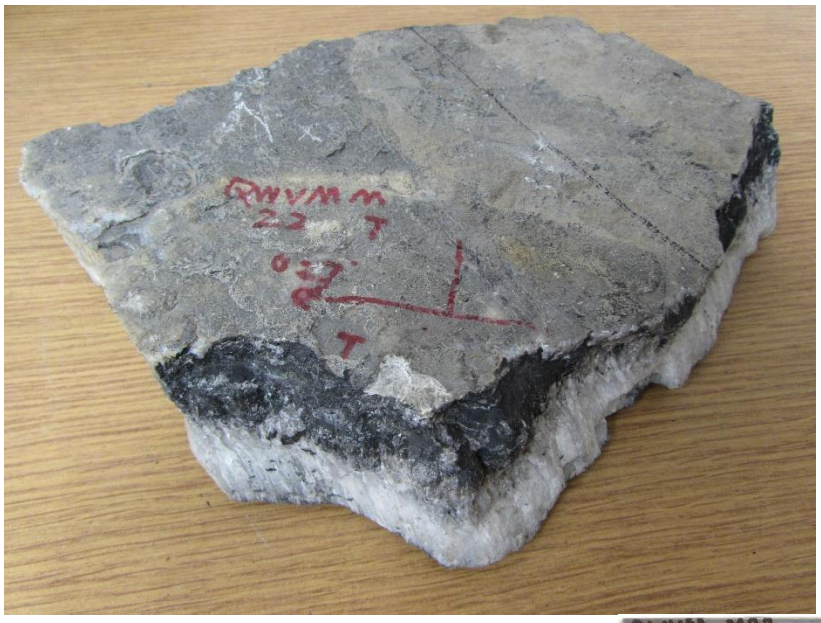

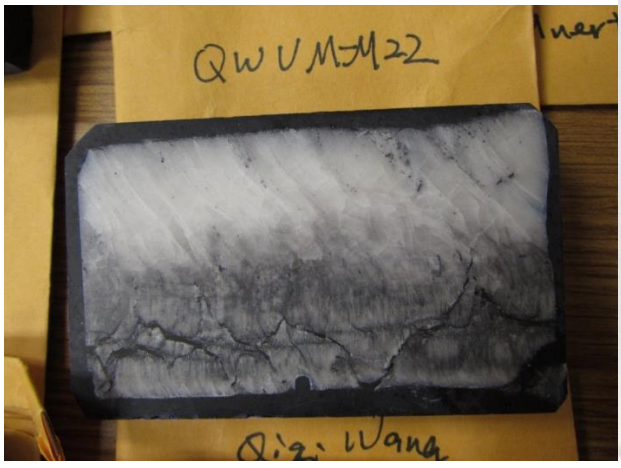

QWVMG01

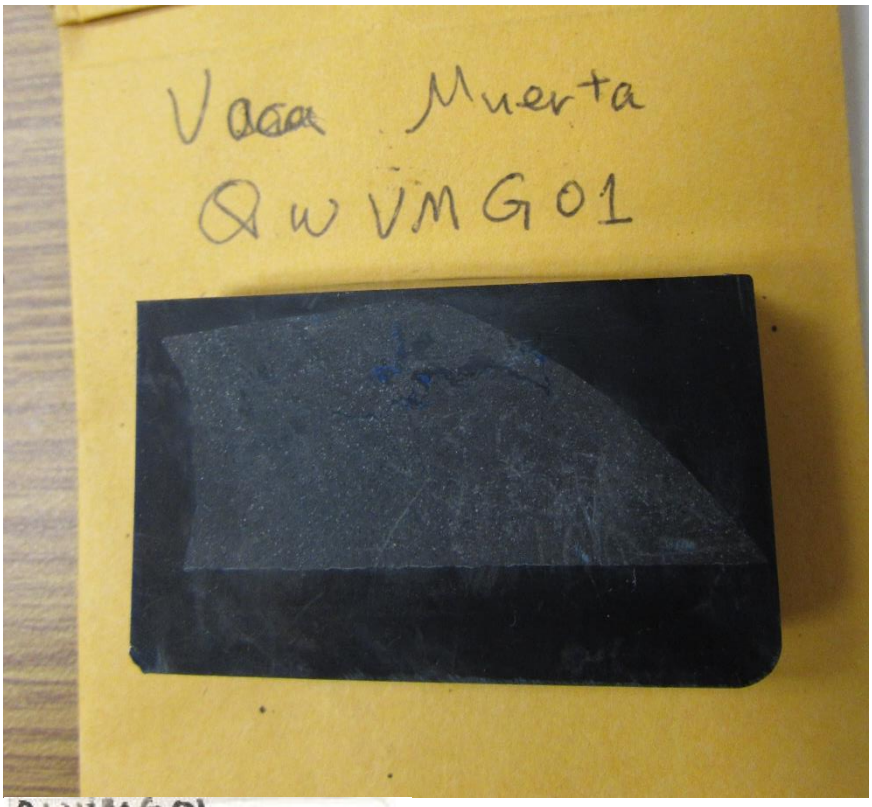

QWVMG02

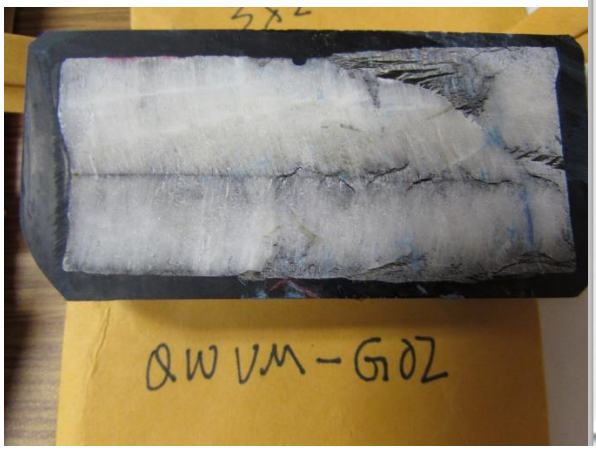

QWVMG03

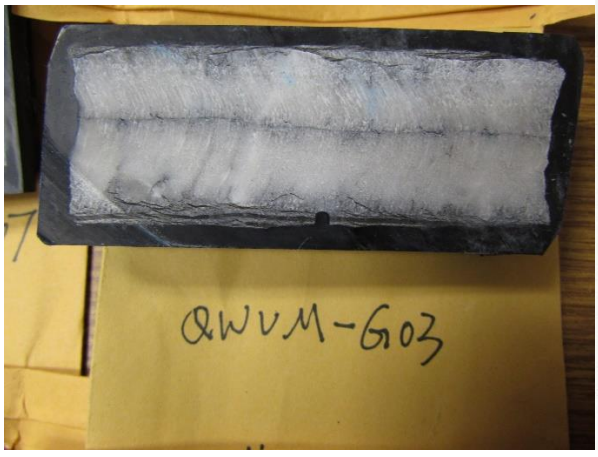

QWVMG04

QWVMG05

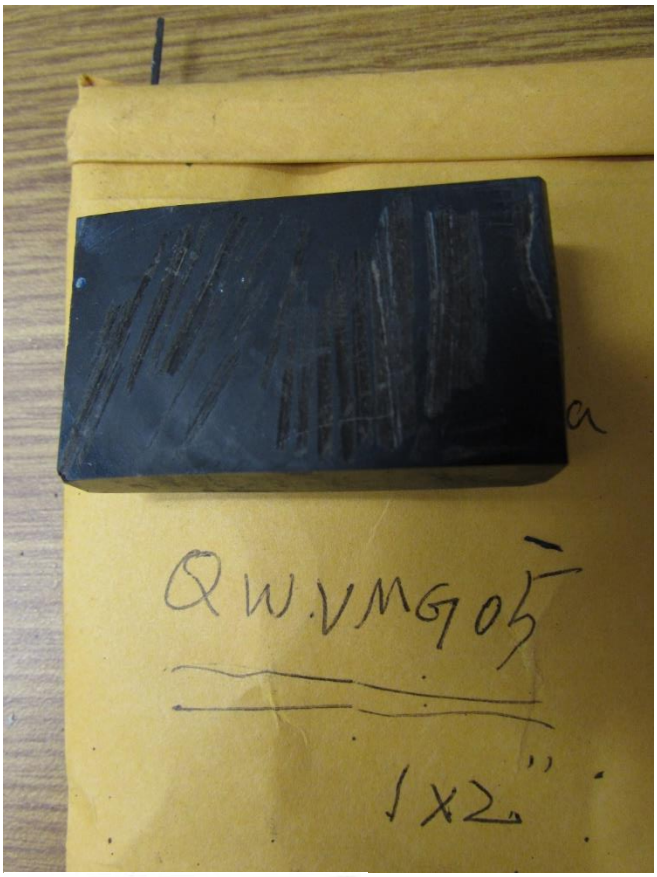

QWVMG06

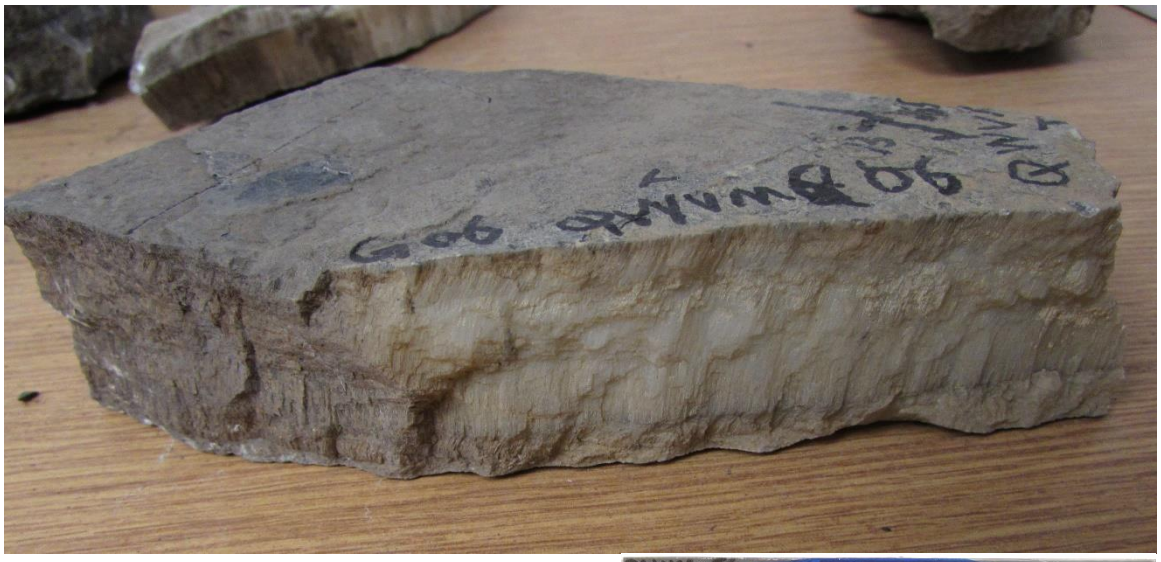

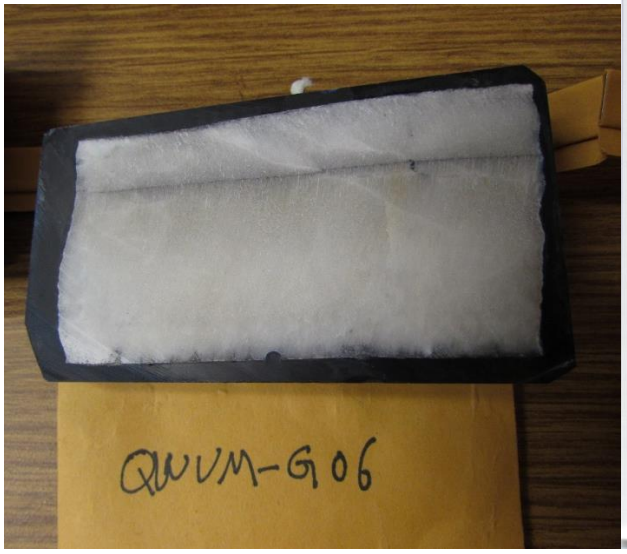

Appendix B: Core Samples

Table 2 List of selected, processed and analyzed core sample from Vaca Muerta wells

VM_Well#1	13 thinsections		note, brief description
VM_Well#1_1-7-M			Stylolite, and vertical frac. OGM filled vertical/subvertical stylolite ~50- 200um, Fibrous and non-fibrous cemented vertical/sub-vertical fracture associated with stylolite
VM_Well#1_1-9-M			Curved beef, multiple beefs developed along calcareous fossil. non-fibrous-multiphase vertical fracture linked to bed-parallel fractures. Hostrock and fluid? Inclusion in vertical frac showing crack seal
VM_Well#1_1-19-M			horizontal slide capturing vertical frac, not fibrous
VM_Well#1_2-7-M			thick beef ~1cm, vertical crack (sample preparation induced?), median line and shale shell. Curve fibers.
VM_Well#1_3-2-M			"T" vertical-low angle frac interaction. Low angle fracture at lithologychange? Material interface.
VM_Well#1_3-3-M			Beef with median line and shale shell, fiber of a different phase of cement(?) at beef median line, dispersed calcite nucleations and phosphate
VM_Well#1_3-5-M		12 standard	multiple beef with oblique fibers, none or asymetric medianline. vertical non-fibrous fracture, vertical hairline and v-frac associated with stylolite. vertical stylolite interact with beef, showing cross cutting relationship. May indicate the way beef grows.
VM_Well#1_3-16-M			stepped vertical fracture, non-fibrous with median line in fossil rich OM rich host rock
VM_Well#1_3-18-M			Beef w/ median line, linked, curve fiber
VM_Well#1_4 6 M			2 beefs w/asymetrical median line, looks like cone in cone tecture in cement
VM_Well#1_4-7-Ma			vertical fracture, non-fibrous. Have cracked Bitumen in the middle, cracks in bitumen perpendicular to the host vertical fracture. fracture break along median line due to thinsectioning
VM_Well#1_4-7-Mb			thick v frac and beef interaction. Thick beef has cone in cone texture. vertical fracture is non-fibrous. I's rim and corehas different texture.
VM_Well#1_4-4-M		1 2x3"	low angle fractures, with thick fiber or not fibrous cement, no median line
VM_Well#2	2 thinsections		
VM_Well#2_sample 1		1 standard	bed-parallel and v frac interaction. vertical fracture split at horizontal fracture and terminates at horizontal material interface
VM_Well#2_sample 2		1 2"x3"	a group of parallel low angle fracs (tention gashes?), constrained within borrow-like features, but no burrow shown under microscope. Looks like kink bands.
VM_Well#3		4 2"x3"	
VM_Well#3-sample 1-A			
VM_Well#3-sample 1-B			
VM_Well#3-sample 2			
VM_Well#3-sample 3			

VM_Well#1_1-7-M

VM_Well#1_1-9-M

VM_Well#1_1-9-M

VM_Well#1_1-19-M

VM_Well#1_2-7-M

VM_Well#1_3-2-M

VM_Well#1_3-3-M

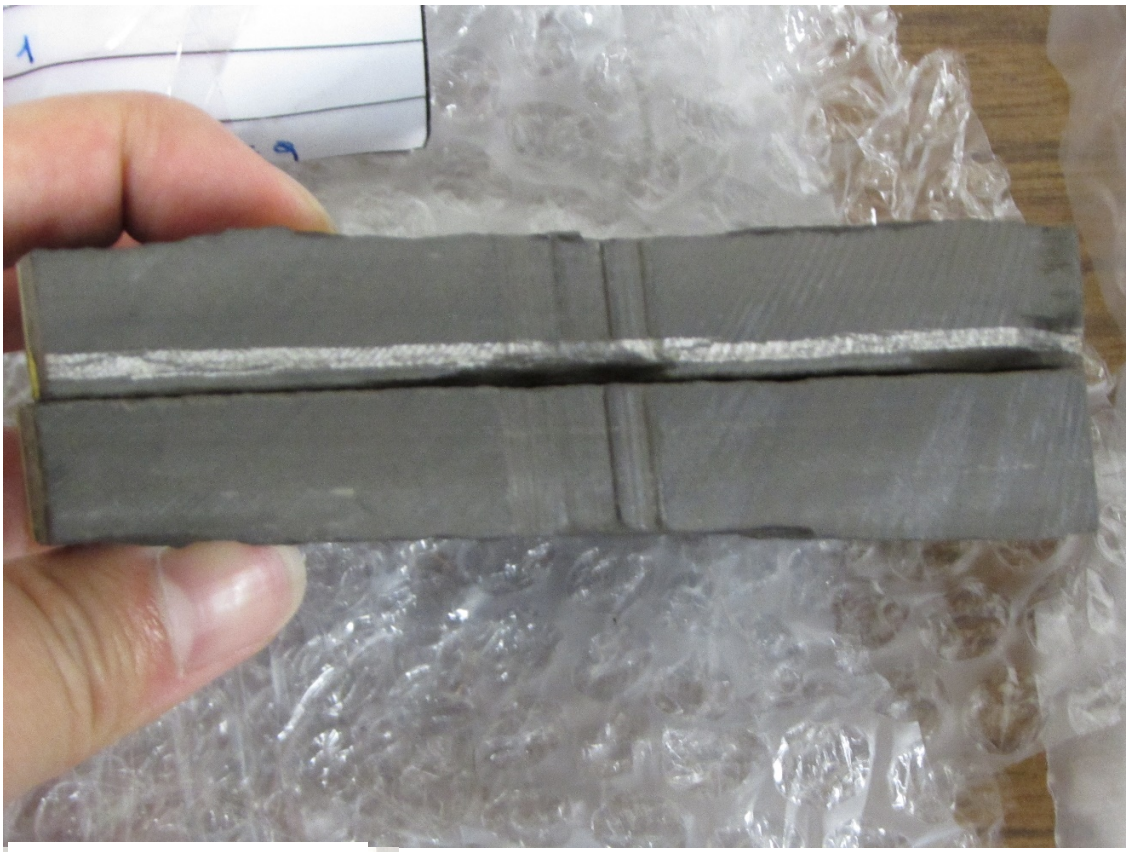

VM_Well#1_3-3-M

VM_Well#1_3-5-M

VM_Well#1_3-16-M

VM_Well#1_3-16-M

VM_Well#1_3-18-M

VM_Well#1_3-18-M

VM_Well#1_4-6-M

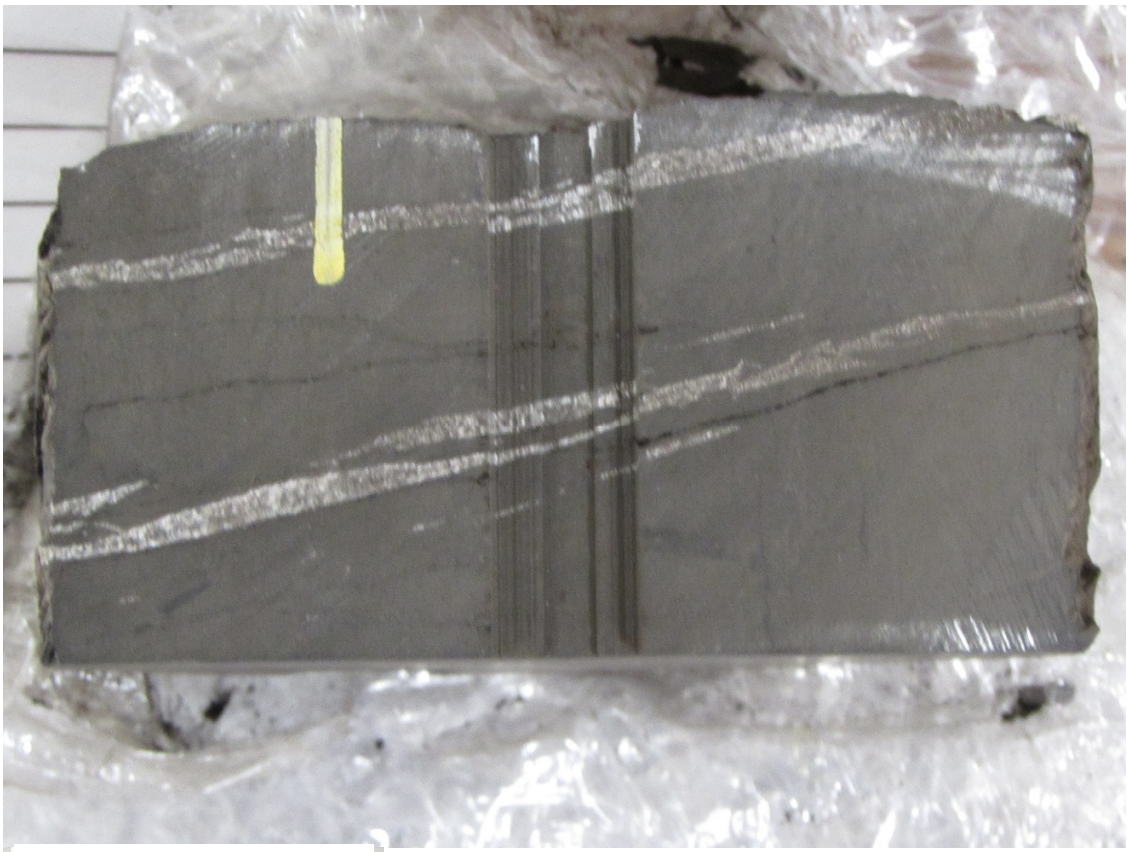

VM_Well#1_4-6-M

VM_Well#1_4-7-M

VM_Well#1_4-7-Ma
VM_Well#1_4-7-Mb

VM_Well#1_4-7-Ma

VM_Well#1_4-7-Mb

VM_Well#1_4-4-M

VM_Well #2_sample1

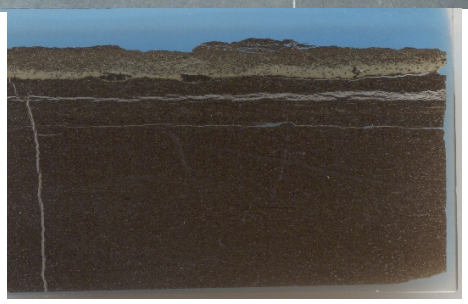

VM Well#2 sample1

VM_Well #2_sample 2

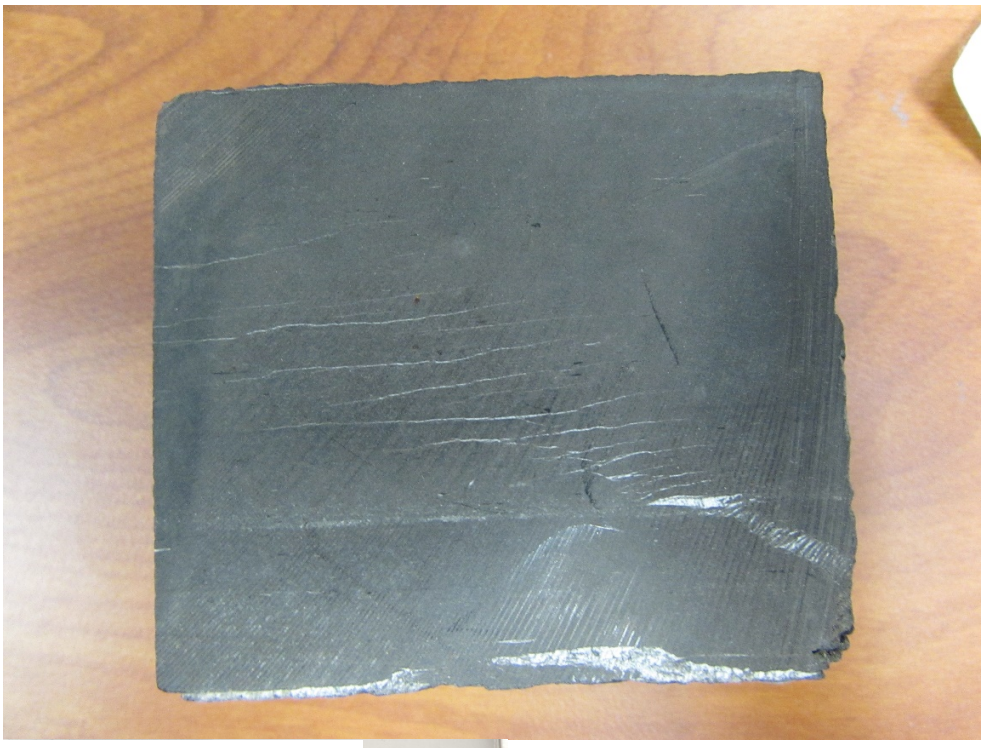

VM_Well#2_sample2

VM_Well #3

VM_Well#3 sample1

VM_Well#3 sample1-A

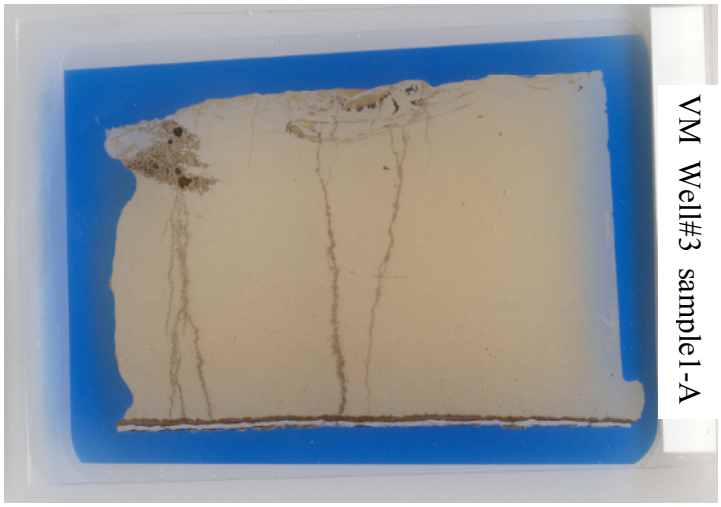

VM_Well#3 sample1-B

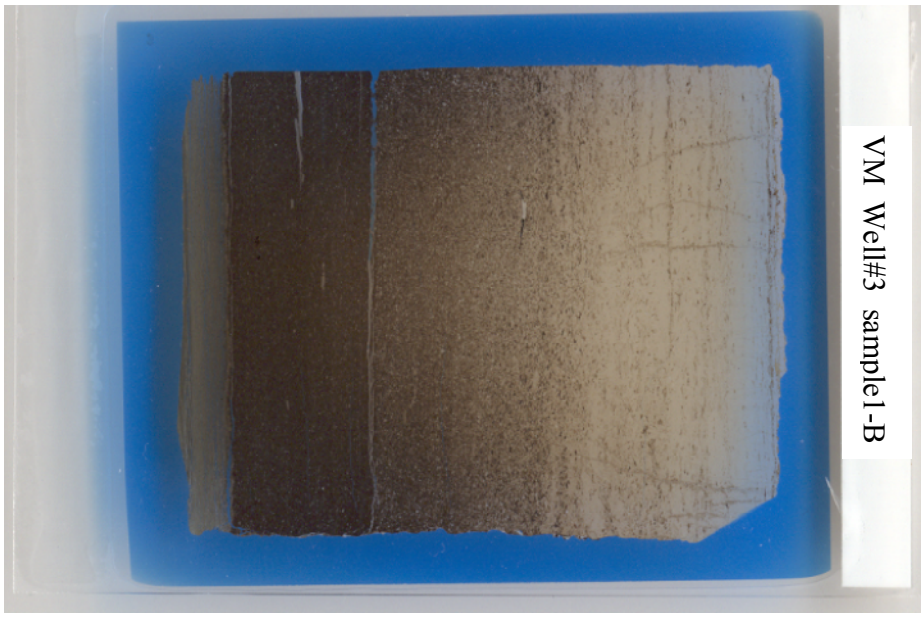

VM_Well#3 sample2

VM_Well#3 sample3

Table 3 List of sample Marcellus cores

Core	Sample #	Sample Thickness (in.)	Depth Interval	Sampled Feature
Marcellus Well #2	SWN-Pr-6512	5.3		Hairline bed-parallel fractures
	SWN-Pr-6579	6.5		Pyrite and calcite bed-parallel veins
	SWN-Pr-6704	2.6		Steplike pyrite and calcite-filled fractures (microfaults?)
	SWN-Pr-6708	6.8		fossil debris layers and calcite-filled fractures (?) with diagenetic (?) pyrite surround
	SWN-Pr-6728.5	4		Diagenetic pyrite layers
	SWN-Pr-6780	3.5		Faults
	SWN-Pr-6812 a & b	(a) 4.5 (b) 3.3		(a) Fossil debris layers & (b) bed-parallel beef vein with slickenfibers on surface
	SWN-Pr-6820	3.3		Stylolite & fossil
	SWN-Pr-6834 a & b	(a) 3.3 (b) 6		(a) Bed-parallel fracture with euhedral crystals & (b) large vertical stylolites with calcite-filled fractures emanating off
	SWN-Pr-6866	1.5		High-angle fractures with calcite fill
	SWN-Pr-6869	7.8		High-angle fractures with calcite fill
	SWN-Pr-6898	3		Concave-up bed-parallel beef veins with thin microfractures
	SWN-Pr-6900	2.2		Bed-parallel beef vein with shale shells
	SWN-Pr-6930	1.5		Composite bed-parallel microfractures with slickenlines on top surface
	SWN-Pr-6936	1.1		Gray silter layer; friable
	SWN-Pr-6992	2.4		Large composite bed-parallel fracture with slickenfibers on top surface and a polished surface below
	SWN-Pr-7001	2.2		Thin vertical fractures with carbonate and chalcopyrite cement
Marcellus Well #1	SWN-Gw-6246.5	4.4		Large vertical fracture with composite fill, offsets a bed-parallel fracture with shear fibers
	SWN-Gw-6311.5	2		Fault with calcite
	SWN-Gw-6358.5 a & b	(a) 3.3 (b) 4.5		(a) Wide vertical vein with 2 different types of fill & (b) Low-angle stylolite/bitumen vein (?) apparently offset
	SWN-Gw-6379	0.9		Cluster of gray siltier layers, bed-parallel fractures, and small vertical fractures connecting layers
	SWN-Gw-6496	0.7		Bed-parallel fractures with shear
	SWN-Gw-6504 a & b	(a) 0.1 (b) 1.8		(a) Disc of calcite cement & (b) Bed-parallel fracture
	SWN-Gw-6505	1.6		Vertical calcite filled fracture
	SWN-Gw-6512 a & b	(a) 1.8 (b) 1.9		(a) Thick bed-parallel calcite vein & (b) bed-parallel beef vein cluster with shale shells
	SWN-Gw-6521	0.6		Fossil?
Marcellus Well #3	SWN-Ed-6301	3.1		Vuggy vertical fractures with fibrous calcite fill and brown (bitumen?) margins
	SWN-Ed-6541	1.5		Bed-parallel veins with slickenfibers and vertical fractures
	SWN-Ed-6545	3.1		Bed-parallel fractures and hairline vertical fractures
	SWN-Ed-6638	3.3		Tension gashes (?) and stylolites
	SWN-Ed-6658	3		Faults
	SWN-Ed-6668	2.9		Faults with vertical stylolites
	SWN-Ed-6674	5		Bed-parallel fractures
	SWN-Ed-6676	2.5		Bed-parallel fractures

Table 4 List of thinsections made from sampled Marcellus cores.

Marcellus Well #2	21 thinsections	**Marcellus Well #1**	11 thinsections	**Marcellus Well #3**	7 thinsections
SWN-Pr-6579		SWN-GW-6246.5		SWN-Ed-6301	
SWN-Pr-6704a		SWN-GW-6358.5A		SWN-Ed-6638	4 standard
SWN-Pr-6704b		SWN GW 6358.5B		SWN-Ed-6674	
SWN-Pr-6708		SWN-GW-6379		SWN-Ed-6676	
SWN-Pr-6812a		SWN-GW-6496	9 standard		
SWN-Pr-6866		SWN-GW-6504B		SWN-Ed-6658	
SWN-Pr-6869a	12 standard	SWN-GW-6505		SWN-Ed-6668	3 2"x3"
SWN-Pr-6869b		SWN-GW-6512B		SWN-Ed-6545	
SWN-Pr-6900a		SWN-GW-6521			
SWN-Pr-6900b					
SWN-Pr-6936		SWN GW 6311.5	2 2"x3"		
SWN-Pr-7001		SWN GW 6512A			
SWN Pr6512					
SWN Pr6728.5					
SWN Pr6780					
SWN Pr6820					
SWN Pr6834b	9 2"x3"				
SWN Pr6898a					
SWN Pr6898b					
SWN Pr6992a					
SWN Pr6992b					

SWN-Pr-6579

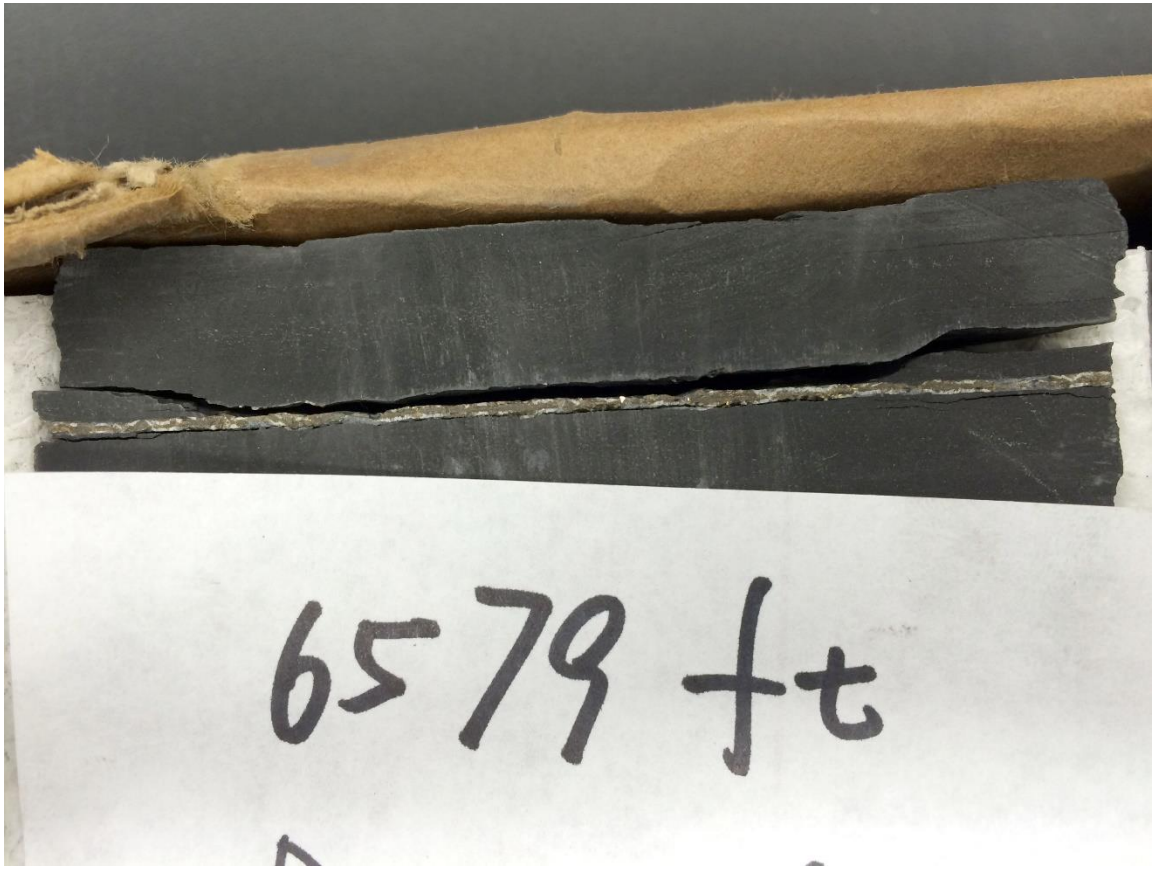

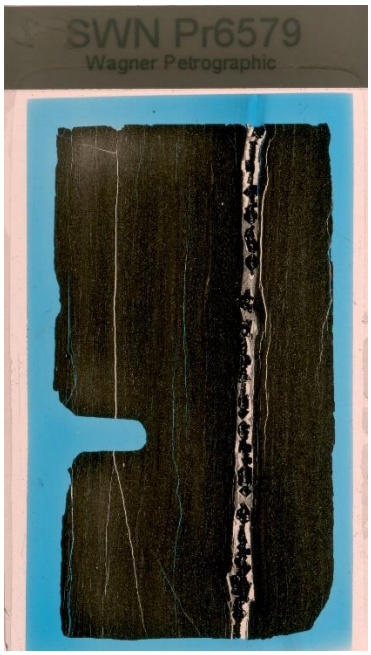

SWN-Pr-6704

SWN-Pr-6704a
SWN-Pr-6704b

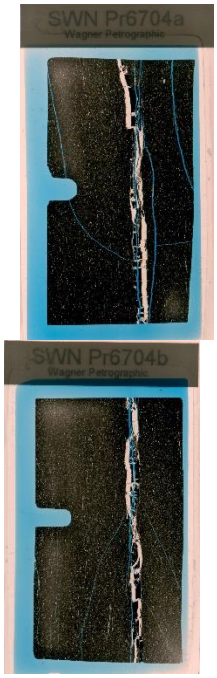
SWN Pr6704a
Wagner Petrographic
SWN Pr6704b
Wagner Petrographic

SWN-Pr-6708

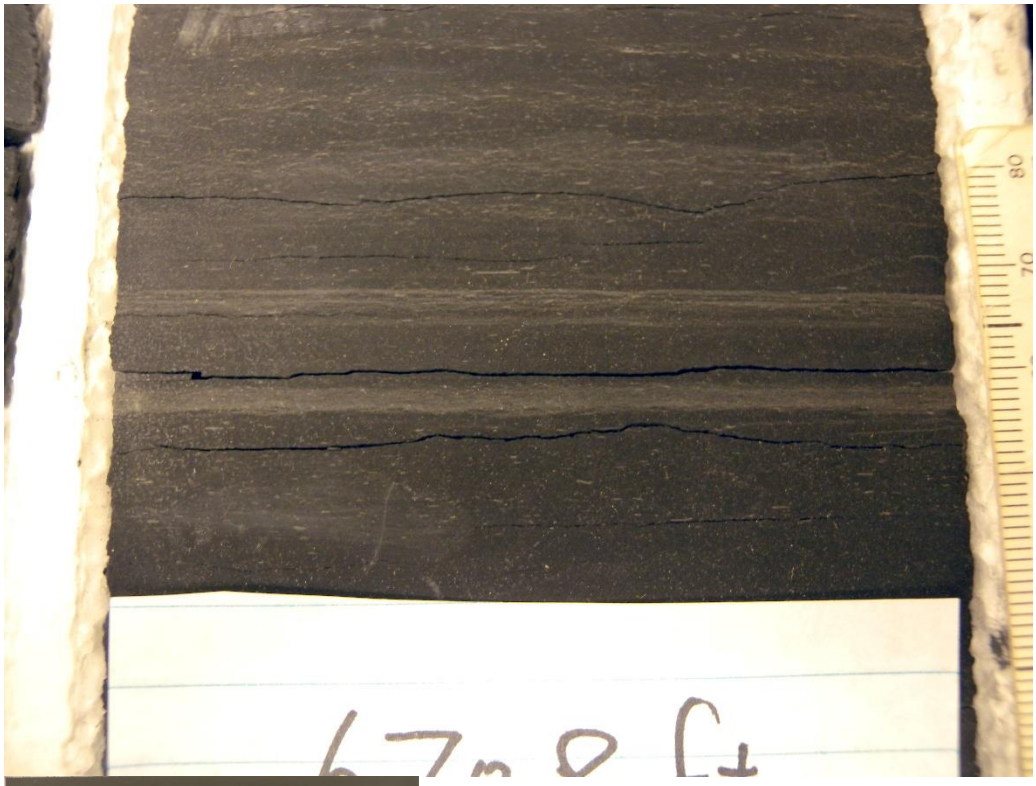

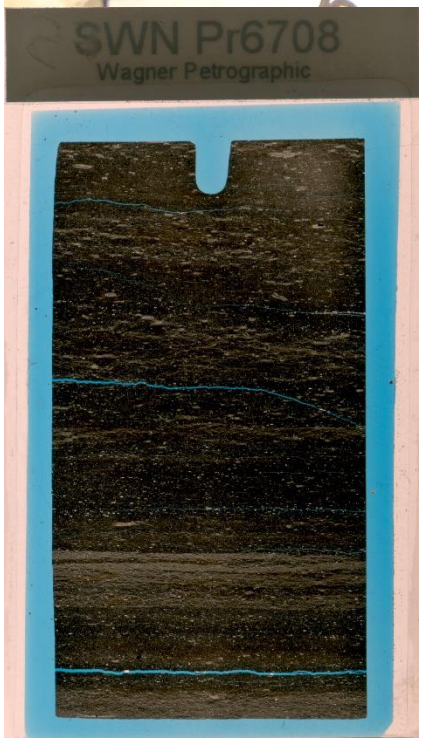
SWN Pr6708
Wagner Petrographic

SWN-Pr-6812a

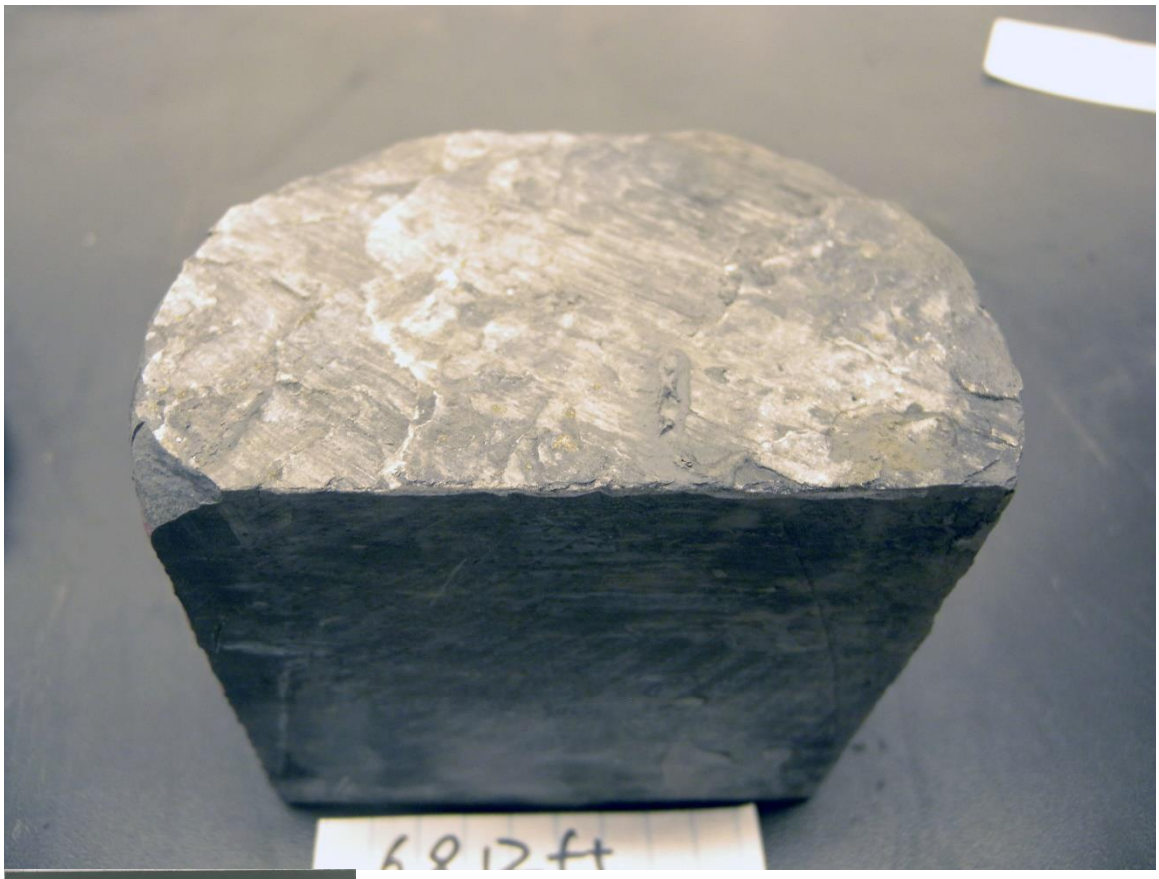

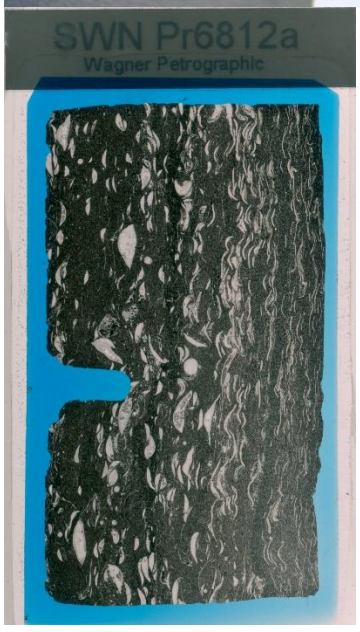

SWN-Pr-6866

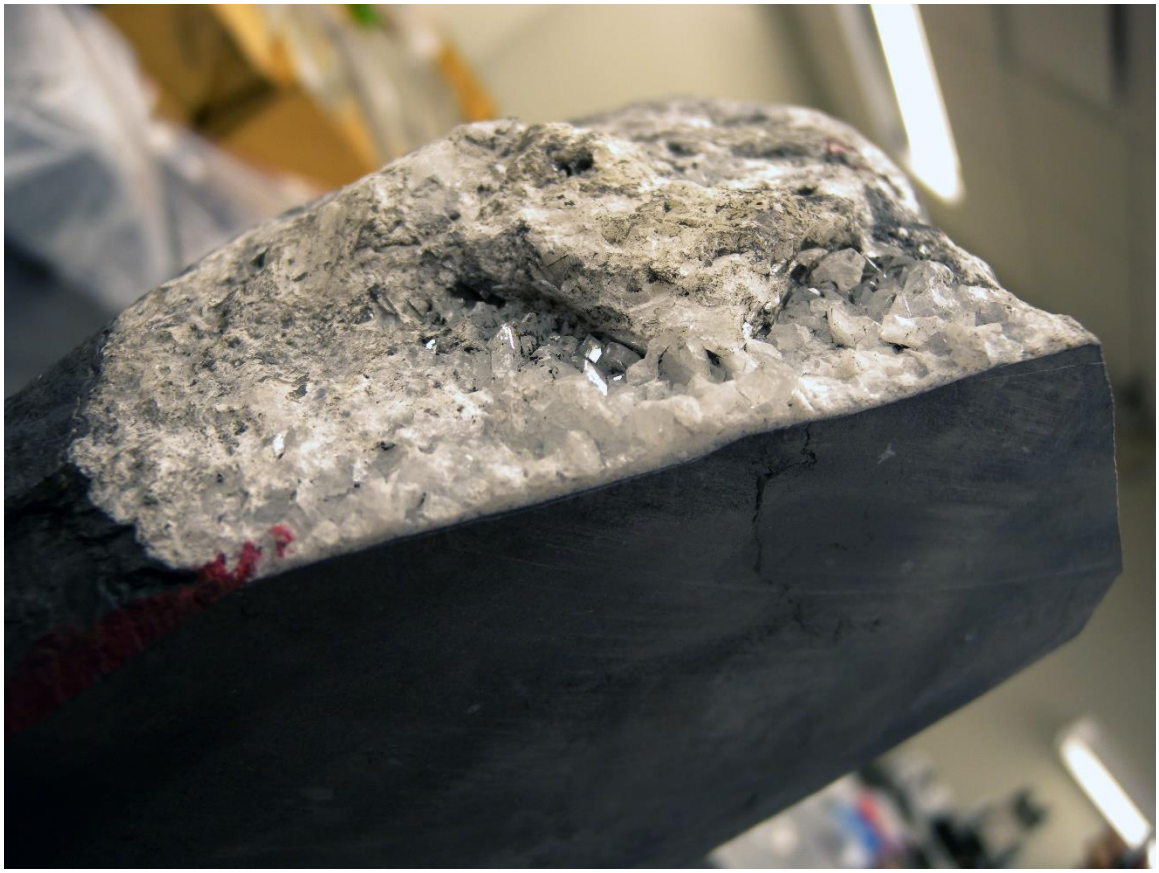


SWN Pr6866
Wagner Petrographic

SWN-Pr-6869

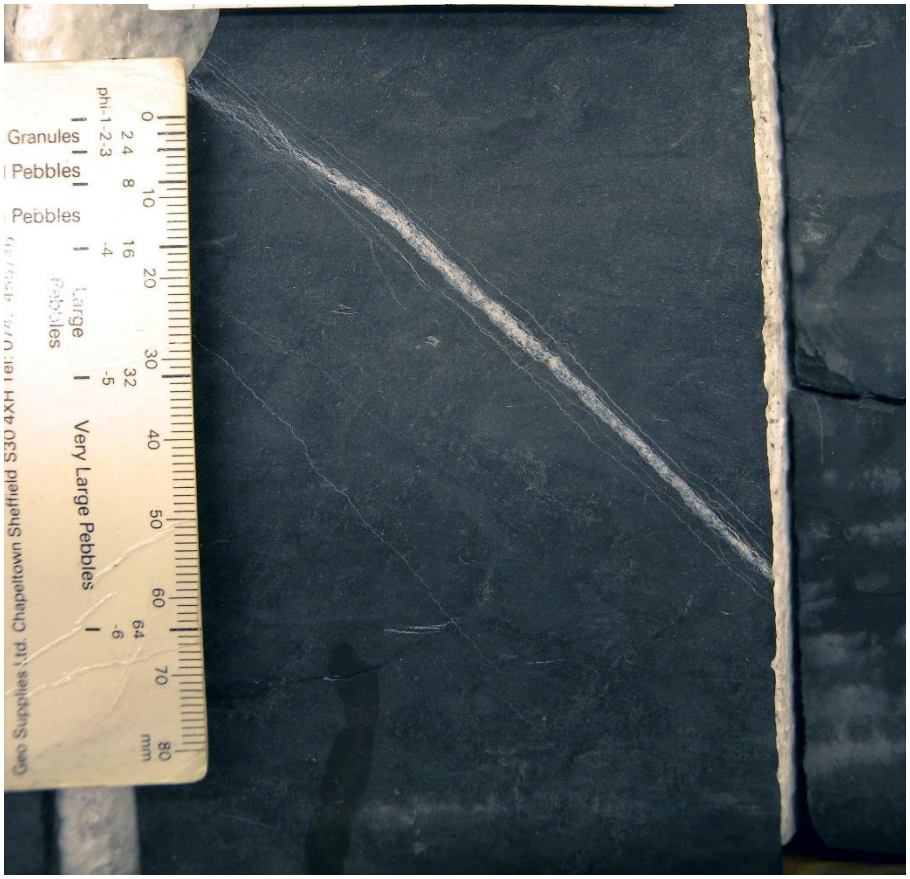
Granules
Pebbles
Pebbles
Very Large Pebbles
mm

SWN-Pr-6869a
SWN-Pr-6869b

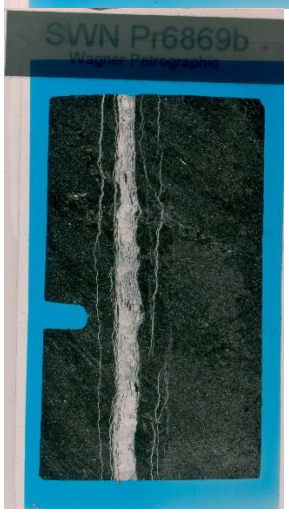

SWN-Pr-6900

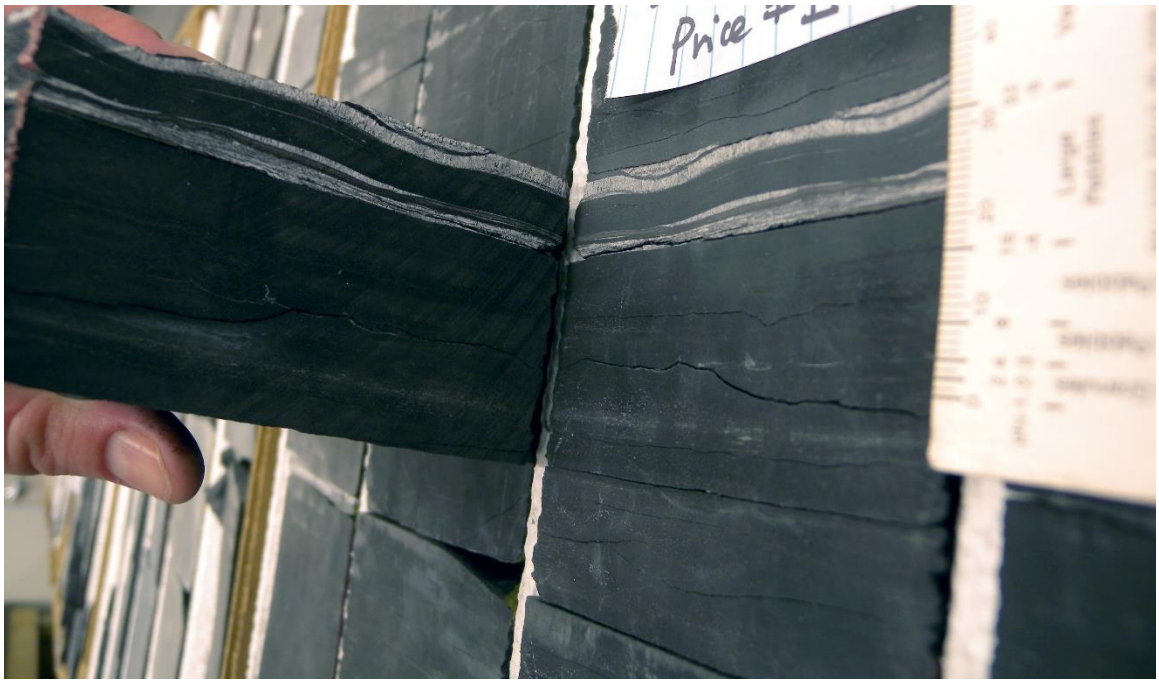

SWN-Pr-6900a
SWN-Pr-6900b

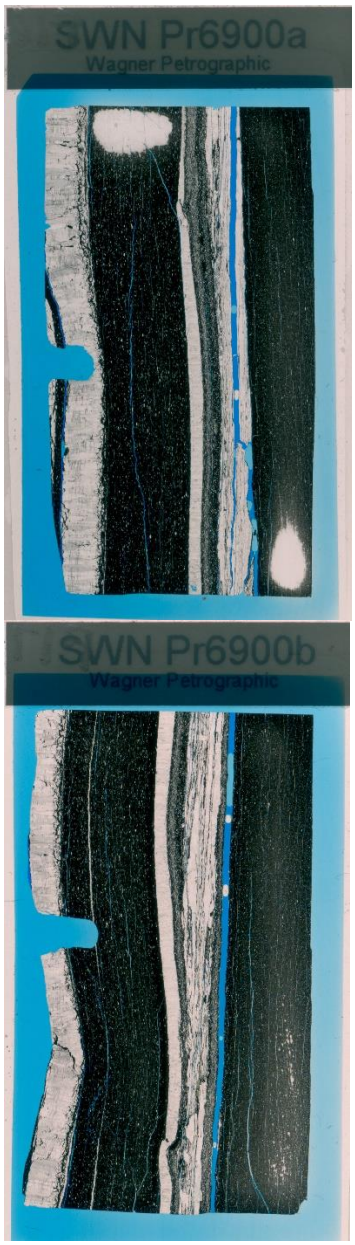
SWN Pr6900a
Wagner Petrographic
SWN Pr6900b
Wagner Petrographic

SWN-Pr-6936

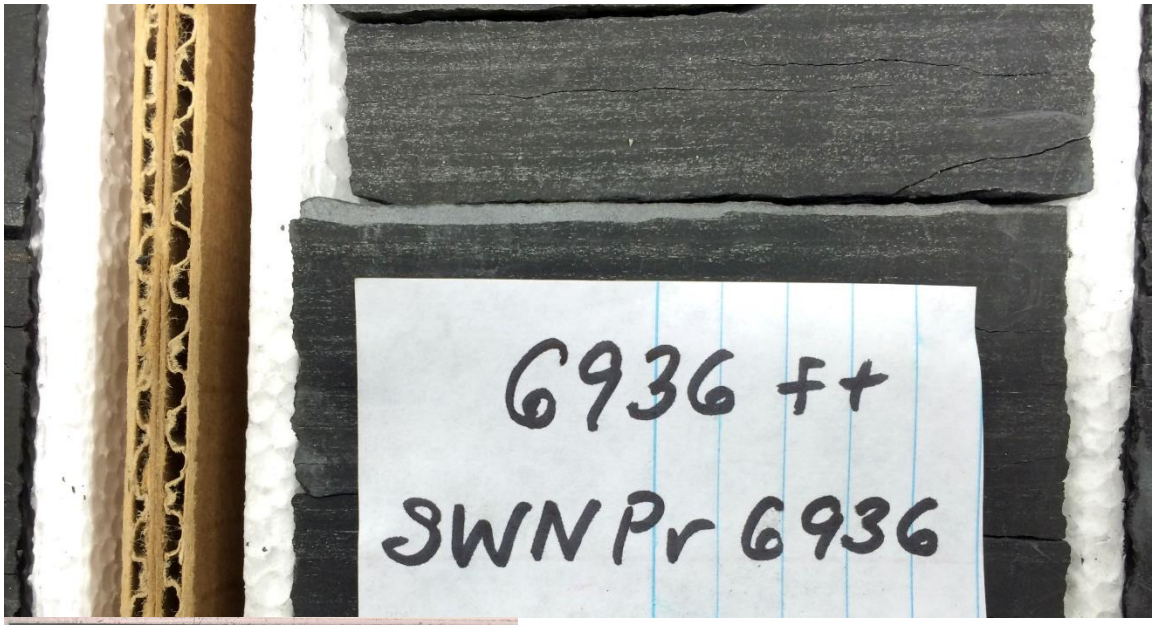

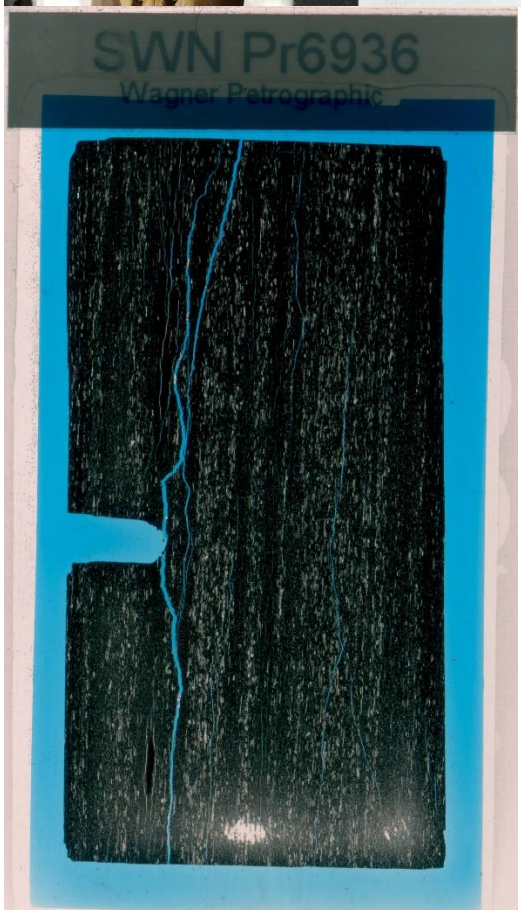

SWN-Pr-7001

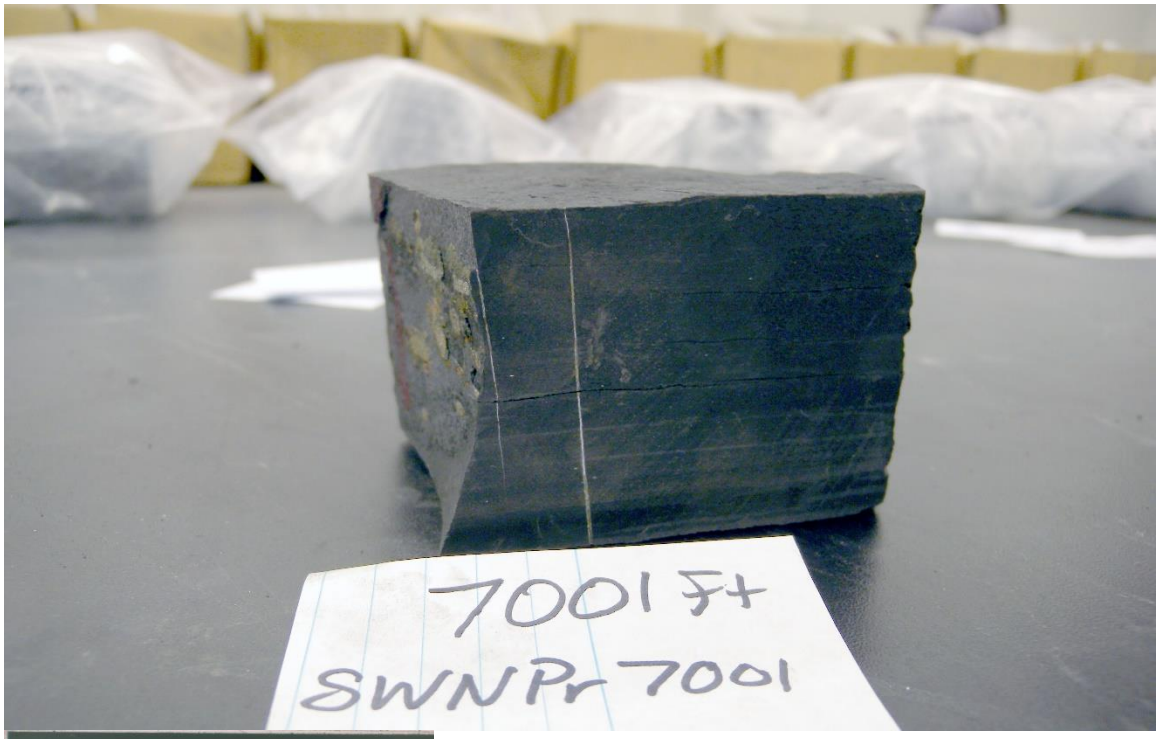
7001 ft
SWNPr 7001

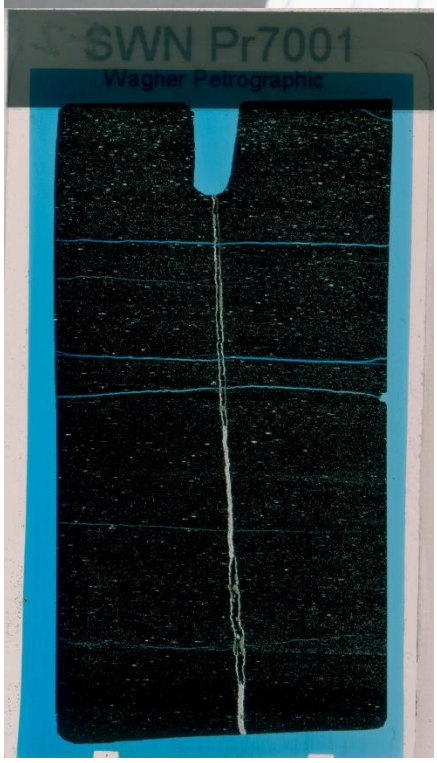
SWN Pr7001
Wagner Petrographic

SWN Pr6512

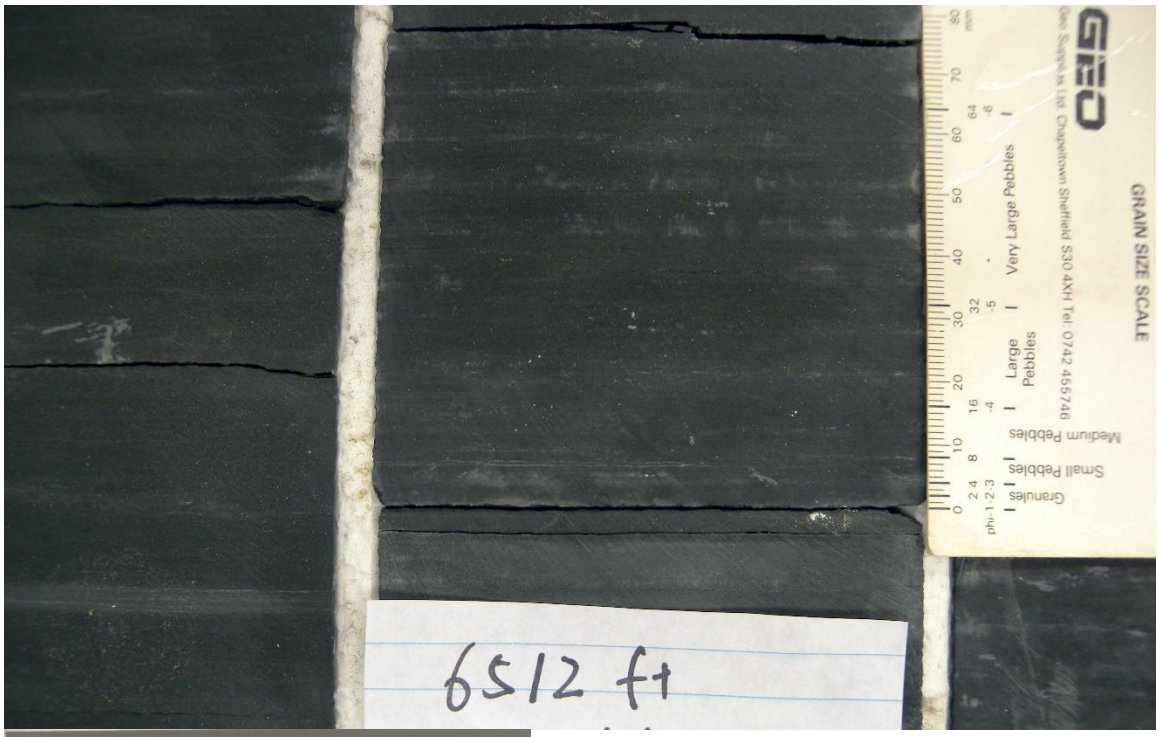
GRAIN SIZE SCALE
GEO
Very Large Pebbles
Large Pebbles
Medium Pebbles
Small Pebbles
Granules
6512 ft


SWN Pr6512
Wagner Petrographic

SWN Pr6728.5

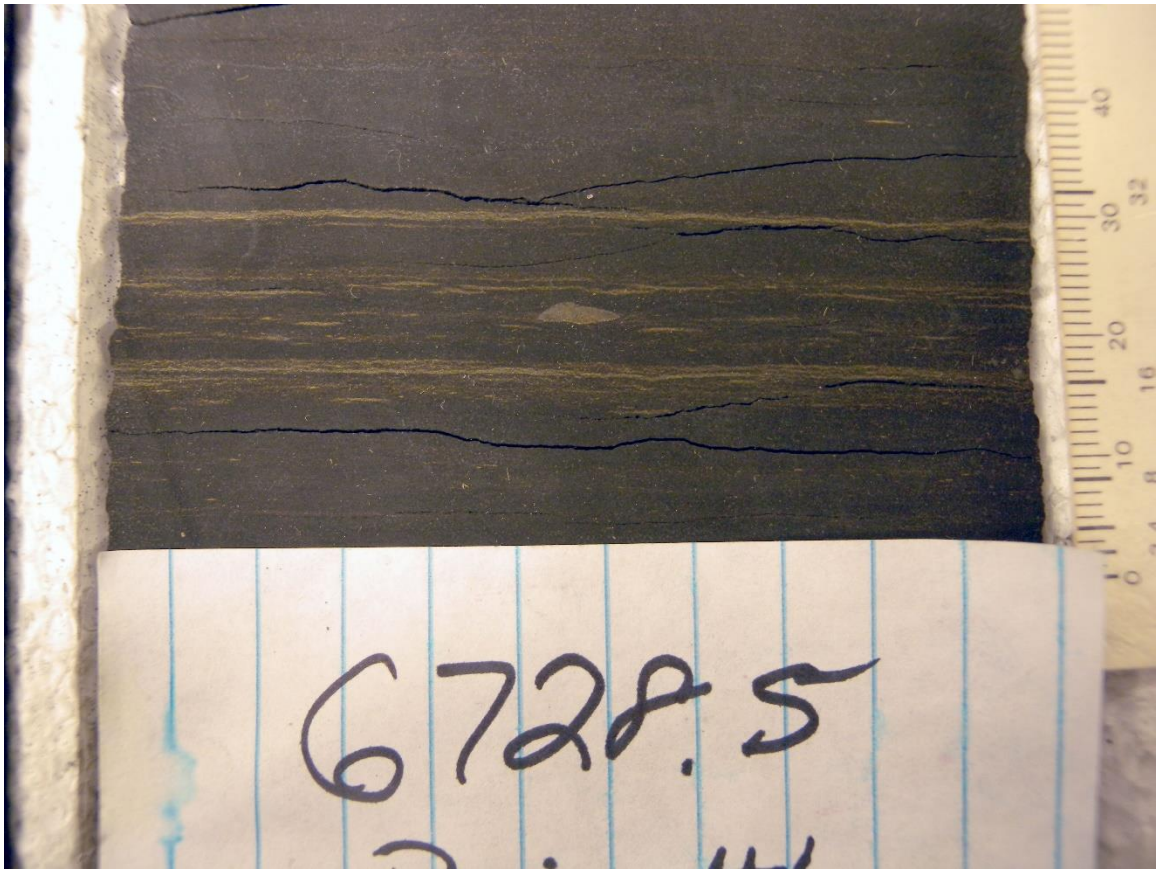

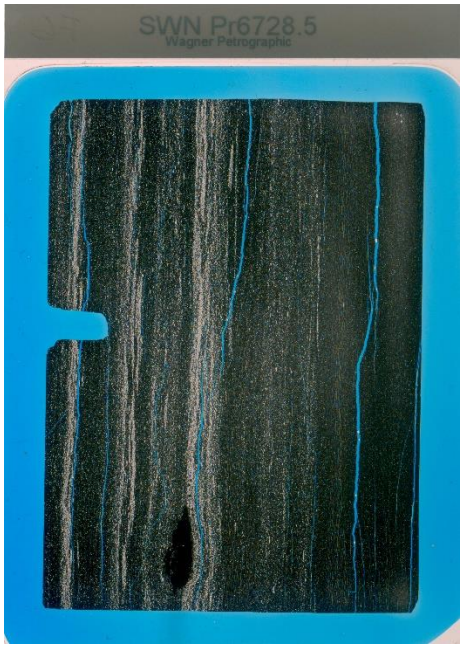

SWN Pr6780

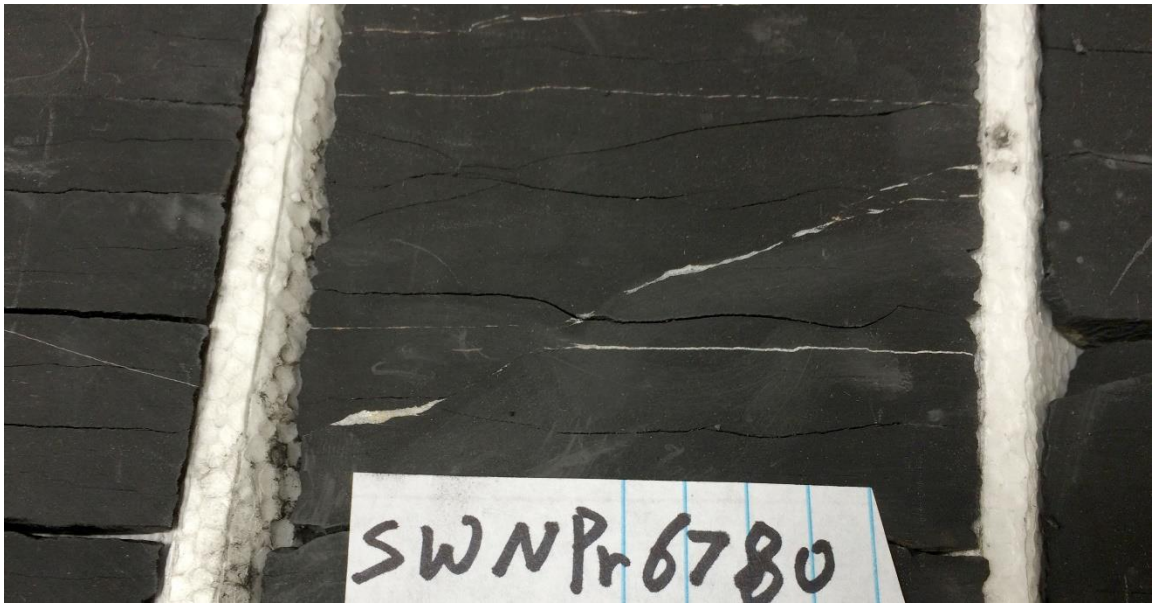

SWN Pr6820

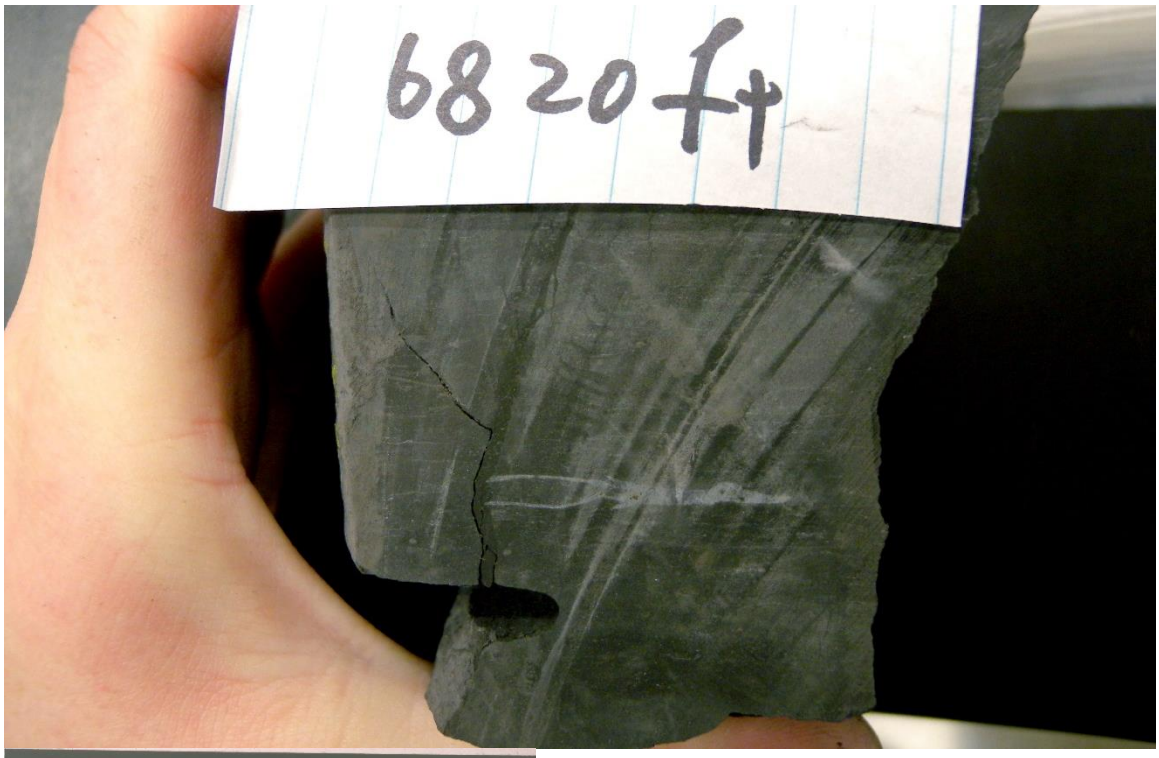

SWN Pr6834b

SWN Pr6898

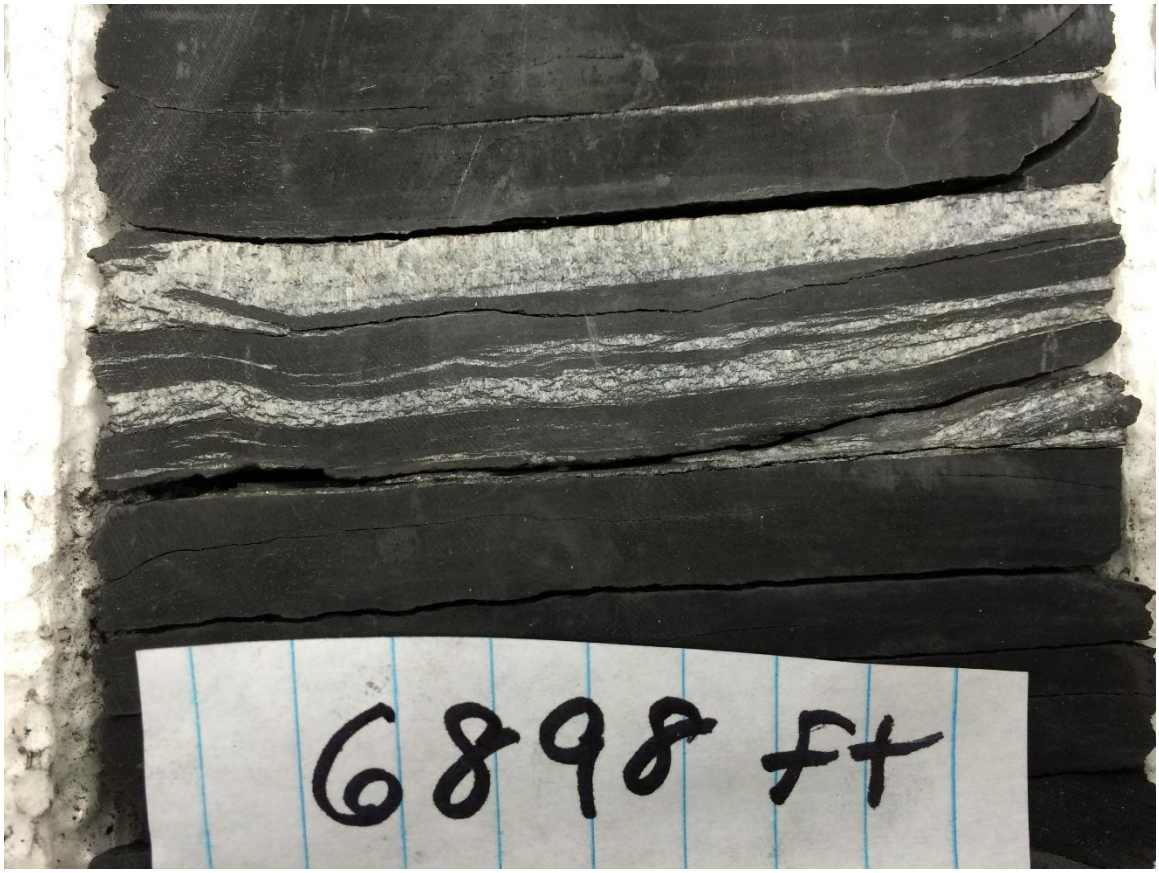

SWN Pr6898a
SWN Pr6898b

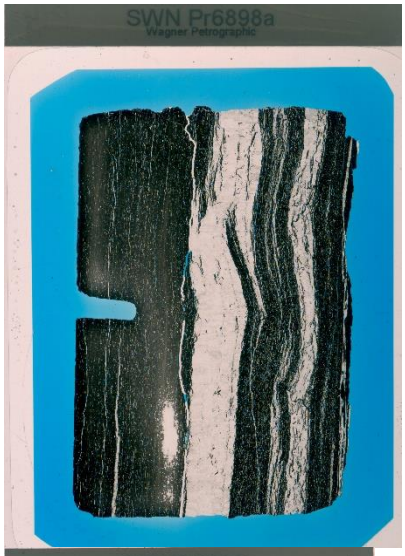
SWN Pr6898a
Wagner Petrographic


SWN Pr6898b
Wagner Petrographic

SWN Pr6992a

SWN Pr6992a
SWN Pr6992b


SWN Pr6992a
Wagner Petrographic
SWN Pr6992b
Wagner Petrographic

SWN-GW-6246.5

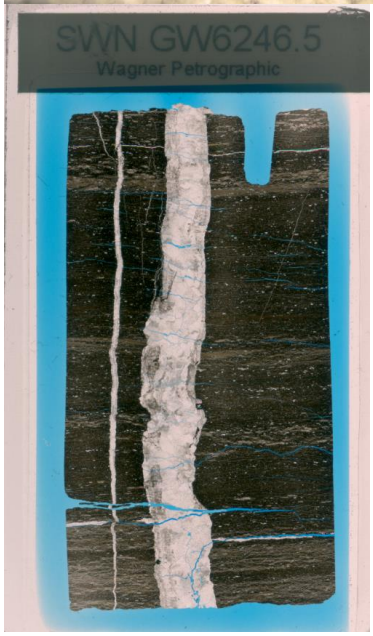

SWN GW 6358.5

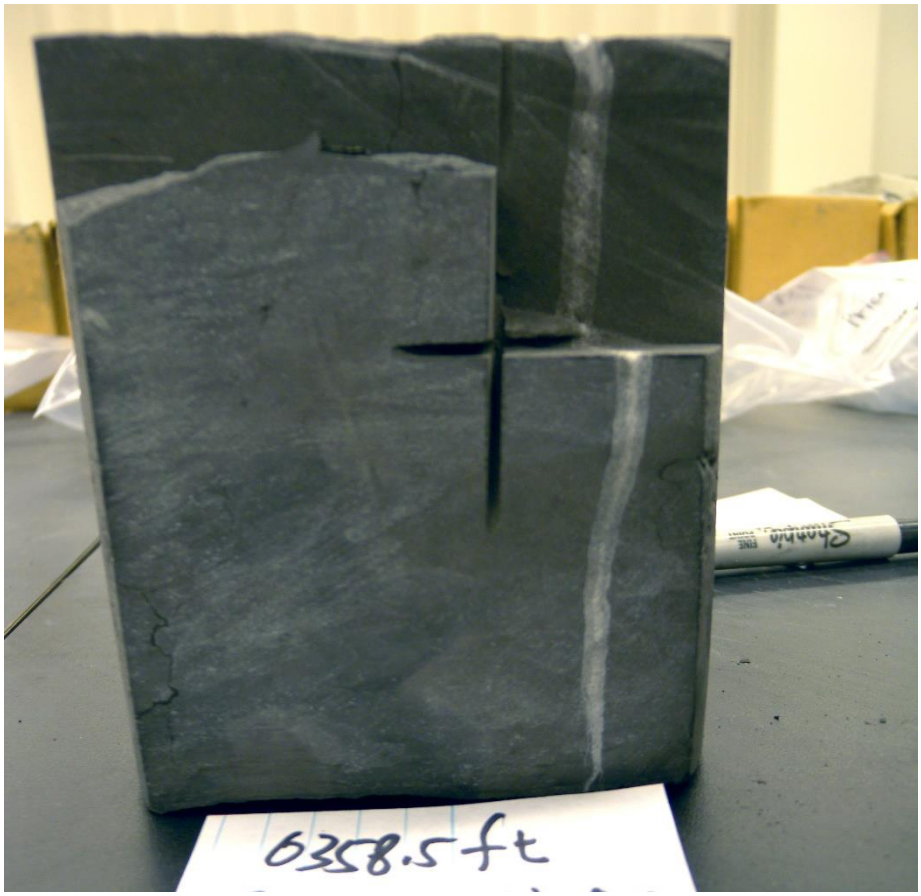

SWN-GW-6358.5A

SWN GW 6358.5B

SWN-GW-6379

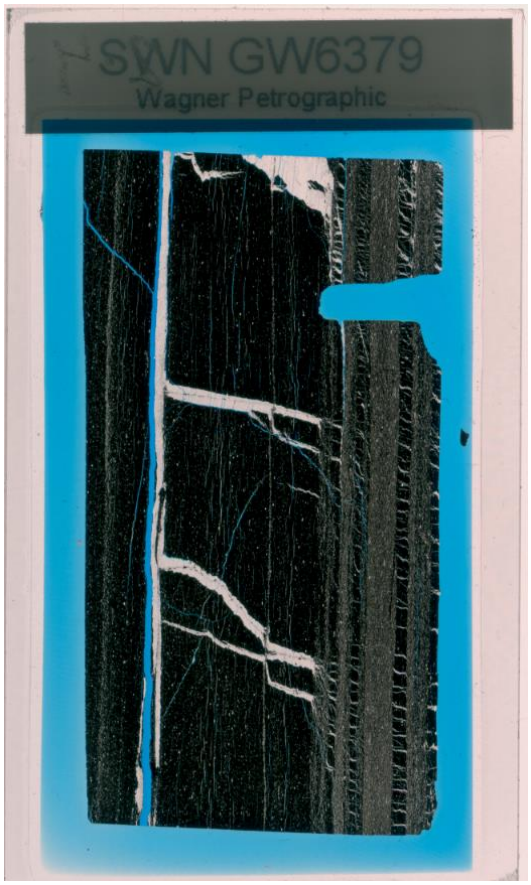

SWN-GW-6496

SWN-GW-6504B

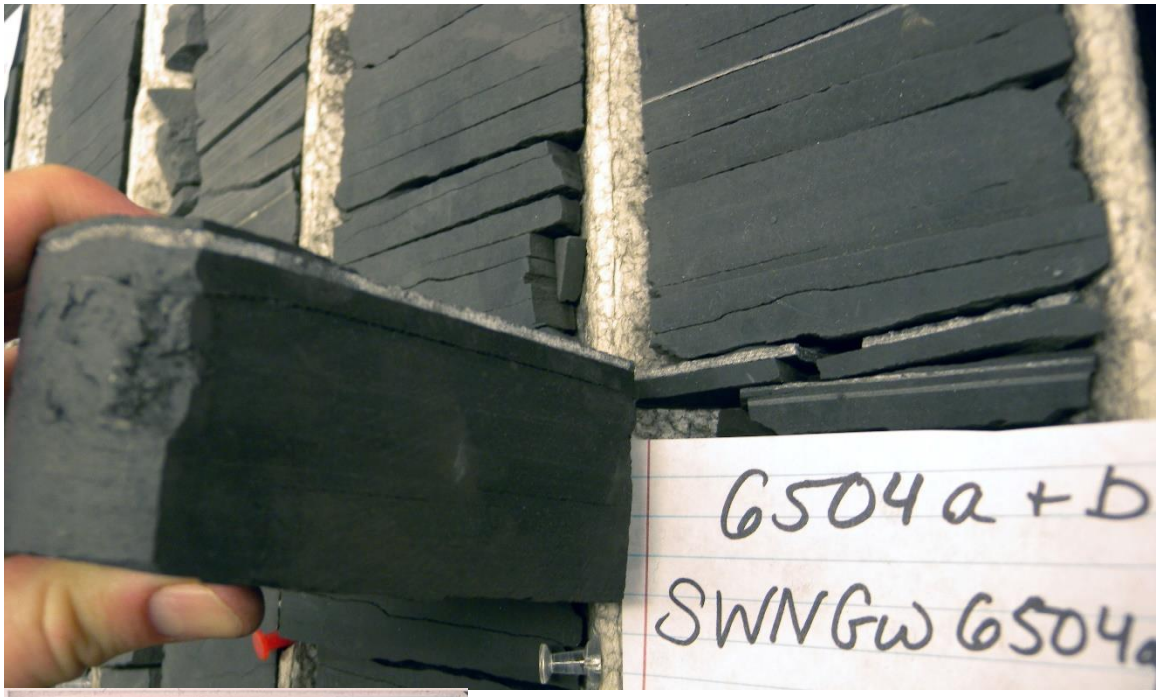

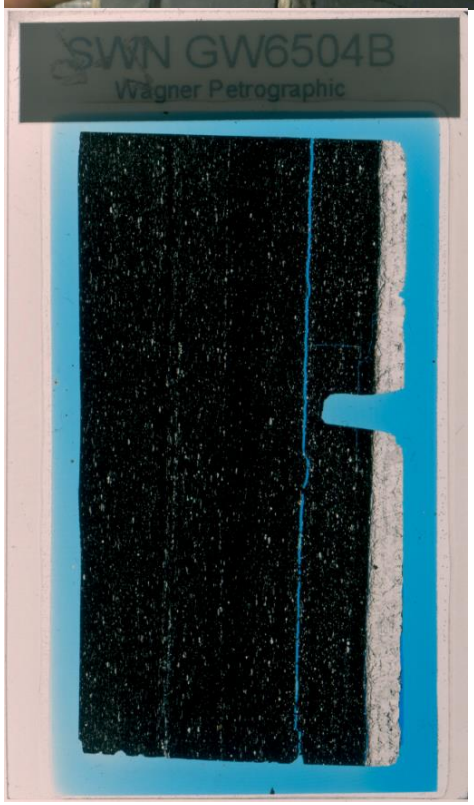

SWN-GW-6505


6505 ft
SWNGW6505

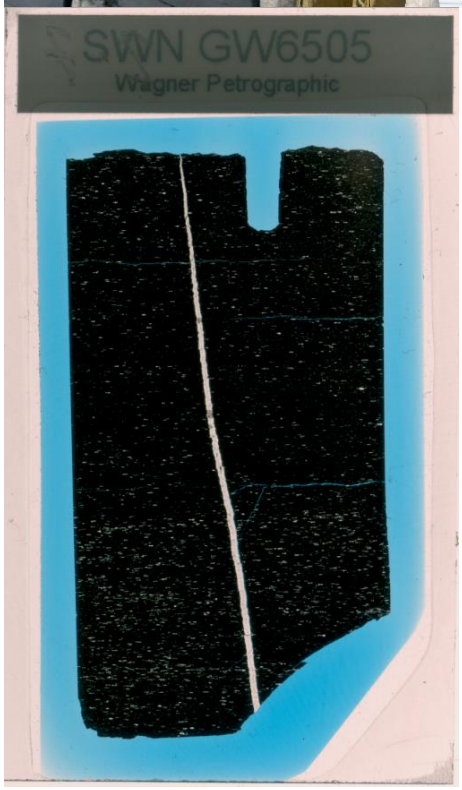
SWN GW6505
Wagner Petrographic

SWN-GW-6512B

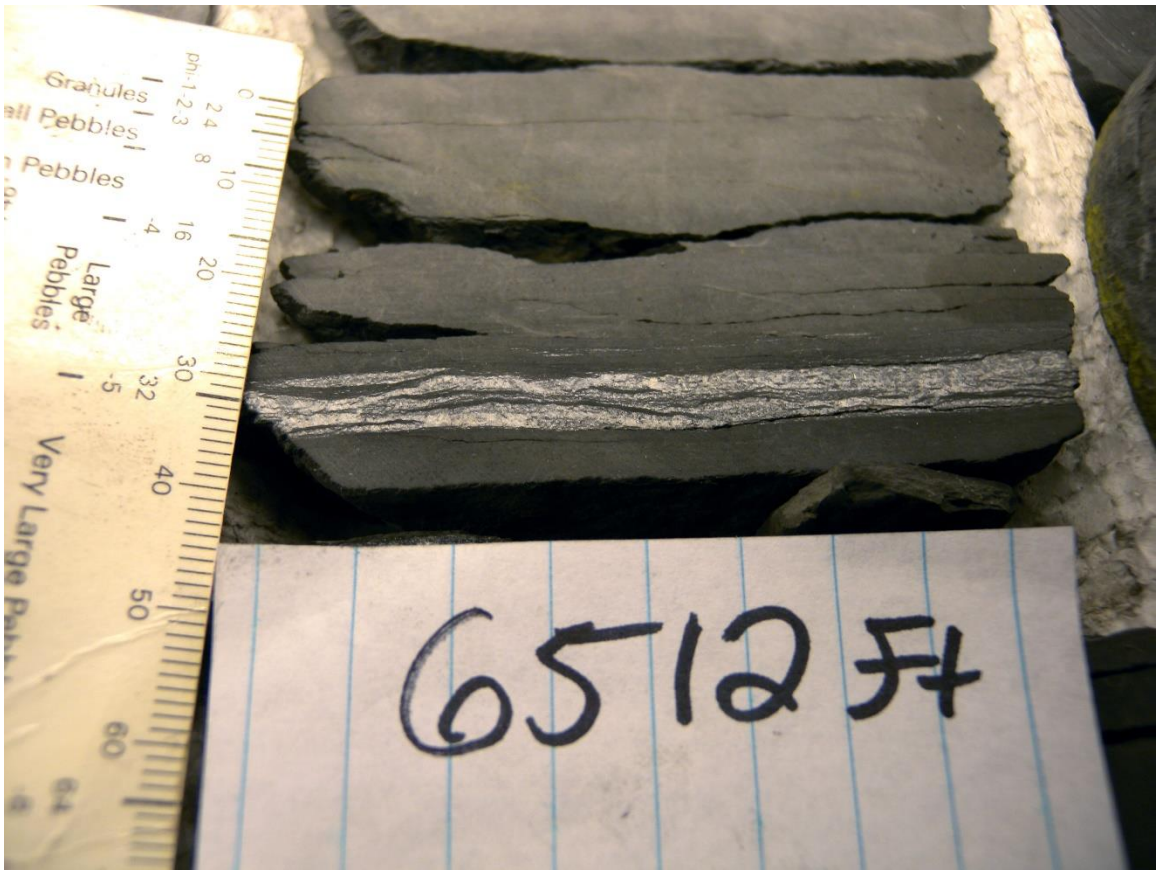

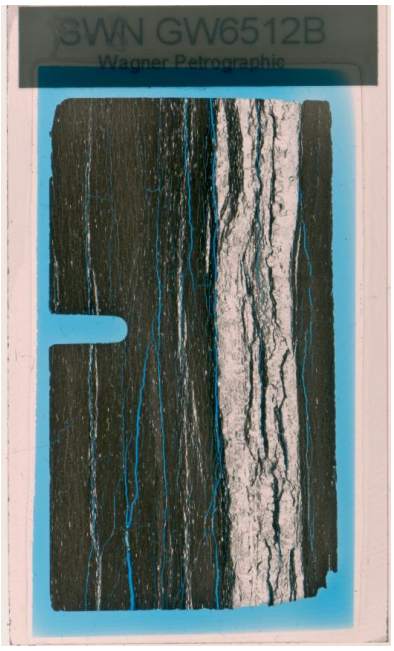

SWN-GW-6521

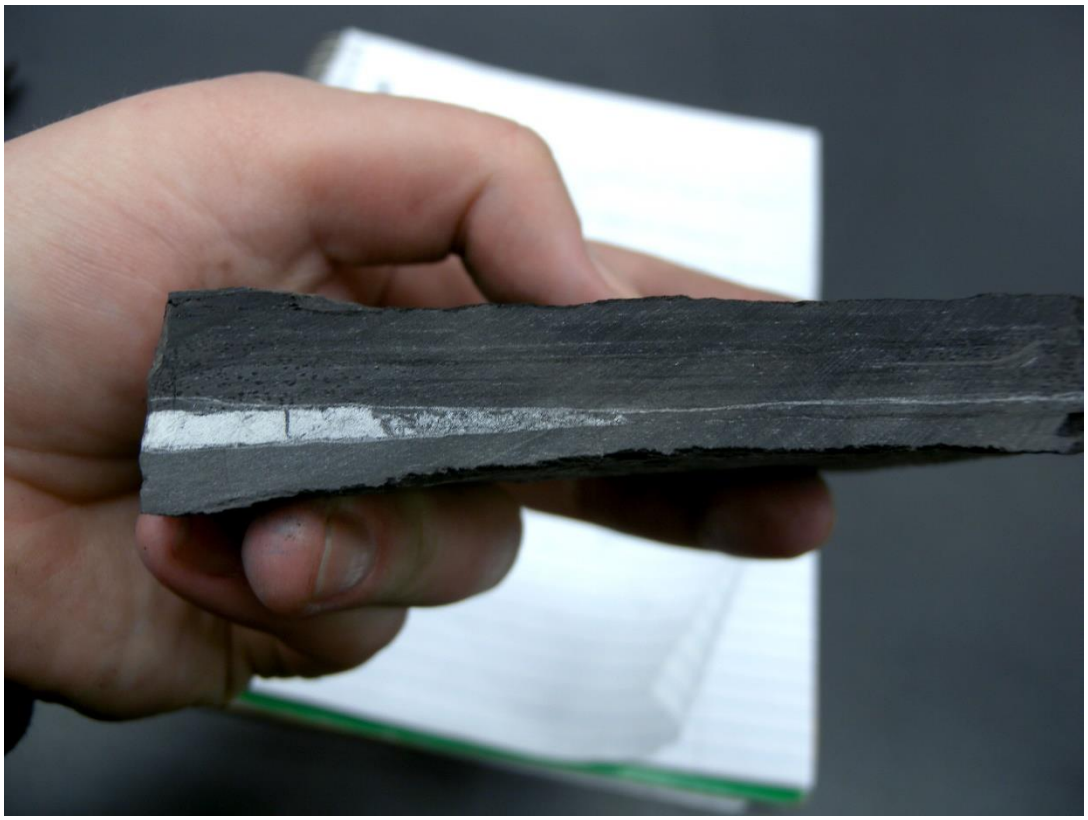

SWN GW 6311.5

SWN GW6512A

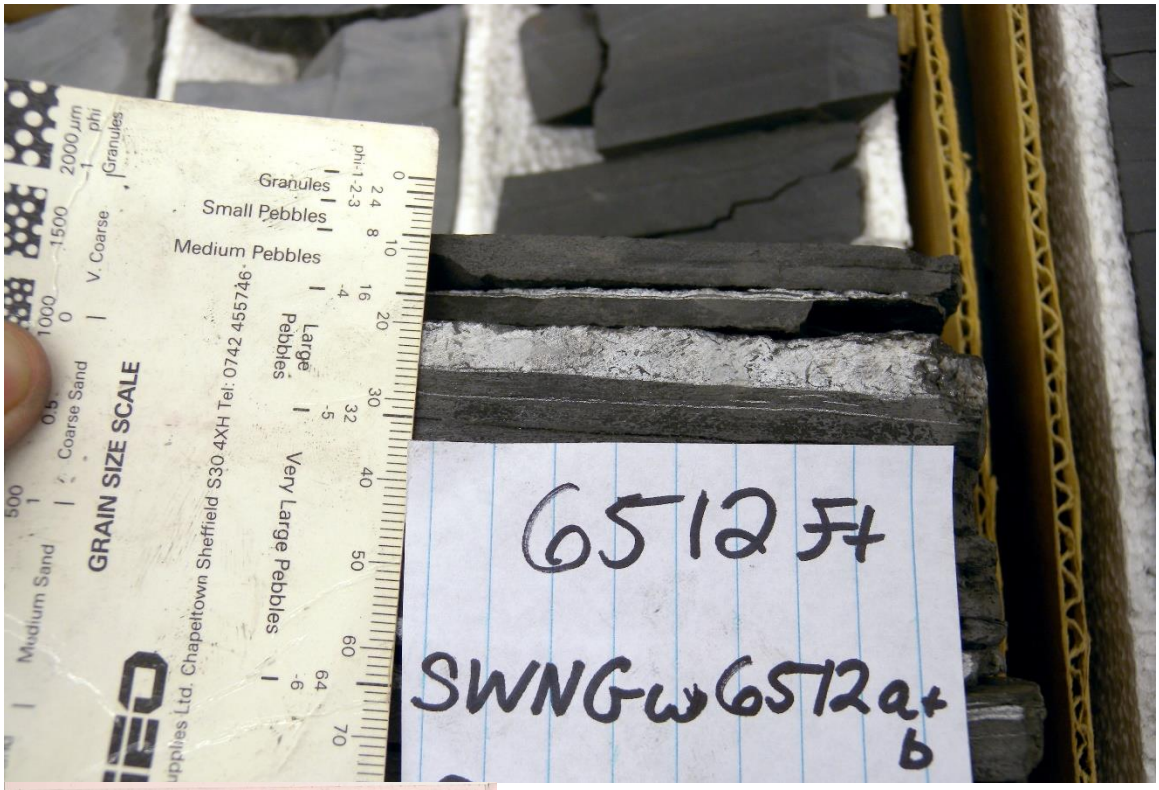
GRAIN SIZE SCALE
Granules
Small Pebbles
Medium Pebbles
Large Pebbles
Very Large Pebbles
Coarse Sand
Medium Sand
V. Coarse
Granules
6512 F+
SWNGW6512a+
b

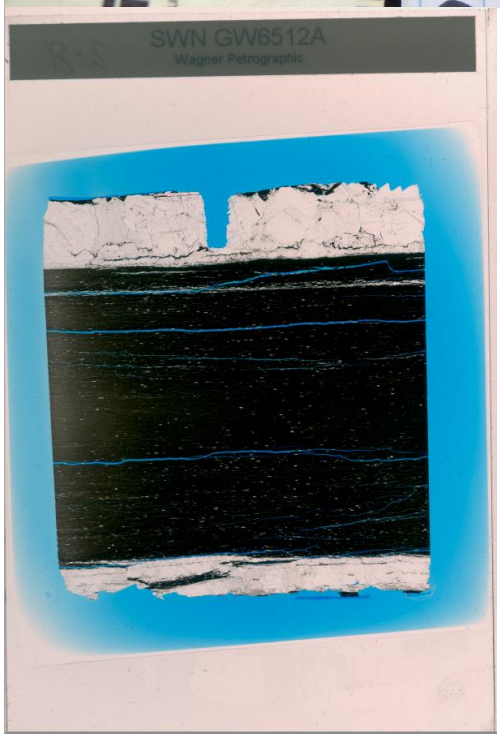
SWN GW6512A
Wagner Petrographic

SWN-Ed-6301

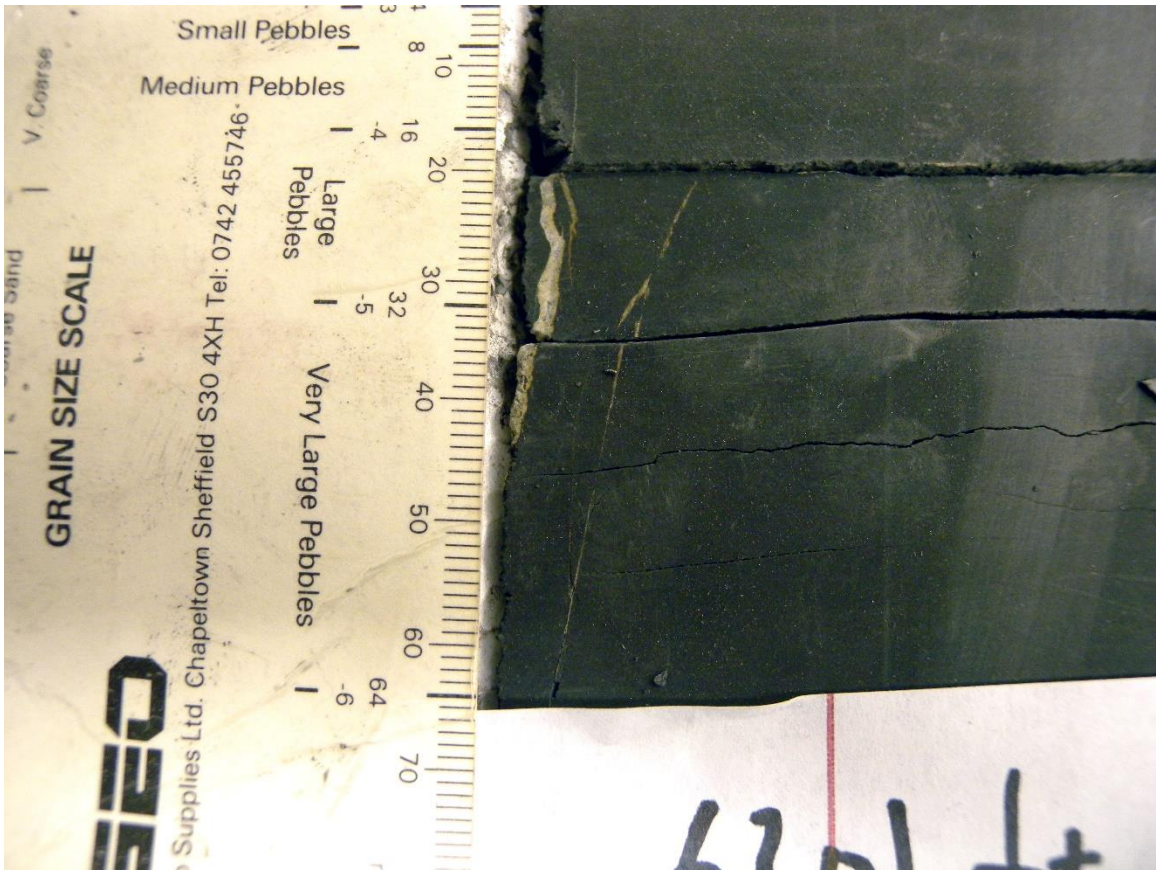
GRAIN SIZE SCALE
Small Pebbles
Medium Pebbles
Large Pebbles
Very Large Pebbles
Supplies Ltd. Chapeltown Sheffield S30 4XH Tel: 0742 455746

SWN-Ed-6638

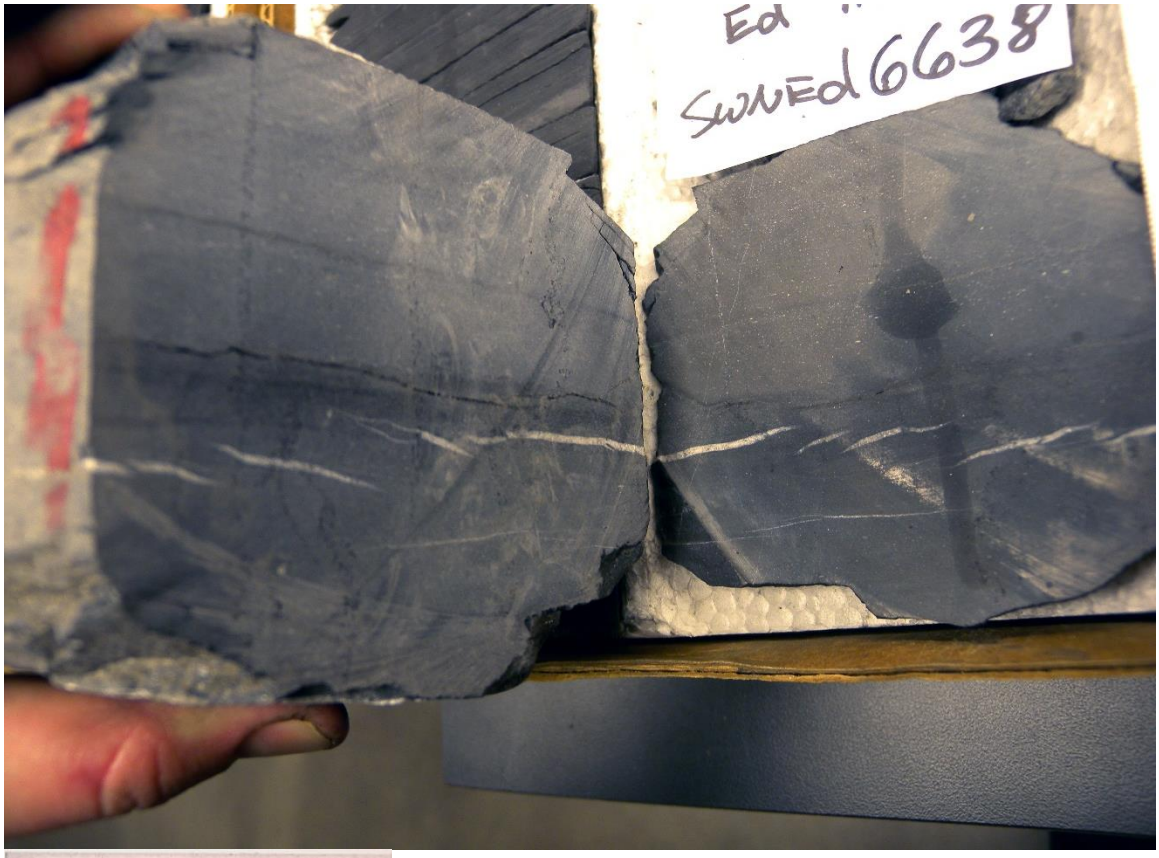

SWN-Ed-6674


6674 ft


SWN Ed6674
Wagner Petrographic

SWN-Ed-6676

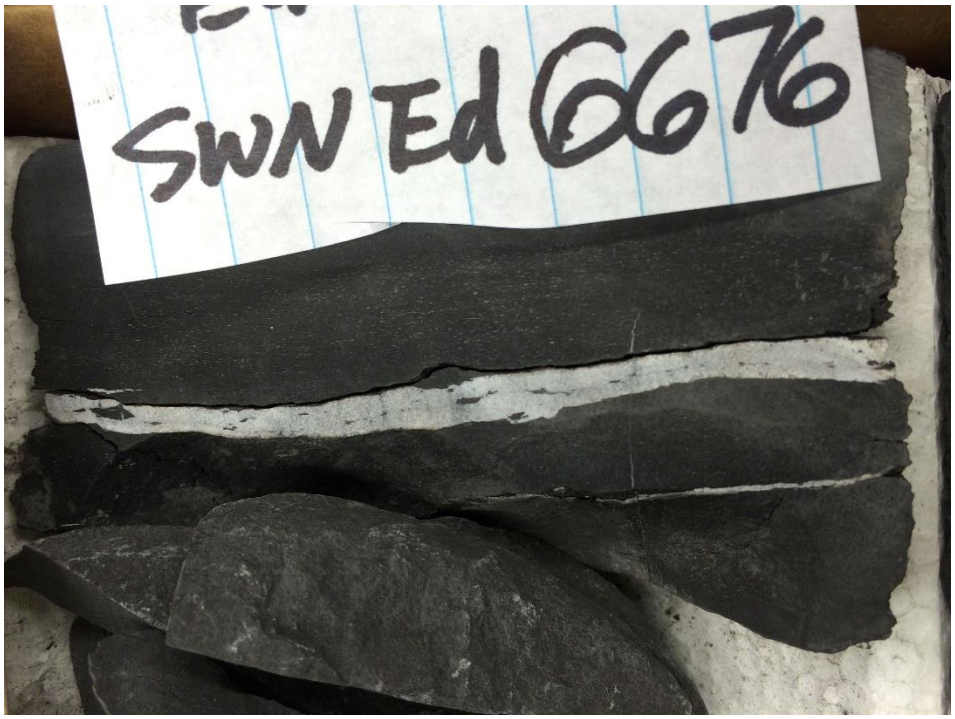

SWN-Ed-6658

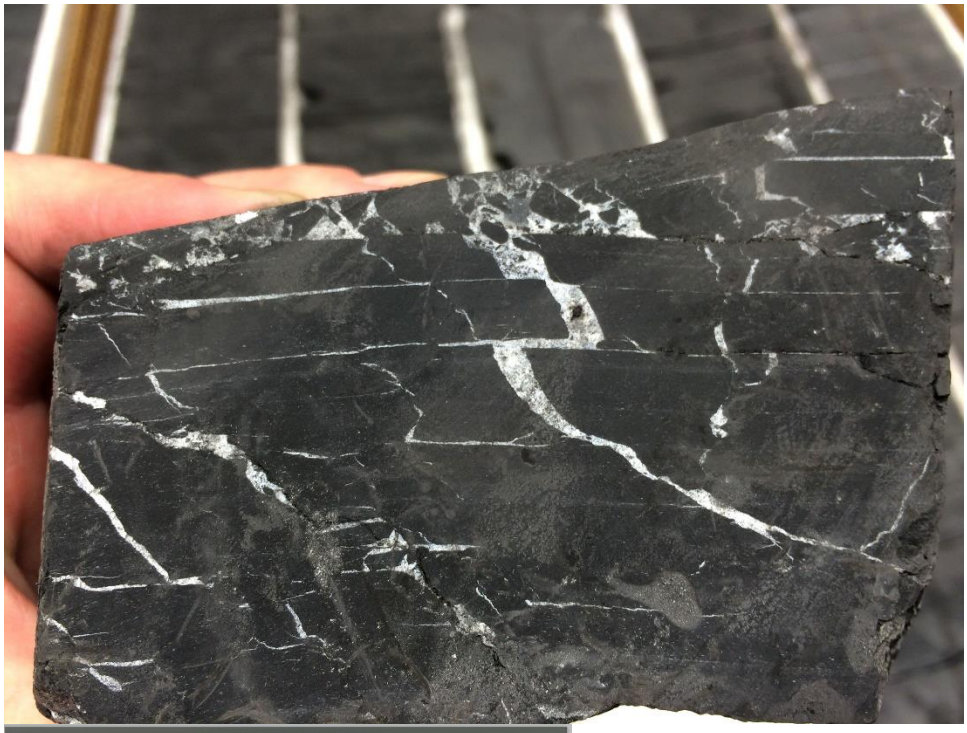

SWN-Ed-6668

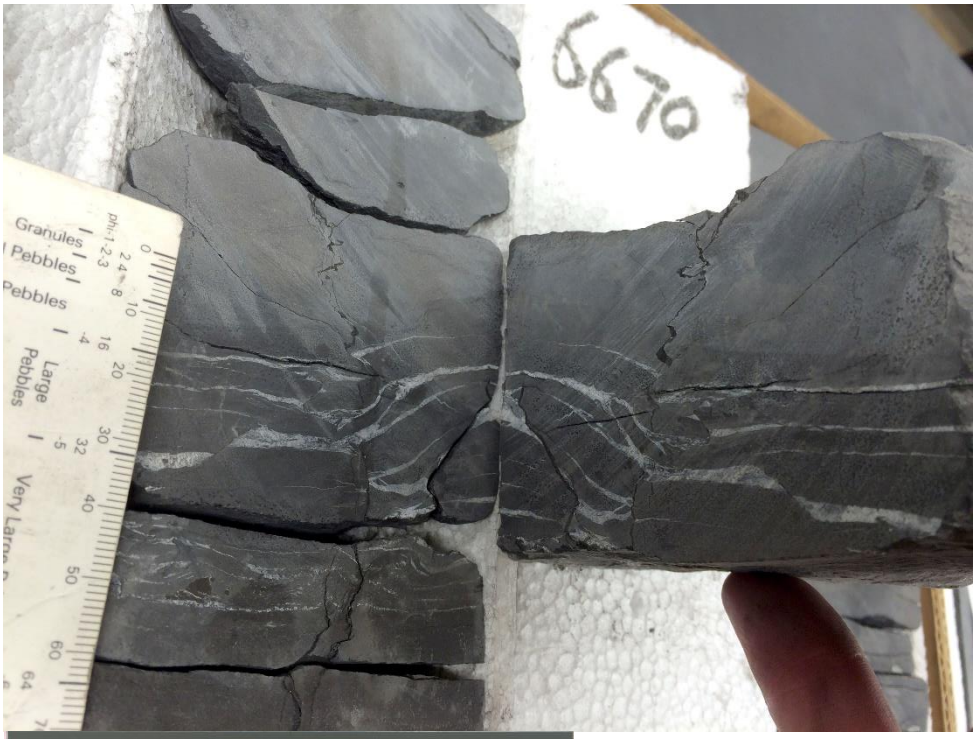
6670
Granules
Pebbles
Pebbles
Large
Pebbles

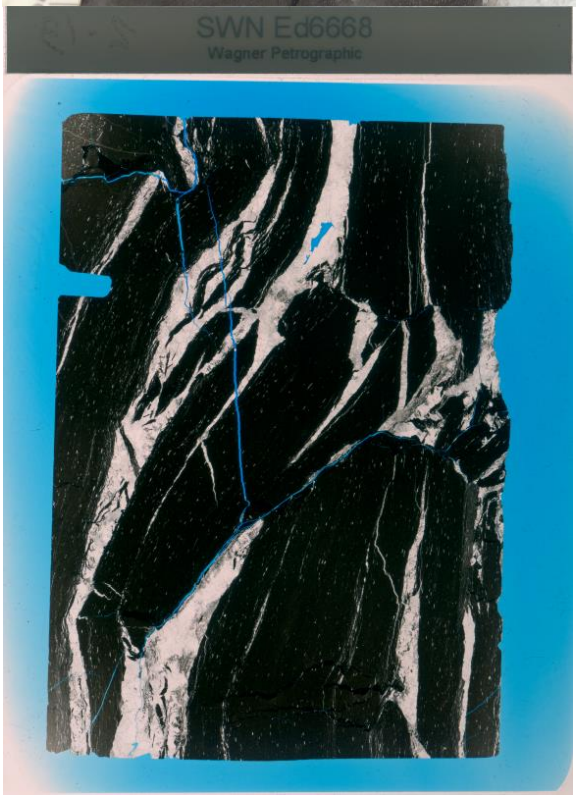
SWN Ed6668
Wagner Petrographic

SWN-Ed-6545

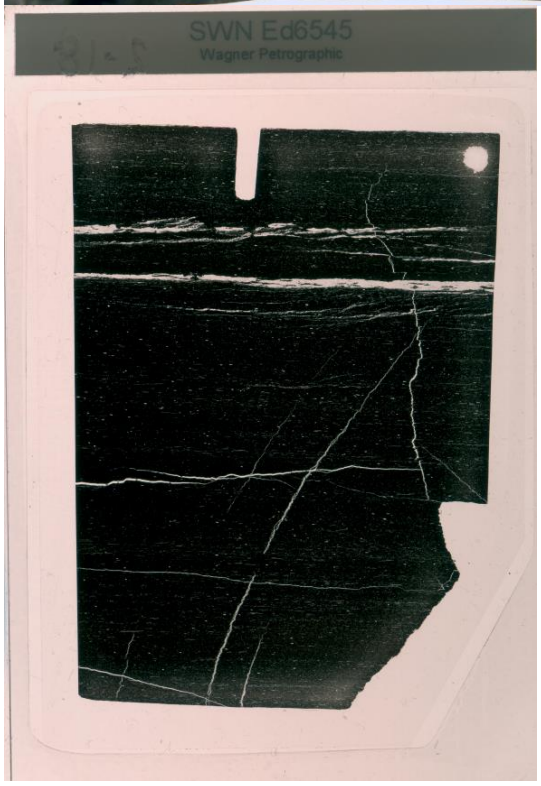

Appendix C: Field Measurements and Raw Scanline Data Spreadsheet.

Appendix C contains the spreadsheets for all 10 vertical scanline datasets collected from outcrops, core scan images, or by direct observation from core, these datasets are archived on a CD. Table columns of fracture#, aperture size, spacing, length and width of fractures (if applicable), cumulative frequency of each aperture sizes and preliminary descriptions of each fracture (if applicable). Datasets were used in fracture aperture scaling and length scaling. For datasets collected from core scan images, these are continuous or non-continuous mosaics, data collected in separate mosaics are listed in separate spreadsheets. The uncertain identification of bed-parallel fractures is marked by yellow. Table 6 is an example of scanline dataset archived (Vaca Muerta well#1, mosaic 1). For the full master scanline datasheet please refer to the CD available in the Walter Geology Library in the Jackson School of Geoscience.

This appendix also includes one separate spreadsheet focuses on the description of each one of the bed-parallel fractures collected along the scanline in the studies cores from three formations. For the full datasheet please refer to the CD available in the Walter Geology Library in the Jackson School of Geoscience.

One spreadsheet includes field bedding and fiber orientation measurements is shown below as Table 5.

Table 0-1 Table showing field bedding, fiber orientation measurements, and the attitude of bedding of 19 points along a mini fold at Arroyo Mulichinco upper section.

Bedding attitude and fiber orientation at outcrop									
Bedding			*Fiber orientation*					*Mini fold at Arroyo Mulichinco*	
Strike dgr.	dip dgr.		Arroyo Mulichinco dgr.		El Puesto dgr.			point#	Strike dgr.	dip dgr.
210	15		Plunge	Trend	Plunge	Trend		1	50	6
215	14		70	230	50	4		2	40	8.5
180	25		70	180	70	290		3	56	7.5
175	22		60	255	60	255		4	62	6
210	14		60	228	90	0		5	152	8
165	9		54	255	75	4.3		6	159	9
200	20		65	220	50	264.3		7	160	11.5
170	19		80	220	70	290		8	170	9.5
160	4				80	255		9	10	8
200	32				60	350		10	170	10
190	10							11	175	13
170	10							12	166	17
150	4							13	163	12
120	7							14	127	5
175	7							15	86	2
165	13							16	55	3
								17	53	5
								18	47	6
								19	70	4

Table 6 Example of scanline dataset archived (Vaca Muerta well#1, Mosaic 1). For the full master datasheet please refer to the CD available in the Walter Geology Library in the Jackson School of Geoscience.

Bed-parallel fracture picking in Vaca Muerta Well #1				2415.00-2433.36m			
#1	**Strip Section 1**	2415.00-2420.30m	*Uncertain ones aperture colored yellow*		unfiltered (includes uncertain observation)		
no.	Aperture (mm)	Spacing(cm)	Note	0.33mm as aperture min. cutoff	Aperture (mm)	cum #	cum freq
		46.9			7	1	0.054015
1	0.75				3.3	2	0.108029
		38.2			2.65	3	0.162044
2	0.33				2.15	4	0.216059
		1.2			1.75	6	0.324088
3	0.5				1.4	7	0.378102
		50			1.15	10	0.540146
4	0.62				0.95	18	0.972263
		10.1			0.75	27	1.458395
5	0.62		Beef? Sampling induced?		0.62	45	2.430659
		57.9			0.5	58	3.132849
6	2.65				0.4	64	3.456937
		138.6			0.33	67	3.618981
7	0.75		Beef? Sampling induced?				
		0.8			filtered (excludes uncertain observation)		
8	0.4		Beef? Sampling induced?		Aperture (mm)	cum #	cum freq
		2.6			7	1	0.054015
9	0.95				3.3	2	0.108029
		99.7			2.65	3	0.162044
10	0.62				2.15	4	0.216059
#1	**Strip section 2**	2420.30-2425.67			1.75	6	0.324088
		125.1			1.4	7	0.378102
11	0.4		Beef? Sampling induced?		1.15	10	0.540146
		9.3			0.95	17	0.918249
12	0.5		Beef? Sampling induced?		0.75	24	1.296351
		3.2			0.62	37	1.998542
13	0.33				0.5	46	2.484673
		1.5			0.4	49	2.646717
14	0.5				0.33	52	2.808761
		1.4					
15	0.75		fracs around concretions, curved, complex(branches or linked)				
		2					
16	0.62						
		1.1					
17	0.5						
		0.5					
18	0.4						
		1.6					
19	0.62		beef or just mud/sampling induced?				
		1.4					
20	0.75		Beef? Sampling induced?				
		4					
21	0.95		Fracs around concretions, curved, complex, some				
		1.7	are branced some are fat and short, some are thin				
22	0.62		but long, branches or linked				
		2.3					
23	0.95						
		0.5					
24	1.4						
		6.6					
25	0.95						
		3.1					
26	0.33						
		1.6					
27	0.62						
		10.4					
28	0.5		beef? Silt layer? Too faded				
		1.4					
29	0.62		Beef? Sampling induced?				
		3.5					
30	7		thick beef, highly branched				
		2.4					
31	0.5		Silt layer? Too faded				
		4.5					
32	1.15		single simple, break				
		17.7					
33	0.75		single simple , break				
		88.5					

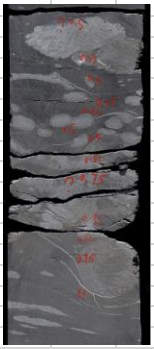

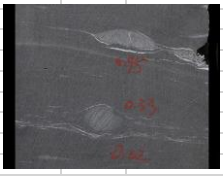

Table 6 continued

34	0.75		
		1	
35	0.62		Curved around concretions, very thin but long, around 6m, simple/single
		1.6	
36	0.62		
		0.2	
37	0.5		
		8.6	
38	0.95		attached at core break
		4.3	
39	0.5		around concretion, thin, simple/single
		2.8	
40	0.5		around concretion, thin, simple/single
		3.7	
41	0.75		around concretion, thin, simple/single
		18.1	
42	0.95		attached at core break
		20.9	
43	1.15		attached at core break
		26.5	
44	0.75		
		0.5	
45	0.4		round Concretion, thin, slightly branche
		60.6	
46	0.62		a group of 3 thing long fracs
		0.4	
47	0.95		simple/single
		2.5	
48	0.75		simple/single
		77.1	
49	0.5		
		0.5	
50	1.15		around concretion, simple, the thickest beef breaks and branches out
		0.5	
51	0.5		
		5.3	
52	2.15		
		2.6	
53	0.62		Thickest part is ~2.15
		41.6	
54	0.62		
		1	
55	0.5		a series of thin and short fracs, curved
		0.6	
56	0.62		
		0.265	
57	1.75		slightly branched with shale shells
		1	
58	1.75		highly branched
		54	
#1	Strip Section 3	2425.67-2431.04	
		171.8	
59	0.4		beef or just plastic box?
		289.1	
60	0.5		
		75.8	
#1	Strip Section 4	2431.04-2433.37	
		35	
61	0.62		beef or plastic box?
		86.3	
62	0.62		single
		9.2	
63	0.4		curved linked
		4.8	
64	0.62		
		22.9	
65	0.95		curved, several short fracs linked together
		63.2	
66	3.3		branched, with shale shells in,cround concretion
		3.9	
67	0.62		single, long curved, around concretion
67 fracs		6	
Total	58.85mm	1845.465 cm	
Length m	18.514		

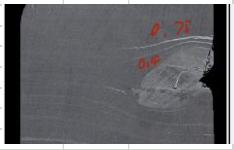

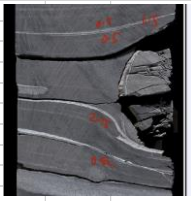

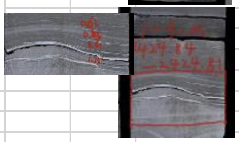

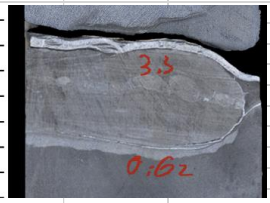

Appendix D: Petrography Photomicropgraphs

Appendix D is located on a CD and contains petrographic images from each Sample from all 3 formations. The digital files are labeled with sample names. The names of pictures indicate the feature of interest within each picture. The setting of microscope used to take that one picture can also be told from the name of each picture. and magnification and allow for better resolution of the images. This CD is available in the Walter Geology Library in the Jackson School of Geoscience.

Appendix E: SEM/EDS/CL Images and Microprobe raw data.

Appendix D is located on a CD and contains all SEM/EDS/CL imagesand the Microp probe raw data from the samples. The digital files are labeled with sample names and magnification and allow for better resolution of the images. This CD is available in the Walter Geology Library in the Jackson School of Geoscience.

References

Abramowitz, M., and Stegun, I.A., 1965, Chapter 9: Handbook of Mathematical Functions with Formulas, Graphs, and Mathematical Tables, p. 355.

Adams, J.E., 1965, Stratigraphic-tectonic development of Delaware Basin: AAPG bulletin, v. 49, p. 2140-2148.
Al Duhailan, M., 2007, Petroleum-expulsion fracturing in organic-rich shales: genesis and impact on unconventional pervasive petroleum systems, PhD Dissertation, Colorado School of Mines.
Andrews, W., 1881, Note on the Purbeck beds at Teffont: Quarterly Journal of the Geological Society, v. 37, p. 251-253.
Andrews, W., and Jukes-Browne, A., 1894, The Purbeck beds of the Vale of Wardour: Quarterly Journal of the Geological Society, v. 50, p. 44-71.
Aydin, A., 2014, Failure modes of shales and their implications for natural and man-made fracture assemblages: AAPG bulletin, v. 98, p. 2391-2409.
Baecher, G.B., and Lanney, N.A., 1978, Trace length biases in joint surveys, 19th US Symposium on Rock Mechanics (USRMS), American Rock Mechanics Association.
Barton, C.A., and Zoback, M.D., 1992, Self-similar distribution and properties of macroscopic fractures at depth in crystalline rock in the Cajon Pass Scientific Drill Hole: Journal of Geophysical Research: Solid Earth, v. 97, p. 5181-5200.
Barton, C.A., and Zoback, M.D., 1992, Self-similar distribution and properties of macroscopic fractures at depth in crystalline rock in the Cajon Pass Scientific Drill Hole: Journal of Geophysical Research: Solid Earth, v. 97, p. 5181-5200.
Belfield, W., and Sovich, J., 1995, Fracture statistics from horizontal wellbores: Journal of Canadian Petroleum Technology, v. 34.
Berg, R.R., and Gangi, A.F., 1999, Primary migration by oil-generation microfracturing in low-permeability source rocks: application to the Austin Chalk, Texas: AAPG bulletin, v. 83, p. 727-756.
Bernard, S., and Horsfield, B., 2014, Thermal maturation of gas shale systems: Annual Review of Earth and Planetary Sciences, v. 42, p. 635-651.
Bogdanov, A., 1947, The intensity of cleavage as related to the thickness of beds: Soviet Geology, v. 16.
Bogdanov, A., 1947, The intensity of cleavage as related to the thickness of beds: Soviet Geology, v. 16.
Bonnet, E., 1996, Localisation de la déformation dans les milieux fragile-ductile: approche expérimentale et application à la lithosphère continentale, Université Rennes 1.
Bonnet, E., Bour, O., Odling, N.E., Davy, P., Main, I., Cowie, P., and Berkowitz, B., 2001, Scaling of fracture systems in geological media: Reviews of geophysics, v. 39, p. 347-383.
Bons, P.D., and Jessell, M.W., 1997, Experimental simulation of the formation fibrous veins by localised dissolution-precipitation creep: Mineralogical Magazine, v. 61, p. 53-63.

Bracaccini, O., 1970, Rasgos tectónicos de las acumulaciones mesozoicas en las provincias de Mendoza y Neuquén, República Argentina: Revista de la asociación Geológica argentina, v. 25, p. 275-284.

Brissón, I., and Veiga, R., 1998, La estratigrafía y estructura de la Cuenca Neuquina: Gira de campo: Buenos Aires, Repsol YPF,(unpublished report).

Brodie, P., 1854, On the insect beds of the Purbeck Formation in Wiltshire and Dorsetshire: Quarterly Journal of the Geological Society, v. 10, p. 475-482.

Carbotte, S.M., and Macdonald, K.C., 1994, Comparison of seafloor tectonic fabric at intermediate, fast, and super fast spreading ridges: Influence of spreading rate, plate motions, and ridge segmentation on fault patterns: Journal of Geophysical Research: Solid Earth, v. 99, p. 13609-13631.

Cheney, M.G., 1940, Geology of north-central Texas: AAPG bulletin, v. 24, p. 65-118.

Chuprakov, D., Melchaeva, O., and Prioul, R., 2013, Hydraulic fracture propagation across a weak discontinuity controlled by fluid injection, ISRM International Conference for Effective and Sustainable Hydraulic Fracturing, International Society for Rock Mechanics.

Chuprakov, D.A., Akulich, A.V., Siebrits, E., and Thiercelin, M., 2011, Hydraulic-fracture propagation in a naturally fractured reservoir: SPE Production & Operations, v. 26, p. 88-97.

Chuprakov, D.A., and Prioul, R., 2015, Hydraulic Fracture Height Containment by Weak Horizontal Interfaces, SPE Hydraulic Fracturing Technology Conference, Society of Petroleum Engineers.

Cladouhos, T.T., and Marrett, R., 1996, Are fault growth and linkage models consistent with power-law distributions of fault lengths?: Journal of Structural Geology, v. 18, p. 281-293.

Clark, M.B., Brantley, S.L., and Fisher, D.M., 1995, Power-law vein-thickness distributions and positive feedback in vein growth: Geology, v. 23, p. 975-978.

Cobbold, P., Diraison, M., and Rossello, E., 1999, Bitumen veins and Eocene transpression, Neuquén basin, Argentina: Tectonophysics, v. 314, p. 423-442.

Cobbold, P., and Rossello, E., 2003, Aptian to recent compressional deformation, foothills of the Neuquén Basin, Argentina: Marine and Petroleum Geology, v. 20, p. 429-443.

CCobbold, P.R., and Rodrigues, N., 2007, Seepage forces, important factors in the formation of horizontal hydraulic fractures and bedding-parallel fibrous veins (‘beef’and ‘cone-in-cone’): Geofluids, v. 7, p. 313-322.

Cobbold, P.R., Zanella, A., Rodrigues, N., and Løseth, H., 2013, Bedding-parallel fibrous veins (beef and cone-in-cone): worldwide occurrence and possible significance in terms of fluid overpressure, hydrocarbon generation and mineralization: Marine and Petroleum Geology, v. 43, p. 1-20.

Cobbold, P.R., Zanella, A., Ruffet, G., Rodrigues, N., and Loseth, H., 2012, Beef (bedding-parallel fibrous veins): worldwide occurrence and significance in terms of fluid overpressure, hydrocarbon generation and mineralization (including

sulfides, emerald, uranium or gold), American Association of Petroleum Geologists Annual Convention.
Cosgrove, J., 1995, The expression of hydraulic fracturing in rocks and sediments: Geological Society, London, Special Publications, v. 92, p. 187-196.
Cosgrove, J., 1995, The expression of hydraulic fracturing in rocks and sediments: Geological Society, London, Special Publications, v. 92, p. 187-196.
Cosgrove, J.W., 2001, Hydraulic fracturing during the formation and deformation of a basin: A factor in the dewatering of low-permeability sediments: AAPG bulletin, v. 85, p. 737-748.
Cosgrove, J.W., 2001, Hydraulic fracturing during the formation and deformation of a basin: A factor in the dewatering of low-permeability sediments: AAPG bulletin, v. 85, p. 737-748.
Cowie, P.A., Sornette, D., and Vanneste, C., 1995, Multifractal scaling properties of a growing fault population: Geophysical Journal International, v. 122, p. 457-469.
Cowie, P.A., Vanneste, C., and Sornette, D., 1993, Statistical physics model for the spatiotemporal evolution of faults: Journal of Geophysical Research: Solid Earth, v. 98, p. 21809-21821.
Cruden, D., 1977, Describing the size of discontinuities, International Journal of Rock Mechanics and Mining Sciences & Geomechanics Abstracts, Volume 14, Elsevier, p. 133-137.
Curtis, J.B., 2002, Fractured shale-gas systems: AAPG bulletin, v. 86, p. 1921-1938.
Damborenea, S., and Leanza, H., 2004, Bivalvos monotoideos tithonianos de la Formación Vaca Muerta, norte de Neuquén, Argentina: Ameghiniana, v. 41.
Dershowitz, W.S., and Herda, H.H., 1992, Interpretation of fracture spacing and intensity, The 33th US Symposium on Rock Mechanics (USRMS), American Rock Mechanics Association.
Deschamps, A., Tivey, M., Embley, R.W., and Chadwick, W.W., 2007, Quantitative study of the deformation at Southern Explorer Ridge using high-resolution bathymetric data: Earth and Planetary Science Letters, v. 259, p. 1-17.
Ding, W., Li, C., Li, C., Xu, C., Jiu, K., Zeng, W., and Wu, L., 2012, Fracture development in shale and its relationship to gas accumulation: Geoscience Frontiers, v. 3, p. 97-105.
Durney, D.W., and Ramsay, J., 1973, Incremental strains measured by syntectonic crystal growths: Gravity and tectonics, v. 67, p. 96.
Durney, D.W., and Ramsay, J., 1973, Incremental strains measured by syntectonic crystal growths: Gravity and tectonics, v. 67, p. 96.
Engelder, T., and Fischer, M.P., 1994, Influence of poroelastic behavior on the magnitude of minimum horizontal stress, Sh in overpressured parts of sedimentary basins: Geology, v. 22, p. 949-952.
Ettensohn, F.R., 1985, The Catskill delta complex and the Acadian orogeny: A model: Geological Society of America Special Papers, v. 201, p. 39-50.

Ettensohn, F.R., 1994, Tectonic control on formation and cyclicity of major Appalachian unconformities and associated stratigraphic sequences: Tectonic and Eustatic Controls on Sedimentary Cycles: SEPM, Concepts in Sedimentology and Paleontology, v. 4, p. 217-242.

Ettensohn, F.R., 2008, The Appalachian foreland basin in eastern United States: Sedimentary basins of the world, v. 5, p. 105-179.

Faill, R.T., 1997, A geologic history of the north-central Appalachians; Part 1, Orogenesis from the Mesoproterozoic through the Taconic Orogeny: American Journal of Science, v. 297, p. 551-619.

Ferrill, B.A., and Thomas, W.A., 1988, Acadian dextral transpression and synorogenic sedimentary successions in the Appalachians: Geology, v. 16, p. 604-608.

Fichter, L.S., Whitmeyer, S.J., Bailey, C.M., and Burton, W., 2010, Stratigraphy, structure, and tectonics: An east-to-west transect of the Blue Ridge and Valley and Ridge provinces of northern Virginia and West Virginia: Field Guides, v. 16, p. 103-125.

Friedman, M., 1969, Structural analysis of fractures in cores from Saticoy Field, Ventura County, California: AAPG bulletin, v. 53, p. 367-389.

Friedman, M., Handin, J., and Alani, G., 1972, Fracture-surface energy of rocks, International Journal of Rock Mechanics and Mining Sciences & Geomechanics Abstracts, Volume 9, Elsevier, p. 757-764.

Gale, J.F., and Holder, J., 2010, Natural fractures in some US shales and their importance for gas production, Geological Society, London, Petroleum Geology Conference Series, Volume 7, Geological Society of London, p. 1131-1140.

Gale, J.F., Laubach, S.E., Olson, J.E., Eichhubl, P., and Fall, A., 2014, Natural fractures in shale: A review and new observations: AAPG bulletin, v. 98, p. 2165-2216.

Gale, J.F., Reed, R.M., and Holder, J., 2007, Natural fractures in the Barnett Shale and their importance for hydraulic fracture treatments: AAPG bulletin, v. 91, p. 603-622.

Galley, J.E., 1958, Oil and geology in the Permian basin of Texas and New Mexico: North America.

Geikie, A., 1903, Text-book of Geology, Macmillan.

Gillespie, P., Howard, C., Walsh, J., and Watterson, J., 1993, Measurement and characterisation of spatial distributions of fractures: Tectonophysics, v. 226, p. 113-141.

Gillespie, P., Walsh, J., Watterson, J., Bonson, C., and Manzocchi, T., 2001, Scaling relationships of joint and vein arrays from The Burren, Co. Clare, Ireland: Journal of Structural Geology, v. 23, p. 183-201.

Gratier, J.-P., Frery, E., Deschamps, P., Røyne, A., Renard, F., Dysthe, D., Ellouz-Zimmerman, N., and Hamelin, B., 2012, How travertine veins grow from top to bottom and lift the rocks above them: The effect of crystallization force: Geology, v. 40, p. 1015-1018.

Gross, M.R., and Engelder, T., 1995, Strain accommodated by brittle failure in adjacent units of the Monterey Formation, USA: scale effects and evidence for uniform displacement boundary conditions: Journal of Structural Geology, v. 17, p. 1303-1318.

Gudmundsson, A., 1987, Geometry, formation and development of tectonic fractures on the Reykjanes Peninsula, southwest Iceland: Tectonophysics, v. 139, p. 295-308.

Gudmundsson, A., Kusumoto, S., Simmenes, T.H., Philipp, S.L., Larsen, B., and Lotveit, I.F., 2012, Effects of overpressure variations on fracture apertures and fluid transport: Tectonophysics, v. 581, p. 220-230.

Gulisano, C., Gutiérrez Pleimling, A., and Digregorio, R., 1984, Análisis estratigráfico del intervalo Tithoniano-Valanginiano (Formaciones Vaca Muerta, Quintuco y Mulichinco) en el suroeste de la provincia del Neuquén, Congreso Geológico Argentino, Volume 1.

Gupta, U.D., 1980, A study of fractured reservoir rocks, with special reference to Mississippian carbonate rocks of southwest Alberta.

Handin, J., Hager Jr, R.V., Friedman, M., and Feather, J.N., 1963, Experimental deformation of sedimentary rocks under confining pressure: pore pressure tests: AAPG bulletin, v. 47, p. 717-755.

Harker, A., and Barrow, G., 1908, The geology of the small isles of Inverness-shire:(Rum, Canna, Eigg, Muck, etc.)(sheet 60, Scotland.), Printed for HM Stationery Off., by J. Hedderwick & Sons, Ltd.

Harper, J., and Kostelnik, J., 2010, The Marcellus shale play in Pennsylvania: PA Geological Survey, Presentation in PDF, available on-line at: http://www. dcnr. state. pa. us/topogeo/oilandgas/Marcellus. pdf.

Harrison, E.P., 1973, Depositional history of Cisco-Wolfcamp strata, Bend arch, north-central Texas.

Hatton, C., Main, I., and Meredith, P., 1994, Non-universal scaling of fracture length and opening displacement: Nature, v. 367, p. 160-162.

Heffer, K., and Bevan, T., 1990, Scaling relationships in natural fractures: data, theory, and application, European Petroleum Conference, Society of Petroleum Engineers.

Heffer, K., and Bevan, T., 1990, Scaling relationships in natural fractures: data, theory, and application, European Petroleum Conference, Society of Petroleum Engineers.

Hills, J.M., 1984, Sedimentation, tectonism, and hydrocarbon generation in Delaware basin, west Texas and southeastern New Mexico: AAPG bulletin, v. 68, p. 250-267.

Hooker, J., Gale, J., Gomez, L., Laubach, S., Marrett, R., and Reed, R., 2009, Aperture-size scaling variations in a low-strain opening-mode fracture set, Cozzette Sandstone, Colorado: Journal of Structural Geology, v. 31, p. 707-718.

Hooker, J., Laubach, S., and Marrett, R., 2013, Fracture-aperture size—frequency, spatial distribution, and growth processes in strata-bounded and non-strata-bounded

fractures, Cambrian Mesón Group, NW Argentina: Journal of Structural Geology, v. 54, p. 54-71.
Hooker, J., Laubach, S., and Marrett, R., 2014, A universal power-law scaling exponent for fracture apertures in sandstones: Geological Society of America Bulletin, v. 126, p. 1340-1362.
Howell, J.A., Schwarz, E., Spalletti, L.A., and Veiga, G.D., 2005, The Neuquén basin: an overview: Geological Society, London, Special Publications, v. 252, p. 1-14.
Hudson, J., and Priest, S., 1979, Discontinuities and rock mass geometry, International Journal of Rock Mechanics and Mining Sciences & Geomechanics Abstracts, Volume 16, Elsevier, p. 339-362.
Hudson, J., and Priest, S., 1983, Discontinuity frequency in rock masses, International Journal of Rock Mechanics and Mining Sciences & Geomechanics Abstracts, Volume 20, Elsevier, p. 73-89.
Jarvie, D.M., 2012, Shale resource systems for oil and gas: Part 2—Shale-oil resource systems.
Judd, J.W., 1871, On the Punfield Formation: Quarterly Journal of the Geological Society, v. 27, p. 207-227.
Judd, J.W., 1878, The secondary rocks of Scotland. Third paper. The strata of the Western Coast and islands: Quarterly Journal of the Geological Society, v. 34, p. 660-739.
Kaiser, P.K., Valley, B., Dusseault, M.B., and Duff, D., 2013, Hydraulic Fracturing Mine Back Trials—Design Rationale and Project Status, ISRM International Conference for Effective and Sustainable Hydraulic Fracturing, International Society for Rock Mechanics.
Keulen, N., Den Brok, S., and Spiers, C., 2001, Force of crystallisation of gypsum during hydration of synthetic anhydrite rock, 13th DRT conference: Deformation Mechanisms, Rheology, and Tectonics.
Klimczak, C., Schultz, R.A., Parashar, R., and Reeves, D.M., 2010, Cubic law with aperture-length correlation: implications for network scale fluid flow: Hydrogeology Journal, v. 18, p. 851-862.
Klimczak, C., Schultz, R.A., Parashar, R., and Reeves, D.M., 2010, Cubic law with aperture-length correlation: implications for network scale fluid flow: Hydrogeology Journal, v. 18, p. 851-862.
Kozlowski, E., Manceda, R., and Ramos, V., 1993, Estructura, 122 Congreso Geológico ArgentinoCongreso de Exploración de Hidrocarburos.
Ladeira, F., and Price, N., 1981, Relationship between fracture spacing and bed thickness: Journal of Structural Geology, v. 3, p. 179-183.
Lang, W.D., Spath, L.F., and Richardson, W.A., 1923, Shales-with-‘beef,’a Sequence in the Lower Lias of the Dorset Coast: Quarterly Journal of the Geological Society, v. 79, p. 47-66.

Lash, G.G., and Engelder, T., 2005, An analysis of horizontal microcracking during catagenesis: Example from the Catskill delta complex: AAPG bulletin, v. 89, p. 1433-1449.
Lash, G.G., and Engelder, T., 2005, An analysis of horizontal microcracking during catagenesis: Example from the Catskill delta complex: AAPG bulletin, v. 89, p. 1433-1449.
Lash, G.G., and Engelder, T., 2011, Thickness trends and sequence stratigraphy of the Middle Devonian Marcellus Formation, Appalachian Basin: Implications for Acadian foreland basin evolution: AAPG bulletin, v. 95, p. 61-103.
Laslett, G., 1982, Censoring and edge effects in areal and line transect sampling of rock joint traces: Journal of the International Association for Mathematical Geology, v. 14, p. 125-140.
Laubach, S. E., Reed, R. M., Olson, J. E., Lander, R. H., and Bonnell, L. M., 2004, Coevolution of crack-seal texture and fracture porosity in sedimentary rocks: cathodoluminescence observations of regional fractures: Journal of Structural Geology, v. 26, no. 5, 967-982.
Lavoie, D., Hamblin, A., Thériault, R., Beaulieu, J., and Kirkwood, D., 2008, The Upper Ordovician Utica Shales and Lorraine Group Flysch in Southern Quebec: Tectonostratigraphic Setting and Significane for Unconventional Gas, Natural Resources Canada.
Leanza, H., 2009, Las principales discordancias del Mesozoico de la Cuenca Neuquina según observaciones de superficie: Revista del Museo Argentino de Ciencias Naturales nueva serie, v. 11, p. 145-184.
Leanza, H.A., Marchese, H., and Riggi, J., 1973, Estudio sobre los cambios faciales de los estratos limítrofes Jurásico-Cretácicos entre Loncopué y Picún Leufú, provincia del Neuquén, República Argentina: Revista de la asociación Geológica argentina, v. 28, p. 97-132.
Leanza, H.A., Sattler, F., Martinez, R.S., and Carbone, O., 2011, La Formación Vaca Muerta y equivalentes (Jurásico tardío-Cretácico temprano) en la Cuenca Neuquina, Congreso Geológico Argentino, p. 113-129.
Lee, G.W., and Buckman, S.S., 1920, The Mesozoic Rocks of Applecross, Raasay, and Northeast Skye, HM Stationery Office.
Lewan, M.D., and Roy, S., 2011, Role of water in hydrocarbon generation from Type-I kerogen in Mahogany oil shale of the Green River Formation: Organic Geochemistry, v. 42, p. 31-41.
Maher Jr, H.D., Ogata, K., and Braathen, A., 2016, Cone-in-cone and beef mineralization associated with Triassic growth basin faulting and shallow shale diagenesis, Edgeøya, Svalbard: Geological Magazine.
Marrett, R., 1996, Aggregate properties of fracture populations: Journal of Structural Geology, v. 18, p. 169-178.
Marrett, R., Ortega, O.J., and Kelsey, C.M., 1999, Extent of power-law scaling for natural fractures in rock: Geology, v. 27, p. 799-802.

McCaffrey, M.A., Legarre, H.A., and Johnson, S.J., 1996, Using biomarkers to improve heavy oil reservoir management: An example from the Cymric Field, Kern County, California: AAPG bulletin, v. 80, p. 898-912.
Means, W., and Li, T., 2001, A laboratory simulation of fibrous veins: some first observations: Journal of Structural Geology, v. 23, p. 857-863.
Meissner, F.F., 1991, Petroleum geology of the Bakken Formation Williston Basin, North Dakota and Montana.
Milliken, K., 2014, A compositional classification for grain assemblages in fine-grained sediments and sedimentary rocks: Journal of Sedimentary Research, v. 84, p. 1185-1199.
Mitchum, R., and Uliana, M.A., 1985, Seismic stratigraphy of carbonate depositional sequences, Upper Jurassic-Lower Cretaceous, Neuquén Basin, Argentina: Seismic Stratigraphy, v. 2, p. 255-83.
Mitchum, R., and Uliana, M.A., 1985, Seismic stratigraphy of carbonate depositional sequences, Upper Jurassic-Lower Cretaceous, Neuquén Basin, Argentina: Seismic Stratigraphy, v. 2, p. 255-83.
Momper, J.A., 1978, Oil migration limitations suggested by geological and geochemical considerations.
Moros, J.G., 1999, Relationship between fracture aperture and length in sedimentary rocks, Unpublished M.S. thesis. The University of Texas, Austin.
Narr, W., 1996, Estimating average fracture spacing in subsurface rock: AAPG bulletin, v. 80, p. 1565-1585.
Narr, W., and Suppe, J., 1991, Joint spacing in sedimentary rocks: Journal of Structural Geology, v. 13, p. 1037-1048.
Nelson, R., 2001, Geologic analysis of naturally fractured reservoirs, Gulf Professional Publishing.
Nur, A., 1982, The origin of tensile fracture lineaments: Journal of Structural Geology, v. 4, p. 31-40.
Ortega, J., 2002, Fracture Size Scaling and Stratigraphic Controls on Fracture Intensity, PhD Dissertation, The Univ. Texas Austin.
Ortega, O., and Marrett, R., 2000, Prediction of macrofracture properties using microfracture information, Mesaverde Group sandstones, San Juan basin, New Mexico: Journal of Structural Geology, v. 22, p. 571-588.
Ortega, O., and Marrett, R., 2000, Prediction of macrofracture properties using microfracture information, Mesaverde Group sandstones, San Juan basin, New Mexico: Journal of Structural Geology, v. 22, p. 571-588.
Ortega, O.J., Marrett, R.A., and Laubach, S.E., 2006, A scale-independent approach to fracture intensity and average spacing measurement: AAPG bulletin, v. 90, p. 193-208.
Pickering, G., Bull, J., and Sanderson, D., 1995, Sampling power-law distributions: Tectonophysics, v. 248, p. 1-20.

Ploszkiewicz, J.V., 1987, Las zonas triangulares de la faja fallada y plegada de la cuenca neuquina Argentina, 10 Congreso Geológico Argentino, Volume 1.
Pommer, L.E., 2013, Natural fracture cementation in the Marcellus Formation, MS. Thesis, The Univ. Texas Austin.
Potter, P.E., Maynard, J.B., and Pryor, W.A., 1980, Sedimentology of Shale: Study Guide and Reference Source, with 154 Figures and a Colored Insert, Springer-Verlag.
Priest, S., and Hudson, J., 1981, Estimation of discontinuity spacing and trace length using scanline surveys, International Journal of Rock Mechanics and Mining Sciences & Geomechanics Abstracts, Volume 18, Elsevier, p. 183-197.
Pryor, W.A., and Ross, C.A., 1962, Geology of the Illinois parts of the Cairo, La Center, and Thebes quadrangles, State of Illinois, Department of Registration and Education, Division of the State Geological Survey.
Ramos, V., 1978, Relatório: Estructura, Geológia y Recursos Naturales del Neuquén: Buenos Aires, Proceedings Asociación Geológica Argentina, VII Congreso Geológico Argentino, p. 99-118.
Ramos, V., 1999, Plate tectonic setting of the Andean Cordillera: Episodes, v. 22, p. 183-190.
Ramos, V.A., and Folguera, A., 2005, Tectonic evolution of the Andes of Neuquén: constraints derived from the magmatic arc and foreland deformation: Geological Society, London, Special Publications, v. 252, p. 15-35.
Ramos, V.A., and Kay, S.M., 1991, Triassic rifting and associated basalts in the Cuyo basin, central Argentina: Geological Society of America Special Papers, v. 265, p. 79-92.
Ramsay, J.G., 1980, The crack-seal mechanism of rock deformation: Nature, v. 284, p. 135-139.
Reid, C., Woodward, H.B., Bennett, F.J., and Jukes-Browne, A.J., 1903, The Geology of the Country Around Salisbury:(Explanation of Sheet 298), HM Stationery Office.
Reynolds, S.H., and Vaughan, A., 1904, The Rhaetic beds of the South-Wales direct line: Quarterly Journal of the Geological Society, v. 60, p. 194-214.
Reynolds, S.H., and Vaughan, A., 1904, The Rhaetic beds of the South-Wales direct line: Quarterly Journal of the Geological Society, v. 60, p. 194-214.
Richardson, L., 1905, The Rhaetic and contiguous deposits of Glamorganshire: Quarterly Journal of the Geological Society, v. 61, p. 385-424.
Richardson, L., 1911, The Rhaetic and Contiguous Deposits of West, MID, & Part of East Somerset: Quarterly Journal of the Geological Society, v. 67, p. 1-74.
Rodrigues, N., Cobbold, P.R., Loseth, H., and Ruffet, G., 2009, Widespread bedding-parallel veins of fibrous calcite (’beef') in a mature source rock (Vaca Muerta Fm, Neuquén Basin, Argentina): evidence for overpressure and horizontal compression: Journal of the Geological Society, v. 166, p. 695-709.
Sanderson, D.J., Roberts, S., and Gumiel, P., 1994, A fractal relationship between vein thickness and gold grade in drill core from La Codosera, Spain: Economic Geology, v. 89, p. 168-173.

Schopfer, M.P.J, Arslan, A., Walsh, J.J., and Childs, C., 2011, Reconciliation of contrasting theories for fracture spacing in layered rocks: Journal of Structural Geology, v. 33, p. 551-565.

Schultz, R.A., Okubo, C.H., and Fossen, H., 2010, Porosity and grain size controls on compaction band formation in Jurassic Navajo Sandstone: Geophysical Research Letters, v. 37.

Schultz, R.A., Soliva, R., Fossen, H., Okubo, C.H., and Reeves, D.M., 2008, Dependence of displacement–length scaling relations for fractures and deformation bands on the volumetric changes across them: Journal of Structural Geology, v. 30, p. 1405-1411.

Short, A.R., 1904, A description of some Rhaetic sections in the Bristol district, with considerations on the mode of deposition of the Rhaetic Series: Quarterly Journal of the Geological Society, v. 60, p. 170-193.

Sibson, R.H., 2003, Brittle-failure controls on maximum sustainable overpressure in different tectonic regimes: AAPG bulletin, v. 87, p. 901-908.

Silver, B.A., and Todd, R.G., 1969, Permian cyclic strata, northern Midland and Delaware basins, west Texas and southeastern New Mexico: AAPG bulletin, v. 53, p. 2223-2251.

Sinclair, S.W., 1980, Analysis of macroscopic fractures on Teton anticline, northwestern Montana, Texas A&M University.

Swarbrick, R.E., Osborne, M.J., and Yardley, G.S., 2001, AAPG Memoir 76, Chapter 1: Comparision of Overpressure Magnitude Resulting from the Main Generating Mechanisms.

Taber, S., 1916, The growth of crystals under external pressure: American Journal of Science, p. 532-556.

Taber, S., 1918, The origin of veinlets in the Silurian and Devonian strata of central New York: The Journal of Geology, v. 26, p. 56-73.

Turienzo, M., Dimieri, L., Frisicale, C., Araujo, V., and Sánchez, N., 2012, Cenozoic structural evolution of the Argentinean Andes at 34º40'S: A close relationship between thick and thin-skinned deformation: Andean Geology, v. 39, p. 317-357.

Udden, J.A., and Bowman, W., 1917, Notes on the Geology of the Glass Mountains, The University.

Valcarce, G.Z., Zapata, T., del Pino, D., and Ansa, A., 2006, Structural evolution and magmatic characteristics of the Agrio fold-and-thrust belt: Geological Society of America Special Papers, v. 407, p. 125-145.

Vera, E.A.R., Folguera, A., Valcarce, G.Z., Bottesi, G., and Ramos, V.A., 2014, Structure and development of the Andean system between 36 and 39 S: Journal of Geodynamics, v. 73, p. 34-52.

Vergani, G.D., Tankard, A.J., Belotti, H.J., and Welsink, H.J., 1995, Tectonic evolution and paleogeography of the Neuquén Basin, Argentina.

Vernik, L., 1994, Hydrocarbon-generation-induced microcracking of source rocks: Geophysics, v. 59, p. 555-563.

Viñes, R., 1985, Estilos estructurales en la Faja Plegada Occidental Neuquina: Yacimientos Petrolíferos Fiscales.

Warbrick, R., and Osborne, M., 1998, Mechanisms that generate abnormal pressure: an overview: Abnormal Pressure in Hydrocarbon Environments, v. 70, p. 13-43.

Warpinski, N.R., Mayerhofer, M.J., Bridges, A.C., and Du, J., 2012, Hydraulic fracture geomechanics and microseismic source mechanisms, SPE Annual Technical Conference and Exhibition, Society of Petroleum Engineers.

Webster, T., 1826, IV.—Observations on the Purbeck and Portland Beds: Transactions of the Geological Society of London, p. 37-44.

Wilkins, S., Mount, V., Mahon, K., Perry, A., and Koenig, J., 2014, Characterization and development of subsurface fractures observed in the Marcellus Formation, Appalachian Plateau, north-central Pennsylvania: AAPG bulletin, v. 98, p. 2301-2345.

Wong, T.F., Fredrich, J.T., and Gwanmesia, G.D., 1989, Crack aperture statistics and pore space fractal geometry of Westerly granite and Rutland quartzite: Implications for an elastic contact model of rock compressibility: Journal of Geophysical Research: Solid Earth, v. 94, p. 10267-10278.

Woodward, H.B., 1893, The Jurassic Rocks of Britain: The Lias of England and Wales (Yorkshire Excepted), HM Stationery Office.

Woodward, H.B., 1893, The Jurassic Rocks of Britain: The Lias of England and Wales (Yorkshire Excepted), HM Stationery Office.

Wu, H., and Pollard, D.D., 1995, An experimental study of the relationship between joint spacing and layer thickness: Journal of Structural Geology, v. 17, p. 887-905.

Yang, K.-M., and Dorobek, S.L., 1995, The Permian basin of west Texas and New Mexico: tectonic history of a" composite" foreland basin and its effects on stratigraphic development: Stratigraphic evolution of foreland basins: SEPM Special Publication, v. 52, p. 149-174.

Young, J., 1886, I. Notes on Cone-in-Cone Structure: Transactions of the Geological Society of Glasgow, v. 8, p. 1-27.

Zanella, A., Cobbold, P.R., Ruffet, G., and Leanza, H.A., 2015, Geological evidence for fluid overpressure, hydraulic fracturing and strong heating during maturation and migration of hydrocarbons in Mesozoic rocks of the northern Neuquén Basin, Mendoza Province, Argentina: Journal of South American Earth Sciences, v. 62, p. 229-242.

Zapata, T., 2003, The Agrio Fold and Thrust Belt: Structural Analysis and its Relationship with the Petroleum System Vaca Muerta-Agrio-Troncoso Inferior (!), Argentina.

Zapata, T., Brissón, I., and Dzelalija, F., 1999, La estructura de la faja plegada y corrida andina en relación con el control del basamento de la Cuenca Neuquina: Boletín de informaciones Petroleras, v. 60, p. 112-121.

Zapata, T., Brissón, I., Dzelalija, F., and McClay, K., 1999, The role of basement in the Andean fold and thrust belt of the Neuquén Basin: Thrust tectonics, v. 99, p. 122-124.

Zapata, T., Córsico, S., Dzelalija, F., and Zamora Valcarce, G., 2002, La faja plegada y corrida del Agrio: Análisis estructural y su relación con los estratos terciarios de la Cuenca Neuquina Argentina, Proceedings, Congreso de Exploración y Desarrollo de Hidrocarburos, 5th: Mar del Plata, Electronic Files.

Zapata, T., and Folguera, A., 2005, Tectonic evolution of the Andean fold and thrust belt of the southern Neuquén Basin, Argentina: Geological Society, London, Special Publications, v. 252, p. 37-56.